General Electric Co., Philadelphia, Pa., Space Div.
SNAP 27: SUMMARY REPORT

CID 1392
CALL # 24-05

GEMS-402

OSTI # 4695921

A Facsimile Report

Reproduced by
UNITED STATES
ATOMIC ENERGY COMMISSION
Technical Information Center
P.O. Box 62 Oak Ridge, Tennessee 37830

SPACE SYSTEMS

~~CONFIDENTIAL~~

DIN: GEMS 402
15 JULY 1970

UNCLASSIFIED

SNAP-27

SUMMARY REPORT (U)

Classification Cancelled
Or Changed To
By Autnority Of D.O.C.
By L. Joffee Date 10/18/71

UNCLASSIFIED

~~CONFIDENTIAL~~

GENERAL ELECTRIC

~~CONFIDENTIAL~~

UNCLASSIFIED

DIN: GEMS 402
15 JULY 1970

NSP NUCLEAR SYSTEMS PROGRAMS
ISOTOPE POWER SYSTEMS OPERATION

AEC RESEARCH AND DEVELOPMENT REP
C-92A
M-3679 EDITION 63
THIS DOCUMENT CONTAINS:

SNAP-27

SUMMARY REPORT (U)

PREPARED FOR:

CONTRACT NO. AT(29-2)-2581
US ATOMIC ENERGY COMMISION
ALBUQUERQUE OPERATIONS OFFICE
ALBUQUERQUE,NEW MEXICO

LAN: 019A-37-2

UNCLASSIFIED

GROUP 3
DOWNGRADED AT 12
YEAR INTERVALS;
NOT AUTOMATICALLY
DECLASSIFIED

C-DI 10-11-72 Paul K. Pinsuvan
CLASS. DATE AUTHORIZED CLASSIFIER

ISOTOPE POWER SYSTEMS OPERATION

GENERAL ELECTRIC
SPACE DIVISION
KING OF PRUSSIA PARK
P.O. BOX 8661 • PHILADELPHIA, PENNA., 19101

~~CONFIDENTIAL~~ UNCLASSIFIED

TABLE OF CONTENTS

BLANK PAGE

TABLE OF CONTENTS (CONT)

TABLE OF CONTENTS (CONT)

TABLE OF CONTENTS (CONT)

TABLE OF CONTENTS (CONT)

TABLE OF CONTENTS (CONT)

TABLE OF CONTENTS (CONT)

TABLE OF CONTENTS (CONT)

LIST OF ILLUSTRATIONS

LIST OF ILLUSTRATIONS (CONT)

LIST OF ILLUSTRATIONS (CONT)

LIST OF ILLUSTRATIONS (CONT)

LIST OF ILLUSTRATIONS (CONT)

LIST OF ILLUSTRATIONS (CONT)

LIST OF ILLUSTRATIONS (CONT)

LIST OF ILLUSTRATIONS (CONT)

LIST OF ILLUSTRATIONS (CONT)

LIST OF TABLES

LIST OF TABLES (CONT)

LIST OF TABLES (CONT)

ABSTRACT

The SNAP-27 Radioisotope Thermoelectric Generator (RTG) System was designed, developed, and fabricated as the prime power supply for the National Aeronautics and Space Administration's (NASA's) Apollo Lunar Surface Experiment Package (ALSEP). The RTG program was carried out by the General Electric Company's Missile and Space Division under the direction of the Atomic Energy Commission. The program began in late 1965, and the first electrically heated units were delivered in late 1966. Initial power requirements of 56 watts were exceeded; each of the five flight units will produce more than 67 watts after one year of lunar operation. The last flight hardware was delivered in May of 1969. Safety approval was granted in June of 1969 for the Apollo 12 and subsequent flights. The SNAP-27 program was extremely successful in that NASA was provided with a power system exhibiting exceptional performance and reliability.

FOREWORD

This report is a synopsis of the SNAP-27 radioisotope fueled thermoelectric generator program completed for the United States Atomic Energy Commission by the Isotope Power Systems Operation of the General Electric Company's Missile and Space Division under Contract No. AT(30-1)-3535.

The major end-items of this program were five fully qualified and flight acceptance tested SNAP-27 RTG Systems to be employed in support of the Apollo Lunar Surface Experiment Program (ALSEP).

A secondary, but nevertheless highly valuable, fall-out from this program is the far-reaching advances which were made in the state-of-the-art relative to the technological disciplines in beryllium fabrication, thermoelectric conversion, isotopic heat source design, reentry mechanics through regions of high-angle superorbital re-entry, nuclear safety analysis and safety testing.

The report is organized in such a manner that all major task descriptions and results are discussed in a logical approach beginning with the development of the various designs, progressing through qualification and acceptance testing, and concluding with a summary of the prelaunch planning.

The information, though it appears massive, is sketchy, particularly in the development area, compared with the wealth of data actually accumulated during the program. It is, however, written at a level of detail wherein the reader may gain insight as to the scope and nature of the various activities which were required to be carried out in order to accomplish the program.

1. INTRODUCTION

1.1 MISSION DESCRIPTION

The SNAP-27 Radioisotope Thermoelectric Generator (RTG) is the primary source of electric power for the Apollo Lunar Surface Experiments Package (ALSEP).

The ALSEP is a group of scientific experiments and support subsystems which will be deployed on the surface of the moon by an Apollo Astronaut. The ALSEP will measure lunar physical and environmental characteristics and will transmit the data to receiving stations on earth for a period of one year. This data will be used to derive information on the composition and structure of the lunar body, magnetic field, atmosphere and solar wind.

On the lunar surface, the ALSEP will be controlled by ground command from the Manned Space Flight Network (MSFN). Commands from earth and automatically generated commands will direct ALSEP operations. Automatic system shut-down is provided after an elapse of two years.

The experiment and support subsystems are mounted on two subpackages. The SNAP-27 RTG and flight handling tool are included in Subpackage No. 2. Both subpackages are stored in the LM descent stage scientific equipment bay. Figure 1-1 shows Subpackage No. 2, and its location in the LM during flight. The Graphite LM Fuel Cask (GLFC) which houses and protects the SNAP-27 fuel capsule is mounted on the outside of the LM descent stage adjacent to the scientific equipment bay by an ALSEP supplied support structure/thermal shield. During the trip to the moon, the ALSEP is inoperative. Upon landing, a crew member will remove the two subpackages from the LM, tilt the GLFC and extract the fuel capsule, insert the capsule into the generator, and then deploy the ALSEP as shown in the pictorial sequence, Figure 1-2 (A through G). Figure 1-3 shows the deployment arrangement of the ALSEP on the moon.

1.2 PROGRAM BACKGROUND

As originally conceived, SNAP-27 was intended for a dual purpose: as the lunar surface generator for the Surveyor Lunar Roving Vehicle (SLRV), and as the power source for the Apollo Lunar Surface Experiment Package (ALSEP).

The SNAP-27 contract was awarded to General Electric Company on March 17, 1965, as a direct successor to the Phase I Study performed by

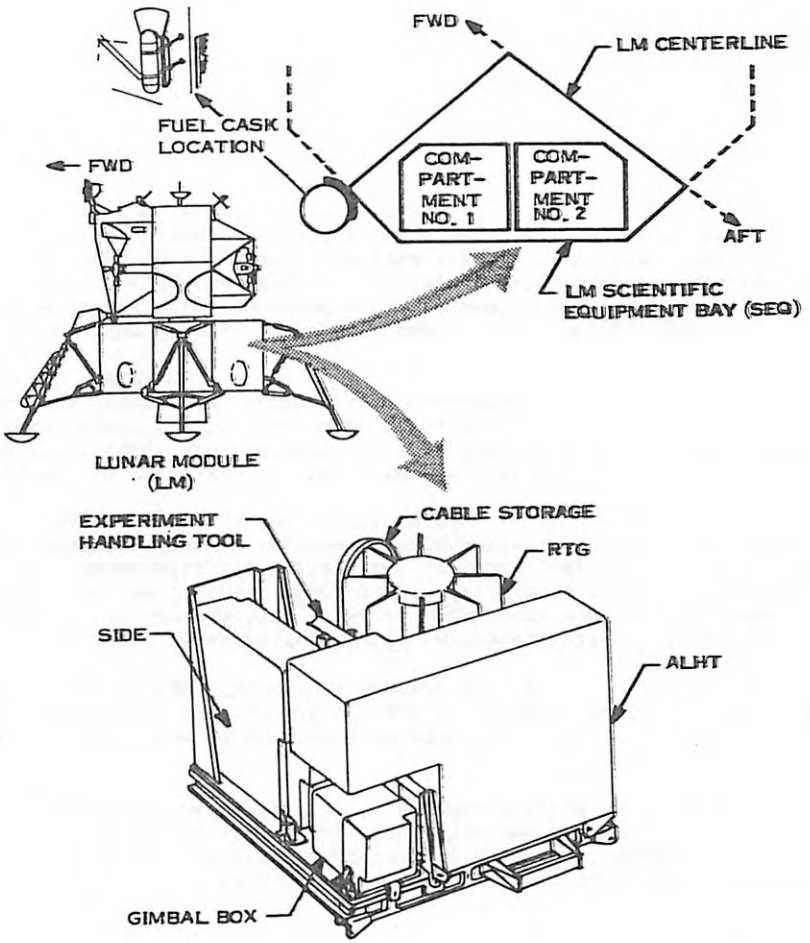

Figure 1-1. SNAP-27 RTG Location on the LM During Flight

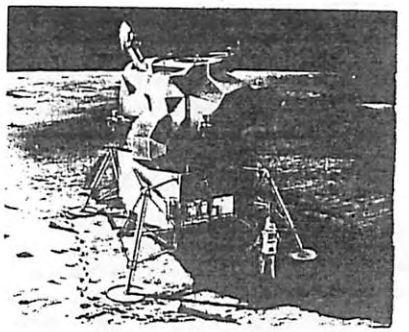

Astronaut Approaching LM for ALSEP Deployment

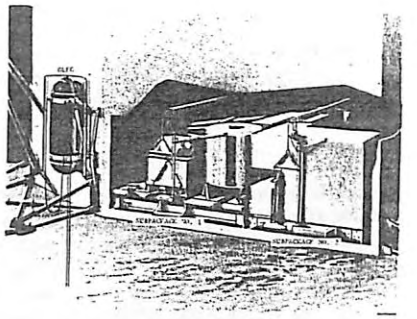

Close-up of Compartments 1 and 2 and Graphite LM Fuel Cask with Heat Source

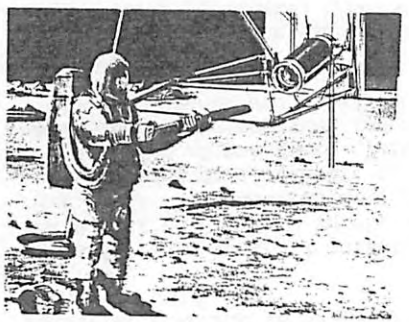

Heat Source Removal from GLFC

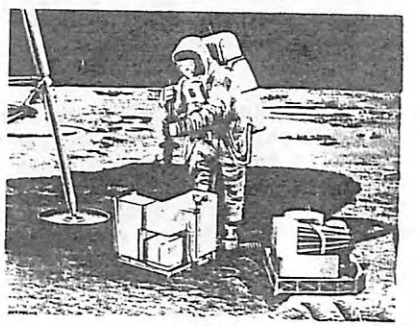

Heat Source Being Inserted in GA

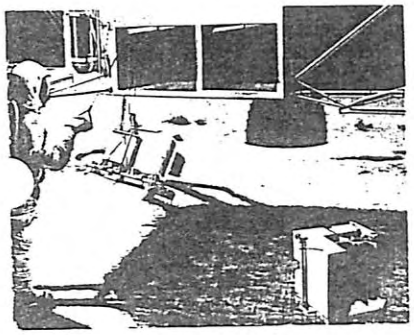

Experiment on Lunar Surface-
Astronaut Now Has Flight
Handling Tool Available

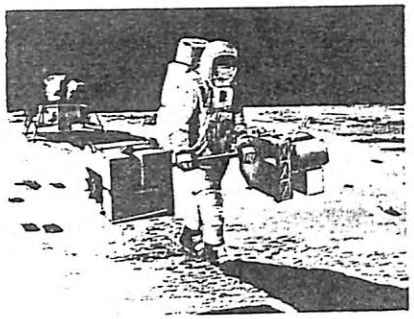

ALSEP Being Carried to
Deployment Site

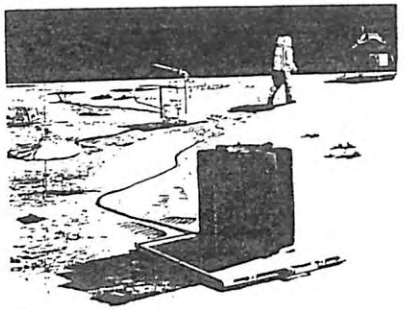

Experiment Deployed

Figure 1-2. SNAP-27 ALSEP Lunar Surface Deployment Sequence

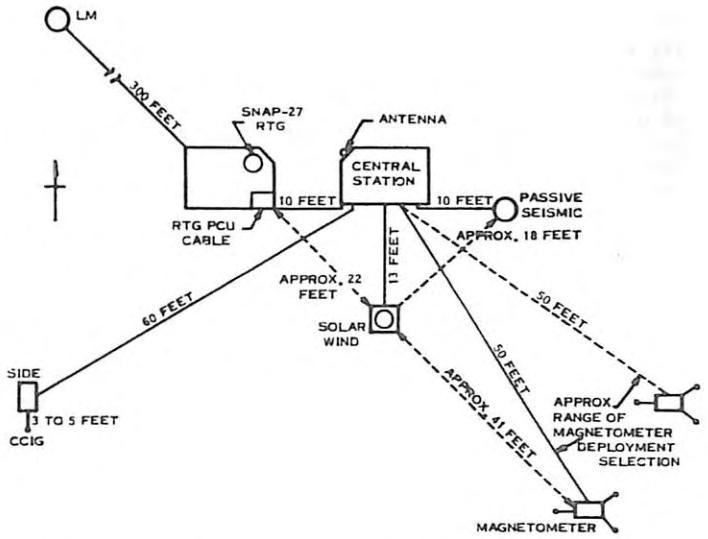

Figure 1-3. ALSEP Deployment Scheme on Lunar Surface

General Electric on a generator for SLRV under contract AT (30-1)-3412.

At the time, the plan was for General Electric to undertake a six to eight month Phase IIA, Technology Development Program, since neither intended user was then able to give more than general performance requirements. The objective of Phase IIA was, therefore, to develop the fundamental design data that would, when detailed performance specifications became available, enable the full generator design and development program to proceed expeditiously. Since there were no schedule pressures at that time, the plan was to define the Phase IIA scope of work, and to fully negotiate the prime contract and all subcontracts before initiating any contractual work.

The combination of Surveyor program schedule slippage and budget limitations subsequently deleted the Block II Surveyors from that program, those carrying the SLRV. On the other hand, the Manned Spacecraft Center initiated an accelerated Apollo Lunar Surface Experiment Package Program and committed itself to an Atomic Energy Commision developed radioisotope powered generator.

The accelerated ALSEP program imposed such severe schedule restrictions on the generator development effort that it soon became obvious

that the Phase IIB effort would have to run in parallel with most of Phase IIA.

The concept at this time was based on "intact re-entry" of a fueled generator. Since this required the fins to withstand the re-entry thermal and mechanical loads, the need for developing a high strength, high temperature fin-to-case joint was the major consideration in selecting beryllium as the basic structural material.

In a NASA study by General Electric in the summer of 1965, this approach was compared against the "separate shipment" approach where the heat source is not launched in the generator, but is contained in a re-entry heat shield structure mounted separately on the LM exterior. In the study, both arrangements of capsule transport were evaluated and trade-offs conducted relating to astronaut handling, thermal integration with the LM, and mechanical integration. Studies were also made by NASA's competing ALSEP contractors in their Phase I Programs. These contractors, Bendix, TRW and Space General, were asked to study both concepts and to provide recommendations to NASA.

A major program change thus occurred on November 15, 1965 when NASA requested the design concept be changed to one incorporating transportation of the fuel capsule to the lunar surface in a separate LM shipping cask. This transferred all the re-entry programs from the generator to the LM shipping cask.

In May, 1966, technical and administrative responsibilities for the program were transferred from NYOO to ALOO. ALOO subsequently administered the program with the Sandia Corporation providing the technical direction.

2. SUMMARY

2.1 PROGRAM IMPLEMENTATION AND MANAGEMENT

Award of the SNAP-27 contract to General Electric was made on March 17, 1965. This was intended to be a six to eight month technology development program to generate fundamental design data.

By early June, 1965, essential agreement had been reached on a work statement, funding level, and subcontractor participation.

General Electric was authorized to proceed on Phase IIA as of August 16, 1965. This was followed by Phase IIA authorizations to Y-12 on September 22, 1965; to Solar on September 27, 1965; and to 3M on September 29, 1965.

The negotiation of a mutually acceptable subcontract with the 3M Company became the major program activity at this time. The Atomic Energy Commission and General Electric were requesting the inclusion of product assurance provisions to increase the confidence in the thermopile capability and to permit meaningful analyses of any failures that might occur. The 3M Company was concurrently seeking adequate protection for its long-standing company investment in its proprietary processes.

On September 8, 1965, the AEC requested that the program include all the development testing needed to fully verify the design, even if the results were scheduled to be available after the major design release points.

The scope of the program was further increased by NASA's inclusion of the full gamut of Apollo management, reliability, quality assurance, and documentation requirements, which were presented to the Commission and the General Electric Company on September 19, 1965.

The commitment of NASA to an AEC generator for the Apollo Lunar Surface Experiments Package (ALSEP), and the acceleration of that program, imposed such severe schedule restrictions on the generator development that Phase IIB was authorized on November 8, 1965 to run in parallel with Phase IIA. The overriding necessity of initiating Phase IIB at the earliest practicable date resulted in the Phase IIA technical efforts being overshadowed by the preparation of the Phase IIB program.

An oral presentation of the technical content of Phase IIB was made on October 18, 1965, followed by a formal quotation submitted on October 25, 1965 for a November 1, 1965 Phase IIB go-ahead. Resolution of the many technical and schedule details of this quotation delayed the release of the authorization to proceed until November 8, 1965.

At this time, the technology development work associated with beryllium fabrication and thermoelectric performance was just underway as part of the original SNAP-27 Phase IIA Technology Program.

The selection of the Phase IIB beryllium supplier was also one of the most critical items in the program, and well illustrated the problems created by the unfortunate, but unavoidable, necessity of conducting Phase IIA and Phase IIB in parallel. This selection was to have been based on the evaluation of the Phase IIA work done by the Solar Division of Internal Harvestor and Y-12 plant of the Oak Ridge National Laboratory, culminating in a mechanical proof test in April of 1966 of one dummy generator from each source. In order to meet Phase IIB schedules, at least one source had to be authorized in early January, 1966, to proceed with the fabrication of parts for the engineering development generators.

A design review was held on January 17, 1966, during which Y-12 indicated that they were not capable of meeting schedules. Solar was thus selected as the Phase IIB beryllium supplier.

The 3M Company was given Phase IIB authorization on December 1, 1965. The work on the electric capsules at Thermo Electron Engineering Corporation (TEECO) was started on January 14, 1966.

Program requirements called for delivery of a prototype generator on December 31, 1966 and for the flight system on July 15, 1967. This short schedule, plus the lack of technological background, required that not only should the SNAP-27 Program be "success" oriented, but that it should provide sufficient technology development to permit rapid solution to problems occurring downstream. Thus the term "component" development was adopted, and the technology effort focused on developing the various functional component characteristics of the RTG system.

Phase IIA and IIB programs were ultimately merged when the overlap between the two subphases made it impractical to continue differentiating between them. The Phase II program then encompassed the total system development and fabrication of all development, prototype and qualification hardware. Basic technology investigations to evaluate finned body re-entry and establishment of a thermoelectric leg product specification were included as adjuncts to the Phase II Program.

Phase III of the program, which consisted of qualification testing of the generator and associated equipment, and the effort necessary to support these activities started in July of 1966, overlapping both Phase II and Phase IV. With the completion of the major portion of the test effort, all remaining Phase III activity was combined with Phase IV in the latter part of 1967. Phase IV extended through June of 1969 and was concerned primarily with the production and delivery of flight units.

The overall SNAP-27 schedule is summarized in Figure 2-1. Review of the figure will show that the first SNAP-27 generator (Mod 5) was completed approximately 12 months after program start. In this period, the thermopile design and beryllium fabrication techniques were developed, and the generator was built and placed on extended life test. Shipment of the first prototype generator (Mod 14) was made to the ALSEP Contractor, Bendix, on December 31, 1966. This was followed then by deliveries of two flight generators in mid-July 1967 per the original schedule. Generator qualification was performed on Mod 10, a unit built to the flight design, which was subjected to dynamic and long term thermal vacuum testing.

The Graphite LM Fuel Cask (GLFC) program was initiated in January 1967 based on program redirection from the AEC. From its inception to the end of April 1969, all development activities, including characterization of Pyrocarb-406 graphite, were completed, casks were fabricated, and a complete qualification program conducted utilizing the fuel capsule and the ALSEP support structure.

Encapsulation of all fuel capsules was completed by Mound Laboratory in November, 1968. After combined acceptance and qualification testing with the GLFC and the ALSEP support structure, the fuel capsules were delivered to the AEC for storage.

Safety work was completed at the end of December, 1968. Flight approval was granted in May, 1969.

2.2 PROGRAM INTERFACES

Interfaces were established early in the SNAP-27 Program to define the system requirements, hardware interface, environmental criteria and program support.

Figure 2-2 shows the major SNAP-27 interfaces, which can be summarized as follows:

AEC/Sandia - technical direction; safety

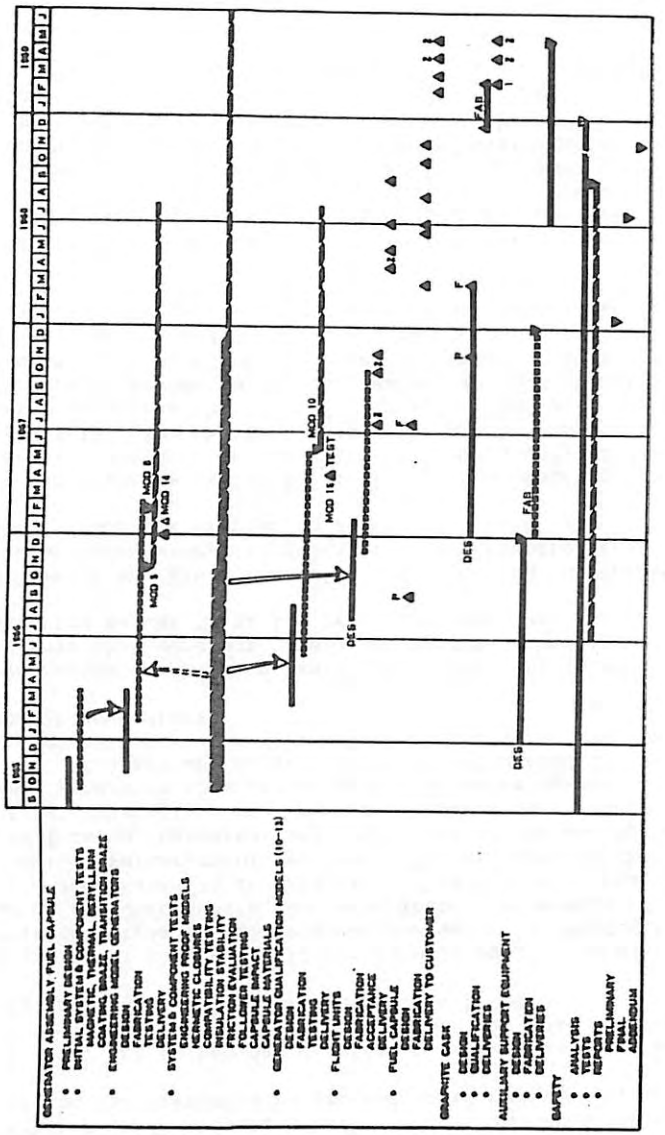

Figure 2-1. Overall SNAP-27 Schedule

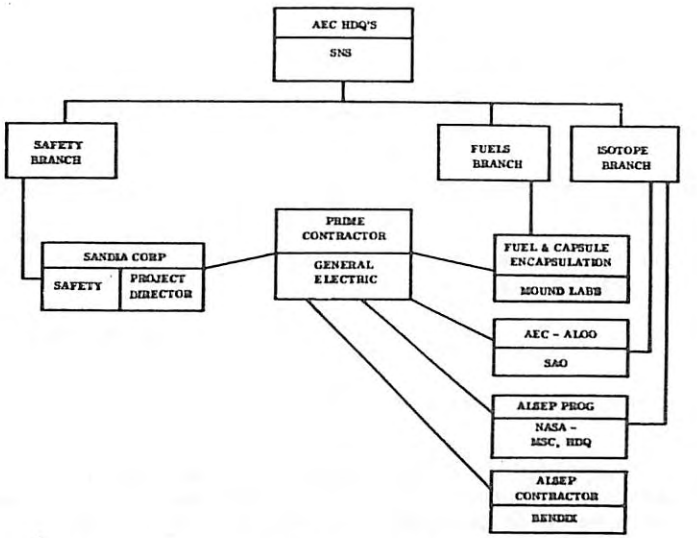

Figure 2-2. SNAP-27 Program Interfaces

NASA/Bendix - environmental criteria; generator and GLFC performance; thermal and mechanical integration

Mound Laboratory - fuel form; fuel characterization; encapsulation

AEC/SAO - contractual requirements.

2.3 SNAP-27 OPERATIONAL SYSTEM

The total SNAP-27 operational system is comprised of the flight hardware and the auxiliary support equipment identified in Table 2-1 and depicted in Figure 2-3. Detailed descriptions of each of these articles are contained in subsequent sections of this report.

Not included as part of the overall SNAP-27 operational system, but provided to NASA and the ALSEP contractor (Bendix) were the following ALSEP test systems, as well as integration and astronaut training articles:

TABLE 2-1. SNAP-27 OPERATIONAL SYSTEM

	GENERAL ELECTRIC DRAWING NUMBER
FLIGHT HARDWARE	
Generator Assembly	47R300779
Fuel Capsule Assembly	47D300400
Graphite LM Fuel Cask	47E301134
Flight Handling Tool	47E300452
AUXILIARY SUPPORT EQUIPMENT	
Electric Fuel Capsule Simulator	47D300331
Test Console	47E300467
Ground Handling Tool	47D300857
Fuel Capsule Ground Shipping Cask	47E300613
Generator Assembly Shipping Cask	47E300754
SLA Handling Tool	47D300855
SLA Transfer Cask	47R301143
Capsule Back Plate Lock Check Tool	47D301112
Port Entry Trough	47R300883

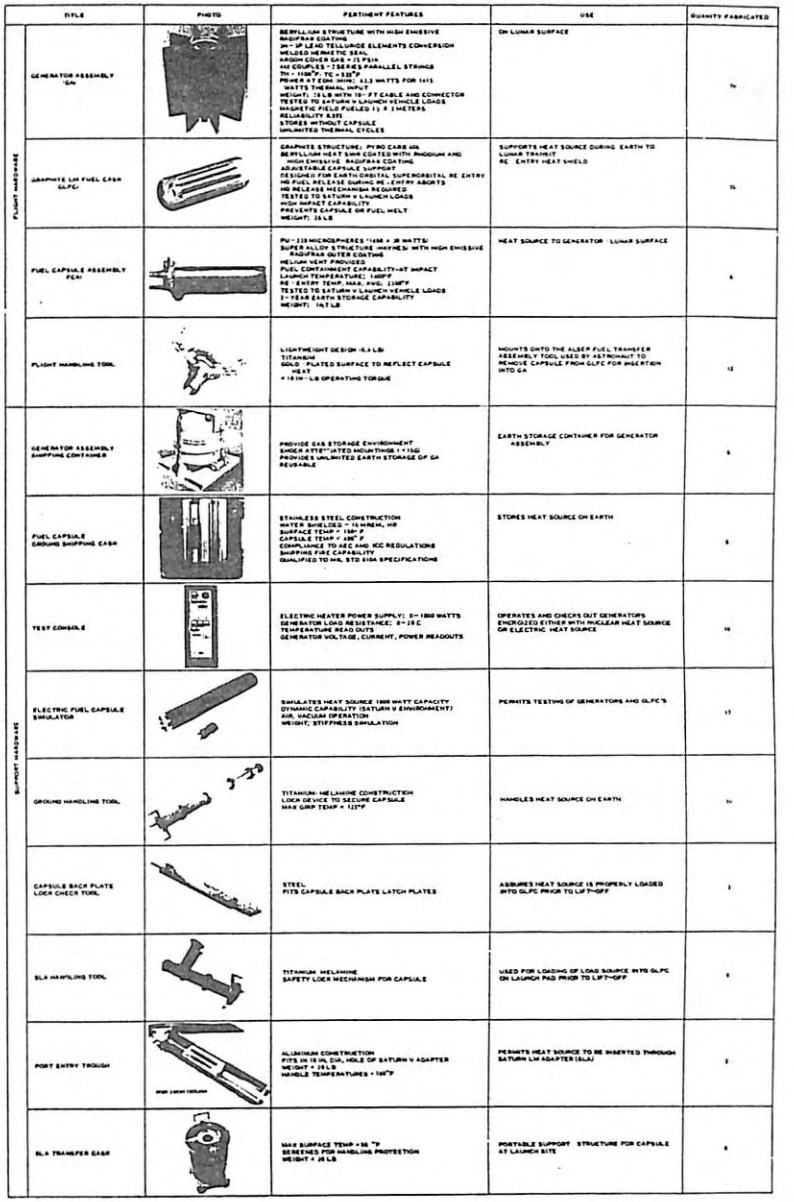

Figure 2-3. SNAP-27 Deliverable End Items

a. ALSEP Test Systems

1. ALSEP prototype test system, Mod 14
2. ALSEP qualification test system, Mod 15.

b. Mock-up Hardware

1. Mechanical Integration Mock-ups, M-1, M-2 and M-3
2. Thermal Test Mock-ups, M-4
3. Mechanical Mock-ups, M-5
4. Training Mock-ups, M-6
5. 1/6 g Training Mock-ups, M-7
6. Final Training Mock-ups, M-8
7. 1/6 g Final Training Mock-ups, M-9
8. Performance test mock-ups.

Table 2-2 is a SNAP-27 end item matrix which summarizes the hardware produced during the program and its allocation.

Table 2-3 summarizes the design and performance characteristics of the three major SNAP-27 flight articles: the generator assembly, the fuel capsule assembly and the graphite LM fuel cask.

2.4 SYSTEM DESIGN

2.4.1 GENERATOR

When the decision was made for the separate shipment approach, a reference generator design was established which, except for some design modifications, remained essentially the same for the program's duration.

2.4.2 POWER CONDITIONING UNIT

At the beginning of the program, General Electric's responsibility also included the design of an associated Power Conditioning Unit (PCU) for the generator. General Electric developed a set of requirements for the PCU and requested bids from industry for its design and fabrication. Three companies responded to the RFP, and during January 1966 the proposals were evaluated. A key milestone at the time was for NASA

TABLE 2-2. SNAP-27 END ITEM HARDWARE MATRIX

	ENGINEERING UNITS		QUAL UNITS		FLIGHT UNITS	TOTAL
	GE	DELIVERED	GE	DELIVERED	DELIVERED	
Generator Assembly	2	1	1	1	5	10
Graphite LM Fuel Cask	2	2	-	1	5	10
Fuel Capsule Assembly	-	-	1	-	5	6
Flight Handling Tool	3	2	1	1	5	12
Generator Shipping Container	-	-	1	-	5	6
Fuel Capsule Ground Shipping Container	-	-	1	-	5	6
Test Consoles	2	4	1	1	2	10
Electric Fuel Capsules	4	6	3	2	2	17
Ground Handling Tool	3	-	1	1	5	10
SLA Inspection Tool	1	-	-	-	2	3
SLA Handling Tool	-	-	1	-	5	6
Port Entry Trough	-	-	-	-	2	2
SLA Transfer Cask	2	-	1	-	5	8
Mock-Ups						
Generator Assembly	-	-	-	-	6	6
GLFC's	-	-	-	1	1	2
FCA	-	-	-	1	1	2

TABLE 2-3. SUMMARY OF SNAP-27 SYSTEM DESIGN AND PERFORMANCE CHARACTERISTICS

Design Life	One year lunar operation preceeded by two years Earth storage
Generator Assembly	
Output Power (minimum)	63.5 watts (end of life)
Output Voltage (nominal)	16 volts dc
Current (nominal)	2 amps in each of two strings
Overall Efficiency (nominal)	4.7 percent
Hot Junction Temperature (max)	1070°F (lunar day)
Cold Junction Temperature (max)	525°F (lunar day)
Overall Generator Diameter (including fins)	15.75 in. max
Overall Generator Length	18.12 in. max
Number of Fins	8
Fin Radial Length	5.0 in.
Fuel Capsule Assembly	
Number of Fuel Capsules	1
Capsule OD	2.511 in. max
Capsule Length	16.481 in. max
Total Dose Rate at 1 Meter	100 mrem/hour
Fuel Capsule Thermal Output (Nominal)	1480 watts (initial)
Fuel Clad Temperature	1390°F max
Fuel Form	$Pu^{238}O_2$ microspheres
Graphite LM Fuel Cask	
Cask OD	8.0 in.
Cask Length	23.0 in.
Free Body Re-entry Capability	Earth Orbit Decay
Free Body Re-entry Capability	Superorbital Re-entry Angle = 6.8 to 38 degrees
Weights (Max)	
Generator Assembly (including cable and connector)	28.0 lbs
Fuel Capsule Assembly	15.46 lbs
Graphite LM Fuel Cask	25.2 lbs
Flight Handling Tool	0.6 lbs

to submit final PCU design requirements by January 7,1966, relative to correct power output characteristics, so that negotiations could begin with the successful bidder. At the January monthly meeting, however, it was agreed that NASA would instead assume responsibility for the PCU design; that General Electric would have the right to review and to reject the PCU design if it was considered to be incompatible with the generator. It was later requested that General Electric impose the technical requirements on NASA (ALSEP) for the PCU hardware necessary to support the SNAP-27 program. This was accomplished in a letter to the AEC dated February 15, 1966.

2.4.3 LM FUEL CASK

The initial reference design of the cask which was to support the fuel capsule in flight was referred to as the LM fuel cask which consisted of a configuration having an Apollo-type nose, a cylindrical midsection and a biconic afterbody. The heat protection system for this cask consisted of an ESM shield/bond composite. The beryllium cask structure provided the support to the fuel capsule, located and supported the ESM heat shields and acted as a controlled heat path to reject capsule heat.

The initial LM fuel cask design was based on requirements for an earth orbital re-entry design. When requirements were subsequently modified by NASA to also include capability for superorbital re-entry, the decision had to be made by the AEC whether a separation subsystem should be incorporated for ejection of the LM fuel cask from the SLA during suborbital or earth orbital periods of the mission (in case of an abort situation) or whether to redesign the LM fuel cask to give it the capability for withstanding the superorbital re-entry conditions. The AEC decision was to take the latter approach even though this meant a substantial increase in cask weight. As a consequence, the design evolved from that of a light-weight beryllium unit to one fabricated primarily of graphite and capable of withstanding all credible abort conditions.

2.4.4 GRAPHITE LM FUEL CASK

The original graphite cask design conceived and developed by General Electric employed a "thermal switch"concept, i.e., the secondary thermal shield consisted of a columbium cylinder with a concentric stack-up of silver rings and SiO_2 insulation rings. Two prime-type secondary heat shields of this design were assembled and received on March 25, 1968 by General Electric but were never utilized in the program. These shields were felt to be fully satisfactory and would have satisfied the stated design requirements.

On April 3, 1968, at the time a production run would have been initiated on the "thermal switch" design, the design of the secondary shield was changed to that of a beryllium structure which offered much greater margins to the GLFC system. The redesign came about in order to satisfy major changes in overall GLFC requirements. These were:

a. Increase in required dynamic capability resulting from a NASA increase in flight loads by a factor of 6.

b. Change in re-entry environments resulting from NASA's reluctance to provide means of release from the LM, and a challenge of the General Electric-Sandia derived re-entry design conditions by NASA Ames.

The adaptation of a beryllium secondary heat shield changed the concept from "thermal switch" to "heat sink" where the high thermal capacitance of the beryllium plus its high thermal conductivity provided the system with the same effective performance characteristics as the original design plus greater structural and re-entry margins.

2.4.5 FUEL CAPSULE

The major change from the initial fuel capsule reference design to that of the intermediate fuel capsule design was the increase from 1400 thermal watts in a single capsule to 1500 thermal watts in a dual capsule. As a result of simulated fuel capsule impact tests, it was determined that the initial reference single capsule design possessed only a slight design margin and that an increase to 1500 watts would possibly eliminate this safety margin. For this reason, the more promising dual capsule was designed to provide greater impact resistance. The fuel was now divided into two separate compartments. Breakage on impact would therefore occur at the midpoint leaving the two capsules intact.

Another advantage of this dual design concept was that this provided design flexibility in fuel location for system thermal matching by means of minor internal changes. Also, the smaller capsules were easier to handle and machine. The change from the intermediate capsule design to the final version consisted in removing the spoiler from the forward end of the capsule, since it proved detrimental to capsule impact survival, and capsule drop tests showed no measurable aerodynamic advantage. The fuel liner was modified by adding a vent and a burst disc assembly at the midsection to be consistent with the desired pressure release. The burst disc is to allow decontamination of the fuel liner assembly after fueling, and is designed to rupture after the fuel liner assembly is safety encased in the cladding. The filter was added to permit venting of the liner while preventing the passage of fuel particles.

2.4.6 10-COUPLE MODULE TESTS

The SNAP-27 program was supported by a comprehensive thermoelectric test program utilizing nineteen 10-couple modules operating at design and off-design conditions. This program was carried out to provided back-up information for the SNAP-27 generator's initial design point which was chosen on a "best estimate" basis, using the relatively incomplete data available at the time. Table 2-4 summarizes the 10-couple module test series. As of June 30, 1969, all modules except three were still on test and had accumulated a total of 3.7×10^6 couple hours without any couple failure.

2.4.7 104-COUPLE MODULE TESTS

The 104-couple module test program extended the objectives of the 10-couple program to provide an experimental basis for predicting generator performance. The module itself was designed and fabricated in a manner identical to a SNAP-27 generator, except that it was highly instrumented and shorter (4 versus 17 rows of couples axially). Use of identical materials, parts, and processes provided the 104-couple modules with the same susceptibilities that the actual generator would have and removed the idealism of the 10-couple module design. Table 2-5 summarizes the 104-couple module testing. As of June 30, 1969, a total of 18.36×10^6 couple hours have been accumulated without any couple failure.

2.4.8 THERMOELECTRIC LEG PRODUCT SPECIFICATION (TELPS) PROGRAM

An extremely comprehensive program was conducted for General Electric by the 3M Company on N-type PbTe and P-type PbSnTe SNAP-27 thermoelectric legs. Included in the end results of the program were:

a. Product specifications for the above mentioned SNAP-27 legs

b. Development of an ingradient test fixture and procedure for making accurate and quick measurements of leg characteristics under various temperature-time conditions

c. Computerized techniques for data reduction through plotting.

2.4.9 NUCLEAR SAFETY

An in-depth SNAP-27 nuclear safety program was carried out (with the assistance of Sandia Corporation, Mound Laboratory, NRDL and NASA-Ames) which covered the design of the system (FCA and GLFC), the assessing of the response of the FCA and GLFC to the full spectrum of possible and remote accidents, the performance of safety tests to verify design

TABLE 2-4. 10-COUPLE MODULE SUMMARY

MODULE	TEST DESCRIPTION	HOT JUNC TEMP-T_H (°F)	COLD JUNC TEMP-T_C (°F)	GAS PRES. P_G (PSIA)	SPRING PRES. P_S (PSI)	TOTAL TIME ON TEST AT 9/5/69
B1	Short Term Stability	1100	525	25	150	Terminated at 2206 hr.
B2	Short Term Stability	1100	525	25	150	28,584 hr.
C3	Short Term Stability	1100	525	25	150	Terminated at 1832 hr.
C4	Short Term Stability	1100	525	25	150	28,259 hr.
C5	Off Design Hot Junction	1130	525	25	150	26,478 hr.
C6	Off Design Hot Junction	1130	525	25	150	26,395 hr.
C7	Off Design Hot Junction	1050	525	25	150	25,901 hr.
C8	Off Design Hot Junction	1050	525	25	150	25,684 hr.
C9	Off Design Hot Junction	1200	525	25	150	26,363 hr
C10	Off Design Hot Junction	1200	525	25	150	Terminated at 23,997 hr (7/19/69)
C11	Lower Gas Pressure	1100	525	25	150	24,397 hr
C12	Lower Gas Pressure	1100	525	2.5 *	150	Terminated at ~6000 hr.
C13	Lunar Cycle	1100/ 1050	525/ 460	25	150	14,767 hr - terminated 9/12/68 after 36 cycles
C14	Increased Spring Pressure	1100	525	25	250	22,413 hr
C15	Increased Spring Pressure	1100	525	25	250	23,099 hr
C16	Lower Gas Pressure	1100	525	7 **	150	17,785 hr
C17	Lunar Cycle	1100/ 1050	525/ 460	25	150	23,197 hr-cycling terminated 4/19/67 after 29 cycles
C18	Off Design Cold Junction	1100	575	25	150	23,363 hr
C19	Off Design Cold Junction	1100	625	25	150	22,868 hr

* Module was originally set at 5.5 psia; outgassing of the insulation increased pressure to 2.5 psia

** Module was originally set at 5.5 psia; outgassing of the insulation increased pressure to 7.0 psia

TABLE 2-5. 104-COUPLE MODULE SUMMARY

MODULE	TEST DESCRIPTION	HOT JUNC TEMP-T_H (°F)	COLD JUNC TEMP-T_C (°F)	TOTAL TIME ON TEST AT 9/5/69
104-81	Off design hot junction	1030	525	7,810 hr
104-82	Efficiency testing with 4-zone heater	1070	525	19,227 hr
104-83	In storage - test start postponed			
104-84	In storage - test start postponed			
104-85	In storage - test start postponed			
104-86	Shock and Vibration	1100	525	Terminated 8/4/67 at 2,413 hr
104-87	On-off cycle performance - Cycling terminated after 17 cycles	1100	525	Terminated 10/19/67 at 5,839 hr.
104-88	Lunar cycle performance - Cycling terminated after 20 cycles	1100/ 1045	525/ 460	Terminated 5/8'68 at 9,451 hr
104-89	Long term stability with Xenon gas	1100	525	21,890 hr
104-810	Efficiency	1100	525	22,229 hr
104-811	Off design hot junction	1130	525	20,757 hr
104-812	Long term stability	1100	525	21,512 hr
104-813	On-off cycle performance - Cycling terminated after 10 cycles, T_H reduced after 2700 hr to 1050°F.	1100	525	21,585 hr
104-814	Reduced hot junction	1050	525	21,318 hr
104-815	Reduced hot junction, spring pressure 250 psi	1050	525	18,859 hr

margins and/or to substantiate the analytical assessment, and the preparation of thorough documentation summarizing the total safety effort.

Sandia provided technical assistance in the definition of significant abort environments such as explosion yields, fireball characteristics and fragmentation distribution typical of an explosion of the Saturn V. Additionally, key testing utilized the special Sandia facilities. Mound Laboratory conducted tests assessing the behaviour of fuel in contact with various materials and media under conditions resulting from potential accidents.

Significant results of the safety program that highlight the margins of the system were:

a. Impact - Containment of fuel at terminal velocity impacts was demonstrated for situations involving a free heat source or a heat source contained in a GLFC.

b. Re-entry - The GLFC and FCA were evaluated for the full range of possible Saturn aborts as influenced by the LM descent stage. Mission analysis indicates that the abort spectrum could be:

1. Earth Orbital - Decay with velocity of 25,567 fps.

2. Superorbital - Velocity 36,333 fps with re-entry angles from 5.5° to 90°DFH.

The GLFC was designed as an omnidirectional re-entry body and its ability to perform as such with sufficient margins to contain fuel had to be verified. Critical re-entry configurations were identified for each abort regime and complete aero thermal and structural analyses were performed.

The results of the analytical program showed integrity of the SNAP-27 system with positive margins existing for the worst case of graphite loadings. Arc tunnel tests at the NASA-Ames facility substantiated that the Pyrocarb-406 was insensitive to local heating caused by protuberances such as trunnions, bands, etc., and that predicted ablation values were realistic.

c. Fragmentation - Tests were run at Sandia's Rocket Sled facility to evaluate the GLFC capability to resist fragmentation impact resulting from a possible S-IVB explosion. Test regimes considered fragmentation impacts edge-on and flat-on for velocities up to 3000 fps.

2.4.10 GENERATOR DEVELOPMENT AND QUALIFICATION TESTS

As originally planned the generator test program at General Electric was based on four functioning engineering units and two qualification units, as follows:

Model Number	Usage
5	Shock and Vibration Test Engineering Model
6	Life Test Engineering Model
7	Performance Test Engineering Model
8B	Simulated Mission Test Engineering Model
10	Load and Environmental Qualification Model
13	Performance and Life Qualification Model (fueled)

The scope of the generator test program was subsequently reduced as a result of funding limitations. Models 6 and 7 were dropped from the program and Mod 13 replaced the damaged Mod 21 generator as a back-up to the flight units.

The three generators, Mods 5, 8B and 10, were subjected to a series of performance, environmental and operational life tests under simulated mission conditions to validate the basic generator design and fabrication techniques as well as to accumulate long life experimental data. Testing was terminated by AEC direction on July 11, 1968, July 9, 1968 and July 15, 1968 on Mod 5, Mod 8B and Mod 10, respectively.

The generators accumulated 28,203 hours with Mod 5 accumulating over 12,000 hours. Thermal sink conditions for all generators were cycled every two weeks to simulate maximum temperatures for lunar day and lunar night operation. A performance summary is given in Table 2-6. Note that Mod 5 was reduced to a power input of 1485 watts after 10,000 hours to simulate a fuel decay.

The normalized power output for the three generators is given in Figures 2-4, 2-5 and 2-6. A theoretical prediction of BOL and EOL power versus heat input (as predicted in May, 1967 and reported in the subsequent SNAP-27 Quarterly) is shown in Figure 2-7. Figures 2-8 and 2-9 show corresponding current-voltage maps for theoretical and actual performance of generator Mod 5 and generator Mod 10.

TABLE 2-6. GENERATOR TEST PERFORMANCE SUMMARY

GENERATOR	TOTAL ACCUM. TEST TIME	POWER OUTPUT BOL		HEAT INPUT WATTS	POWER OUTPUT EOL	
		LUNAR DAY	LUNAR NIGHT		LUNAR DAY	LUNAR NIGHT
Mod 5	12,165	70.8	73.0	1500 after 10,000 hr reduced to 1485 watts	66.6	68.7
Mod 8B	8,341	*65.0	66.0	*1415	62.0	62.9
Mod 10	7,771	71.2	73.3	1505	71.5	73.1

Total accumulated couple hours = 12,465,726 hours

Total energy produced since start of test - 1,842,675 watt-hours

* Mod 8B operating at reduced Q to simulate low-end tolerance on fuel capsule.

2.4.11 FLIGHT GENERATOR ACCEPTANCE TESTS

The performance characteristics of each of the five flight units are summarized in Table 2-7. Each generator has its performance characteristics determined for a possible variation in heat source thermal loading (1415 to 1505 watts) and the maximum temperature extremes representative of lunar day and lunar night. Each generator is tested not less than 500 hours, of which at least 200 hours are in a thermal-vacuum environment. Note the consistency in performance and weight. Since each heat source is very close to 1480 watts, power for the ALSEP mission will be approximately 67 watts.

2.4.12 KENNEDY SPACE CENTER PRELAUNCH SUPPORT

In support of the planning, preparation and execution of the various activities required to successfully carry out the checkout of the SNAP-27 flight systems, as well as accomplishment of the actual on-board prelaunch loading of the capsules, General Electric was requested by the AEC to provide special handling and loading tools for the fuel capsule, necessary procedures for all activities in the field and personnel trained to perform the loading. Due to the uncertainties

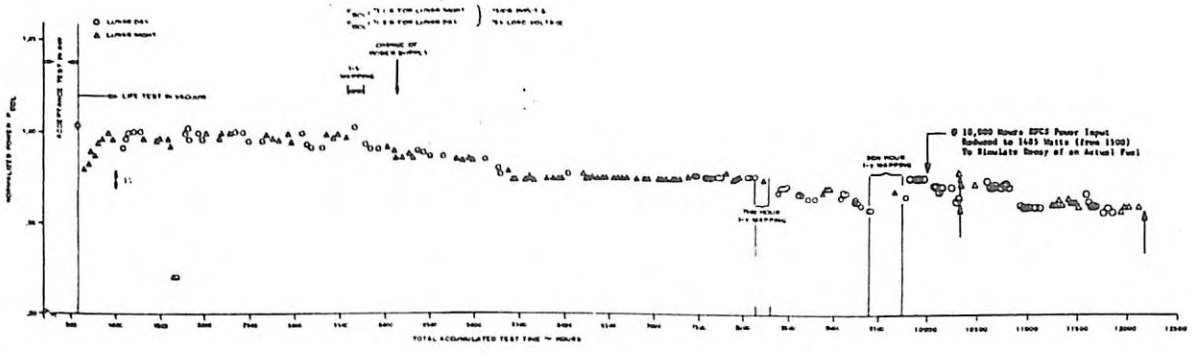

Figure 2-4. Mod 5 Life Test Data

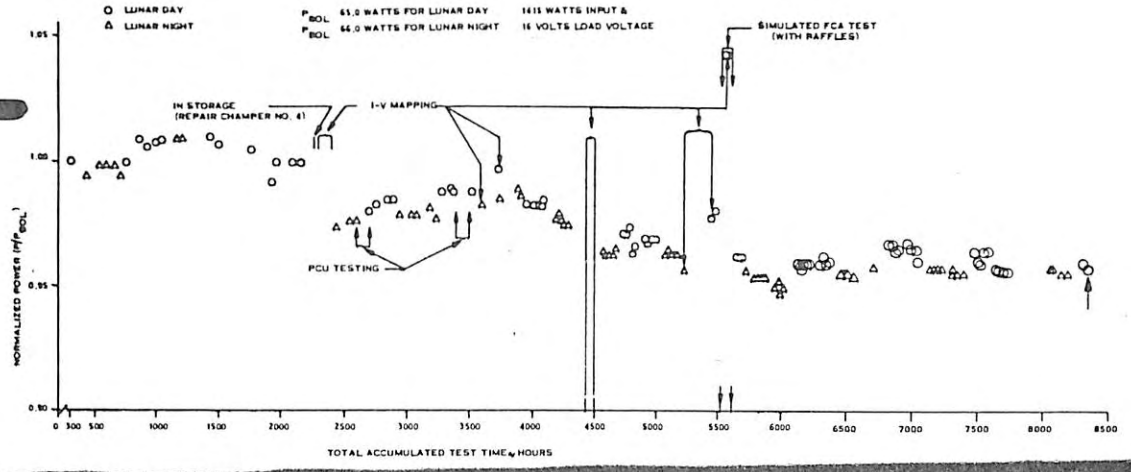

BLANK PAGE

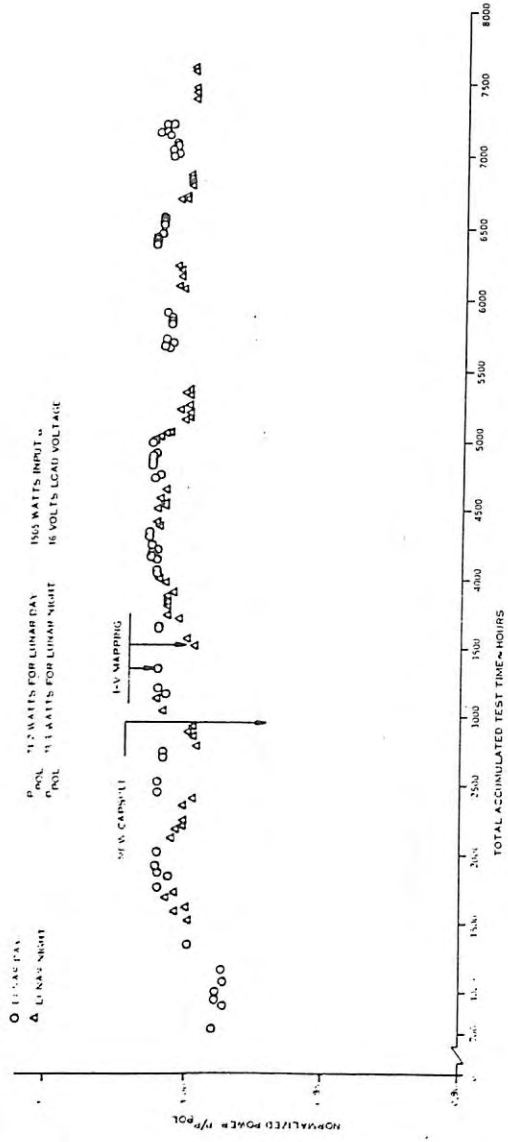

Figure 2-5. Mod 8B Life Test Data

Figure 2-6. Mod 10 Life Test Data

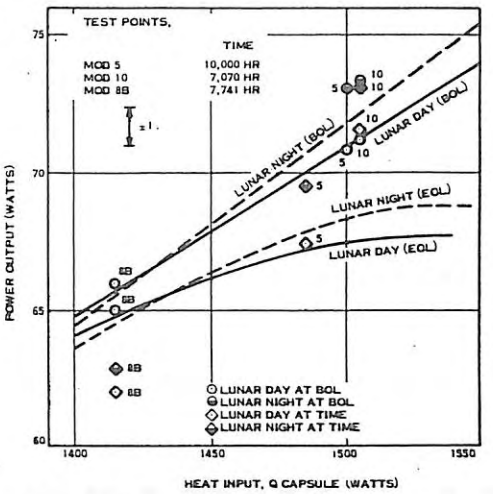

Figure 2-7. Comparison of Predicted and Actual SNAP-27 Performance

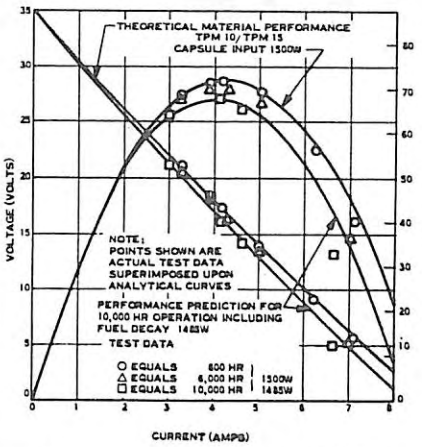

Figure 2-8. Generator Mod 5 Theoretical versus Actual Performance

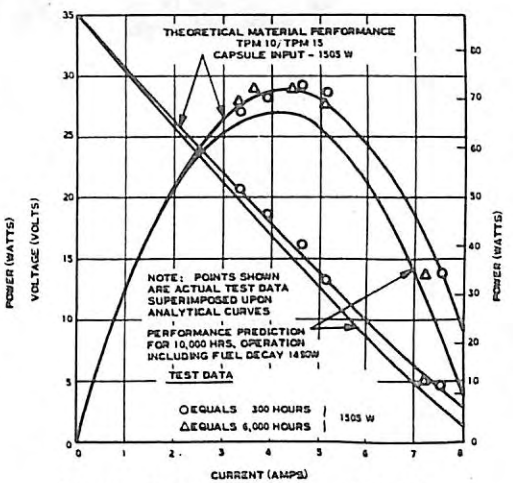

Figure 2-9. Generator Mod 10 Theoretical versus Actual Performance

TABLE 2-7. TEST SUMMARY FOR THE SNAP-27 FLIGHT GENERATOR ASSEMBLIES

OPERATING CONDITIONS			MOD 13 GA S/N 6320006	MOD 19 GA S/N 6320009	MOD 21 GA S/N 6320011	MOD 22 GA S/N 6320012	MOD 23 GA S/N 6320013
POWER INPUT	EQV. LOAD	SINK TEMP. (^{o}F)					
1505W	16 V	+170^{o}F	69.8W	69.1W	68.2W	68.3W	70.7W
1455W	16 V	+170^{o}F	67.1W	67.5W	66.0W	66.2W	67.9W
1415W	16 V	+170^{o}F	64.3W	64.7W	63.2W	63.2W	65.0W
1505W	16 V	-280^{o}F	72.5W	72.9W	71.3W	71.3W	72.9W
1455W	16 V	-280^{o}F	68.8W	68.8W	66.7W	67.3W	68.9W
1415W	16 V	-280^{o}F	65.3W	65.3W	64.0W	64.1W	65.1W
1450W	4.7 OHMS	AMBIENT	69.6W	69.7W	67.9W	69.1W	70.2W
TOTAL ACCUMULATED OPERATIONAL TIME (AIR & VACUUM) (HOURS)			550	593	581	640	571
OPERATIONAL TIME IN A VACUUM			240	264	256	303	233
FINAL GA LEAK RATE IN STD CC/SEC OF ARGON WHILE OPERATING IN A +170^{o}F SINK AT 4.7 OHMS LOAD			2.50×10^{-6}	4.36×10^{-7}	1.09×10^{-6}	3.7×10^{-7}	LESS THAN 3.92×10^{-7}
STORAGE CONTAINER SERIAL NO.			6287007	6287004	6287006	6287005	6287003
TOTAL WEIGHT ~ POUNDS, (LESS PROTECTIVE CABLE SLEEVING).			27.83	27.77	27.96	27.86	27.80

associated with launch scheduling, as well as the time span involved covering all the launches, the KSC support program was subsequently terminated and the capsule loading responsibility transferred to the Sandia Corporation. All required capsule tools and equipment were designed and provided, as well as the necessary field procedures.

3. SNAP-27 FLIGHT SYSTEM

3.1 GENERATOR ASSEMBLY

The generator assembly consists basically of a thermopile, a hermetically sealed structure to house the thermopile, a heat rejection system, internal wiring, an external power cable with connector, and six platinum Resistance Temperature Detectors (RTD's). In the unheated state (no fuel capsule), the generator is an inert device which produces no electric power. When mated with a nuclear fueled capsule, the assembly becomes a dc power producer. It is then referred to as either a Radioisotopic Thermoelectric Generator (RTG), or an Integrated Power Unit (IPU). For test purposes, an electrically heated fuel capsule is employed as the thermal source.

3.1.1 DESIGN

The SNAP-27 generator assembly with fuel capsule installed is shown in Figure 3-1. Note that the heat source is not permanently assembled into the generator and can be removed or inserted as required by ground

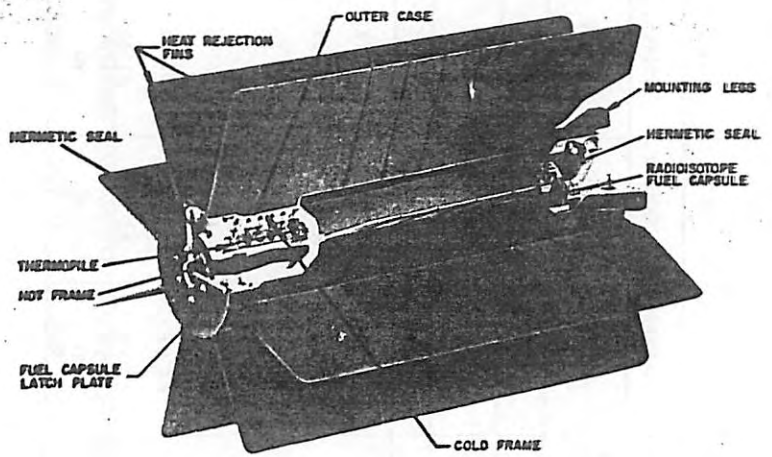

Figure 3-1. Isometric Cutaway of an Integrated Power Unit Showing Thermopile and Fuel Capsule Assembly.

BLANK PAGE

operational considerations. Heat from the nominal 1480 watt fueled $^{238}PuO_2$ capsule is transmitted to the generator hot frame via radiation coupling. Both surfaces are coated with a high emissive radifrax coating, with the heat source having a minimum emissivity of 0.85 and the hot frame 0.80. Corresponding temperatures during operations are 1350°F for the capsule and 1125°F for the hot frame.

Heat received by the hot frame is transmitted to the thermoelectric couple hot side by passing through a boron nitride electrical insulator, an iron plated copper electrode, and finally a 1010 carbon steel hot button. Total temperature drop through these three components is 25 to 45°F, which establishes the SNAP-27's hot junction temperature at 1080 to 1100°F. Heat flow (~1250 watts) through the system's 442 couples is such that the cold side thermoelectric temperature is maintained at 525°F in the normal operating temperature. Heat loss due to leakage between the couples is kept to an absolute minimum due to the very high density packing of powdered Min-K insulation having a thermal conductivity of 0.04 Btu/ft^2-hour. The heat, after passing through the couples, is transferred into beryllium oxide followers which interface directly on the cold copper cap. The heat then flows into a massive beryllium cold frame which serves to "smear" out any possible temperature maldistribution and which in turn reflects inconsistent temperature characteristics of the couple. A block diagram depicting the thermal coupling techniques is shown in Figure 3-2.

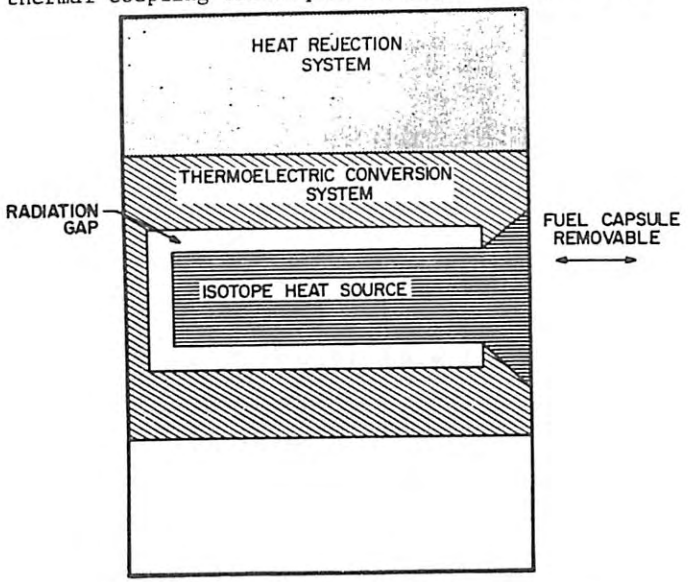

Figure 3-2. Thermal Coupling Techniques

The interface between the cold frame and the outer case is maintained by a shrink fit with an interference up to 0.002 inch. The outer case is the prime structural member of the generator. It is a hot-pressed block beryllium structure with a 0.060 inch thick cylindrical wall with eight cross-rolled sheet beryllium fins integrally attached by silver braze and two transistion rings of 19-9 DL stainless steel, which are likewise brazed. The transistion rings provide the interface for attachment of both IN-102 end seals, which are welded at final assembly to establish and maintain the hermetic seal. Stainless steel (19-9 DL) was selected based on its thermal coefficient compatibility with beryllium. Hermetic seals are used between the hot frame and the outer case at the aft end to maintain an argon plus 1 percent helium atmosphere of 25 psia (operational) around the thermoelectric elements.

The internal wiring is designed to interconnect the thermopile rows so that two series-parallel strings of thermocouples are formed. Careful selection of materials and the use of forward and aft degaussing loops reduce the current-induced magnetic field intensity around the generator to less than one gamma at three meters.

The SNAP-27 couple design and arrangements are worthy of mention. The material selected was the 3M Company's well-developed and proven 3N, 3P lead telluride used extensively in their commercial convertors and in the AEC programs, such as SNAP-17, SNAP-21 and SNAP-23. Each leg forming the couple (one N and one P) is integrally assembled such that the hot side interface is bare and the cold side is soldered to spherical copper caps. Between the caps and the actual leg material are a cold electrode and a stainless steel barrier disc to prevent migration of the leg materials into the copper. Two series strings of 221 couples, each connected in parallel and each couple electrically laddered to prevent string loss (given a couple open failure), comprise the electrical arrangement. Normal operating voltage of the thermopile lies between 14 and 16 volts dc. Each leg is preloaded into its hot button by individual springs sized and shimmed to establish a leg bearing pressure of 150 psi. This preload is the chief degradation mechanism arrestor of the SNAP-27 thermopile. The basic design of a thermoelectric couple is shown in Figure 3-3, which depicts the relationship of the components as well as the flow of the positive and negative charges in their respective directions.

Figure 3-4 is a functional block diagram of the generator.

Detailed descriptions of the generator's components are discussed in Section 5.

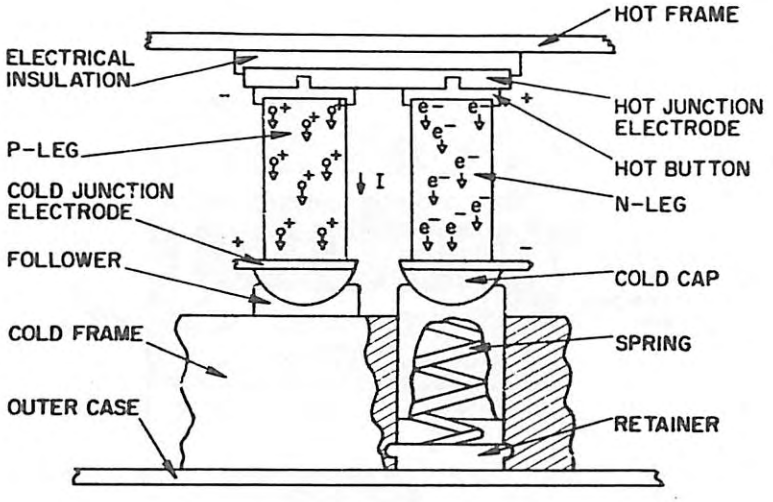

Figure 3-3. Thermoelectric Couple Operation

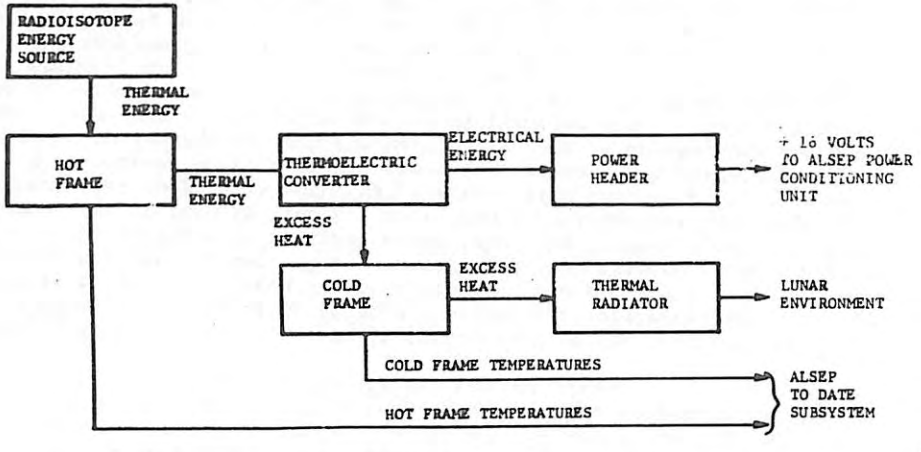

Figure 3-4. SNAP-27 Functional Block Diagram

3.1.2 THEORY OF OPERATION

Electrically, the generator is similar to a dc voltage source with an internal resistance; the source being the electromotive force developed by the thermoelements (Seebeck voltage) and the resistance being that of the thermoelements and all interface resistance of the thermopile. Since both the Seebeck voltage and the resistance of the thermoelements are temperature dependent, the electrical characteristic of the generator becomes a function of the thermal operating conditions, i.e., the hot and cold junction temperatures of the thermoelectric elements.

The heat supplied by the fuel capsule to the thermoelectric elements at any one time is practically constant and only varies over longer time periods according to the decay of the isotope. This, however, does not mean that the temperature conditions of the RTG are constant since there are various heat transport and absorption phenomenon which are current dependent and thus are a function of the electrical load condition. Under normal operating conditions (maximum power), these phenomena account for about 25 percent of the total heat flow and are, for purposes of approximation, directly proportional to the current flow. This means, that since the heat flow is constant, the temperature difference across the thermoelement will increase with decreasing current flow and vice versa. Since the cold junction temperature is nearly constant, due to the radiator and the heat rejection system (the heat supplied by the isotope is constant), the hot junction temperature will increase with decreasing current flow. (Erratic load removal can therefore cause serious temperature damage to the thermoelectric elements.) Typical performance characteristics of a SNAP-27 generator assembly are illustrated in Figure 3-5. Power-current and voltage-current characteristics are shown for steady state operation at a total heat input from the isotope of 1505 watts and sink temperature of 170°F (consistent with a lunar day operating condition near the equator). Also shown on this figure is hot junction temperature versus current. The cold junction temperature stays practically constant (533°F) and only increases about 10°F at the open and short circuit condition where the electrical power normally removed as energy has to be additionally dissipated by the radiators. For currents below 3.5 amperes, the hot junction temperature will exceed 1100°F, a condition which would cause appreciable degradation of the thermoelectric elements if it prevailed. The range below 3.5 amperes is therefore considered undesirable for long term operating conditions.

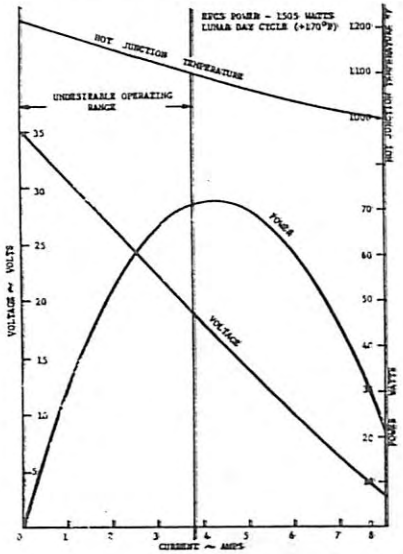

Figure 3-5. Typical Characteristics of SNAP-27 Generator Assembly

3.2 FUEL CAPSULE ASSEMBLY

The SNAP-27 fuel capsule assembly, shown in Figure 3-6, is comprised of three basic subassemblies plus interconnecting hardware. These are:

a. Haynes-25 Backplate Assembly - Bolts to the fueled capsule and contains provisions for handling the capsule in the ground operational flow by use of proper mating auxiliary support equipment; securing the heat source in the generator assembly for astronaut handling; securing the heat source in the GLFC during the environments and mission profile of the earth to lunar transit and, finally, secures the capsule in any of earth storage or support equipment.

b. Fuel Annulus Ring(s) - Two Haynes fuel annulus rings for supporting the fuel plus the fuel topping agent.

c. Haynes Outer Clad/Filtration System - Provides structural capability to the system and allows the filter system to permit helium generated by the PuO_2 to pass from each annulus ring to the outer clad center section.

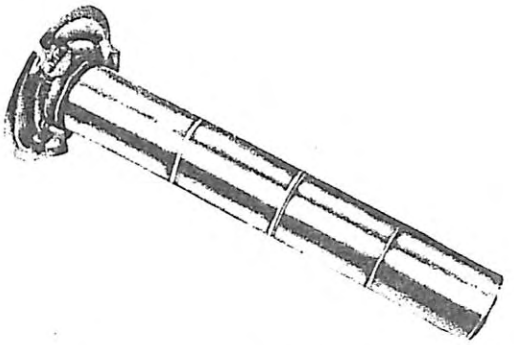

Figure 3-6. SNAP-27 Fuel Capsule Assembly

Each annulus ring assembly is approximately 7.7 inches long, fabricated from 0.020-inch Haynes 25 sheet. The annulus volume is sized to contain ~ 740 watts $^{238}PuO_2$ microspheres at time of loading. After fuel is inserted, the annulus is welded tight with a thin Haynes end cap containing a burst disc. Each welded annulus is then inserted into the 0.060-inch thick outer clad, and the dome and flange ends are welded to ensure a hermetically sealed unit. The large volume in the center of the outer clad contains the two helium gas filters. At some predetermined time (weeks after fueling), the annulus burst discs rupture and the helium gas is allowed to migrate to the center cavity. The migration occurs without the transport of any particulate material. As the capsule ages, this pressure continues to increase; critical point is reached after approximately five years where the loading will be sufficient to rupture the center section at the plane of separation. This rupture is in the form of a hairline crack. The fuel enclosed halves will continue to build up helium and allow the gas migration without release of fuel. All stresses on the clad and liner will have been eliminated.

The capsule as fabricated is 16.5 inches long and 2.5 inches in diameter and weighs slightly less than 15 pounds, including the backplate. After fabrication, iron titanate coating with demonstrated long-term emissivities of greater than 0.85 is applied by a plasma torch. The capsule has successfully passed the ALSEP/Saturn V qualification environments and is designed to perform on the lunar surface for the ALSEP mission.

Capsule operating temperatures are as follows:

a. Ground storage ~ 500°F

b. Steady state (air) ~ 900°F

c. In graphite cask ~ 1400°F

d. In generator ~ 1350°F

Additional capsule design details are covered in Section 6.

3.3 GRAPHITE LM FUEL CASK

The Graphite LM Fuel Cask (GLFC), shown in Figure 3-7, supports the fuel capsule assembly during the operational mission from launch to lunar surface deployment and, in the event of a credible abort of the spacecraft, provides re-entry protection and containment for the fuel until it impacts on the earth. The GLFC is mounted to the outside of the LM descent stage by an ALSEP support structure, Figure 3-8.

The GLFC is not only configured to support the fuel capsule assembly through the lunar surface landing, but also to permit the astronaut to readily remove the fuel capsule assembly for insertion into the generator assembly. The external shape, as well as most of the design details including the selection of materials and coatings and inclusion of special hardware such as the secondary thermal shield, are governed by re-entry considerations and the requirements that the fuel will be contained in a credible abort.

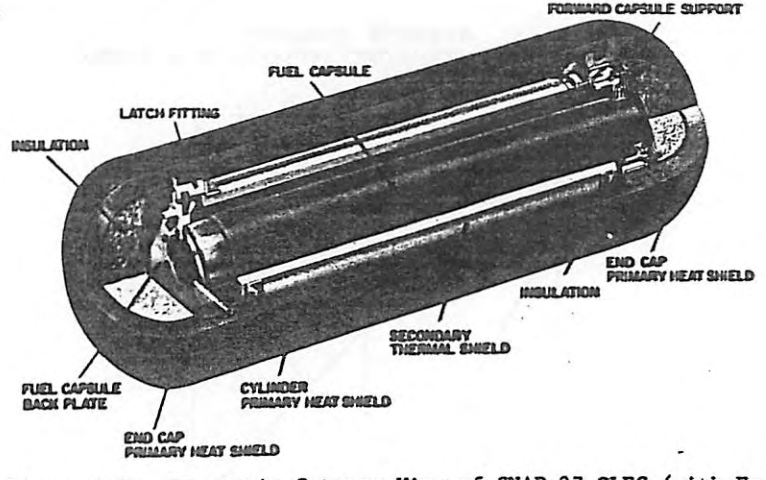

Figure 3-7. Isometric Cutaway View of SNAP-27 GLFC (with Fuel Capsule)

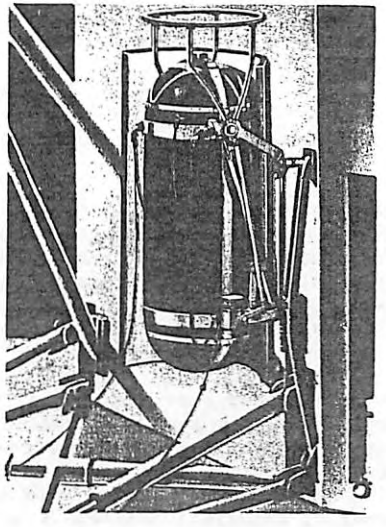

Figure 3-8. GLFC and Support Structure

Basically, the GLFC is a cylindrical container 23-inches long by 8-inches in diameter consisting of a primary heat shield, secondary thermal shield and fuel capsule support structure. The primary heat shield which forms the external shell of the GLFC consists of a cylinder and two nominally hemispherical end caps. The graphitic material used in the primary heat shield is Hitco Pyrocarb-406, formed by infiltrating a pyrolized square weave graphite composite with pyrolitic graphite. The primary heat shield protects the fuel capsule during reentry by heat sink, re-radiation, and ablation methods. The heat rejected by the fuel capsule in normal vacuum operational conditions is transmitted through the secondary heat shield and absorbed by the primary heat shield where it is both re-radiated to external environment and conducted to the GLFC support structure.

The end caps are attached to the cylinder by a single-spline breech type joint to facilitate end cap installation and removal. Once installed, the end caps are locked to the cylinder by means of a tantalum-ceramic spline which is inserted into a hole formed by matching grooves in the cylinder and end cap at their interface. A tantalum pin is attached to a tantalum wire strung with aluminum oxide beads which extend further into the curved length of the hole. Upon installation, the

wire deforms and takes a permanent set which prevents the tantalum pin from vibrating loose during launch or re-entry.

3.4 FLIGHT HANDLING TOOL

The flight handling tool, Figure 3-9, when mated with an ALSEP supplied handle will be used by the astronaut on the lunar surface to remove the fuel capsule assembly from the LM-mounted GLFC for insertion into the generator assembly. It is carried to the lunar surface mounted on the same ALSEP pallet as the generator assembly.

The tool is similar in design to the jaw mechanism of the ground handling tool, discussed in Section 13, differing in reduction of the cross section of the sliding jaws to reduce weight and in the addition of gold plating to the surface of the flat disc which views the capsule backplate. The tool is constructed of titanium and weighs approximately 0.6 pounds (less ALSEP handle) on earth. The grooved spiral plate contains a low emissive coating on the face which comes closest to the fuel capsule backplate to minimize the heat radiated to the flight handl- tool in a vacuum environment. A separate handle, which includes a locking device to lock the flight handling tool in the engaged position to ensure attachment to the fuel capsule during astronaut handling, is provided by the ALSEP contractor for integration with the tool.

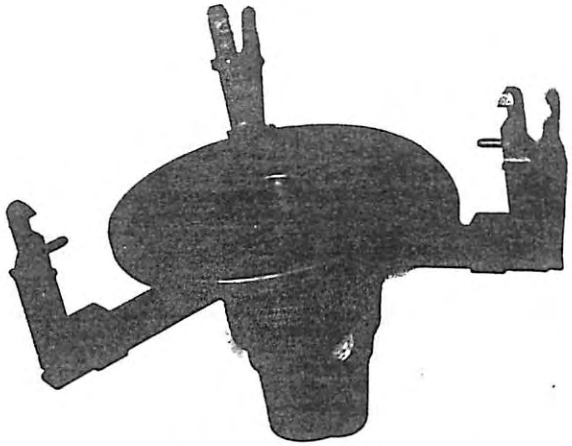

Figure 3-9. Flight Handling Tool

After the flight handling tool is inserted into the fuel capsule backplate, twisting of the handle translates the latch fingers of the movable jaw assembly into an opening/closing motion. A locking device on the handle locks the flight handling tool in the engaged position during handling operations.

Performance characteristics are as follows:

a. Engagement force - less than ten pounds (earth)

b. Torque required to lock and unlock the tool from the fuel capsule - less than ten inch-pounds

c. Number of complete turns (360 degrees) of flight handling tool between full unlocked position to full lock position - $2 \pm 1/4$ turns

d. Temperature of the threaded interface where attached to the ALSEP supplied handle - will not exceed 300°F after the flight handling tool has been supporting a fuel capsule for 15 minutes in vacuum

e. The flight handling tool can support a load of at least 30 pounds, the center of gravity of which is applied at 7.80 inches from the latch mechanism jaw on an axial axis. Application of load may be in either vertical or horizontal directions.

4. SNAP-27/ALSEP INTERFACES

4.1 SPECIFICATIONS AND DRAWINGS

The requirements relating to the various interfaces between the SNAP-27 and ALSEP Systems, such as electrical, mechanical, thermal, magnetic and nuclear radiation are defined in the following specifications and drawings:

ORIGINATOR	TITLE	IDENTIFICATION
Bendix Aerospace	Interface Control Specification for Electrical Power Subsystem (SNAP-27 Integrated Power Unit System)	IC 314119
Bendix Aerospace	Interface Control Specification for Graphite LM Fuel Cask (SNAP-27 Integrated Power Unit System)	IC 314121
Bendix Aerospace	GLFC Interface	Dwg. ICD2334552
General Electric	GE/Bendix GLFC Interface (Ref. only)	Dwg. 47D301139
General Electric	IPU Interface	Dwg. 47C300112
General Electric	Fuel Capsule Assembly Interface	Dwg. 47D300186
General Electric	Flight Handling Tool Interface	Dwg. 47D300644

4.2 MECHANICAL INTERFACES

4.2.1 GENERATOR

Throughout the mission (launch, translunar flight and lunar operation), the generator is permanently attached to the pallet of ALSEP Subpackage No. 2 by means of eight bolts which pass through the eight generator mounting feet and engage threaded inserts anchored in the pallet.

ALSEP envelope requirements specified for the generator to ensure compatibility with the pallet and the Lunar Module (LM) stowage compartment are given as 18.12 inches absolute height by 17.2 inches

BLANK PAGE

diameter (circle drawn through the fin tips). Actual measurements for the generator are 18.12 inches high by 15.75 inches in diameter.

4.2.2 GRAPHITE LM FUEL CASK (GLFC)

During launch and translunar flight, the GLFC (with its fuel capsule cargo) is attached to the LM vehicle by means of an ALSEP-furnished support assembly (Bendix drawings 2337960 and 2338660). This structure supports the GLFC on the outside surface of the LM vehicle. It consists of:

a. Tension bands which contact the GLFC and provide attachment points

b. A truss to which the bands are attached and which transfer loads to the LM vehicle structure

c. Quick disconnect latches and tilt mechanism used to position the GLFC for capsule removal

d. Thermal shield which protects sensitive portions of the LM against direct thermal radiation from the hot GLFC.

The structural support concept involves positive constraint through all axes using flexible metallic bands designed to apply positive pressure against the cask throughout the entire mission.

The maximum allowable tensions in the support assembly bands which hold the GLFC are specified at 70 $\pm$ 30°F as follows:

Upper circumferential bands	900 pounds
Axial bands	900 pounds
Lower circumferential bands	775 pounds

A requirement exists that the force which the astronaut must exert to extract the GLFC end dome locking spline should not exceed a pull of 20 pounds. Also, the torque required to rotate the end dome is not to exceed 80 inch-pounds. During test on flight units, all values were experimentally determined as below one pound to remove the spline lock and as a maximum of 25 inch-pounds for rotating the dome.

On the lunar surface, an ALSEP Dome Removal Tool is used to remove the GLFC dome.

For extraction of the fuel capsule from the GLFC cavity and for

insertion into the generator on the lunar surface, a Fuel Transfer Assembly Tool is used which is comprised of the SNAP-27 Flight Handling Tool, an ALSEP-supplied handle and a Tie Down Release Tool. The Flight Handling Tool (FHT) supplied by General Electric becomes a part of the ALSEP Fuel Transfer Assembly Tool (FTAT).

The support structure and tools are described in detail in Section 15.

4.3 ELECTRICAL INTERFACE

The electrical interface between an operating generator and the ALSEP central station has been established at the connector assembly which terminates the generator cable (General Electric Drawing 47D300951G1 or Bendix Drawing 2331952). The connector is provided by Bendix and is physically joined to the cable at General Electric. A schematic identifying the electrical connections between the cable and connection is shown in Figure 4-1.

The dc power output of the generator on the lunar surface when mated to the power conditioning unit of the ALSEP central station is required to be at least 63.5 watts at 16 volts nominal, continuously for a full year under both lunar day and night conditions. This capability was amply demonstrated during generator tests.

The six platinum resistance thermometers mounted to the generator for determining generator operating temperatures are connected to the ALSEP central station via conductors present in the generator cable. These leads are also shown in the cable schematic, Figure 4-1.

A block diagram demonstrating the functional relationship of the SNAP-27 RTG to the ALSEP electrical power system is shown in Figure 4-2.

4.4 THERMAL INTERFACES

The generator interface specification requires that the supporting baseplate (ALSEP Subpackage No. 2 pallet) shall allow a conducted heat flow of 20 to 80 watts into the baseplate through the generator mounting feet. It is also required that the top surface of this baseplate should have an emittance of at least 0.85 with the α / ϵ ratio a minimum.

Relative to the GLFC, a thermal requirement exists that the GLFC, when attached to the LM by the ALSEP support structure, shall not have an external surface temperature exceeding 835°F, nor a circumferential temperature gradient in excess of 150°F.

A thermal interface requirement also exists between the GLFC and Space

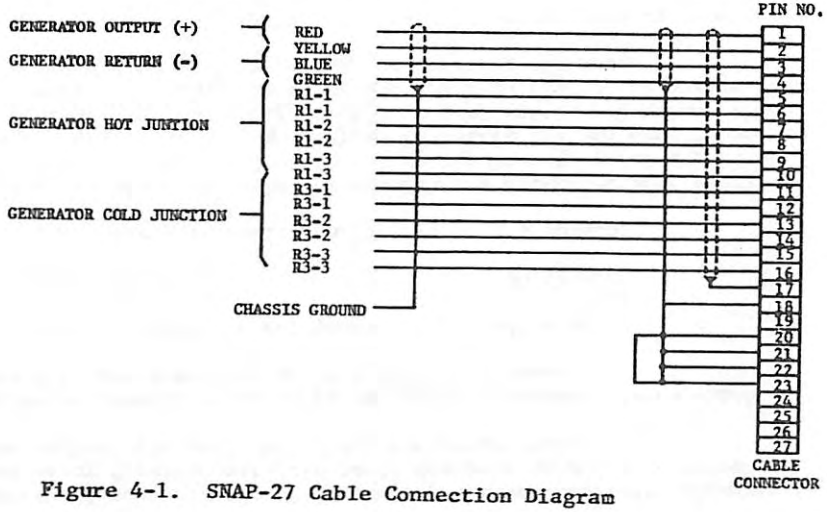

Figure 4-1. SNAP-27 Cable Connection Diagram

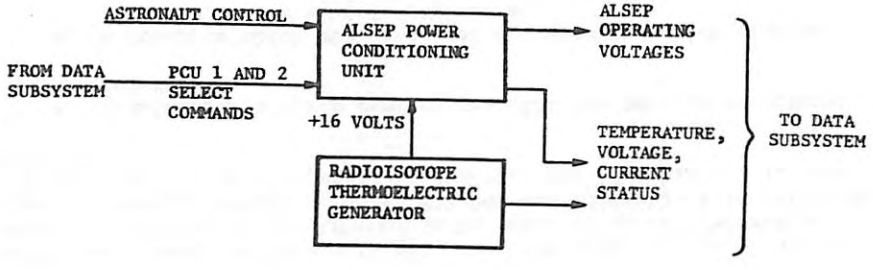

Figure 4-2. ALSEP Electrical Power Subsystem, Functional Block Diagram.

Vehicle which specifies that during on-pad operation, the GLFC shall be actively cooled to a maximum external surface temperature of 350°F and to a minimum average of 125°F. (This latter requirement has been imposed for safety purposes to preclude the possibility of inadvertent ignition of hypergolic fuels and vapors which might be present in the vicinity of the GLFC.)

4.5 MAGNETIC FIELD INTERFACE

The interface specification requirement is that the magnetic field at a distance of 50 feet from the operating generator on the lunar surface should not exceed 0.1 gamma. As can be seen by Figure 4-3, magnetic field tests conducted on Generator Mod 10, energized by a fuel capsule, indicated that this requirement was readily met.

4.6 NUCLEAR RADIATION

The interface specification requirement for nuclear radiation is that the tissue equivalent dose rate from the FCA should not exceed 70 millirem per hour at a distance of one meter in any direction. This number as a maximum was apparently based on early predicted radiation values for the capsule and is not rigid. Measured values for the flight capsule are given in Section 14.

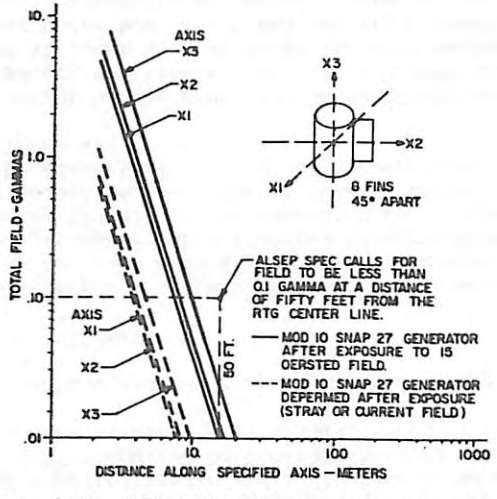

Figure 4-3. SNAP-27 Magnetic Field Measurements

5. GENERATOR ASSEMBLY DESIGN AND DEVELOPMENT

5.1 DESIGN REQUIREMENTS

The reference design of the generator assembly was based on the initial requirements shown in Table 5-1, established in 1965 by the Atomic Energy Commission.

TABLE 5-1. INITIAL GENERATOR DESIGN REQUIREMENTS

ELECTRICAL OUTPUT	56 watts end of two foot cable 56.2 watts - aft hermetic seal power interface
INSTRUMENTATION	Six sensors, for diagnostic monitoring
RELIABILITY	0.995 for 1 year lunar operation
DESIGN ENVIRONMENTS	Temperature -300°F to +250°F (equiv. sink -280°F to +170°F) Pressure 1 x 10^{-10} mmHg
STORAGE	Up to two years
MAGNETIC FIELD	1 γ @ 3 meters
WEIGHT	38.5 pounds with fuel capsule

These initial requirements were subsequently updated and expanded primarily as a result of the ALSEP interface. Final SNAP-27 RTG design and performance characteristics are shown in Table 5-2.

5.2 COMPONENT DESIGN

5.2.1 THERMOELECTRIC ELEMENTS

5.2.1.1 Thermoelectric Material Selection

Three factors were considered in the selection of the optimum N and P

BLANK PAGE

TABLE 5-2. SNAP-27 DESIGN AND PERFORMANCE CHARACTERISTICS

MISSION APPLICATION	POWER APOLLO LUNAR SURFACE EXPERIMENT PACKAGE (ALSEP)	
CONVERSION CONCEPT	Pu^{-238} FUELED THERMOELECTRIC SYSTEM USING LEAD-TELLURIDE ALLOY THERMOCOUPLES IN TWO SERIES PARALLEL STRINGS.	
DESIGN LIFE	ONE YEAR LUNAR OPERATION PRECEEDED BY TWO YEARS EARTH STORAGE.	
GENERATOR PERFORMANCE		
OUTPUT POWER		
SPECIFIED (WATTS)	65 (BOM)*	63.5 (EOM)* MIN.
MEASURED (WATTS)	73.3 (BOM)	68.5 (EOM)**
OUTPUT VOLTAGE (NOMINAL)		16 VOLTS DC
CURRENT (NOMINAL)		4 AMPS
OVER-ALL EFFICIENCY (NOMINAL)		4.75%
AVERAGE HOT JUNCTION TEMPERATURE		1075°F (580°C)
AVERAGE COLD JUNCTION TEMPERATURE		525°F (271°C)
FUEL CAPSULE THERMAL OUTPUT (NOMINAL)		1450 WATTS
MECHANICAL CHARACTERISTICS		
OVER-ALL DIAMETER OVER FINS		15.7 INCHES
OVER-ALL LENGTH		18.1 INCHES
NUMBER OF FINS		8
FIN RADIAL LENGTH		5.0 INCHES
FIN AXIAL LENGTH		18.0 INCHES
WEIGHT		
GENERATOR ASSEMBLY (INCLUDES CABLE, CONNECTOR, AND INSTRUMENTATION)		28.2 POUNDS
RADIOISOTOPE FUEL CAPSULE ASSEMBLY		14.5 POUNDS
FUELED GENERATOR		42.7 POUNDS

* BEGINNING (OR END)-OF-MISSION
** 1485 WATT THERMAL INPUT, 12, 113 HOURS

materials for the generator: (1) efficiency, (2) chemical stability/compatibility, and (3) mechanical compatibility. For materials having comparable efficiencies, the one exhibiting the greater Seebeck voltage is preferred since fewer couples are required to meet electrical power requirements. Fewer parts, less generator weight, fewer contacts, and lower extraneous resistance result from the use of higher voltage material. It was also desirable, from design and assembly considerations, to select a pair of N and P materials for which the length-over-area ratio geometries of optimum performance are similar.

The following N- and P-type materials were surveyed:

N-Type	P-Type
TPM-10 (PbTe)	TPM-15 (PbSnTe)
TPM-11 (PbTe)	TPM-19 (PbTe)
TPM-108 (PbTe)	

The maximum theoretical leg conversion efficiency was computed for the design temperature of $T_H = 1100^oF$ and $T_C = 525^oF$. The efficiencies and the corresponding load voltages are summarized in Table 5-3.

TABLE 5-3. THERMOELECTRIC MATERIAL COMPARISON

MATERIAL	MAXIMUM EFFICIENCY PERCENT	LOAD VOLTAGE AT MAXIMUM
TPM 108	6.33	33.2 mv
TPM 10	5.95	38.5 mv
TPM 11	5.13	53.8 mv
TPM 19	6.40	48.8 mv
TPM 15	6.10	37.3 mv

In spite of its higher efficiency, TPM 19 was not considered for this application because of insufficient documented evidence to establish stability. Therefore, TPM 15 was selected as the P-leg material for this application. Chemical and mechanical stability and compatibility had been demonstrated for this material used in commercial generators.

It has also been used exclusively as the hot-end P-material in other SNAP generators and substantial documented test data demonstrating its performance with time has been accumulated.

Selection of the N-type material was not as clear cut. Several factors were taken into consideration and engineering judgements made based on past experience.

Table 5-4 shows a comparison of the three N-type materials with the selected P-material and a comparison of the three couple combinations.

TABLE 5-4. COMPARISON OF THERMOELECTRIC MATERIAL THEORETICAL PERFORMANCE CHARACTERISTICS

Material	I(L/A) at Maximum Efficiency, Amps/Inch	Open Circuit Voltage, Millivolts	Load Voltage at Maximum Efficiency, Millivolts	Maximum Theoretical Efficiency, Percent	Total Couples Required for Two 14-Volt Circuits
P-Leg TPM-15	20.5	65.8	37.3	6.10	-
N-Leg TPM-108	37.1	58.3	33.2	6.33	-
Couple TPM-15 TPM-108	-	124.1	70.5	6.21	397
N-Leg TPM-10	26.4	68.4	38.5	5.95	-
Couple TPM-15/ TPM-10	-	134.2	75.8	6.04	370
N-Leg TPM-11	19.3	79.2	43.8	5.13	-
Couple TPM-15/ TPM-11	-	145.2	81.1	5.52	345

Notes:
1. Number of couples indicated here represent ideal conditions, not actual generator.
2. Conditions were as follows:
   a. No extraneous resistance included.
   b. Hot junction temperature = 1100°F.
   c. Cold junction temperature = 525°F.

The N-type material TPM-11 has a major disadvantage in that its efficiency is significantly lower than the other two types.

The length-to-area ratio of TPM-108 is almost twice as great as that of the P-leg, which is not desirable. It required significantly more couples than the other types. With this material, little fabrication or test experience has been accumulated.

Material TPM-10 yields a couple efficiency less than three percent lower than that of TPM-108. This is not considered significant since the difference is within the measured precision of the property values. TPM-10 requires fewer couples than TPM-108 and its length-to-area ratio is sufficiently near that of the P-leg.

On the basis of these considerations, TPM-10 was selected as the N-type thermoelectric material to be used in the SNAP-27 couple.

5.2.1.2 Couple Design (Leg Size Determination)

5.2.1.2.1 Length-To-Area Ratio - Leg sizes were initially established by determining the optimum length-to-area (L-A) ratio of each leg. In this determination, first cut electrodes and contacts were taken into account. The amount of resistance added for each leg was based on results of tests conducted under a SNAP-A and a SNAP-B program. The electrode hardware in these programs was very similar in size and configuration to that used in the SNAP-27 couple design.

Examination of test data (recorded from individually instrumented legs used in SNAP-A test modules and prototype generators) showed a range of extraneous resistance associated with the N-leg of from less than one milliohm to three milliohms. The extraneous resistance associated with the P-leg generally exhibited a much wider variation due to the fact that it is inherently more difficult to achieve a low resistance, hot contact. The variation shown in the SNAP-A data is typical in the range of one to ten milliohms. Table 5-5 shows a limited amount of data at specific points of time.

Examination of these data shows the relative extraneous resistance values associated with the N and P-legs. The values selected for the couple design are 1.7 milliohms for the N-leg and 3.0 milliohms for the P-leg. Requirement for additional margins could be made up by numbers of couples selected.

A computerized analysis was conducted for each leg in order to study the effect of variation in leg geometry (L-A) upon efficiency and load voltage. Figures 5-1 and 5-2 (Reference 5-1) summarize the results of this analysis for the design temperature conditions and for a design load current of 2.0 amperes. Plotted on the ordinate is the ratio of

TABLE 5-5. SNAP-A TYPICAL EXTRANEOUS RESISTANCE

DEVICE	N-LEG R_x (MILLIOHMS)	P-LEG R_x (MILLIOHMS)	TIME OF OPERATION (HOURS)
Module A1	0.2	6.1	1250
Module A3	1.9	2.5	2700
Module A4	1.9	2.1	2256
Prototype No. 3	0.7	1.1	96
Prototype No. 3	1.2	9.4	2280
Prototype No. 3	0.7	7.2	2280
Prototype No. 4	2.5	2.9	24
Prototype No. 5	1.0	5.9	24
Prototype No. 5	2.0	9.9	24

load current to the matched load current. With the load current held fixed at 2.0 amperes, the matched load current varies by allowing the L-A ratio to vary. This variation in L-A ratio is plotted, as well as efficiency and load voltage.

In the selection of the design point, it was desirable to achieve the highest load voltage while maintaining near-maximum efficiency. The efficiency curve is relatively flat over a wide range of the current ratio, while the load voltage decreased linearly with increasing current ratio.

Thus, it was desirable to select the design point at the far left of the flat portion of the efficiency curve. This yields highest load voltage with negligible loss in efficiency from the maximum efficiency point.

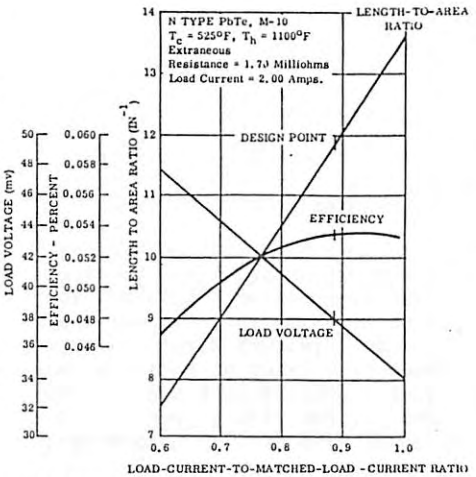

Figure 5-1. N-Leg Geometry Analysis

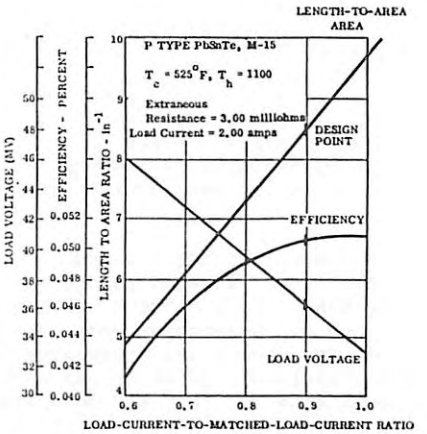

Figure 5-2. P-Leg Geometry Analysis

Based on these considerations, the design point conditions were selected. These are summarized in Table 5-6.

TABLE 5-6. LEG DESIGN CHARACTERISTICS

CHARACTERISTICS	N-LEG	P-LEG	TOTAL COUPLE
Length-to-Area Ratio ($inch^{-1}$)	11.88	8.40	-
Efficiency (percent)	5.36	5.08	5.2
Load Voltage (Millivolts)	37.8	36.2	74.0
Power Output (watts)	0.076	0.072	0.148
Heat Input (watts)	1.42	1.43	2.85
Load Current (amperes)	2.0	2.0	2.0
Hot Junction Temperature (°F)	1100	1100	1100
Cold Junction Temperature (°F)	525	525	525
Extraneous Resistance (milliohms)	1.7	3.0	4.7

Figures 5-3 through 5-6 (Reference 5-1) show the predicted performance of each leg with load current variation from open circuit to short circuit conditions.

5.2.1.2.2 Leg Geometry - The following factors were considered for determination of the actual leg geometry:

a. Previous manufacturing experience has shown that length-over-diameter ratio should not be greater than four

b. Legs should be of equal length to facilitate bonding

c. Previous manufacturing experience has shown that the leg diameter should not be less than 0.187 inch

d. The longer the leg, the less shifting of the cold frame (with respect to the hot frame) would influence the hot-side contact

e. The longer leg is less sensitive to ingradient thermal stresses

f. A short leg reduces the size and weight of the generator

g. A short leg is difficult to install into the generator.

These considerations were taken into account to determine the actual leg geometry. Emphasis was on selection of a leg size which would result in a reliable design.

To keep weight to a minimum, the legs would perforce have to be very small, but this conflicts with some of the other considerations. A very long leg would help satisfy some of the considerations but would conflict with the length-over-diameter ratio maximum of four. A length of 0.400 inches was selected for both the N and P-legs.

This selection was based on judgement from past experience in building thermoelectric generators. From the previously determined length-over-area ratios of the N- and P-legs, the diameters were calculated. The diameter of the N-leg was 0.207 inches and the P-leg, 0.247 inches.

5.2.2 THERMOPILE ASSEMBLY

The thermopile is an annular hermetically sealed volume containing 442 lead telluride thermoelectric couples (884 individual legs). As illustrated in Figure 5-7, each leg assembly begins with the boron nitride electrical insulation block mounted in the molybdenum spacer strip which contact the generator hot frame. Subsequent components are the

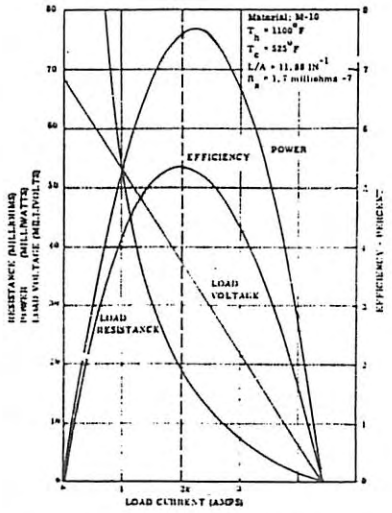

Figure 5-3. N-Leg Performance Characteristics

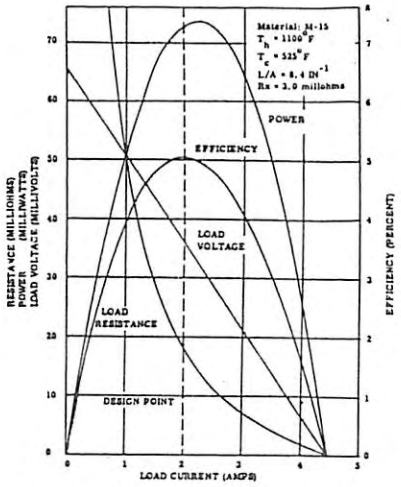

Figure 5-4. P-Leg Performance Characteristics

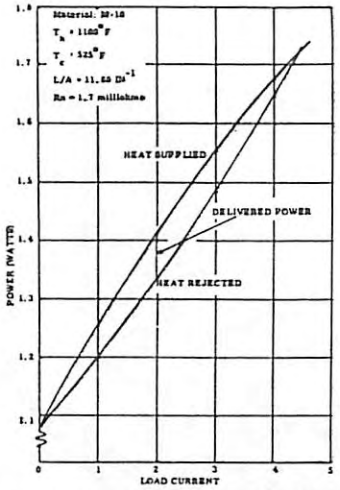

Figure 5-5. N-Leg Predicted Thermal Performance Characteristics

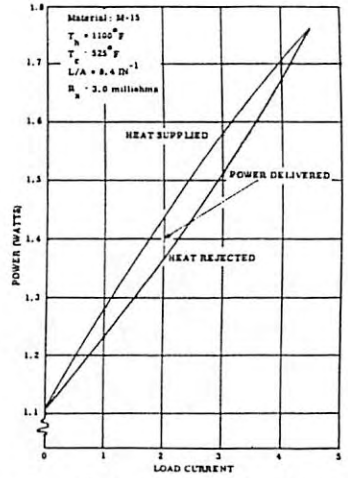

Figure 5-6. P-Leg Predicted Thermal Performance Characteristics

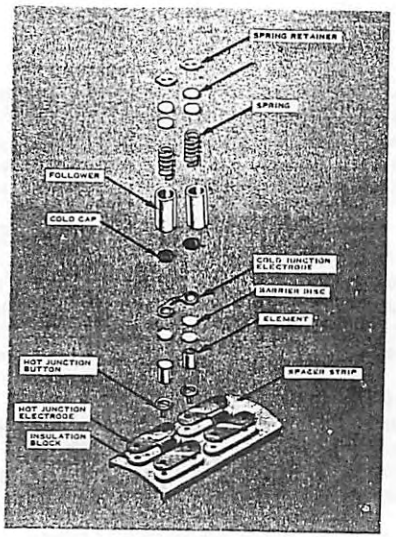

Figure 5-7 Thermocouple Leg Assembly Detail

the hot junction electrode, the hot junction button, the thermoelement (either N- or P-type), the barrier disc, and the cold junction electrode, which completes the thermocouple electrical circuit. Thermal contact with the hot frame is assured by a spring assembly system, including the cold cap, the beryllium oxide followers, the spring, the shims, and the spring retainer which attaches to the cold frame. Figure 5-8 depicts an end view of an assembled thermopile. An argon gas mixture of 25 psi envelopes the thermopile to assist heat transfer at contact areas and to prevent sublimation of the thermoelectric materials.

The basic elements of the electrical system comprise 442 couples arranged in 26 rows, each row having 17 couples. Each couple consists of one N-leg and one P-leg, attached by an integral copper strap.

The couples are electrically connected by way of Armco iron-plated copper hot shoes. Laddering between rows is obtained by electrically connecting two hot shoes. Two series parallel strings are formed and the four power leads are brought through the hermetic seal. As wired, the system has a floating ground. Electrical shorting of the thermoelectrics is prevented by the high resistance beryllium oxide follower on the cold side and by the resistance of boron nitride on the hot side.

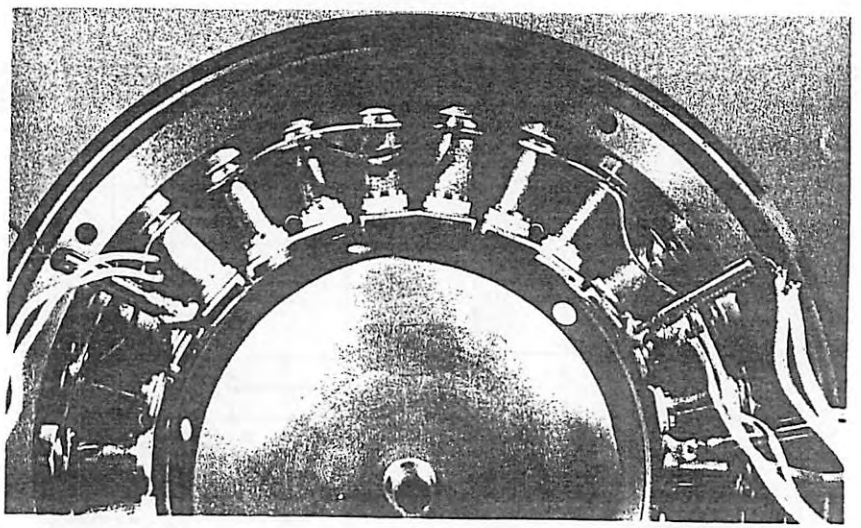

Figure 5-8. End View of Thermopile Assembly

The temperatures in the thermopile vary from 1075°F at the hot junction to 525°F at the cold junction at BOM. These are average values between the approximately axial gradient along the thermopile caused by variation in axial heat rejection. Powdered Min-K insulation is packed about the thermoelements to minimize heat flow bypassing the elements.

5.2.3 OUTER CASE/FINS ASSEMBLY

The outer case (Figure 5-9) is the principal structural member of the generator. The outer case also forms the outer boundary for the hermetically sealed thermopile, supports the fuel capsule and is the mount for the eight-fin heat rejection system. Eight feet are provided at the aft end of the outer case for bolting to the ALSEP baseplate. It is fabricated of hot pressed block beryllium with a 0.060-inch thick cylindrical wall, has eight 18-inch long by 5-inch wide cross-rolled sheet beryllium fins integrally attached by silver braze, and two transition rings of 19-9DL stainless steel, which are likewise brazed. The transition rings provide the interface for attachment of both Inconel (IN-102) end seals, which are welded at final assembly to establish and maintain the hermetic seal. Stainless steel (19-9DL) was selected based on its thermal coefficient compatibility with beryllium.

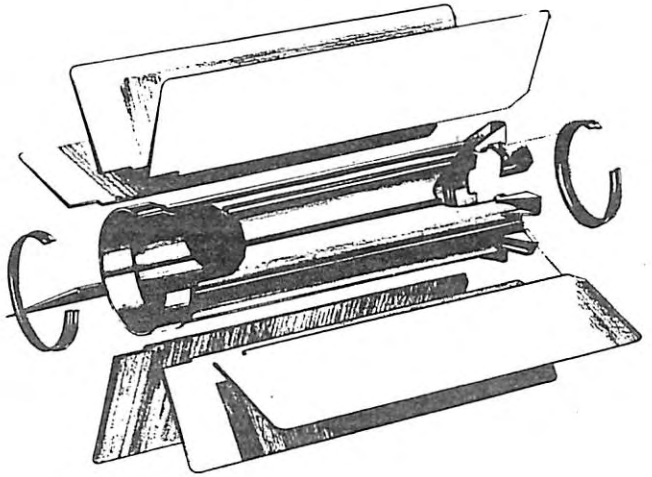

Figure 5-9. Outer Case Radiator Assembly Showing Fins, Case and Transition Rings

The interface between the outer case and cold frame is maintained by a shrink fit with a maximum interference of 0.002 inch.

Serious design and manufacturing problems, encountered during the initial processing and test phases on the outer case assembly, were resolved through the joint effort of General Electric and Solar. The major design and processing changes which resulted are summarized below.

On the first four engineering outer case assemblies, Solar experienced warpage of the fins and oversized bore (excessive out-of-round condition) during the braze cycle. In addition, cracking was experienced earlier on practice shrink fit units. Fin warpage was eventually eliminated by refinements in fixturing, reduction in mandrel wall thickness and extension of the cool down cycle. However, the out-of-round condition as well as the cracking problem remained. An analysis postulated a possible differential coefficient of expansion between the fins and case which could account for the stress producing the out-of-roundness condition.

The initial fin design depicted in Figure 5-10 (a) was that of a one

piece solid construction without any slots or holes. This early design was used on Generator Mod 1. In an attempt to reduce the stress, the fins were slotted as shown in Figure 5-10 (b). This approach was used on Generators Mods 5, 6 and 14. Results after brazing indicated great improvement and pointed towards the "split-fin" design, Figure 5-10 (c), for the next assembly. It was hoped that this design would thereby reduce the stress causing the center out-of-roundness at midpoint. This approach was used on Generator Mod 7, and after brazing, it was found that the center out-of-roundness was completely reversed from the preceding assembly.

A compromise between approaches (b) and (c) was suggested to General Electric in the form of varying lengths of slots in a "Christmas Tree" pattern as shown in Figure 5-10 (d). However, this approach was not tried.

Instead, the outer case wall thickness was increased from 0.060 to 0.100-inch, which would permit post-brazing machining of the wall to size and the "slotted fins" of Figure 5-10 (b) were retained. This design was then employed on Generator Mod 8.

Following the General Electric-Solar review of the failure analysis data on Practice Shrink Fit Numbers 1 and 2 outer cases, it was agreed that the principal contributor to structural weakness apparently was the case geometry in the area of the fillet at the forward flange. Coupled with the inherent tendency of the braze alloy to agglomerate in the same area at the fin notch, the two factors combined to form a stress riser. When combined with residual stress in the case wall induced by differential contraction of fins and case during the braze cool down cycle, small external loads were sufficient to cause fracture. It was decided that a redesign was required to strengthen the fillet zone and eliminate the fin notch. All activity on the qualification and flight units was halted pending the redesign which incorporated a high fin rib in the case and an unnotched fin running straight for the full length of the case.

On December 16, 1966, the decision was made to slot the fins into seven segments as a means of reducing the residual stress in the case, as shown in Figure 5-10 (e). Generators, Mods 8B, 10, 15 and flight generators, Mods 13, 14, 21, 22 and 23 employ this design consisting of a heavy wall (with post-braze machining), high fin buttresses and through slotted fins.

5.2.4 COLD FRAME

The cold frame, Figure 5-11, is a hollow cylinder of beryllium with radial holes to accommodate the thermoelectric element followers and

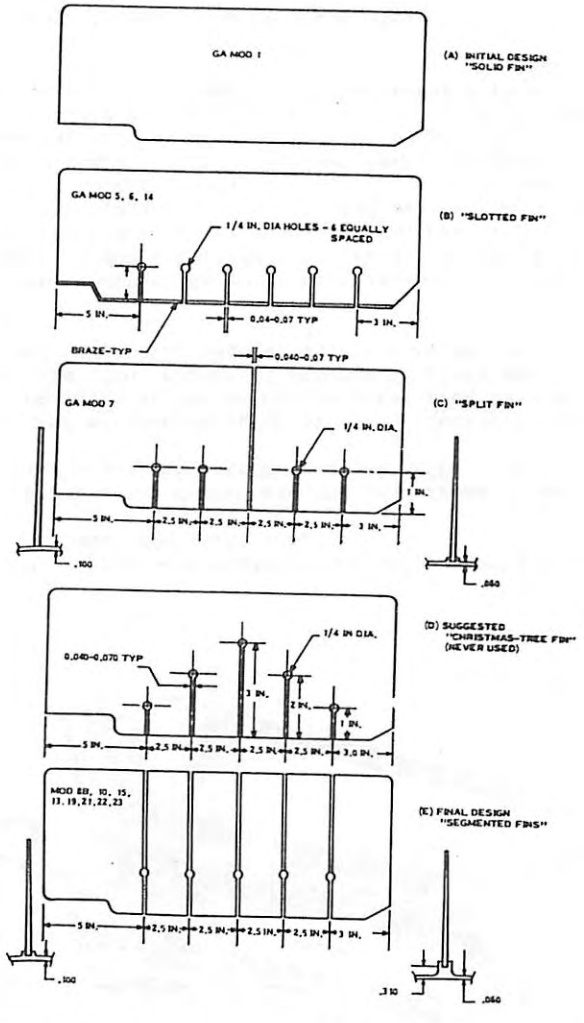

Figure 5-10. Evolution of Outer Case Fin Design

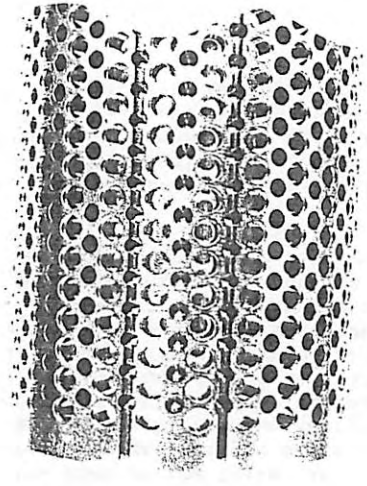

Figure 5-11. Cold Frame

other holes for lightening the structure. The cold frame provides the outer structural support for the thermopile and conducts heat from the thermopile to the heat rejection system.

5.2.5 HOT FRAME

The hot frame, (Figure 5-12), fabricated on 0.020-inch thick IN-102 steel, provides the inner support for the thermopile and serves as the inner boundary for the inert gas control atmosphere. The hot frame receives heat from the fuel capsule by thermal radiation and conducts it to the thermoelements via sliding contact with the insulation blocks.

5.2.6 HERMETIC SEALS

At each end of the thermopile, Inconel (IN-102) discs provide the seals for the pressurized inert gas mixture. The forward seal supports the thermal gradient between the hot and cold frames. The electrical leadthrough assembly is brazed to the aft hermetic seal, Figure 5-13. The two pinch-off tubes, Figure 5-14, are also located in the aft hermetic seal; these are employed to purge the generator and fill it with the argon inert gas mixture.

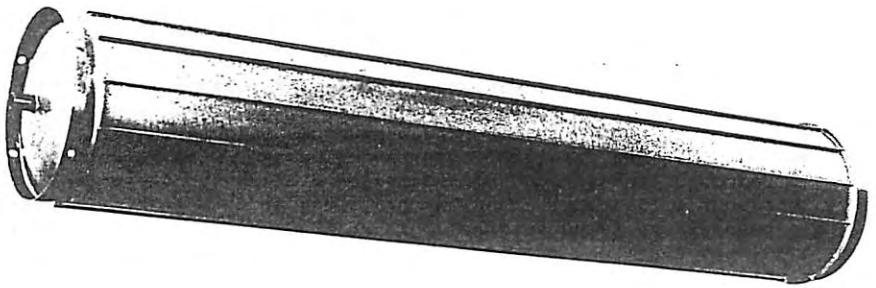

Figure 5-12. Hot Frame

Integrity of the hermetic seal was demonstrated through extensive testing of engineering qualification and flight generators. Each of these units has undergone full environmental testing, including vibration, thermal cycling, air operation and vacuum operation. A helium tracer (one percent) gas is used with the thermopile argon fill gas to permit monitoring of generator leak rates at any time in the test cycle. Leak rates of the five ALSEP flight generators (after all testing) measured prior to shipment were as follows:

Flight Generator	Rate in cc/sec Argon
(1) Mod 13	2.5×10^{-6}
(2) Mod 19	4.36×10^{-7}
(3) Mod 21	1.09×10^{-7}
(4) Mod 22	3.7×10^{-7}
(5) Mod 23	3.92×10^{-7}

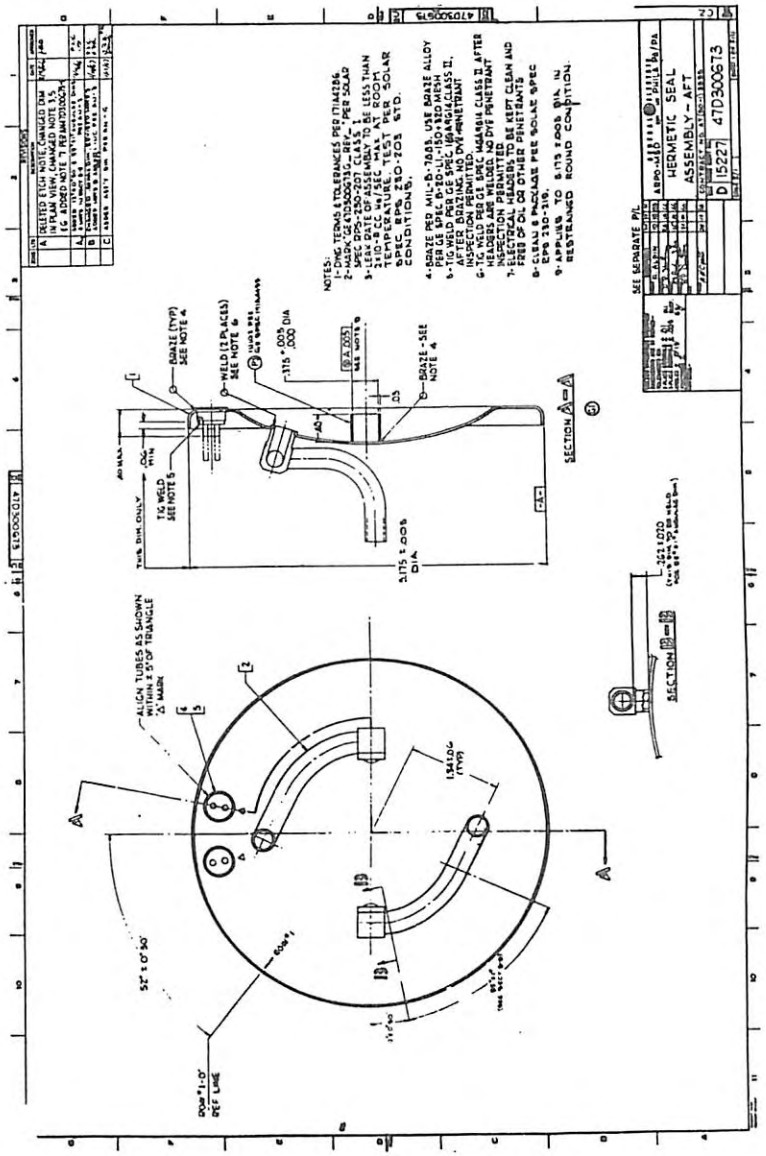

Figure 5-13. Aft Hermetic Seal Assembly

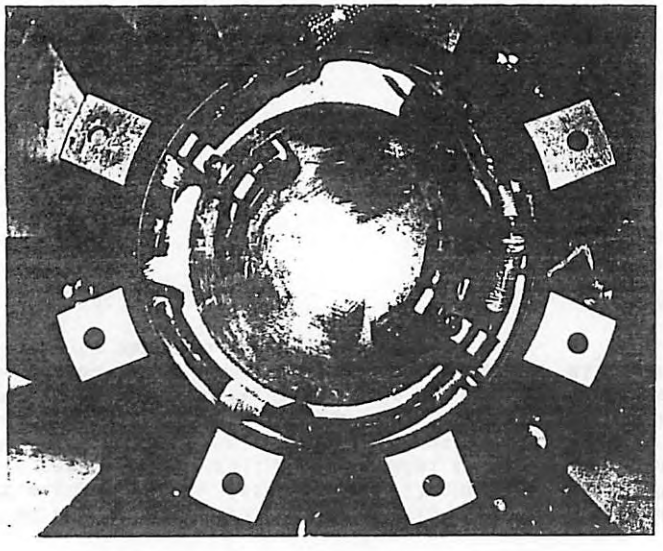

Figure 5-14. Aft Hermetic Seal Showing Cable Pinch-off Tubes

The highest of these rates, 2.5×10^{-6} cc/sec, is consistent with maintaining a thermopile internal pressure well above 10 psia after five years of operation.

It was shown by the 10-couple module tests that thermoelectric performance at the hot junction temperatures will not be affected until argon pressure drops well below 10 psia, and even then the influence is slight until very low pressures (several psia) are reached. Long term vacuum testing of the first engineering prototype generator (Mod 5), which has extensive penetrations for non-flight instrumentation, including a pressure transducer, also confirmed the hermetic seal design. This generator, which operated beyond 11,000 hours in a simulated lunar environment, has shown a gradual decline in pressure to 16 psia, and at currently measured leak rates, would still retain over 10 psia after five years.

Due to the multitude of potential leak paths of Mod 5 associated with instrument lead penetrations and the fact that this was the very first full size generator to be fabricated, this is considered to be a worst case example.

5.2.7 DEGAUSSING LOOPS

5.2.7.1 Design

To reduce the generator magnetic field, all permeable materials were eliminated in the design except for a small deposition of pure iron (0.002 to 0.005 inch thick) on the hot shoes, a degaussing loop was incorporated at each end of the generator to "buck" the ring current and the return power lines were judiciously placed to minimize the longitudinal fields. Figure 5-15 shows the resultant wiring schematic for the generator. Note that the ring currents are countered by the two degaussing rings and that the two return power leads are positioned between the thermoelectric rows, whose current is opposite.

During assembly of the generator, the longitudinal lengths of the degaussing loops are led down the outside of the cold frame to the power headers as shown in Figure 5-16. The construction of the degaussing loops is shown in Figure 5-17.

5.2.7.2 Degaussing Loops Failures

Some early failures were experienced on degaussing loop lead wires. On two occasions the silver lead-in wire for a degaussing loop fractured at the silicon-ceramic seal.

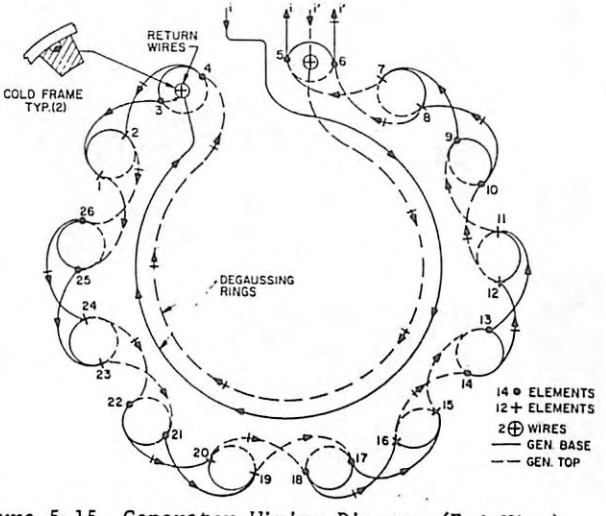

Figure 5-15. Generator Wiring Diagram (End View)

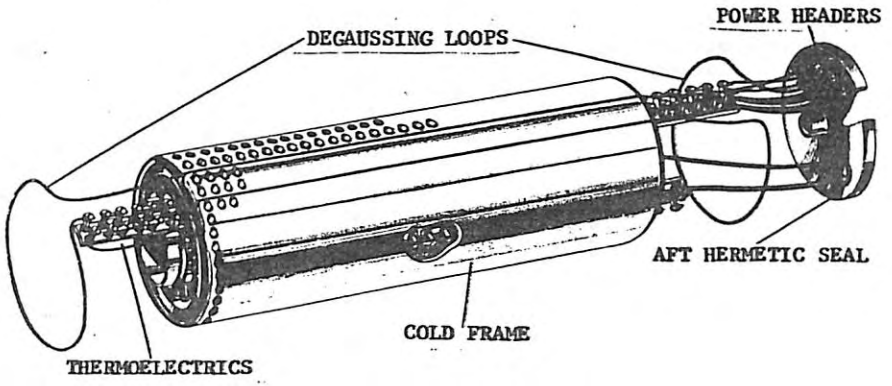

Figure 5-16. Module Assembly Showing Degaussing Loops

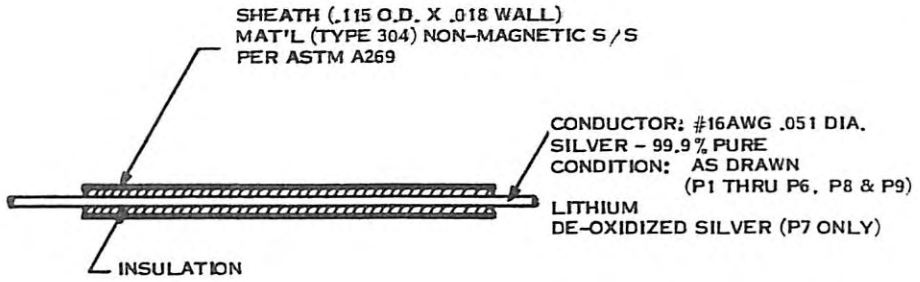

Figure 5-17. Degaussing Loop Design

Metallurgical examination of the failed wires disclosed unusually large grain structure in the vicinity of the seal and a normal fine-grained structure throughout the rest of the wire. A formation of this localized large-grain structure, with the subsequent wire embrittlement, was attributed to overheating of the silver wire during formation of the seal. The functions of the seal are to retain the insulation material and to prevent moisture pickup.

Consultation with the vendor disclosed that the capabilities of seal were far in excess of the temperature requirement for the degaussing loops. Application of this seal required high temperature for its formation, which resulted in wire embrittlement. The vendor recommended a lower temperature seal material, and supplied sample degaussing loop pieces for test. Elevated temperature tests were performed at 600°F for over 500 hours on the samples with no significant deterioration of insulation resistance taking place and the lead-in wires remained free of embrittlement.

5.2.8 CABLE/CONNECTOR

At the outset of the SNAP-27 Program, it was planned that only a two-foot "pigtail" would extend from the generator, and that this would be tied to the ALSEP Central Station by Bendix Corporation using some suitable means. As the ALSEP program evolved, it became desirable to have a thirteen foot cable with a connector coming from the generator to tie in to the ALSEP Central Station. Bendix Corporation designed this cable using the NASA guidelines appropriate to mission requirements and astronaut use. The astronaut connectors themselves were furnished to General Electric by Bendix.

After the Bendix design specifications had been revised to provide a more workable combination of performance and construction requirements in conjunction with realistic acceptance tests, the required units proceeded through manufacture and test. A major difficulty resulted from water tightness requirements in that the specified construction H-film (Kapton) and ML varnish bonding agent were not sufficiently flexible. This difficulty was recognized when the outer covering of the cable cracked during the severe 3.75-inch bend radius test performed at -65°F. This type of construction is not recommended for watertight applications since the purpose of the ML varnish is only to prevent unravelling and shifting of H-film insulation layers.

Difficulties experienced by the initial cable vendor resulted in the consideration of a backup cable using Teflon coated H-film which appeared to be watertight, as well as offering greater resistance to abrasion and cracking. Ultimately this design was adopted and the cable obtained from another vendor.

d. Capable of withstanding the SNAP-27 environmental conditions.

Figure 5-19 shows the assembly details of the feed-through header.

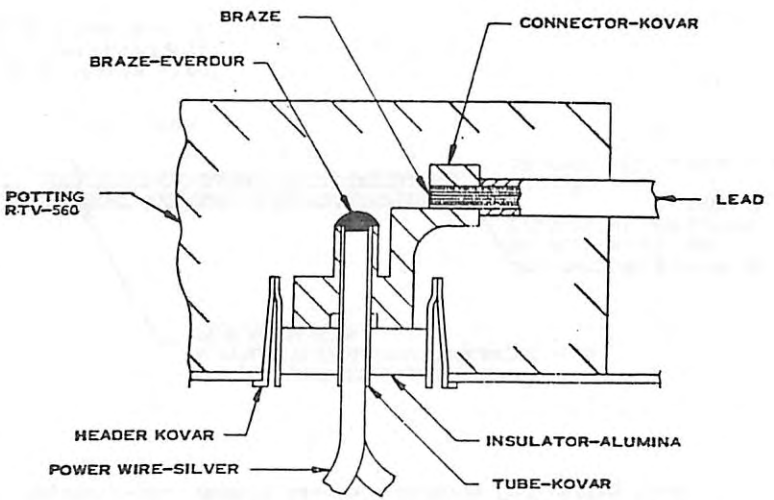

Figure 5-19. Electrical Feed-through Assembly

5.2.9.2 Failures in Header Pin Weld

The appearance of excessive porosity in sample power header pin welds prepared by 3M Company for weld certification prompted an investigation into methods of improving the weld integrity. The configuration of this weld was originally a silver wire passing through a closely fitting Kovar tube. The end of the silver wire (positioned just above the end of the Kovar tube) was struck with a Tungsten Inert Gas (TIG) arc to make the silver flow over and wet the end of the Kovar tube; this created a hermetically tight seal and provided electrical continuity.

The excessive porosity encountered was attributed either to evaporation of the silver or decomposition of silver oxide on the wire surface during welding, resulting from the approximately 500°F differential between the melting points of Kovar and silver. To make the silver and Kovar more compatible with each other during welding, a filler metal, Everdur 1010 (an alloy of copper and silicon), with a melting temperature between that of Kovar and silver, was introduced to the weld joint configuration.

The configuration of the joint before applying the TIG arc was arranged with the silver wire depressed below the top surface of the Kovar feed-through tube. A small ball of Everdur was then placed on top of the silver wire. When the joint configuration is struck by the TIG arc, the higher melting Everdur acts as a heat shield for the silver. At the same time, the Everdur provides fusion between itself and the silver at a lower temperature than wetting of the Kovar by the silver was accomplished in the previous configuration. Consequently, vaporization of the silver is reduced.

Sections of welded specimens using the Everdur in conjunction with radiography of Mods 10, 13 and 19 generators, indicated excellent results with much less porosity than the previous configuration, and results were within the requirements of the TIG welding specification for the power header pin weld.

5.2.10 RTG INSTRUMENTATION

5.2.10.1 Design

Platinum wire resistance temperature devices (RTD's) are used on all generators to obtain temperature measurements of the interior of the hot frame and of the outer case. Six RTD's are present on each generator. Three are positioned 120 degrees apart on the inner diameter of the hot frame and held by two retaining rings. Three units are attached to the outer case by means of clips. Figure 5-20 depicts installation of the RTD's on a generator.

The sensing elements and sheath construction for both the flight and engineering units were identical except for the following items.

a. A two-pin header on the sheath transition piece was used on flight units; whereas, pigtail leads were used on the engineering units

b. The flight units had the sheaths and headers vented in order to eliminate any moisture entrapment.

The need for venting the RTD's became apparent when in the course of running stability checks on 30 of these sensors, 6 of the units showed low resistance to ground. It was established that moisture, both entrapped and entering through flaws in the hermetic seals, was the source of the trouble. During the course of running stability checks on prime resistance temperature sensors (RTD's) prior to installation on generators, 6 out of 30 hot frame units on test showed low resistance to ground. This occurred after periods ranging from 75 to 400 hours at a soak temperature of 1100°F, with as many as four thermal

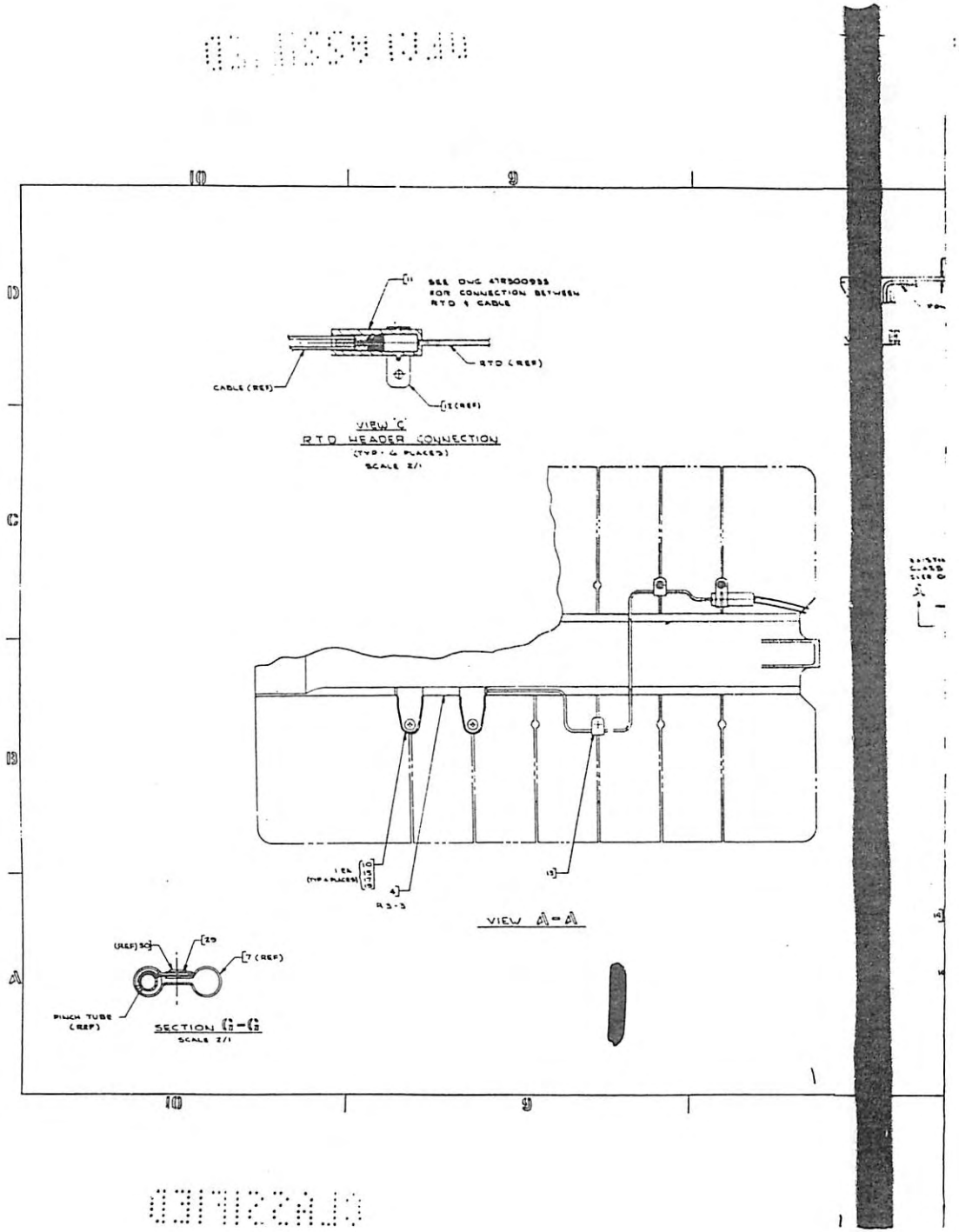
SEE DWG 4785009SS FOR CONNECTION BETWEEN RTD & CABLE
RTD (REF)
CABLE (REF)
VIEW 'C'
RTD HEADER CONNECTION
(TYP. 6 PLACES)
SCALE 2/1
VIEW A-A
SECTION G-G
SCALE 2/1
PITCH TUBE (REF)
7 (REF)

BLANK PAGE

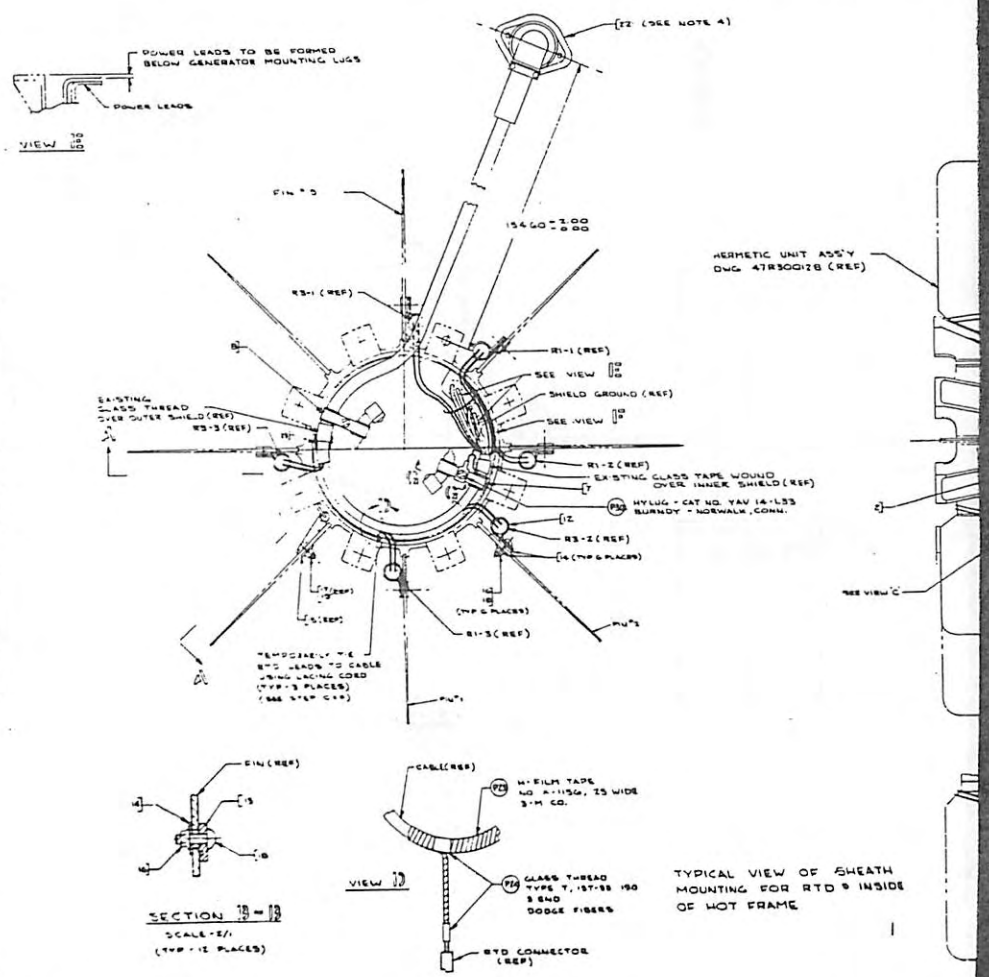
POWER LEADS TO BE FORMED BELOW GENERATOR MOUNTING LUGS
POWER LEADS
VIEW
[12 (SEE NOTE 4)
FIN #3
15460 +2.00 -0.00
R3-1 (REF)
R1-1 (REF)
SEE VIEW
SHIELD GROUND (REF)
SEE VIEW
EXISTING GLASS THREAD OVER OUTER SHIELD (REF)
R3-3 (REF)
R1-2 (REF)
EXISTING GLASS TAPE WOUND OVER INNER SHIELD (REF)
HYLUG - CAT NO. YAV 14-L33 BURNDY - NORWALK, CONN.
R3-2 (REF)
(TYP 6 PLACES)
(TYP 6 PLACES)
R1-3 (REF)
HERMETIC UNIT ASS'Y DWG 47R300128 (REF)
SEE VIEW 'C'
TEMPORARILY TIE RTD LEADS TO CABLE WITH LACING CORD (TYP - 3 PLACES) (SEE STEP C-5)
FIN (REF)
SECTION - SCALE - 5/1 (TYP - 12 PLACES)
CABLE (REF)
M-FILM TAPE NO. A-1156, 25 WIDE 3-M CO.
GLASS THREAD TYPE T, 187-38 150 3 END DODGE FIBERS
VIEW
RTD CONNECTOR (REF)
TYPICAL VIEW OF SHEATH MOUNTING FOR RTD'S INSIDE OF HOT FRAME

2

BLANK PAGE

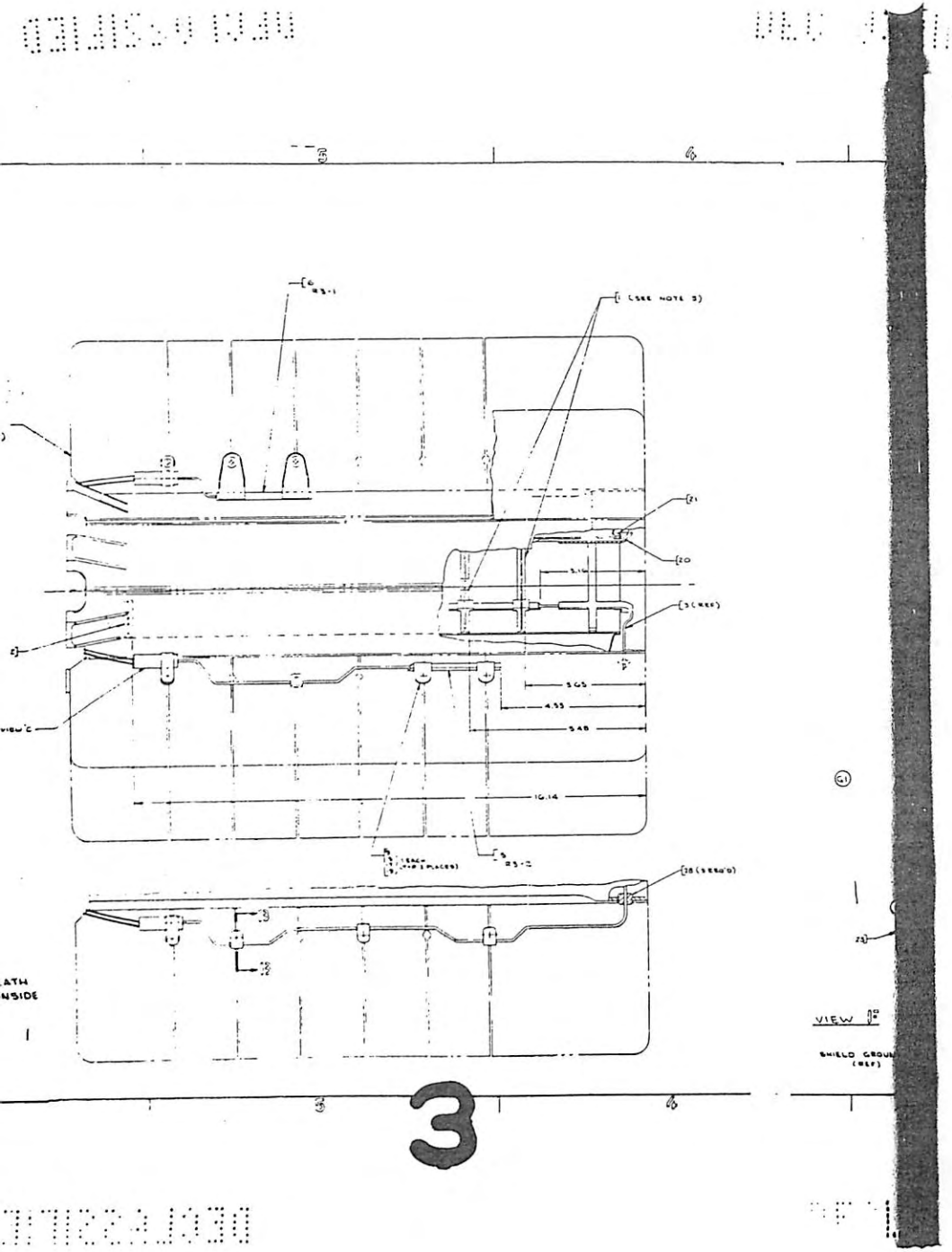

3

BLANK PAGE

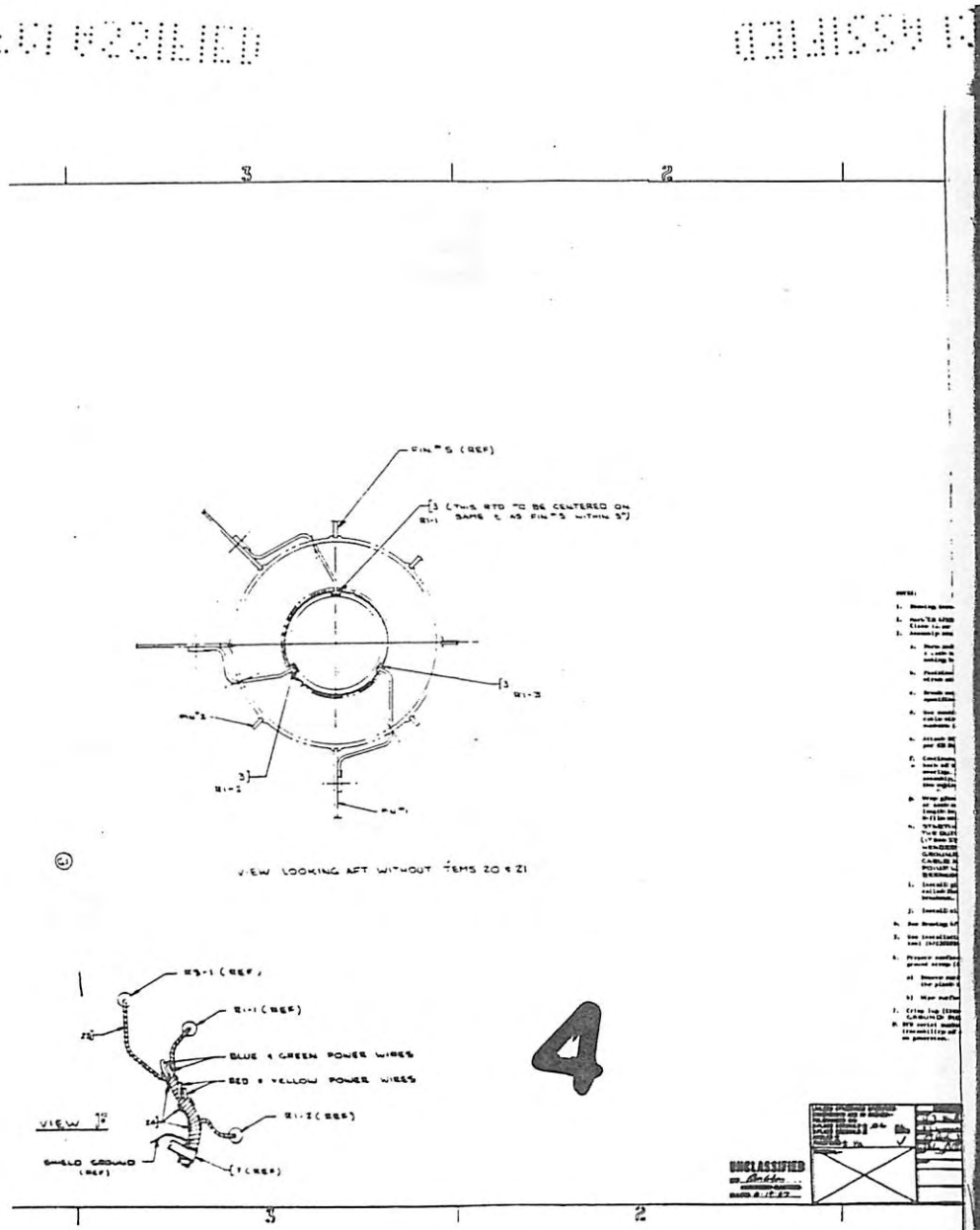

Figure 5

BLANK PAGE

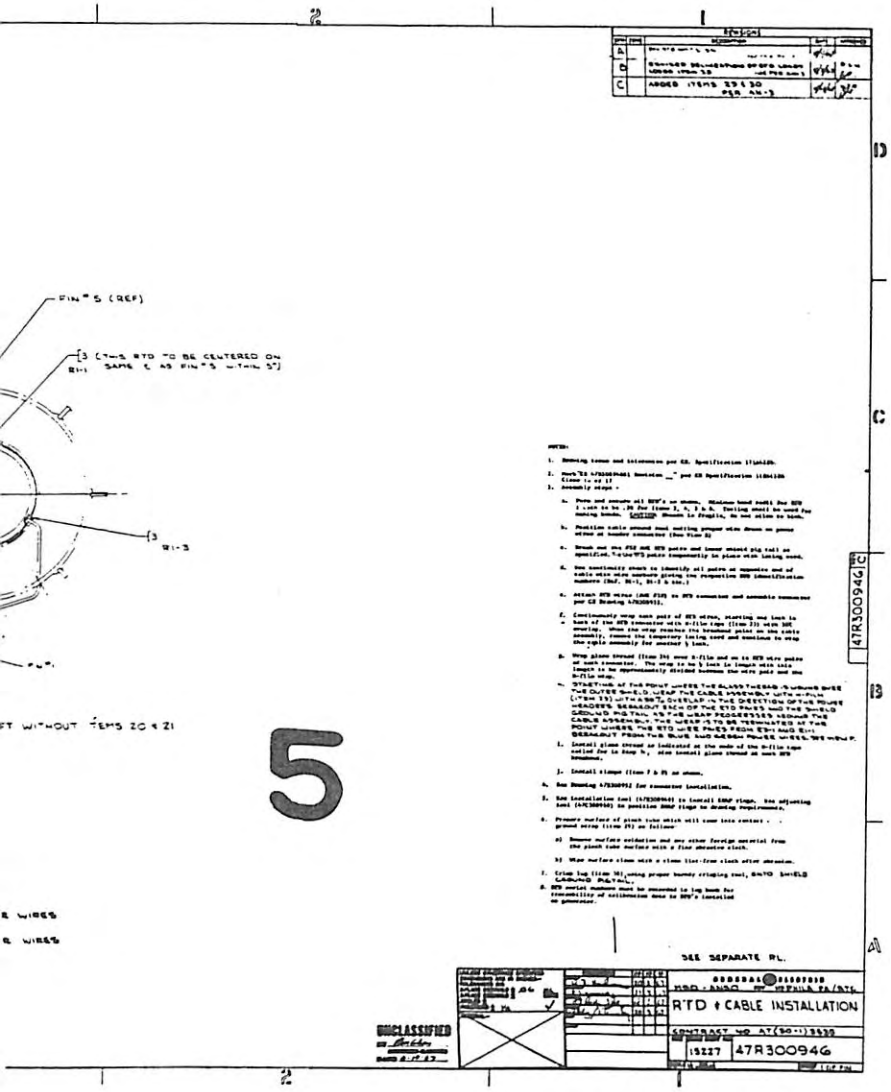

Figure 5-20. RTD and Cable Installation

cycles incurred between periodic 32°F calibration checks. The low sensor resistance was caused by inadequate insulation resistance in the areas of the sensor sheath and the header which acted as a shunt on the element. It was established that moisture, both entrapped and entering through flaws in the hermetic seals, was the source of the trouble. Leaks were found in some of the units at braze and weld joints, and at micro-cracks in the sheaths.

The design was subsequently changed to include the venting of these RTD's by introducing a 0.060-inch diameter hole in both the sheath and header such that any moisture present would be driven off as the units came up to stabilization temperature during operation.

5.2.10.2 Hot Frame Temperature Determination

The only thermal instrumentation present on flight generators are three resistance temperature detectors (RTD's) on the generator hot frame and three on its cold frame. As a result, thermoelectric hot and cold junction temperatures have to be determined by correlation with the RTD readings and curves, Figures 5-21 and 5-22, which were derived from tests on a generator instrumented with 12 additional thermocouples attached to the fins at a radial location of 1/4-inch from the fin roots and tested under vacuum conditions.

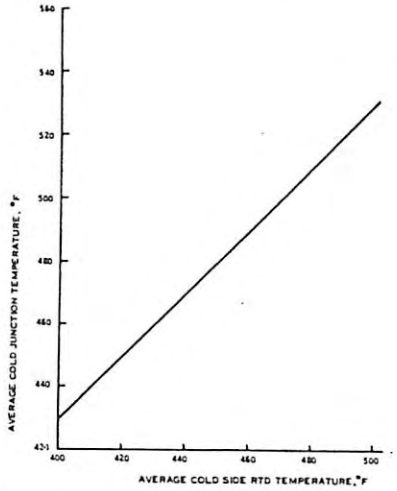

Figure 5-21. Cold Junction Temperature

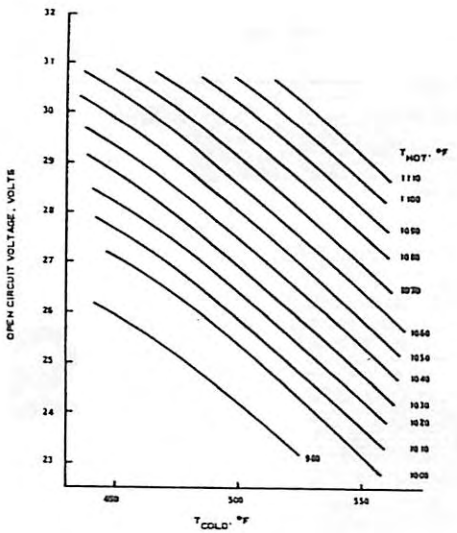

Figure 5-22. Hot Junction Temperature

The average axial location of the RTD's from the top of the generator is as follows:

RTD	AVERAGE LOCATION
Cold Side R3-1	12 inches on base of fin root
Cold Side R3-2	6 inches on fin at 1/4-inch radially
Cold Side R3-3	6 inches on base of fin root
Hot Side R1-1 to R1-3	4.8-inches on hot frame

Figure 5-21 shows the cold junction temperature as a function of the average cold side RTD temperature. The curve is based on:

a. A 454 node THT-D analysis of the SNAP-27 generator for maximum and minimum lunar sinks

b. Mod 5 long life test thermal vacuum results for +170°F sink and 280°F sink

c. Mod 5 engineering environmental thermal vacuum test at a +170°F sink

d. Mod 15 thermal vacuum acceptance test for +170°F and -280°F sinks.

The hot junction temperature is presented as a function of the generator open circuit voltage and cold junction temperature. These curves are analytical results of a thermoelectric computer program. Temperature is determined as follows:

a. Use of average of the three cold side RTD's to represent average fin root (outer shell) temperature

b. Use Figure 5-21 and the average cold side RTD temperature to determine the average cold junction temperature

c. The average hot junction temperature can be found from Figure 5-22 if the generator open circuit voltage and the cold junction temperature are known

d. As a cross check on the average hot junction temperature, subtract 28°F from the average hot side RTD's

e. The average of the hot side RTD temperatures represents the maximum hot junction temperature.

5.3 DESIGN ANALYSIS

5.3.1 AC EQUIVALENT CIRCUIT

An ac equivalent circuit was analytically derived early in the program to determine the RTG system's response characteristics to support various techniques of generator protection and power conditioning. The effort included:

a. Synthesis of the equivalent ac circuit for an individual couple of the configurational arrangement in the SNAP-27 generator assembly

b. Assessment of the electrical capacitance at the thermocouple level

c. Buildup of the equivalent circuit to the thermopile row-level and subsequent assessment of the mutual inductance between rows

d. Determination of the equivalent inductance of the degaussing loops

e. Determination, from previous work, of the equivalent resistance of the thermopile and power wiring

f. Buildup of the circuit to the generator assembly level and subsequent determination of total equivalent lumped parameter values.

The results of the analysis, as presented here, reflect only the iginal follower design which was being used at the time, i.e., a coated beryllium follower instead of the present BeO follower.

5.3.1.1 Thermopile Pair Equivalent Circuit

The ac equivalent circuit of a paralleled thermocouple pair is shown in Figure 5-23.

Capacitance linkage to the generator frame is contributed by two sources:

a. Followers - The follower is isolated from the thermocouple leg cold cap and from the generator cold frame by a thin coating; thus, the follower/cold cap close proximity with intervening dielectric acts as a capacitor

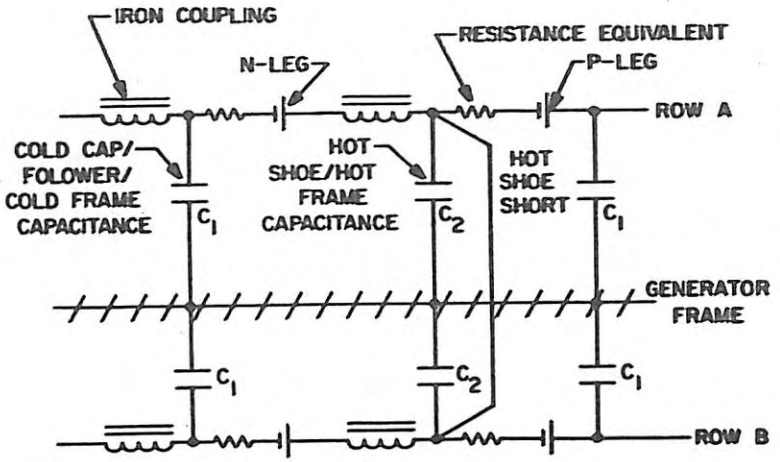

Figure 5-23. AC Equivalent Circuit of a Paralleled Couple Pair

b. Hot Shoes - The current-carrying hot shoe is isolated from the hot frame by a Boron-nitride insulator; thus, a capacitance exists at the hot shoe in each couple.

Inductance is due largely to the mutual inductance between rows of couples. The iron linkage shown is due to the thin Armco iron coating on the hot shoes.

Each individual leg in the thermocouples generates a voltage and has associated with it a resistance that can be "lumped" in with the power wiring and contact resistances as shown in the figure.

Each row contains 17 couples. Paralleling between couples in row-pairs is achieved at the hot shoes and additional paralleling is provided at the header interface.

The wiring arrangement used in derivation of overall lumped parameter values is shown in Figure 5-24, which illustrates the buildup of thermocouple pairs into rows, wiring between rows, degaussing loop connection, and feedthrough to external circuitry.

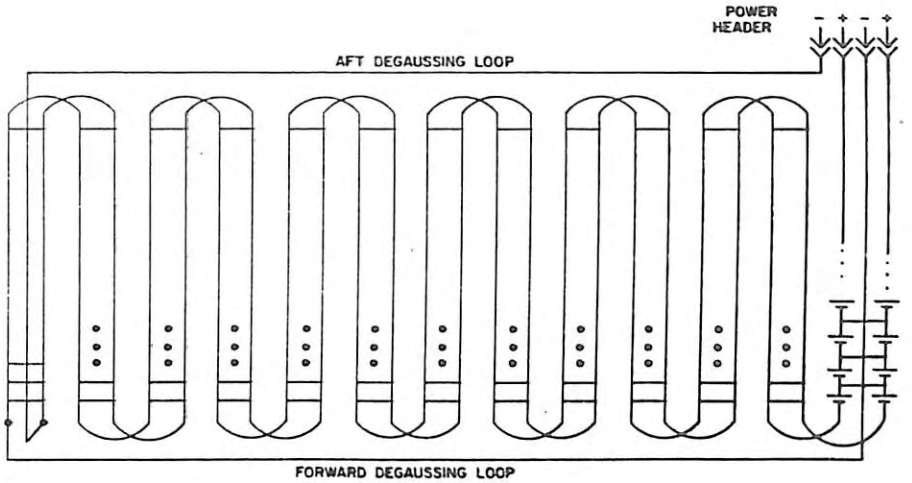

Figure 5-24. Generator Wiring Diagram

5.3.1.2 Capacitance (Follower)

Figure 5-25 shows the follower capacitance model which is approximately equivalent to two capacitors in series; capacitance between cold cap and follower in series with capacitance between follower and cold frame.

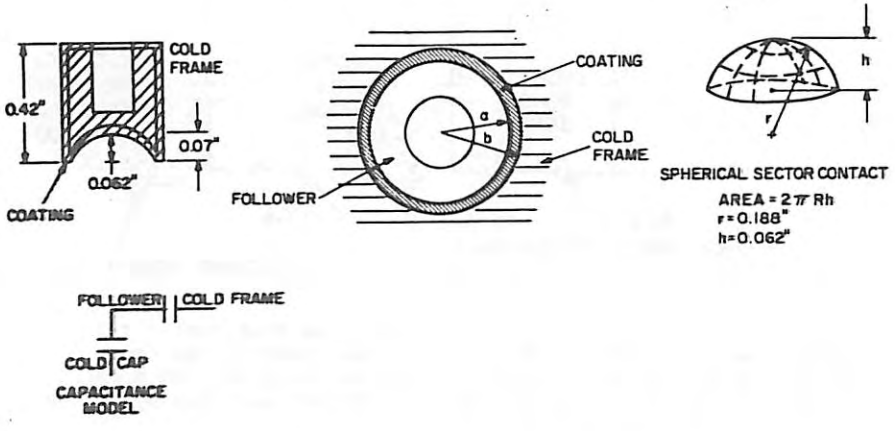

Figure 5-25. Follower Capacitance Model

5.3.1.3 Inductance

The inductance in the system arises primarily from the mutual inductance between rows in the thermopile and from the mutual inductance between the degaussing loops and end-cold strap assemblies.

For the thermopile, the mutual inductance was calculated on IBM 7094 for each row inductively linked with every other row and summed over the total thermopile. The summation resembled a finite alternating series because of the changing current direction as each row was taken into account. The degaussing loop was treated using the same formulation.

5.3.1.4 Approximate Thermopile Equivalent Circuit

The circuit suggested for use is shown in Figure 5-26. The distributed capacitance has been summed over the thermopile and lumped into three areas as shown. The thermopile inductance was divided along with the series resistance to allow illustration of a capacitance that can be considered to be near the center of the thermopile. The degaussing loops have been lumped at the output terminal. Note that all paralleling between thermopile rows and between the degaussing loops has already been taken into account in this figure.

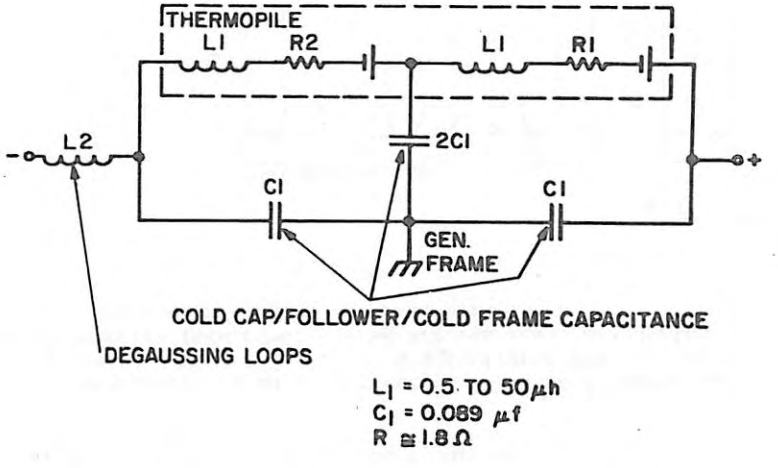

Figure 5-26. Approximate AC Equivalent Circuit

5.3.1.5 Generator Power Losses

An estimate was made of the RTG power losses due to in-line path resistances and leakage currents. The analysis is based on dc operation at a current of four amperes.

The wiring diagram for the generator is shown in Figure 5-24. Twenty-six rows of thermocouples lie parallel to the generator longitudinal axis. Couples in each row are connected in series and adjacent couples in rows of two groups; each are paralleled at the hot shoe interface.

Each paralleled row group is series connected to the next paralleled group for voltage buildup. Thermopile negative terminal connections interface with the generator forward and aft-end degaussing loops, which carry 1/2 of the current on each loop and terminate at the hermetically sealed header on the bottom of the generator. The thermopile positive terminals interface with the same header, which therefore provides four power lead pins (two positive and two negative. The flight cable is attached to the power header.

To evaluate the dc series path losses of the RTG, three equivalent dc circuits were developed:

a. Thermocouple - The equivalent circuit for one thermocouple parallel pair is shown in Figure 5-27(a). Each in-line and parallel path contributory loss is shown. Thermocouple paraleling occurs at the hot shoe. For the purposes of this analysis, it has been assumed that under nominal operating conditions a voltage differential does not exist across the hot shoe (between the two thermocouple legs common to the shoe).

b. Thermopile Rows - The equivalent circuit for a series-parallel thermopile row is illustrated in Figure 5-27(b). It consists simply of 17 series-connected thermocouples paralleled at each hot shoe with another row of 17 couples, and the addition of the equivalent resistance at the end of the row to account for the connection into the next series-parallel row.

c. Generator Assembly - The equivalent circuit for the generator assembly is shown in Figure 5-27(c). It consists of the 13 series-parallel rows, which are connected in series, with the addition of the positive and negative terminal equivalent circuits terminating in the power header. The cable, which runs from the generator to the PCU of the ALSEP package, is simply another series line loss that is added to the header lines.

Equivalent resistances and corresponding power losses are shown in Table 5-7. Included in the table, for purposes of illustration, are losses for five feet of harness. Equivalent resistance values reflect paralleling of conductors in the RTG.

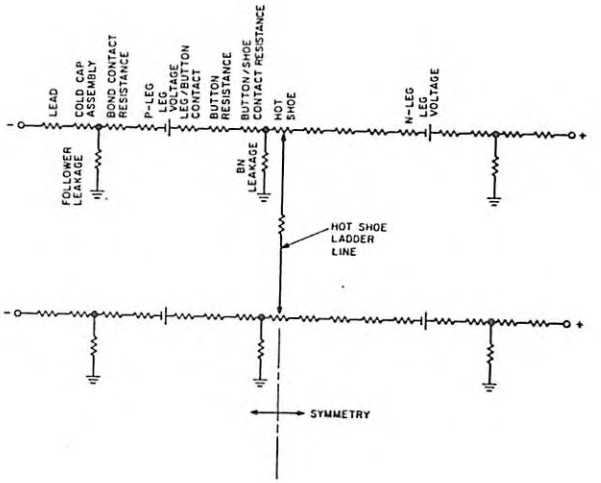

(a) One Thermocouple Parallel Pair

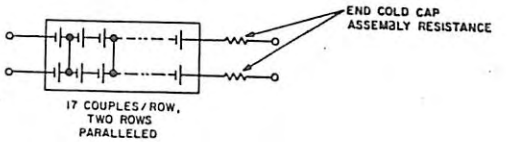

(b) Series-Parallel Connected Thermopile Row

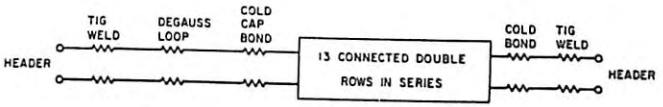

(c) Generator Assembly

Figure 5-27. Generator Assembly DC Equivalent Circuit

TABLE 5-7. RTG DC SERIES POWER LOSSES

ITEM	EQUIVALENT RESISTANCE (OHMS x 10^{-2})	POWER LOSS AT 4 AMPS (WATTS x 10^{-1})	COMMENT
End Cold Strap Assembly	0.70	1.12	
Degaussing Loop	0.57	0.91	
Lead Lines to Output	0.63	1.00	Lead lines to degaussing loop and positive terminals
TOTAL RTG	1.90	3.03	
Harness (10 feet of wire - 5 feet of cable)	2.45	3.92	No. 16 wire, four conductors
TOTAL (Including 5-foot Harness)	4.35	6.95	

5.3.2 GENERATOR THERMAL ANALYSIS

A detailed 500 node thermal model of the SNAP-27 generator was run (Reference 5-2). The model represents the final design, and with few exceptions, describes in detail the thermal behavior of a 22.5 degree segment of the generator. The generator segment chosen was described in sufficient detail to yield the following:

a. Hot and cold junction temperatures for each thermoelectric couple

b. Removal of generated electrical power from thermal model at the cold junction, and minor post-computer run calculations given total power generated by system

c. Calculation of temperature drops at hot and cold junctions due to thermal resistances. These resistances are based on latest test results and can readily be adapted to new test figures

d. Accurate description of radiation interchange between fins themselves, between a fin and the base plate, and between the fins and the lunar environment

e. Mounting plate temperature distribution

f. Accurate thermoelectric representation described by temperature dependent properties

g. Circumferential temperature gradients existing between fin bases

h. Temperature distributions, and heat balances throughout the generator and capsule.

The results are summarized in Figures 5-28 and 5-29.

5.3.3 DYNAMIC ANALYSIS

5.3.3.1 Generator Assembly

An analysis was made of the most critical conditions (lateral) seen by the generator assembly, with the responses computed according to input qualification vibration and shock levels (Reference 5-3). The analysis was based upon a linear system and did not consider any non-linearities.

The calculated natural frequencies for the generator assembly were found to be high despite the fact that the fin stiffnesses were neglected. A separate analysis for the fins was conducted (Paragraph 5.3.3.2) which confirmed the large difference between the fin frequencies and the generator assembly, and hence verified the mathematical model used.

Calculated responses at the most important locations are summarized in Table 5-8. As can be seen, critical design conditions for the generator assembly resulted from the applied random vibration. The lowest natural frequency for the generator assembly was far greater than 200 cps, and thus the component will act as a rigid body during the applied sinusoidal qualification input exitation.

5.3.3.2 Generator Fins

A dynamic analysis of the fins was conducted to determine the most critical condition of the generator fins due to sinusoidal and random base excitation (Reference 5-4). The fins were considered uncoupled from the generator frequencies, based upon previous analyses. The

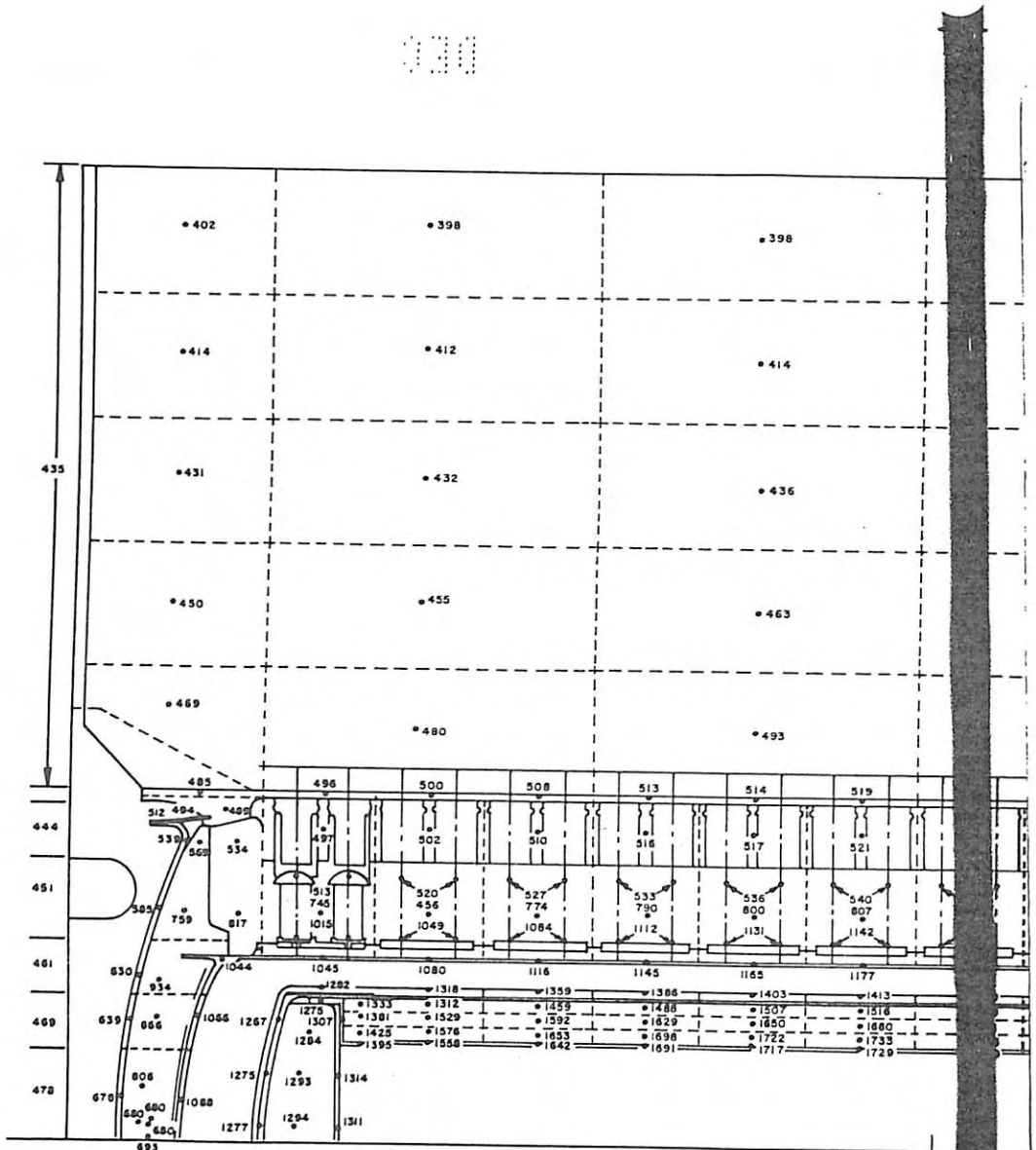
435
444
451
461
469
478
402
398
398
414
412
414
431
432
436
450
455
463
469
480
493
485
496
500
508
513
514
519
512
494
405
497
502
510
516
517
521
339
562
534
513
745
1015
520
456
1049
527
774
1084
533
790
1112
536
800
1131
540
807
1142
585
759
817
630
1044
1045
1080
1116
1145
1165
1177
934
1282
1318
1359
1386
1403
1413
639
866
1275
1307
1284
1333
1381
1425
1395
1312
1529
1576
1558
1459
1392
1653
1642
1488
1629
1696
1691
1507
1650
1722
1717
1516
1660
1735
1729
1056
1267
806
678
680
680
680
693
1275
1293
1294
1277
1314
1311
1068

BLANK PAGE

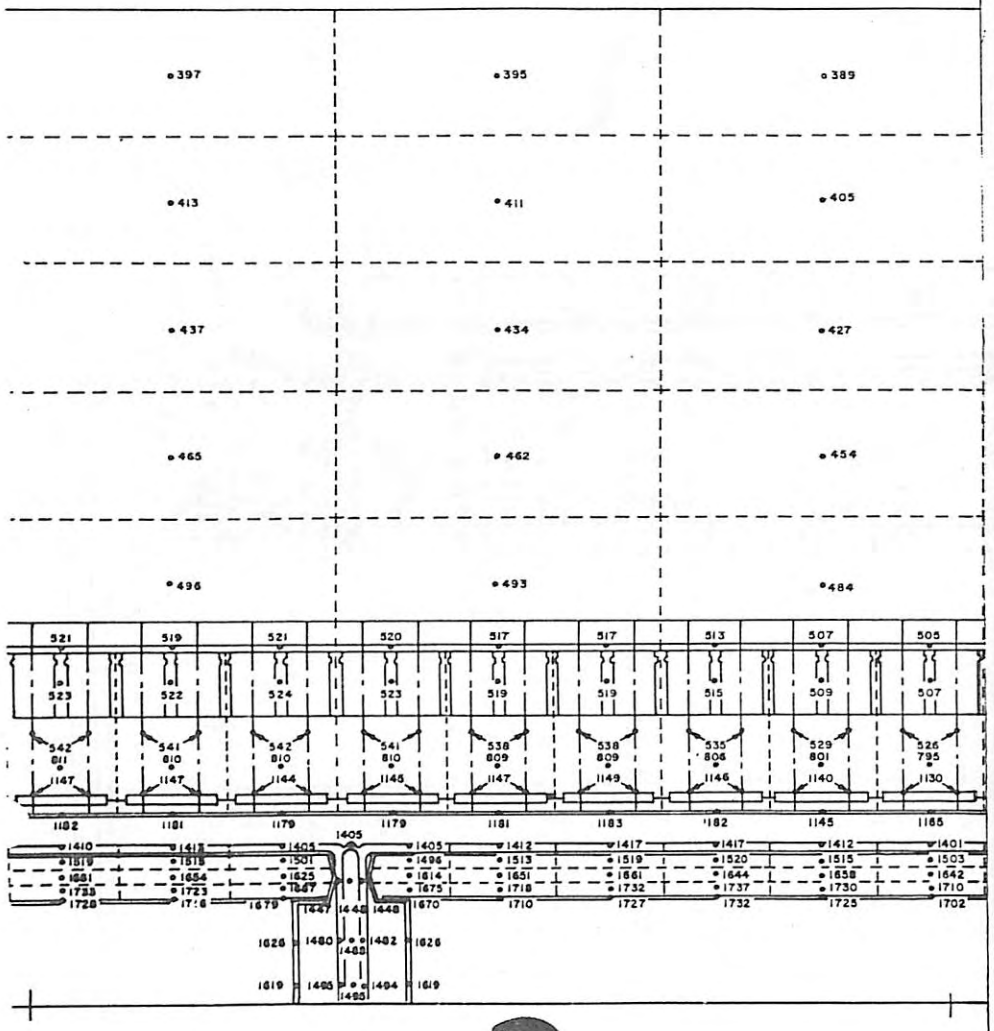

2

BLANK PAGE

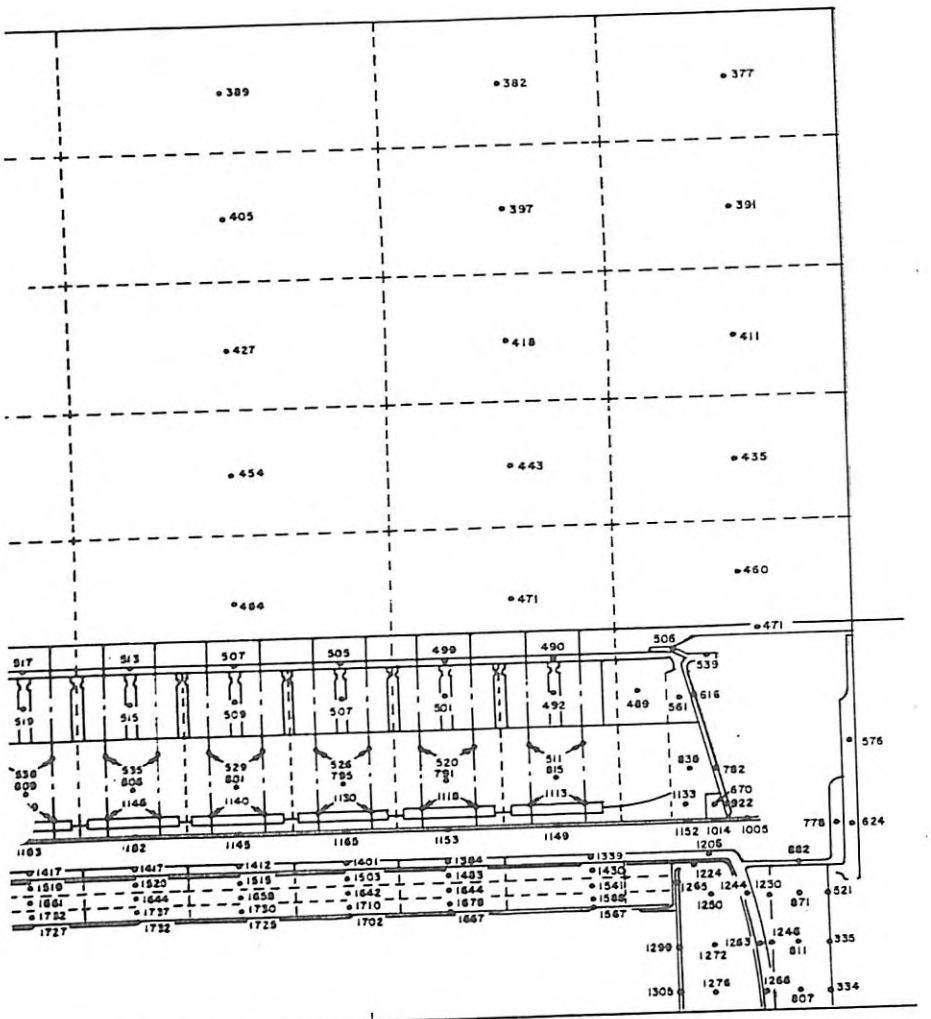

Figure 5-28. Generator Model Fin, Plane Nodal Temperature Map (Maximum Sinks = 237°F, Top 169°F, Sides).

5-41/5-42

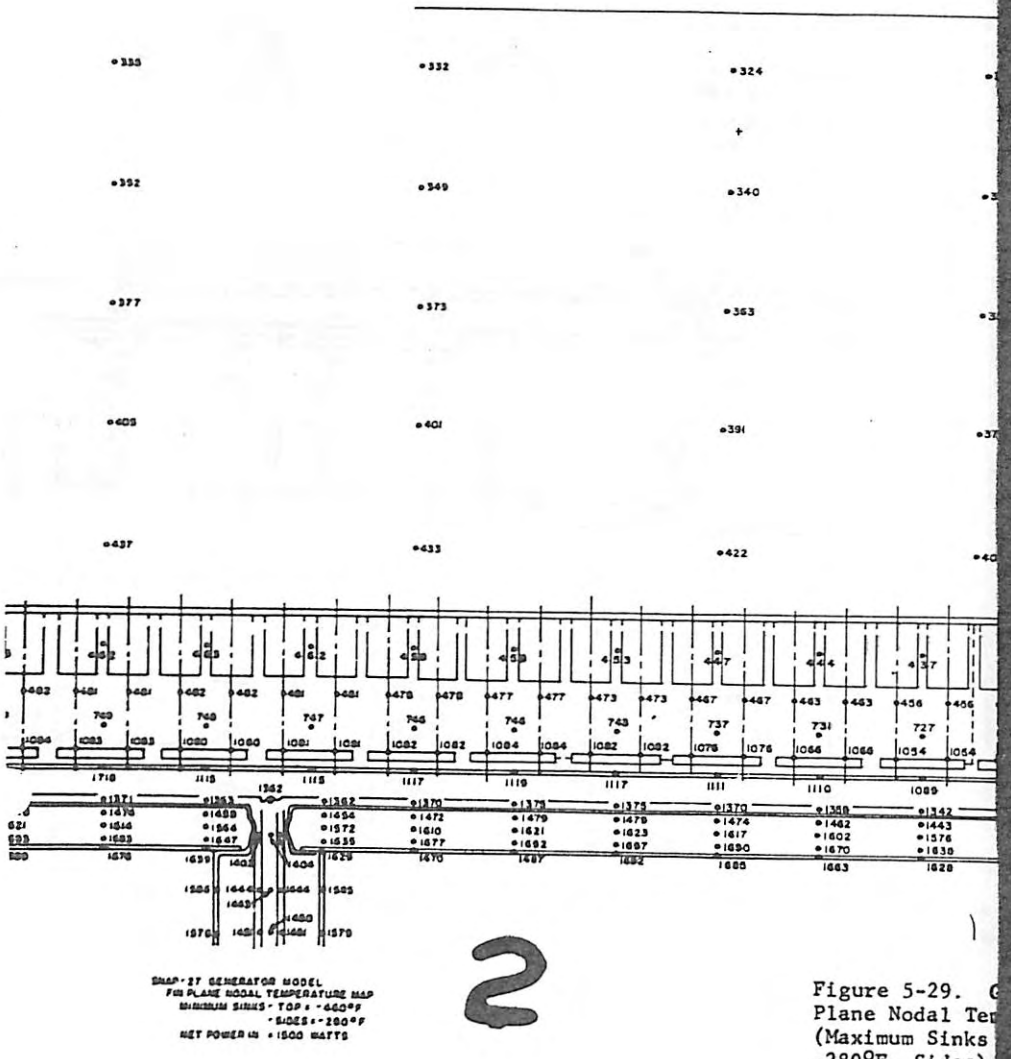

Figure 5-29. G
Plane Nodal Te
(Maximum Sinks
-280°F, Sides)

BLANK PAGE

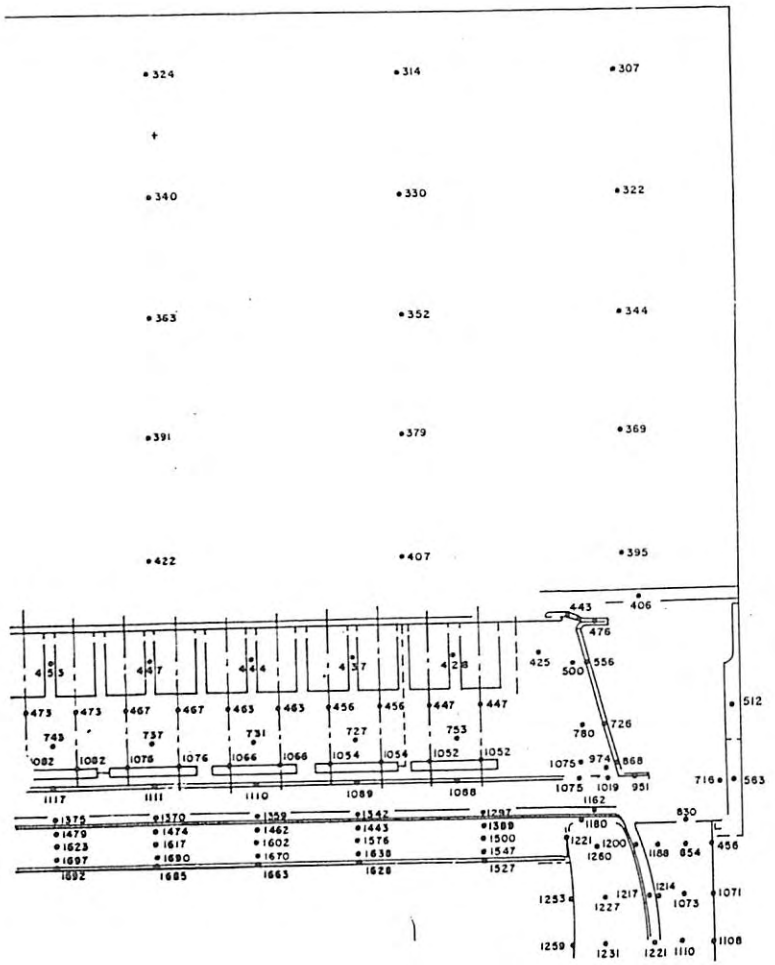

Figure 5-29. Generator Model Fin, Plane Nodal Temperature Map (Maximum Sinks = -460°F, Top, -280°F, Sides)

3

5-43/5-44

TABLE 5-8. SUMMARY OF GENERATOR ASSEMBLY DYNAMIC RESPONSE(1)

TYPE OF RESPONSE	ACCEL.	AXIAL LOCATION AND ELEMENT	REMARKS
Response to a 1 g Sinusoidal Input 1st mode	2.12 g	6.93 (cold frame)	410 cps
	5.72 g	11.37 (cold frame)	
	10.04 g	16.31 (cold frame)	
	10.19 g	16.485 (cold frame-trans.)	
	11.38 g	17.95 (cold frame)	
	10.72 g	16.835 (hot frame-trans.)	
	10.66 g	16.310 (hot frame)	
	8.78 g	11.37 (hot frame)	
	4.25 g	6.73 (hot frame)	
2nd mode	0.74 g	6.93 (cold frame)	687 cps
	1.09 g	16.31 (cold frame)	
	1.11 g	16.485 (cold frame-trans.)	
	1.36 g	17.95 (cold frame)	
	1.17 g	16.835 (hot frame-trans.)	
	1.10 g	16.310 (hot frame)	
	1.74 g	11.37 (hot frame)	
	1.56 g	6.73 (hot frame)	
3rd mode	3.29 g	6.93 (cold frame)	1433 cps
	2.55 g	11.37 (cold frame)	
	1.12 g	16.31 (cold frame)	
	1.21 g	16.485 (cold frame-trans.)	
	1.99 g	17.95 (cold frame)	
	1.97 g	16.835 (hot frame-trans.)	
	2.64 g	16.310 (hot frame)	
	5.10 g	11.37 (hot frame)	
	6.16 g	6.73 (hot frame)	
Response to a Random Input	11.85 g (rms)	0.4 (cold frame)	See note (2)
	12.09 g (rms)	0.8 (cold frame)	
	12.21 g (rms)	1.49 (cold frame)	
	18.84 g (rms)	6.93 (cold frame)	
	19.81 g (rms)	11.37 (cold frame)	
	29.12 g (rms)	16.31 (cold frame)	
	29.67 g (rms)	16.485 (cold frame-trans.)	
	34.39 g (rms)	17.95 (cold frame)	
	31.92 g (rms)	16.835 (hot frame-trans.)	
	32.03 g (rms)	16.310 (hot frame)	
	31.07 g (rms)	11.37 (hot frame)	
	25.54 g (rms)	6.73 (hot frame)	
Shock	18.0 g -28.4 g	1.49 (cold frame)	See note (3)
	21.8 g -17.8 g	6.93 (cold frame)	
	18.0 g -32.0 g	11.37 (cold frame)	
	32 g -46 g	16.31 (cold frame)	
	32 g -47 g	16.485 (cold frame-trans.)	
	34.6 g -49 g	17.95 (cold frame)	
	35 g -45 g	16.835 (hot frame-trans.)	
	36 g -50 g	16.310 (hot frame)	
	38 g -41.8 g	11.37 (hot frame)	
	21.6 g -35 g	6.73 (hot frame)	

NOTES: (1) Input excitation applied at Base Mounting Plate
(2) Random input excitation was qual. levels
(3) Shock input level was 45 g - 11 ms - peak terminal sawtooth

thermal power for a lunar day environment. (This increases to 0.8 watt change for a 10 thermal watt change for a lunar night environment.) Therefore, there will be an average decrease of 0.9 watt in the electrical output power as a result of isotope decay given in BOL fuel loading of 1480 watts.

The effect on electrical output power due to thermoelectric degradation was based on previously determined correlations. Thermoelectric degradation was analyzed only for the ± 8 percent unsymmetric loading of the liner assemblies.

Table 5-11 shows the hot junction temperatures for both lunar day and lunar night environments and the corresponding EOL power ratio, P/P_{TH}. The lunar day hot junction temperatures were obtained from Figure 5-30(c); the lunar night hot junction temperatures were evaluated by having a knowledge of previous generator/capsule analyses.

The EOL power ratio was 0.957; translated, this means a 2.9 watt decrease in the electrical power output due to thermoelement degradation. The final EOL electrical power output of the generator for the ± 8 percent unsymmetric loading of the liner assemblies is then 63.9 watts.

5.3.5 DEGRADATION MECHANISM OF THE SNAP-27 TYPE THERMOELEMENTS

The SNAP-27 thermoelements are referred to by the 3M Company terminology of 3N (N-type) and 3P (P-type). The N-type is a lead-tellurium compound with iodine added in various amounts as a doping agent to achieve optimum thermoelectric properties over a particular temperature operating range. The P-type is a lead-tin-tellurium compound with sodium as the doping agent. The P-type also contains some manganese which also appears to act as a dopant.

Review of test data and physical examination of couples after testing has established that the controlling mechanism responsible for the decrease in power output of the SNAP-27 type couple is the sublimation of the N element material at the hot junction. This sublimation phenomena eventually results in the N element geometry changing from a cylinder to a domed cylinder as illustrated below.

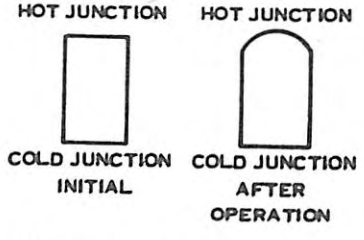

TABLE 5-11. HOT JUNCTION TEMPERATURES VERSUS EOL POWER RATIOS FOR LUNAR DAY/NIGHT

AXIAL ROW	HOT JUNCTION TEMPERATURE (°F)		P/P_{TH}	
	Lunar Day	Lunar Night	Lunar Day	Lunar Night
1	1022	975	1.0	1.0
2	1023	976	1.0	1.0
3	1027	981	1.0	1.0
4	1033	989	1.0	1.0
5	1041	998	1.0	1.0
6	1052	1010	0.988	1.0
7	1065	1023	0.971	1.0 1.0
8	1082	1039	0.938	1.0
9	1098	1055	0.898	0.984
10	1111	1068	0.858	0.966
11	1122	1079	0.832	0.944
12	1125	1081	0.826	0.941
13	1121	1076	0.834	0.951
14	1111	1068	0.858	0.966
15	1095	1052	0.906	0.988
16	1075	1033	0.953	1.0
17	1066	1026	0.969	1.0
		Ave. P/P_{TH}	0.931	0.984
		Overall Average	0.957	

This modified shape represents a decrease in the effective area to length ratio of the leg and consequently results in an increase in the electrical resistance of the leg with a subsequent decrease in power output at constant hot and cold junction temperature. The sublimation phenomena is much less severe in the P-leg. A thin manganese complex layer has been found at the P-leg surface. It is postulated that this is partially responsible for the reduced sublimation of the P-leg.

The sublimation of the N-leg with its resulting decrease in effective area to length ratio results in a decrease in the thermal conductance of the leg. This means that for constant hot and cold junction temperatures, less heat can be conducted through the leg or couple. Conversely, for a constant heat input to the couple, the hot junction temperature must rise to a higher level. Since the sublimation rate is a function of temperature, the higher the temperature the greater the sublimation rate and, consequently, a self-aggravating process exists. In addition to this thermal conductance decrease phenomenon, there is a reduced Peltier cooling effect. This effect also tends to drive up the hot junction temperature for a constant heat input system. Therefore, in test programs where the hot junction temperature is controlled to a constant value, as in single-couple or 10-couple module tests, the significant information obtained is the change in internal electrical resistance as a function of time at that particular operating temperature.

Constant heat input tests cannot be performed on a configuration with a small number of couples because the extraneous heat losses are usually larger than the heat input for the couples. Any tendency for the hot junction temperature to rise is greatly suppressed by the increased extraneous losses with increasing temperature. However, constant hot junction temperature tests are valuable if they are conducted for a wide range of temperatures. This data can then be incorporated into a digital computer program to predict the internal resistance.

At this point, the SNAP-27 program has established the internal resistance rate of change as a point function of hot junction temperature. A theoretical model has also been developed to correlate the increase in internal resistance with the decrease in thermal conductance.

Prior to presenting the results of the theoretical model, another facet of the degradation phenomena must be considered. As the hot junction temperature rises, the emf or open circuit voltage of the couple or generator increases. The power output can be approximated by

$$P = C_1 \frac{E_{oc}^2}{R_I} = \frac{(\bar{\alpha}_{N+P} \Delta T)^2}{R_I}$$

where

P = power output

C_1 = a constant

E_{oc} = open circuit voltage

R_I = internal electrical resistance

$\bar{\alpha}_{N+P}$ = average Seebeck coefficient

ΔT = hot to cold junction temperature difference

Therefore, if there were a one to one correspondence between an increase in internal resistance and a decrease in thermal conductance, the net effect would be an increase in power output because of the second power effect of ΔT in the numerator.

The first attempt to determine the relationship between the thermal conductance and electrical resistance has been made by analysis of the SNAP-27 Mod 5 generator which has accumulated about 10,000 hours of test time with a lunar day hot junction of ~1075°F and a lunar night temperature of 1015°F. During testing, the hot junction temperature increased by ~20°F as determined from open circuit voltage measurements. This generator exhibited a measured internal resistance increase of approximately 15 percent which would have resulted in a power decrease of the same magnitude if there were no corresponding increase in hot junction temperature. The actual power output decrease was ~5 percent. Analysis of the test data indicated that a proportionality constant of 0.45 between thermal conductance decrease and electrical resistance increase fit the experimental data quite well. However, when this same proportionality constant was used to predict performance at higher initial hot junction temperatures, the results in some cases indicated a decrease in power initially, followed by a leveling off of the power as the hot junction continually increased. In some cases of high initial hot junction temperature of 1200°F, the power output for 1 year increased slightly after an initial 10 percent decrease. As of this writing, the theoretical model is still under development.

5.4 DEVELOPMENT TEST PROGRAMS

Representative tests which were conducted during development of the generator are discussed here.

5.4.1 COLD FRAME MODEL TEST

This test was conducted by Solar to make an early evaluation of the shrink fit assembly process. An outer shell with brazed dove tail fins was shrunk fit onto an inner cold frame, the outer heated to 615°F and allowed to stabilize. The cold frame was then inserted into the uter case, and the assembly (Figure 5-31) allowed to cool. Dimensional data before and after shrink fitting are given below:

a. Inner case, before shrink fit
   OD (avg) = 4.98776 inches
   ID (avg) = 3.99726 inches

b. Outer case, before brazing and shrink fit
   T (avg) = 0.0702 inches
   ID (avg)= 4.9844 inches

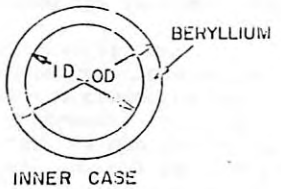

c. Outer case, after brazing of fins, before shrink fit
   Between fins, ID (avg)
   = 4.98403 inches
   Under fins, ID (avg)
   = 4.98581 inches
   Average of total, ID
   = 4.98492 inches

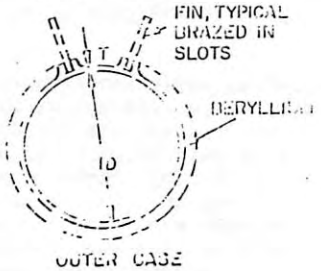

d. Inner case, after shrink fit
   ID (avg) = 3.996765 inches

5.4.2 SHRINK FIT THERMAL TEST

This test was conducted by Solar to make an early evaluation of heat transfer effectiveness of the shrink fit concept in terms of interference fits and faying surface finishes.

The test was run by soaking the outer case at 545 ± 15°F for one-hour. The inner cold frame was then inserted manually into the outer case. The power to the outer case was turned off and the assembly allowed to cool slowly.

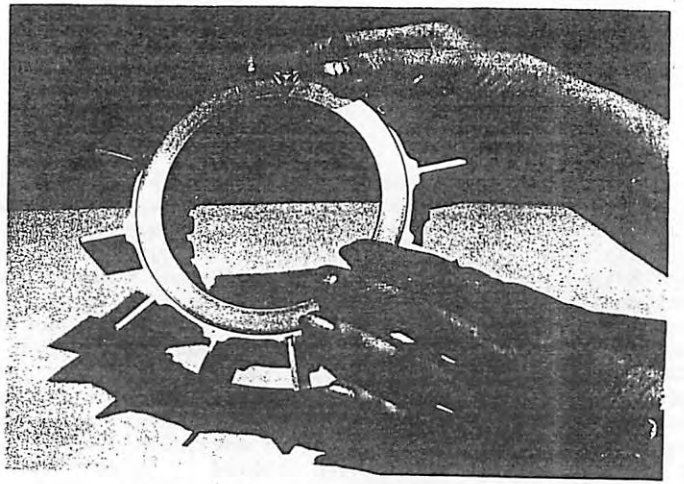

Figure 5-31. Shrink Fit Assembly

Evaluations of the heat transfer effectiveness of the faying surfaces were performed by thermal and infrared methods. In essence, the thermal test technique relied on gauging the rate of flow of heat in the solid material. The readout is accomplished by remote surface measurements with an infrared radiometer. A-scan radiometer plots were taken and the effectiveness of faying surface heat transfer evaluated. By being rotated upon its axis on a turntable, the assembly was subjected to constant speed circumferential scans on the outside cylindrical surface with a small radiant heat spot; the heat spot is followed by the focus of an infrared radiometer, which measures the surface temperature (see Figure 5-32).

Outer surface temperature is therefore a function of interface contact quality; it will be hotter than normal if any of the following conditions are present at the interface:

a. A hole in the cold frame

b. Poor contact because of surface preparation

c. Poor contact because of eccentricity or other geometric anomoly

d. Gross defects in the faying surfaces causing interface voids.

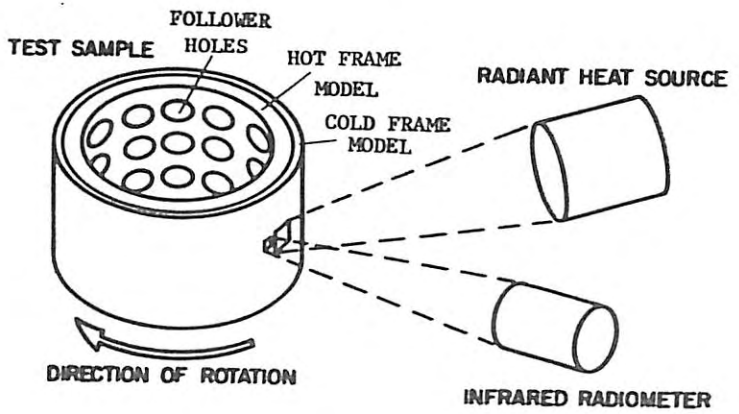

Figure 5-32. Measurement of Surface Temperature on Shrink Fit Thermal Test Unit

5.4.3 FIN VIBRATION TESTS

A cross-rolled sheet fin and a hot pressed block fin each of the split design (Figure 5-33), were vibrated perpendicular to the plane of the fins to determine their structural integrity. The fins were instrumented with a miniature accelerometer on each of the three different-size fin sections. The first phase in the testing was a low-level sine resonance search to determine the natural frequency of each of the three different sized fin sections. Following this, a five-minute sine dwell was maintained at each of the three natural frequencies, at a sine "g" input equivalent to the qualification test random levels of 0.044 G^2/cps, with no visual evidence of failure for any of the sections for either fin noticed. At the conclusion of the foregoing, a low-level sine resonance search was run to determine any change of natural frequency, thus indicating failure of the fin section. No appreciable change was noted. The hot-pressed block fin then was subjected to additional testing in an effort to determine its point of failure. Another five-minute sine dwell at each of the three natural frequencies was run, this time at a "g" input equivalent to the old qualification random levels of 0.075 G^2/cps, with no visual evidence of failure noticed. Another low-level sine resonance search was run to determine any

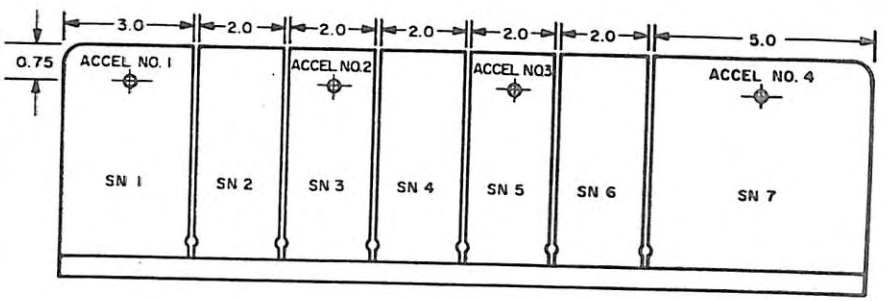

DIRECTION OF VIBRATION PERPENDICULAR TO PLANE SHOWN

Figure 5-33. Split Design Fin

change of natural frequency, with no appreciable change noted. The final attempt to fail a fin section was to increase the input to 30 g's at the natural frequency of the larger (five inches) fin section (this section showed the highest response during other testing). At 30 g's input, the response at the tip of the fin was 950 g's with no evidence of any failure. This was the force limitation of the electrodynamic exciter used. It was therefore concluded, that either the hot pressed block or the cold-rolled sheet fin will perform adequately under the SNAP-27 vibration environment.

5.4.4 GENERATOR MOD 1 PROOF TESTS

This early model was a full size 12-fin generator less a thermopile, (Figure 5-34). The final configuration of this generator had to be modified due to difficulties encountered in fabrication and assembly of the power and instrumentation headers. The solid pin headers were replaced by stainless steel tubes and "potted" with silicon rubber cement. During the thermal vacuum tests, the hermetic seal enclosure was pressurized with argon, at 15 psia, through a line which penetrated the vacuum chamber and terminated outside the chamber at a pressure regulator attached to an argon source. The generator was heavily instrumented with thermocouples to measure temperature gradients across

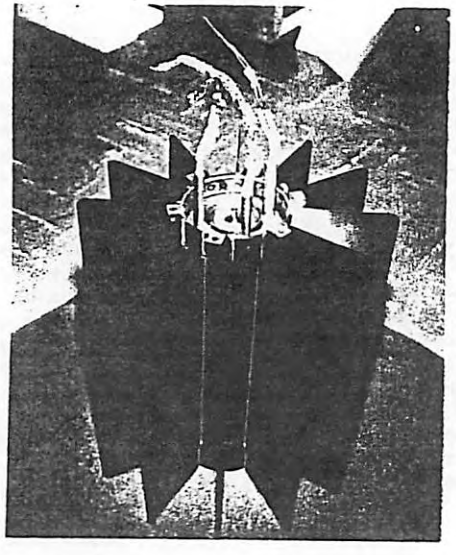

Figure 5-34. Generator (Base View)

the outer case fins, end-plates and seals. Internal pressure was monitored by a pressure transducer.

The testing was divided into three separate phases:

a. Phase A - Thermal vacuum conditions for a thermal power level of 1400 watts (supplied by an electric heater). Chamber pressure of 10^{-5} torr and sink temperatures of -280°f, + 40°F, + 110°F and + 170°F.

b. Phase B - Shock and vibration tests.

c. Phase C - Repeat of Phase A with the additional tests at power levels of 1500 watts and 1200 watts for sink temperatures of +170°F.

Results from the thermal vacuum testing indicated that the heat conducted through the mounting feet to the mounting plate was 80 to 90 watts total, that the outer case temperatures appeared to be 20 to 40°F below the predicted values and that the temperature gradients radially outward through the cold frame and outer case (across the shrink fit) were excessive.

Dimensions recorded for the cold frame outer diameter and outer case inner diameter prior to shrink fit indicated the possibility of the existence of at least a five mil gap between the shrink fit in some areas which would have accounted for the large ΔT's recorded during the test.

Vibration and shock tests were performed as follows:

a. Vibration

1. Sinusoidal - The generator was vibrated in each of the three major orthogonal axes for five minutes per axis at the following levels applied at a constant sweep rate from 5 to 2000 to 5 cps.

Amplitude	Frequency (cps)
+ 0.11 inch DA	5 to 16
1.4 g	16 to 150
1.98 g	150 to 300
4.52 g	300 to 2000

2. Random - The generator was also vibrated for two minutes in the three major orthogonal axes at the following levels:

Level	Frequency (cps)
0.3 g^2cps	10 to 300
6 db/octave decrease to 0.1 g^2/cps	300 to 520
0.1 g^2/cps	520 to 1200
12 db/octave decrease	1200 to 2000

b. Shock - The generator was subjected to a shock impulse of sawtooth configuration having peak value of 45 g's and a duration of 11 milliseconds with a 2-millisecond decay.

The shock and vibration tests produced no visible damage to the generator.

5.4.5 THERMOELECTRIC LEG PRODUCT SPECIFICATION (TELPS) PROGRAM

The lead telluride family of thermoelectric materials has been used successfully in commercial generators since the mod-1950's. However, certain thermopile tests indicated performance changes with time. It was the opinion of the Minnesota Mining and Manufacturing Company that lead telluride and lead tin telluride as fabricated by them was stable when subjected to a temperature gradient in a suitable protective environment and that any degradation of output, if present, should not be blamed on the leg proper. At the direction of the AEC, General Electric and Minnesota Mining and Manufacturing Company devised and conducted a program designed to resolve this question of variation in leg performance with time and temperature.

The Thermoelectric Leg Product Specification Program (TELSP) embodied several test series including material characterization, simulated performance and post performance tests.

The objectives of the overall program were defined as follows:

a. Preparation of a thermoelectric leg product specification, with all necessary supporting test and process documents, that identifies the manufactured properties and parameters of specific SNAP-27 thermoelectric material grades as consistent with demonstrated performance

b. Preparation of documents and development of inspection procedures to permit selection and acceptance of thermoelectric materials within the scope of the specification in (a) above

c. Development and demonstration of a standard performance test for SNAP-27 elements

d. Acceptance by both General Electric and Minnesota Mining and Manufacturing Company of the validity of the documents, tests and procedures developed under (a), (b) and (c) above.

Ground rules that generally guided the sense of the program effort are summarized below:

a. The aim of the task was twofold. Initial emphasis was placed upon characterizing production material and providing workable acceptance tests. In addition, correlation of physical parameters with performance was performed so that a specification could be prepared for long life material

b. The ultimate test criterion was chosen to be stable, reproducible life. A basic assumption was made that a suitable test environment could be provided for each test specimen for the duration of each test

c. Acceptance tests were to be oriented toward grading materials with respect to particular parameters rather than establishing go-no-go conditions

d. The assumption was made that reproducible, predictable performance depends upon uniformity in critical parameters in the fabricated element

e. The assumption was also made that the technology for production of long-lived materials exists; this program was directed toward weeding out, from typical parameter variations encountered in production, those combinations of parameters that result in early failure

f. Likewise, it was assumed that satisfactory values for each parameter to be measured lay within the distributions encountered in the current product. Efforts were directed toward establishing and selecting mean values which were consistent with stability until other values were shown to lead to better life performance

g. Maximum effort was made to utilize other SNAP-27 efforts in the execution of this task. Separate tests were proposed only where required to avoid duplication.

An additional aspect of this program was that no data of a confidential and/or proprietary nature was utilized or generated during its execution and that results would be rapidly and widely dispersed through public information channels. It was hoped that the thermoelectric characterization and performance test equipment and procedures generated by this program would eventually gain industrial approval and acceptance as a routine standard.

Tests were performed on N-type PbTe and P-type PbSnTe SNAP-27 thermoelectric legs, designated by production drawings B-45-1001, Rev. 1 and B-45-1002, Rev. 1 (Figure 5-35).

Legs which were out of nominal tolerance on dimensions or on thermoelectric properties were not rejected, but were included in the test program to ascertain the influence of these deviations on performance and life.

NOTES:
1. MATERIAL TPM-211 RAW MATERIAL INSPECT PER TPI-71 LEVEL II, FINISHED LEG INSPECT PER TPI-71 LEVEL III
2. DENSITY LOWER LIMIT -129 gm/in³
3. INSPECT PER TPI 89

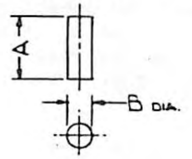

PHYSICAL		
	DIM'S.	TOL.
A	.400	±.005
B	.207	±.003

ELECTRICAL	
	PROPERTIES
ρ	108 TO 132 μ Ω in (TEMP 75°F)
Es	Min. 48 mv @ 600°F ΔT (Tc-75°F REF)

a. Leg N-Type B-45-1001

NOTES:
1. MATERIAL TPM-206 RAW MATERIAL INSPECTED PER TPI-71 LEVEL II, FINISHED LEG INSPECTED PER TPI-71 LEVEL III
2. DENSITY LOWER LIMIT 103 gm/in³
3. INSPECT PER TPI 89

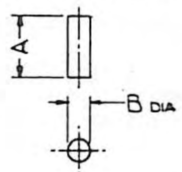

PHYSICAL		
	DIM'S.	TOL.
A	.400	±.005
B	.247	±.003

ELECTRICAL	
	SPEC'S.
ρ	320 TO 450 μ Ω in (TEMP 75°F)
Es	Min. 62 mv @ 800°F ΔT (Tc-75°F REF)

b. Leg P-Type B-45-1002

Figure 5-35. Thermoelectric Legs

All legs for these tests were accepted from regular SNAP-27 Phase III production batches after quality control procedures were completed. Legs were drawn at the rate of approximately 40 per batch.

Four lots were represented in this test program:

Lot 4 Lot 5	N-type P-type	35 batches 25 batches	Lots 4 and 5 are used in 10-couple, early 104-couple modules and engineering generators
Lot 9 Lot 10	N-type P-type	35 batches 35 batches	Lots 9 and 10 are used in late 104-couple modules, qualification and flight generators

The change from Lot 4 and 5 production to Lot 9 and 10 production took place during September and October 1966 and represented primarily tighter process control and in-process testing by 3M during leg production.

Results from the long-term ingradient tests did not succeed in universally demonstrating the degree of stability of performance of which the materials are believed capable. In general, the changes observed in resistance, Seebeck voltage and power with time were more severe and occurred more rapidly than the counterpart tests on instrumented legs conducted in hermetically sealed modules in other SNAP-27 tests. Thus, the question of ultimate stability of the materials remains unresolved. The observed behavior strongly suggests that the performance changes are at least partially due to environmental influences. The drop in Seebeck voltage and resistance of the P-legs and the increase in power are consistent with the changes which have been observed on legs diliberately contaminated by water vapor. The P-leg property changes are confined to the hot end of the leg and as such are beneficial to a degree in that the S^2/ρ distribution along the leg length is improved over that of a freshly manufactured leg; that is, the leg beneficially segments itself during operation with respect to its ability to produce power. The effects of such changes on thermal conductivity have not been studied. It is not known, therefore, what the effect on efficiency is.

Some of the resistance change noted in both N- and P-legs is due to changes in the leg geometry with time and temperature. At 1090°F hot junction temperature, the N-leg geometry changes are due primarily to plastic deformation of the hot end since no significant change in leg volume with leg length was noted. The P-leg, however, shows definite evidence of swelling since dV/dL is negative and an order of magnitude higher than that observed for the N-legs. For both P- and N-legs at higher hot junction temperatures, the leg geometry versus time and

temperature is governed by the rate of sublimation. The rate of material loss due to sublimation was determined in the absence of junction electrode buttons and thermal insulation material surrounding the legs. The possible influence of these factors on sublimation rates is not known.

In addition to the changes in area and length of the legs with time and temperature, the rounding of the hot end and consequent loss of hot junction area with time and temperature further complicates the interpretations of the resistance measurements.

In summation, the test program accomplished a number of goals:

a. Product specifications for SNAP-27 N-type PbTe and P-type PbSnMnTe were developed on the basis of the results of an extensive test and test development program

b. An ingradient test fixture and test procedure were developed which demonstrated capability of making rapid, accurate and precise measurements of ingradient resistance and Seebeck voltage values of SNAP-27 PbTe and PbSnMnTe thermoelectric legs over extended periods of time and various junction temperatures without the need of special electrical contacts

c. Computerized techniques were developed to handle the tasks of data reduction, normalization of performance data to specific operating junction temperatures, data sorting, and ultimate data plotting

d. A new rapid technique for the simultaneous determination of the thermoelectric properties S, K, and $K \cdot \rho$ of individual test specimens as functions of temperature was developed and tested. These test results have been used to establish beginning of life specification limits on the thermoelectric properties of SNAP-27 materials

e. An ingradient soak test fixture and testing technique was developed which demonstrated the feasibility for large-scale ingradient testing of thermoelectric legs

f. A number of physical, chemical, and metallurgical characteristics of SNAP-27 legs were determined and included in the specification for engineering references

g. Oxygen content in PbSnMnTe was identified as a critical characteristic and acceptance limits established.

The final report on this test program is summarized in Reference 5-5.

5.4.6 10-COUPLE MODULE TEST PROGRAM

This program was carried out to provide backup information for the SNAP-27 generator's initial design point which was chosen on a "best estimate" basis, using the relatively incomplete data available at the time. A total of 19 10-couple modules participated in the test program. Table 2-4, shown previously, summarizes the test conditions for each of these modules as well as the total time on test. The objectives of this program were:

a. To demonstrate performance and obtain data on the thermopile assemblies in extremes of expected environments

b. To obtain possible failure modes and material interactions

c. To provide an experimental basis for predicting thermopile performance

d. To establish, if necessary, environmental limits of operation.

Figures 5-36 and 5-37 show a 10,000 hour thermopile assembly, Figures 5-38 and 5-39 show the complete 10-couple module, and Figure 5-40 shows the 10-couple module test laboratory.

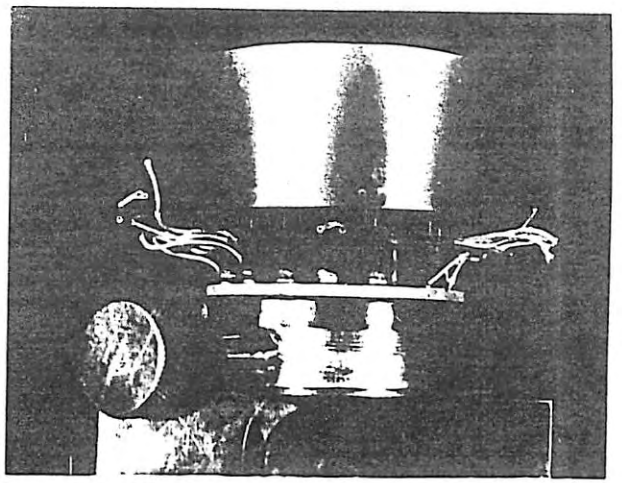

Figure 5-36. Typical 10-Couple Thermopile Assembly

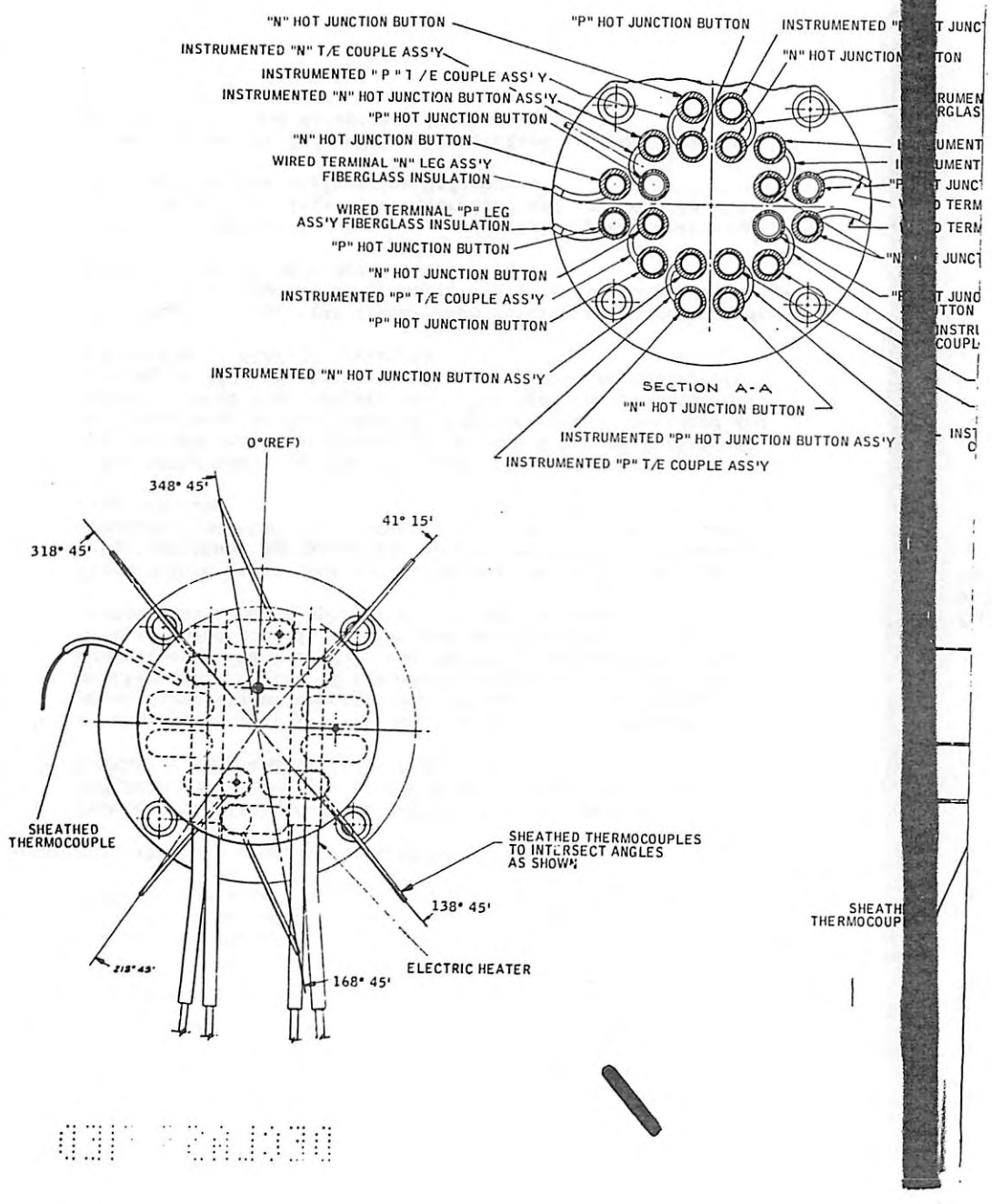
"N" HOT JUNCTION BUTTON
INSTRUMENTED "N" T/E COUPLE ASS'Y
INSTRUMENTED "P" T/E COUPLE ASS'Y
INSTRUMENTED "N" HOT JUNCTION BUTTON ASS'Y
"P" HOT JUNCTION BUTTON
"N" HOT JUNCTION BUTTON
WIRED TERMINAL "N" LEG ASS'Y FIBERGLASS INSULATION
WIRED TERMINAL "P" LEG ASS'Y FIBERGLASS INSULATION
"P" HOT JUNCTION BUTTON
"N" HOT JUNCTION BUTTON
INSTRUMENTED "P" T/E COUPLE ASS'Y
"P" HOT JUNCTION BUTTON
INSTRUMENTED "N" HOT JUNCTION BUTTON ASS'Y
"P" HOT JUNCTION BUTTON
INSTRUMENTED "N" T/E COUPLE ASS'Y
"N" HOT JUNCTION BUTTON
SECTION A-A
"N" HOT JUNCTION BUTTON
INSTRUMENTED "P" HOT JUNCTION BUTTON ASS'Y
INSTRUMENTED "P" T/E COUPLE ASS'Y
0°(REF)
348° 45'
41° 15'
318° 45'
SHEATHED THERMOCOUPLE
SHEATHED THERMOCOUPLES TO INTERSECT ANGLES AS SHOWN
138° 45'
ELECTRIC HEATER
168° 45'

BLANK PAGE

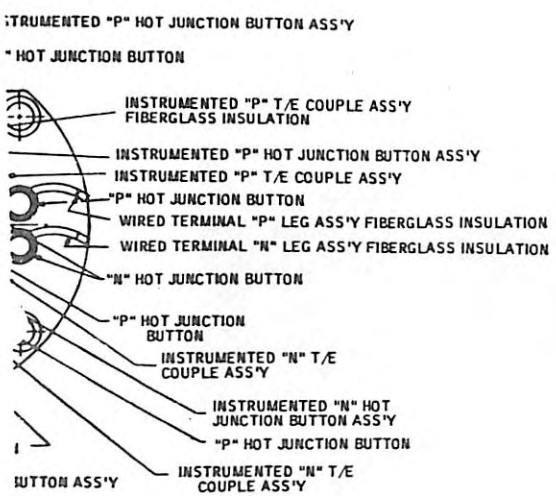

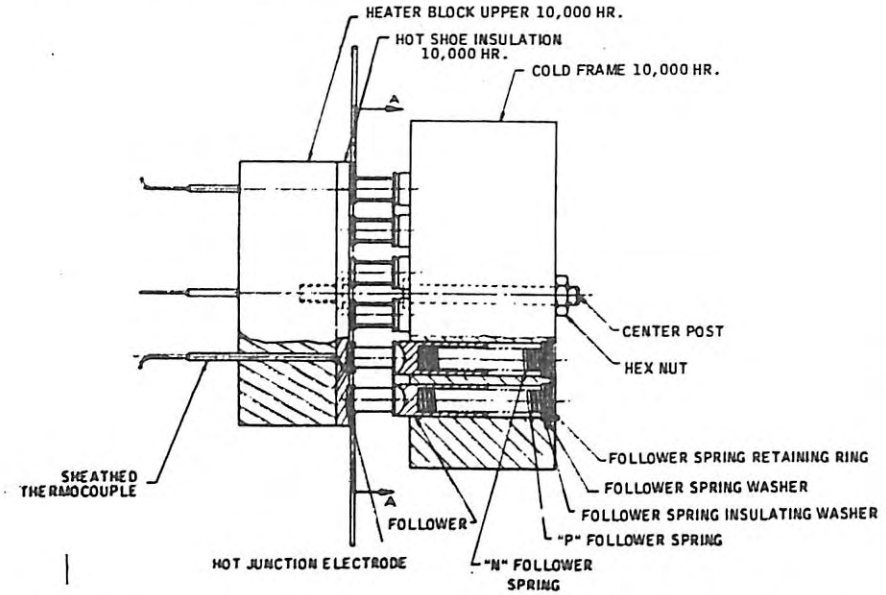

Figure 5-37. Thermopile Assembly, 10,000 Hours

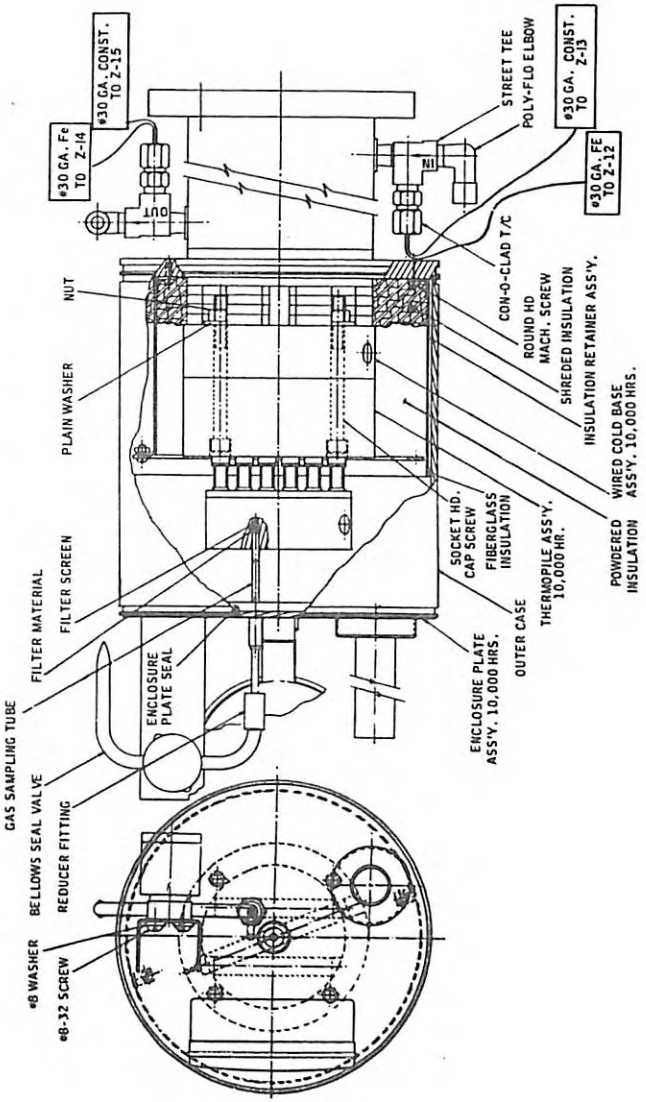

Figure 5-38. Typical 10-Couple Module

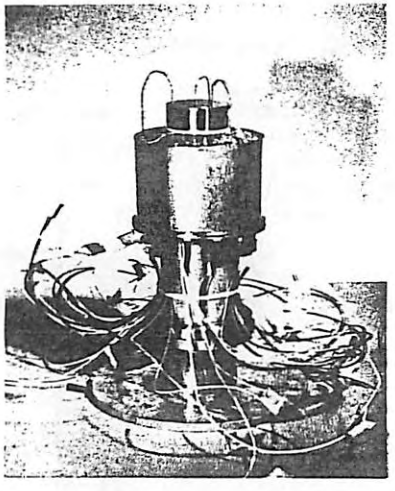

Figure 5-39. Typical 10-Couple Test Fixture

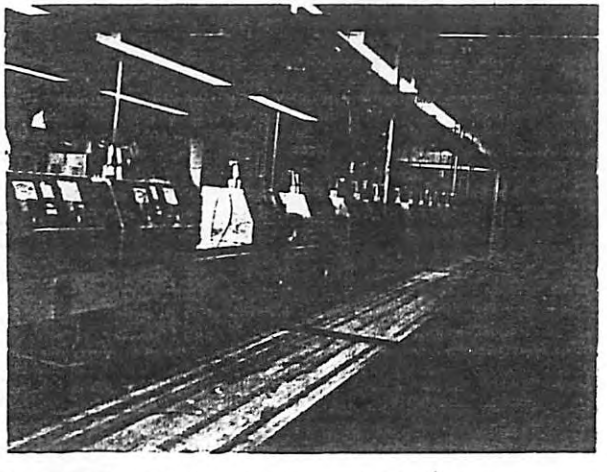

Figure 5-40. Test Laboratory, 10-Couple Module

A typical 10-couple test module is about 17 inches in height, 6 inches in diameter, and weighs about 25 pounds. The test module consists primarily of a heat source, thermoelectric couples, a heat sink, and an insulation subsystem.

The heat source specified for the test modules is a controlled electrical heater. The heater input power will be adjusted until the modules are operating at specified temperatures.

The thermoelectric couple assembly provides direct energy conversion within the module. The thermoelectric couples are sandwiched between the hot frame and cold frame. Each couple consists of a P- and N-leg. The P-leg is 0.400-inch in length and 0.207-inch in diameter and the N-leg is 0.400-inch in length and 0.207-inch in diameter. The legs are connected in electrical series and thermally in parallel. Each module contains two circuits, each circuit consisting of five thermoelectric couples. Each circuit is externally terminated with its own resistive load.

The heat sink consists of a cold frame and cold base. The cold frame transfers the rejected heat from the cold junction of the thermoelectric couple to the cold base. The cold base rejects this heat to a water coolant.

The voids between the components within the module are packed with thermal insulation (Min-K 1301) to a nominal density of 14 pounds per cubic foot. Prior to packing within the module, the thermal insulation is baked to remove the binder and crushed to a particle size of 30 to 50 mesh. The particle insulation is temperature-treated to remove the moisture.

After the module has been packed with thermal insulation, it is processed and then backfilled with argon gas to a pressure of 25 psia at operating temperatures of 1100 to 525°F except for the reduced pressure modules. The modules are provided with a pressure gauge so that the internal pressure may be monitored. A gas sampling tube is provided to facilitate post-test gas analysis.

Table 2-4 outlines the 10-couple module test program and operating conditions. Testing of short term stability modules, B-1 and C-3, was prematurely terminated after 2225 hours and 1832 hours, respectively, due to erratic thermoelectric performance. The performance degradation was indicated by:

a. A decrease in open circuit voltage of all P-legs

b. An increase in some P-leg hot button contact resistances.

A post-test investigation indicated that the decrease in P-leg open circuit voltage was caused by a loss of manganese near the hot end of the element. The increase in P-leg hot button contact resistance was due to the oxidation of this manganese at the hot button-element interface. Manganese oxidation may have been caused by an air leak in the module. There was no significant evidence of contamination of either the P- or N-legs by any of the thermocouple or module hardware. In particular, there was no evidence of beryllium contamination of the thermoelectric materials in Module B-1.

Module C-12, designed to investigate low pressure effects, operated at 2.5 psia and was taken off test after power had dropped to 60 percent of its theoretical value. On all other modules, testing is continuing and, as of June 30, 1969, 3.7 x 10^6 couple hours had been accumulated without any couples failures.

A performance summary for the various test conditions is given in Figures 5-41 through 5-43. It should be noted that the power ratios given here are the ratios of the actual power output of the module divided by the theoretical output, based on the same hot and cold junction temperatures and operating conditions. Power ratios larger than one, which are sometimes experienced, do not reflect inaccuracies in the reduction technique, but show a slightly higher performance of the acutal material than the theoretical data used on the SNAP-27 design (TPM-10-N material and TPM-15-P material).

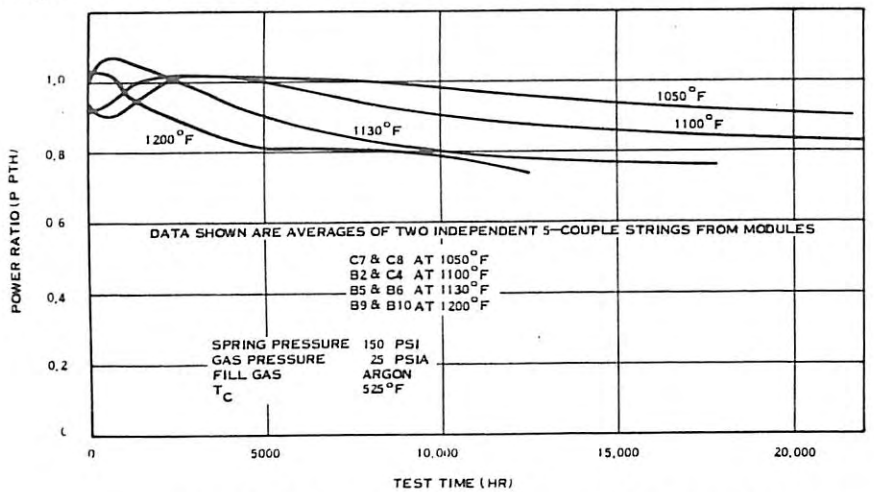

Figure 5-41. Influence of Hot Junction Temperature

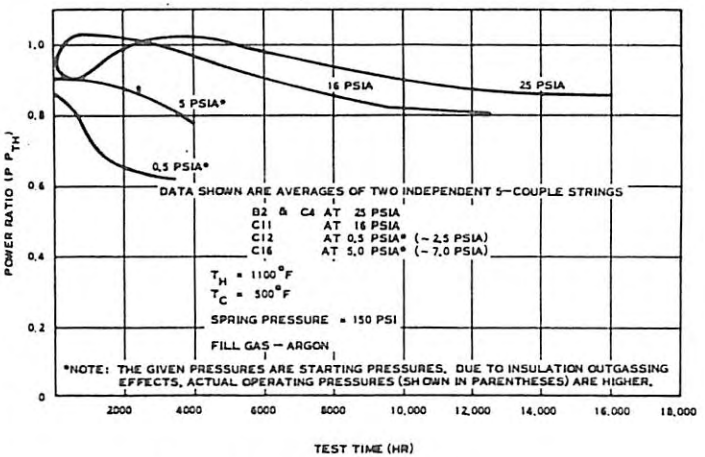

Figure 5-42. Influence of Gas Pressure

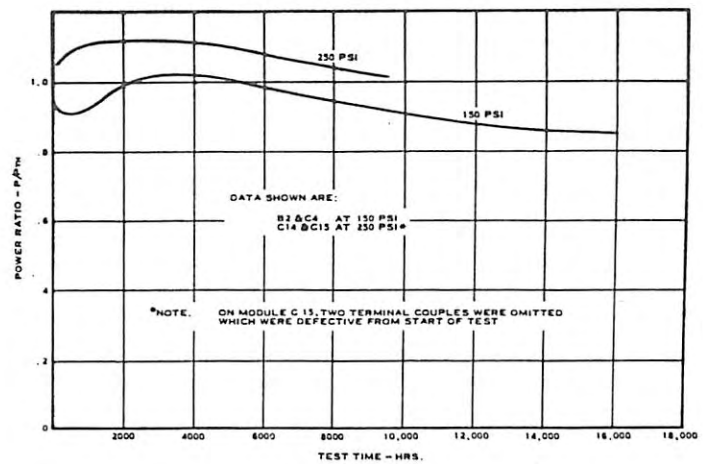

Figure 5-43. Influence of Spring Pressure

The influence of hot junction temperature is summarized in Figure 5-41. All modules below 1200°F show a normal and expected performance-time history. The sudden change in slope for the modules operating at 1200°F around 5000 hours might reflect a change in leg geometry due to sublimation losses and creep deformation; the data are not necessarily meaningful beyond this point, even though they would yield a more optimistic performance pattern. A large portion of the degradation is experienced at the N-leg due to sublimation of thermoelectric material at the hot junction.

Figure 5-42 shows the sensitivity of performance to gas pressure. This is due to the same sublimation effect, as mentioned above, which is suppressed at higher surrounding gas pressures. On Module C-12, a post-test analysis was conducted and a substantial material loss on the N-leg was found with an appreciable geometry change.

Figure 5-43 displays the effect of higher spring pressure on the elements. It can be seen that higher spring pressures have a pronounced effect on "burn in" characteristics at BOL which are an important factor for lower temperature operation. Furthermore, equivalent resistance increases are experienced at considerably later times. The mechanism is also discussed with the degradation model. The performance of the modules which were subjected to an accelerated lunar cycle simulation (35 cycles for C-13 and 24 cycles for C-17) showed that cycling does not have any detrimental effects on performance. This experience was further confirmed on the 104-couple module series and the generators. Higher cold junction temperatures (up to 625°F) were also found to have no effect upon long term performance.

5.4.7 104-COUPLE MODULE TEST PROGRAM

The 104-couple module test program extended the objectives of the 10-couple module test program and provided an experimental basis for predicting full-size generator performance. A total of 15 modules were tested under various operating conditions to determine their performance characteristics, degradation rates and operational reliability.

The 104-couple modules are scale model thermoelectric generators manufactured and assembled for General Electric by the 3M Company. The test module consists primarily of a heat source, the thermoelectric couples, a heat sink and insulation. The design was based on a full size SNAP-27 generator assembly, with the center section removed and the two remaining ends brought together. The removal of the fins was necessitated by the fact that heat rejection rates required for the 104-couple module testing at ambient conditions far exceed that provoded by the fins which were designed for space application. A heat

rejection device called a thermojacket was used in place of fins. A typical 104-couple test module test module is about 7 inches high, 6 inches in diameter and weighs about 20 pounds. The 104-couple module is shown in Figure 5-44; the thermopile assembly is shown in Figure 5-45. The materials and processes used in the 104-modules are the same as those used for the SNAP-27 engineering, qualification and flight generators. The heat source is a one zone (3 circuit) or a four zone controlled electric heater block as shown in Figure 5-46, which is inserted into the hot frame of the module. Heater power is adjustable to provide specified operating temperatures at the thermopile hot junction. The thermoelectric couple assembly provides direct energy conversion within the module. The couples, each consisting of an N-leg and a P-leg, are sandwiched between the hot and cold frames. P-legs are 0.400-inch long and 0.247-inch in diameter; N-legs are 0.400-inch long and 0.207-inch in diameter. Each module contains two circuits of 52 thermocouples each, electrically laddered (or paralleled) by straps connecting adjacent pairs of hot electrodes. The thermopile consists of four axial rows of couples with 26 circumferential positions in each row. The heat sink consists of a cold frame and a thermojacket (Figure 5-47). Heat from the thermojacket is dissipated to the surroundings. Voids between the components in the module are packed with Min-K 1301 thermal insulation. Prior to packing the thermal insulation into the module, the insulation is baked to remove the binder and crusher to a particle size of 30 to 50 mesh. Moisture is removed from the insulation particles by temperature treatment. After the module has been packed with thermal insulation, it is processed and backfilled with argon gas to a pressure of 25 psia at operating temperatures of 1100°F at the hot junction and 525°F at the cold junction. Modules are provided with a pressure transducer so that internal pressures can be monitored. A gas sampling tube is also provided to fabricate post-test gas analysis.

Figure 5-48 depicts a typical 104-couple module thermopile assembly; Figure 5-49 depicts the 104-couple module internal construction details and Figure 5-50 depicts the 104-couple module test lab.

Table 2-5, shown previously, summarizes the 104-couple module testing. As of June 30, 1969, a total of 176,544 couple hours were achieved without failures.

Data is taken on an automatic data acquisition system and stored on tape for further processing. The easiest and most meaningful presentation of data pertinent to generator operation with constant heat input is efficiency versus time, which is almost a direct measure of power output versus time. Figure 5-51 shows module efficiency as a function of time for all modules. Efficiency is herein defined as the measured power output over the total measured heat input of the module. Testing is

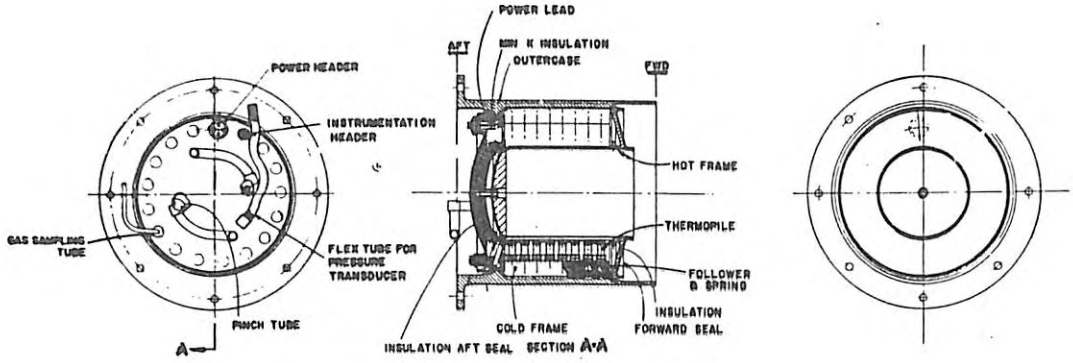

Figure 5-44. Module Assembly

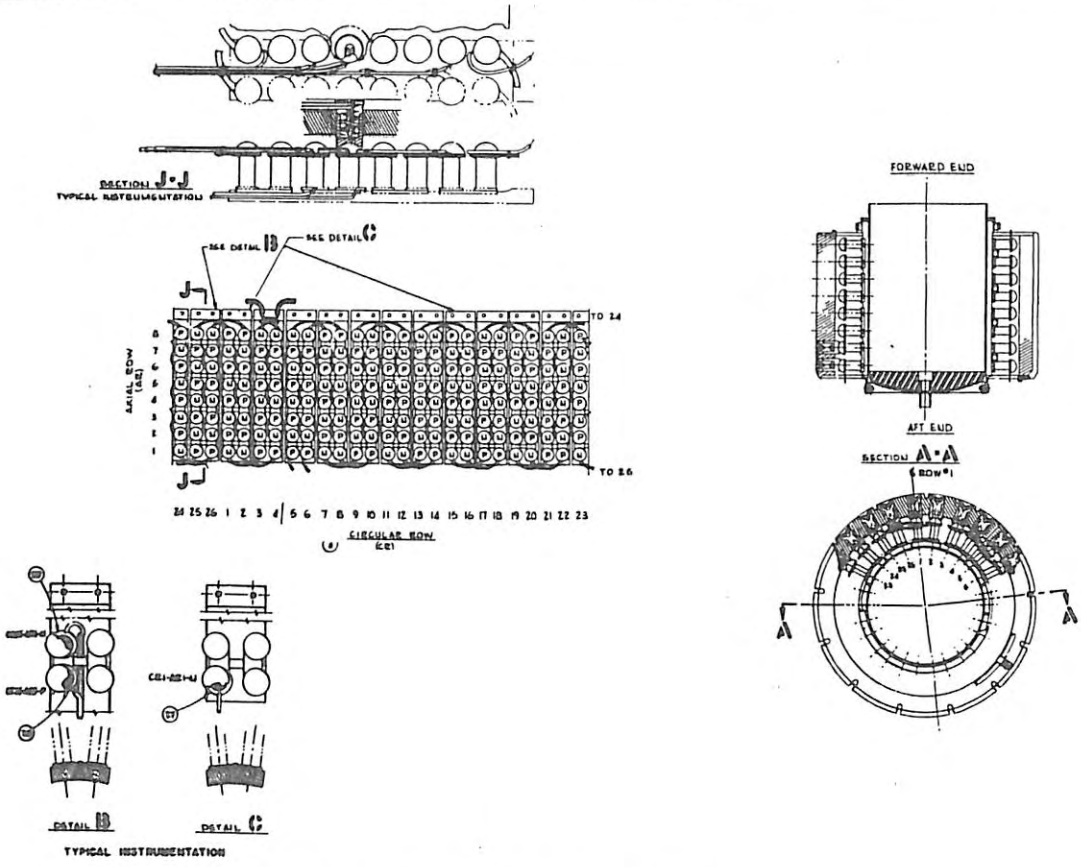

Figure 5-45. Mechanical Thermopile Assembly

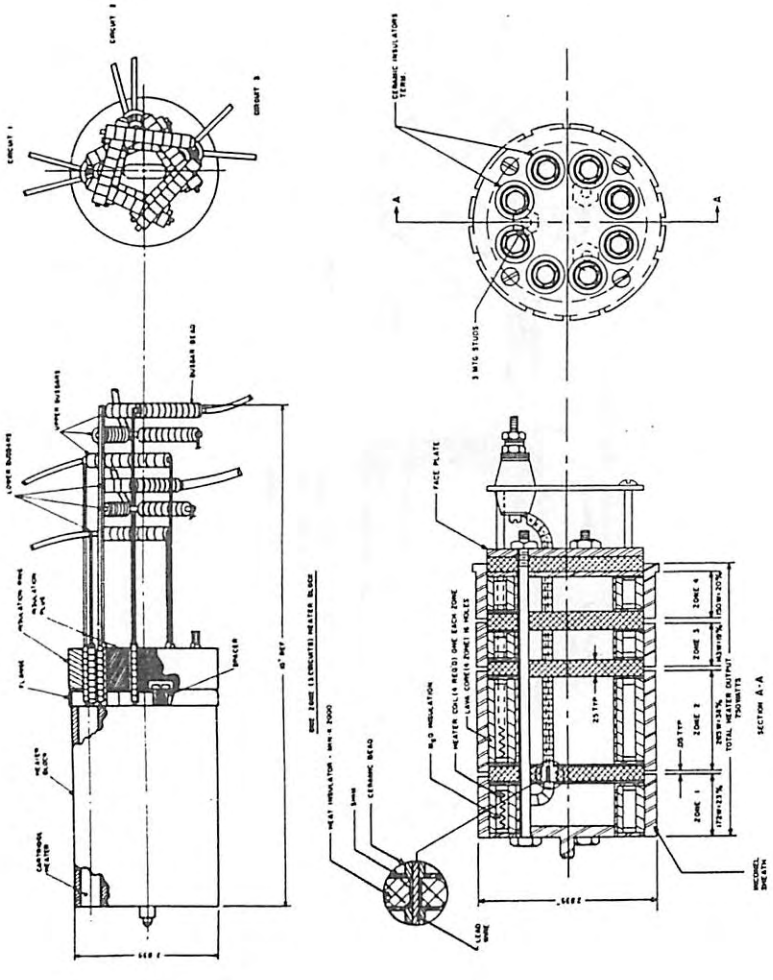

Figure 5-46. Heater Block Assembly

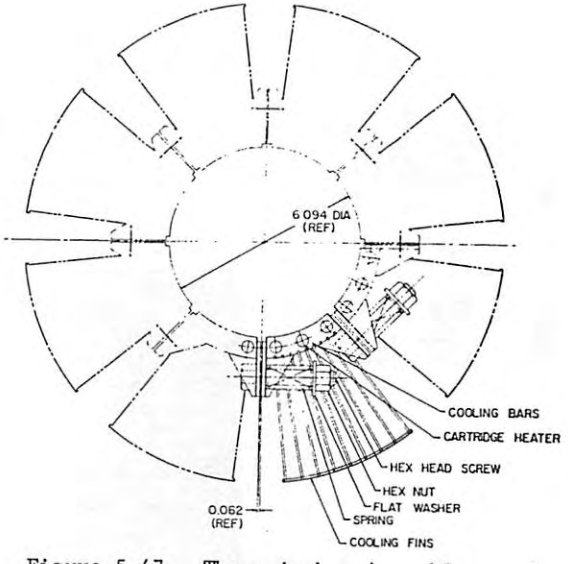

Figure 5-47. Thermojacket Assembly

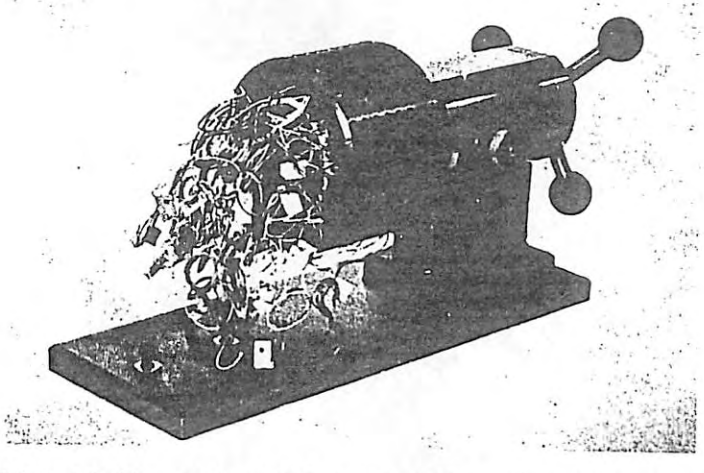

Figure 5-48. Typical 104-Couple Module Thermopile Assembly

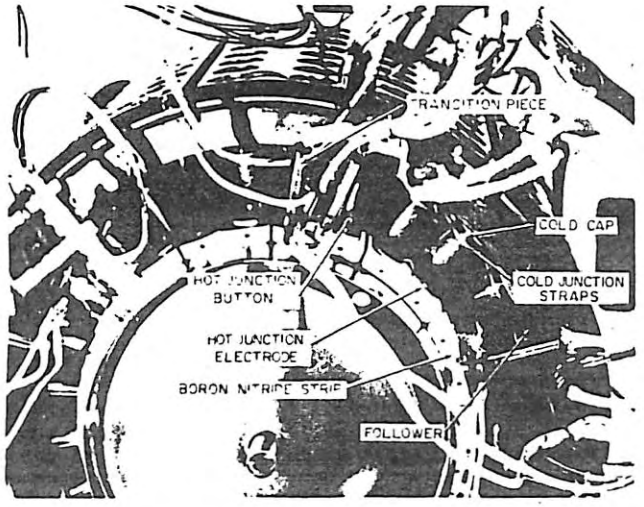

Figure 5-49. Internal Construction Details, 104-Couple Module

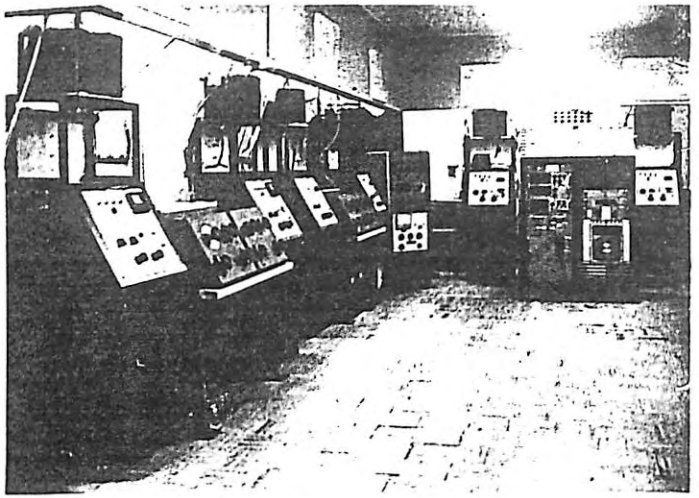

Figure 5-50. Test Laboratory, 104-Couple Module

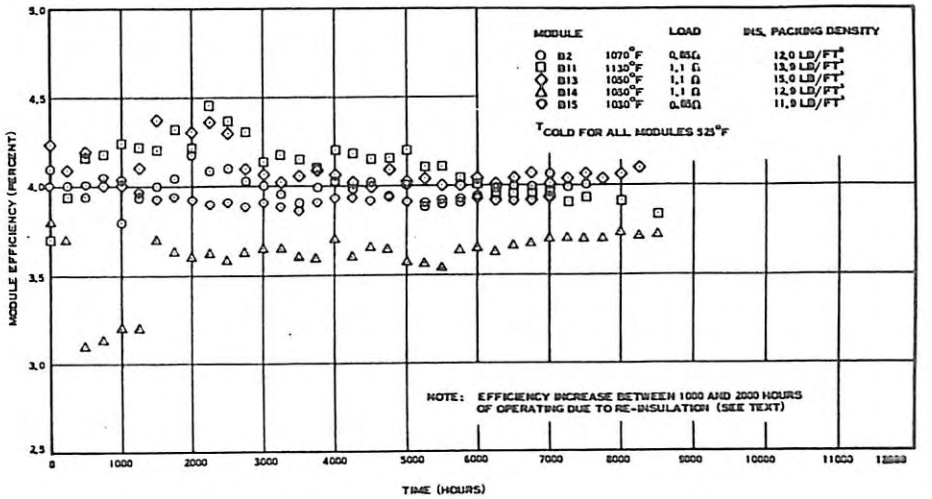

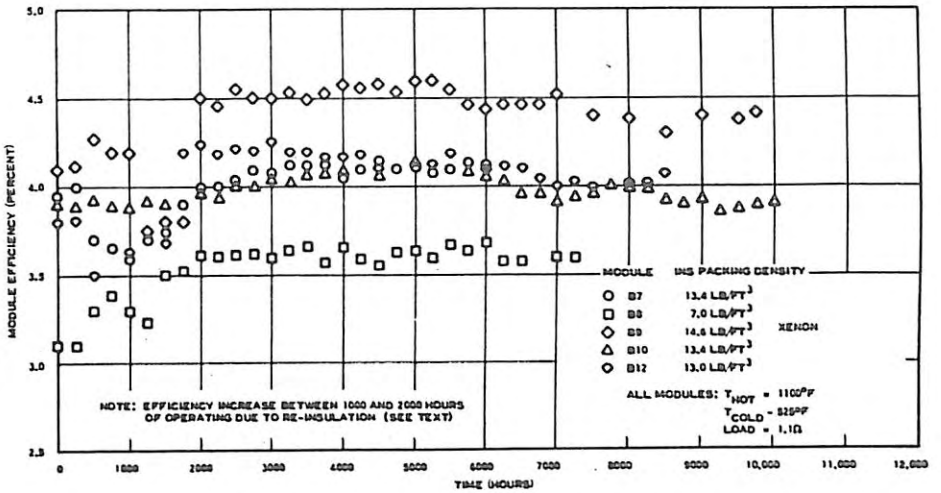

Figure 5-51. Life Test Data, 104-Couple Module

performed under a constant load condition of 1.1 ohms for all modules except for Module 104-B2 and Module 104-B15, which are tested at 0.85 ohm. A load equal to 1.1 ohms was chosen in accordance with the 4.7 ohm load requirements earlier in the SNAP-27 program, which was the analytically determined optimum efficiency load after one year of operation at 1100/525°F. A load resistance of 0.85 ohm is closest to the maximum efficiency operation point at BOL.

Some modules show a significant increase in efficience between 1000 and 2000 hours. This stems from a reinsulation of the module test stations after it was discovered that the insulation originally used was insufficient and its performance was not reproducible. Data shown for the first 300 hours are acceptance test results taken at the 3M Company.

The exceptionally low efficiency of Module 104-B8 can be attributed to the extremely low Min-K 1301 insulation packing density of seven pounds per cubic foot, which is about 50 percent of normal packing. This was due to an error during processing where part of the insulation was inadvertently sucked out of the module and therefore, major voids can be expected in this module. Voids not only have a pronounced effect on the efficiency, but also will produce increased degradation due to increased sublimation.

5.4.8 GENERATOR MOD 5 ENGINEERING DEVELOPMENT TESTS

Generator Mod 5 was the first full-size operating unit representative of the qualification and flight generators. It differed from the prime units primarily in that the fins were slotted instead of segmented, the fin buttresses were not as rugged as on prime units, the followers were beryllium instead of beryllium oxide, considerable thermocouple instrumentation was present internally for obtaining direct hot and cold junction temperatures and an integral pressure transducer was present for measuring internal gas pressure. In addition, the cable and connector were of the original design.

Generator Mod 5 was subjected to the following series of tests, in the order shown:

a. Acceptance Tests
   1. Visual Examination
   2. Resistance measurements
   3. I-V mapping, in air
   4. Leak rate determination (non-operating)
   5. Operability assurance vibration
   6. I-V mapping, thermal vacuum

b. Sinusoidal Vibration Test - qualification levels

c. Operational Life Test - thermal vacuum

All performance testing was conducted using an electric fuel capsule as the heat source.

The test program was initiated on October 31, 1966 and terminated on July 9, 1968 by AEC direction. During this period, Generator Mod 5 accumulated a total of 12,165 hours of operation, nearly all of it under thermal vacuum conditions.

5.4.8.1 I-V Mapping

Performance characteristics of Generator Mod 5 are summarized in Figures 5-52 through 5-54.

Figure 5-52 shows curves of pre-acceptance performance measurements made by the 3M Company prior to shipment to General Electric, together with measurements made by General Electric during acceptance testing, superimposed on theoretical performance curves. Figures 5-53 and 5-54

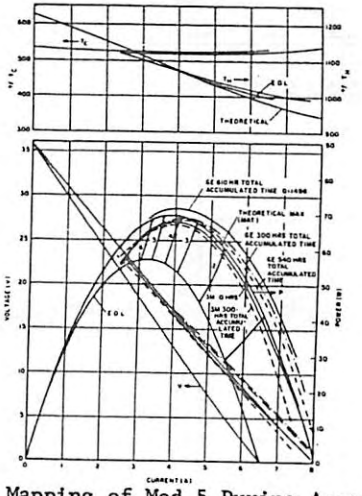

Figure 5-52. I-V Mapping of Mod 5 During Acceptance Testing

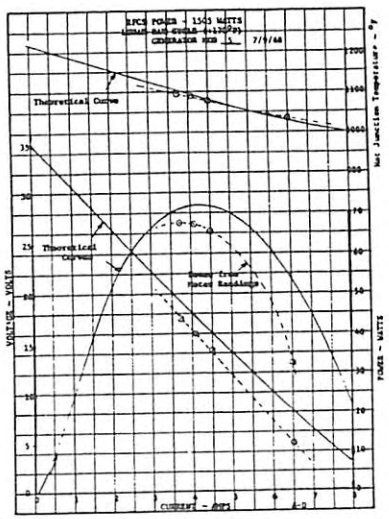

Figure 5-53. Final I-V Mapping of Mod 5 (Lunar Day Cycle)

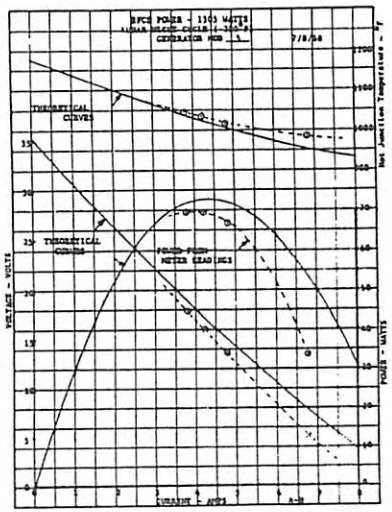

Figure 5-54. Final I-V Mapping of Mod 5 (Lunar Night Cycle)

show curves of the final mapping made on the generator at the completion of the operational life test, for both lunar day and night conditions with a power input of 1505 watts to the generator.

The data obtained at General Electric during the first I-V mapping in air, the first I-V mapping in thermal vacuum and of the concluding maps at the completion of the life testing can be found in the Appendix.

5.4.8.2 Sinusoidal Vibration

a. Frequency Survey - Prior to qualification level vibration, the generator was subjected to a one g sine survey along each of its three major axes over the frequency range of 5 to 2000 cps to determine its dynamic response and mode shapes for comparison and verification of the design analysis. The predominant frequency in the longitudinal axis was determined as 1200 cps, with one accelerometer recording a major response at 1400 cps. The calculated first natural frequency in the longitudinal direction is 1189 cps.

The generator, when vibrated in the lateral axes, induced

oscillating motion in the longitudinal axes. Tabulated below are the predominant experimental values for both the lateral and the induced longitudinal frequencies. For reference, the theoretical frequencies are also shown.

LATERAL (EXPERIMENTAL)	LATERAL (THEORETICAL)	INDUCED LONGITUDINAL (EXPERIMENTAL)
280 cps	188	280
340 to 380 cps	410	480
900 to 920 cps	687	900 to 920
1300 cps	1433	1300
1700 cps	1678	1700

The experimental results in most cases substantiated assumptions used in the analytical model. Considering the assumptions made, and the lack of precise thermopile spring constants, the calculated frequencies (except for the second mode) compared quite favorably with the experimentally determined frequencies. The agreement between experimental and theoretical longitudinal frequencies was extremely favorable. The analytical assumption of the fins being uncoupled from the generator was borne out by the experimental results. However, the omission of the fin elasticity in the mathematical model compromised the second mode frequency.

b. Vibration - Qualification Levels - Generator Mod 5 was subjected to qualification level sinusoidal vibration along each of its three axes. The frequency range covered and vibration levels employed were as follows:

FREQUENCY	VIBRATION LEVEL
5 to 20 Hz	0.39 inch Double Amplitude
20 to 35 Hz	± 7 g
35 to 100 Hz	± 10.4 g

The frequency range was swept at a rate of three octaves per minute along each axis, increasing frequency only. For this

test, the generator was heavily instrumented with strain gages and accelerometers as shown in Figure 5-55. No indications of damage were noted.

5.4.8.3 Operational Life Tests

This test was performed in the Long Life Test Chamber shown in Figure 5-56 under temperature and vacuum conditions simulating lunar day and night. Thermal sink conditions were cycled between -280°F and +170°F. Each temperature extreme was maintained for two weeks. At periodic intervals during the test, I-V mapping was performed to determine if any significant degradation in operation was occurring. After 10,000 hours of test, the power to the electric fuel capsule was reduced to 1485 watts to simulate fuel decay.

The performance of Generator Mod 5 over the total test period at General Electric, i.e., acceptance through termination of life testing, is summarized in Figures 5-57 through 5-60. Figure 5-57 shows the normalized power output versus accumulated time; Figure 5-58 shows normalized open circuit voltage; Figure 5-59 shows generator resistance ratio, and Figure 5-60 shows generator internal pressure (from its transducer).

5.4.9 GENERATOR MOD 8B ENGINEERING DEVELOPMENT TESTS

Generator Mod 8 (subsequently redesignated as Mod 8B) was intended to be identical in construction to Generator Mod 5, but during the processing cycle at the 3M Company, outer case cracking was experienced. The thermopile was salvaged and installed in a new outer case of the type used on the prime units. Since a replacement aft hermetic seal with instrumentation feedthroughs and provision for a pressure transducer was not available at the time, a prime generator seal was used instead. As a result, the internal instrumentation wires and pressure transducer leads were left unconnected. The generator was, therefore, not considered as an "optimum" unit, and its performance was not expected to turn out as "typical". A new cable and connector were also incorporated.

Generator Mod 8B was subjected to the following series of tests, in the order shown:

a. Acceptance tests

   1. Visual examination

   2. Resistance measurements

   3. I-V mapping in air

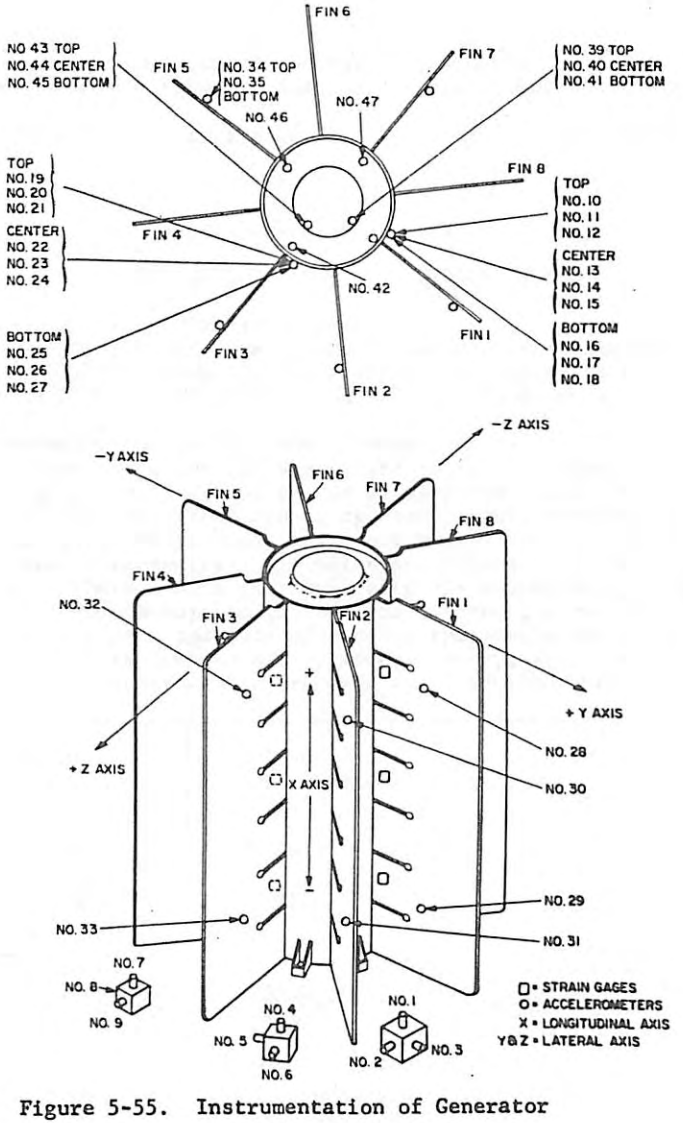

Figure 5-55. Instrumentation of Generator

test, the generator was heavily instrumented with strain gages and accelerometers as shown in Figure 5-55. No indications of damage were noted.

5.4.8.3 Operational Life Tests

This test was performed in the Long Life Test Chamber shown in Figure 5-56 under temperature and vacuum conditions simulating lunar day and night. Thermal sink conditions were cycled between -280°F and +170°F. Each temperature extreme was maintained for two weeks. At periodic intervals during the test, I-V mapping was performed to determine if any significant degradation in operation was occurring. After 10,000 hours of test, the power to the electric fuel capsule was reduced to 1485 watts to simulate fuel decay.

The performance of Generator Mod 5 over the total test period at General Electric, i.e., acceptance through termination of life testing, is summarized in Figures 5-57 through 5-60. Figure 5-57 shows the normalized power output versus accumulated time; Figure 5-58 shows normalized open circuit voltage; Figure 5-59 shows generator resistance ratio, and Figure 5-60 shows generator internal pressure (from its transducer).

5.4.9 GENERATOR MOD 8B ENGINEERING DEVELOPMENT TESTS

Generator Mod 8 (subsequently redesignated as Mod 8B) was intended to be identical in construction to Generator Mod 5, but during the processing cycle at the 3M Company, outer case cracking was experienced. The thermopile was salvaged and installed in a new outer case of the type used on the prime units. Since a replacement aft hermetic seal with instrumentation feedthroughs and provision for a pressure transducer was not available at the time, a prime generator seal was used instead. As a result, the internal instrumentation wires and pressure transducer leads were left unconnected. The generator was, therefore, not considered as an "optimum" unit, and its performance was not expected to turn out as "typical". A new cable and connector were also incorporated.

Generator Mod 8B was subjected to the following series of tests, in the order shown:

a. Acceptance tests

   1. Visual examination

   2. Resistance measurements

   3. I-V mapping in air

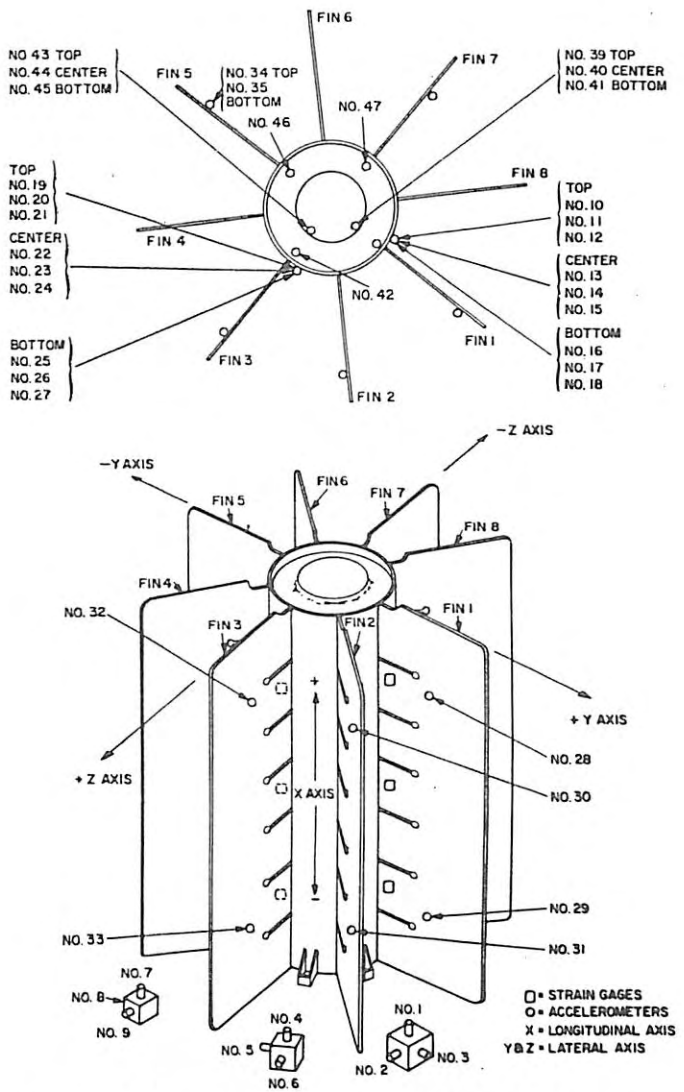

Figure 5-55. Instrumentation of Generator

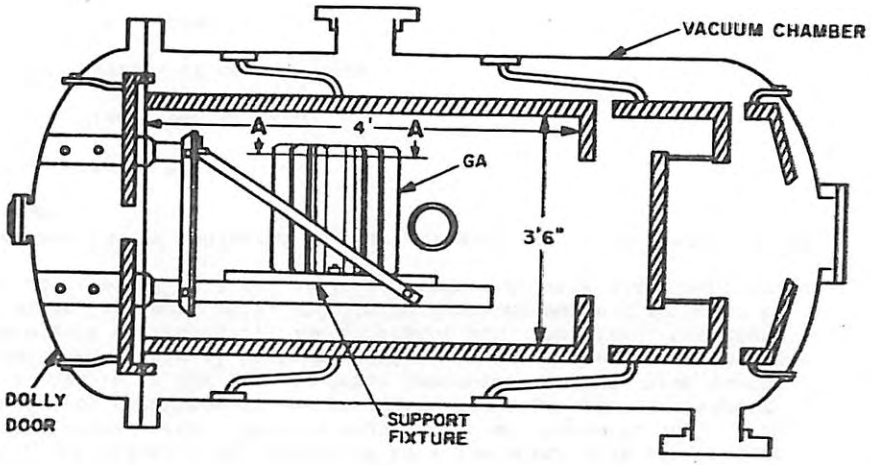

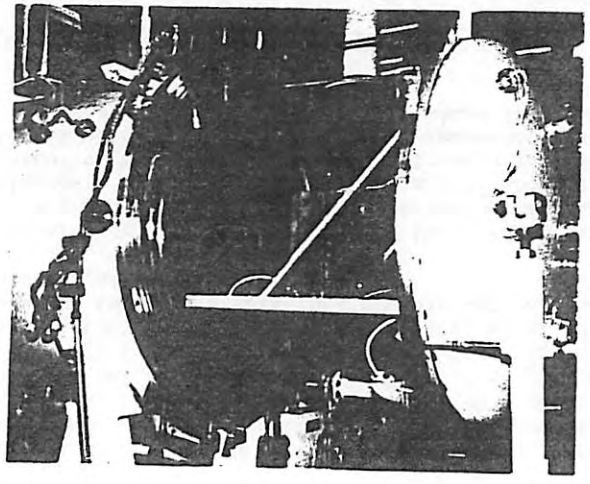

Figure 5-56. Generator Installation in Long Life Test Chamber

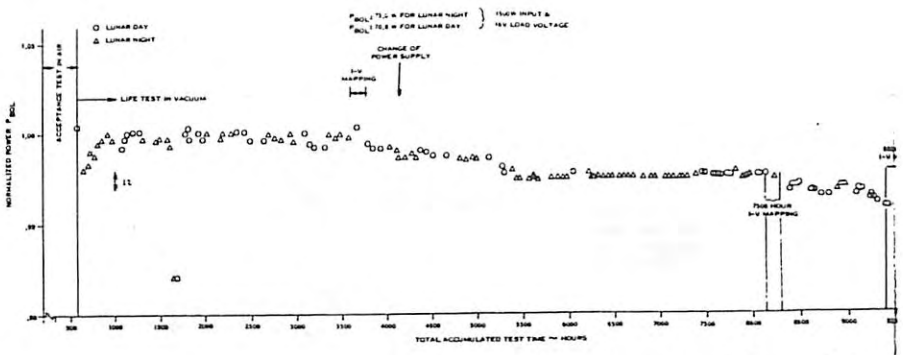

Figure 5-57. Mod 5 Generator Normalized Power Output

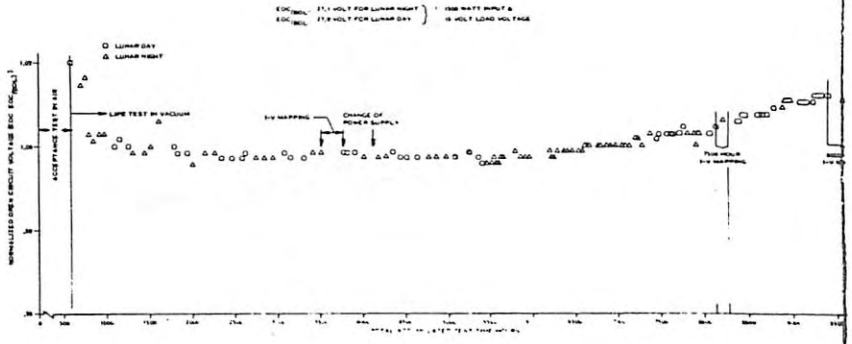

Figure 5-58. Mod 5 Generator Normalized Open Circuit V

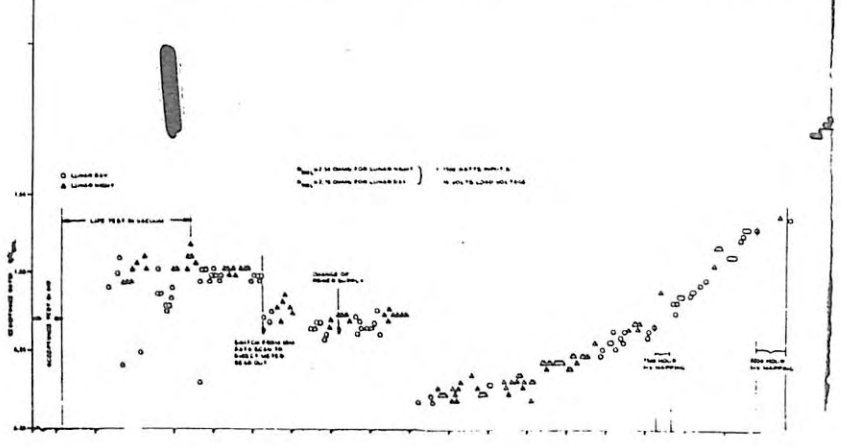

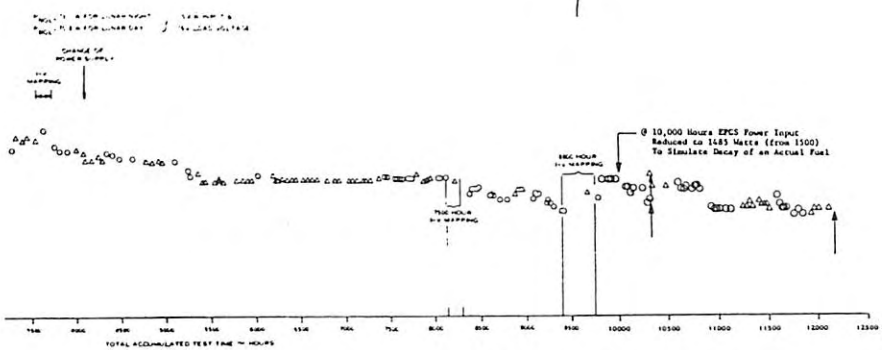

5-57. Mod 5 Generator Normalized Power Output

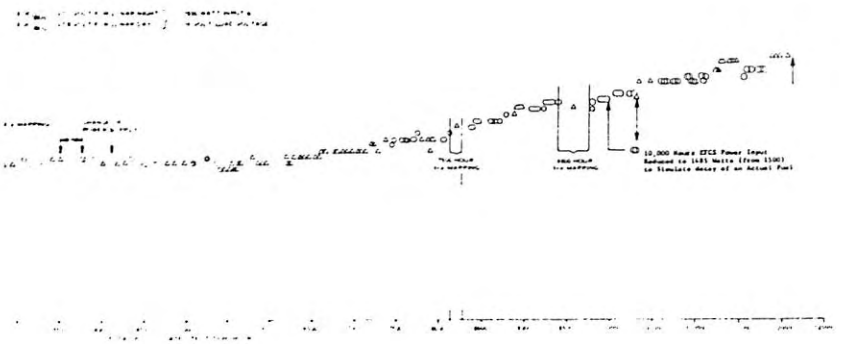

Mod 5 Generator Normalized Open Circuit Voltage

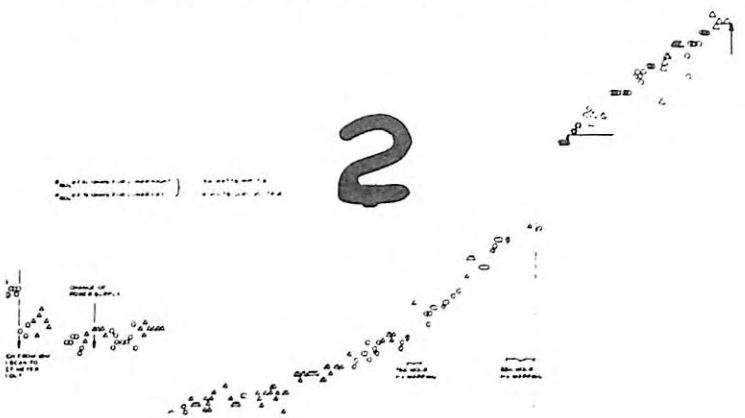

BLANK PAGE

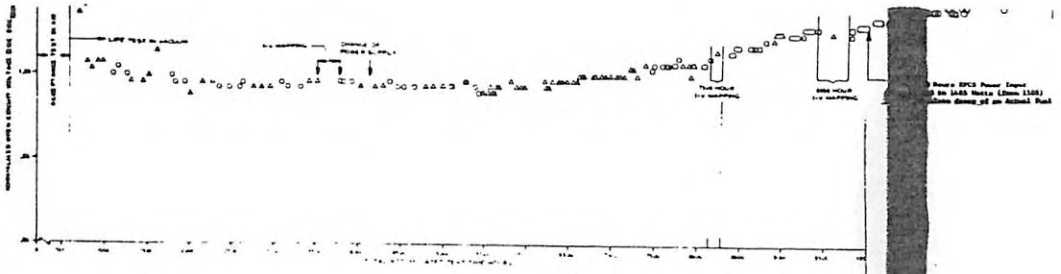

Figure 5-58. Mod 5 Generator Normalized Open Circuit Volt

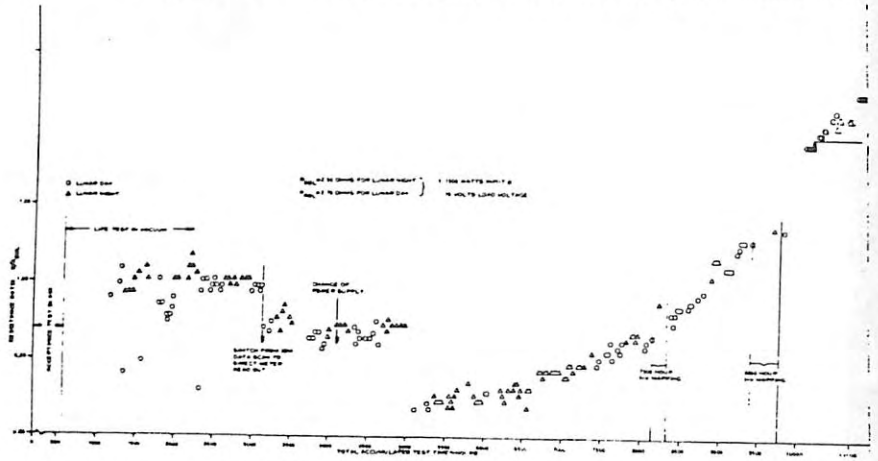

Figure 5-59. Mod 5 Generator Resistance Ratio

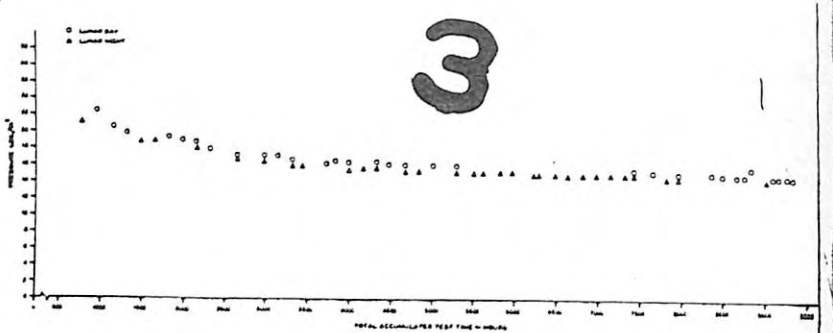

Figure 5-60. Mod 5 Generator Internal Pressure

BLANK PAGE

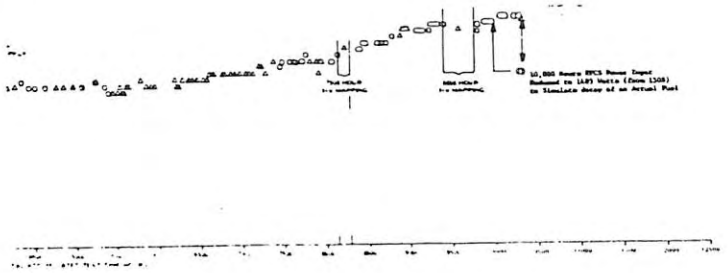

5 Generator Normalized Open Circuit Voltage

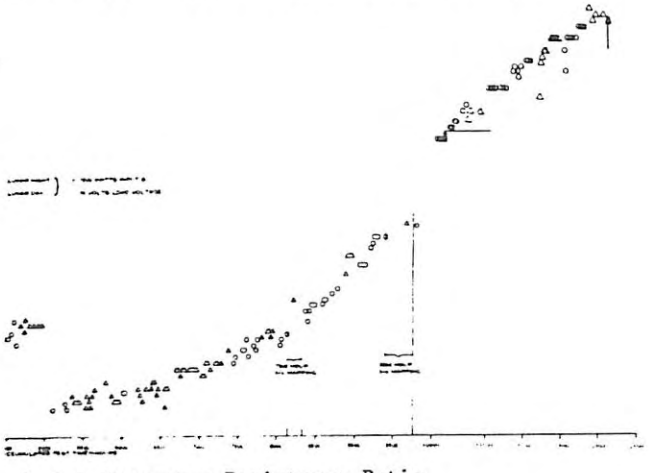

Mod 5 Generator Resistance Ratio

4

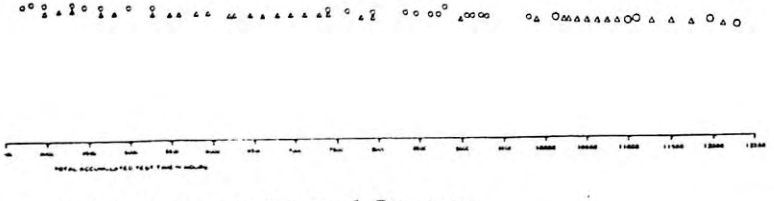

50. Mod 5 Generator Internal Pressure

4. Leak rate determination (non-operating)

5. Operability assurance vibration test

b. Magnetic evaluation test (NASA-Goddard)

c. I-V mapping (vacuum) and leak rate check

d. Hot EFCS insertion test

e. Thermal vacuum test

f. ALSEP PCU/IPU compatibility tests

g. Sinusoidal vibration test (qual level)

h. Random vibration test (qual level)

i. Shock test

j. Acceleration test

k. Operational life test (thermal vacuum)

Performance testing was conducted in nearly all instances with an electric fuel capsule. Some performance data was, however, obtained using a nuclear fueled capsule.

The test program on Mod 8B was initiated on March 22, 1967 and terminated on July 9, 1968 by AEC direction. During this period of time, Generator Mod 8B accumulated a total of 8,341 hours of operation; 8,093 hours under thermal vacuum conditions.

5.4.9.1 I-V Mapping

Performance curves of the first I-V mapping in air performed on the generator following its receipt from the 3M Company are summarized in Figure 5-61; curves of the data obtained during the first I-V mapping in vacuum at 10^{-6} torr are summarized in Figures 5-62 and 5-63. Curves of the maps for lunar day and night conditions at the completion of 7500 hours operational life testing are shown in Figures 5-64 and 5-65. Corresponding data sheets are included in Appendix C.

5.4.9.2 Sinusoidal Vibration Test - Qual Levels

Generator Mod 8B was subjected to qualification levels sinusoidal vibration sequentially along each of its three major axes, over the

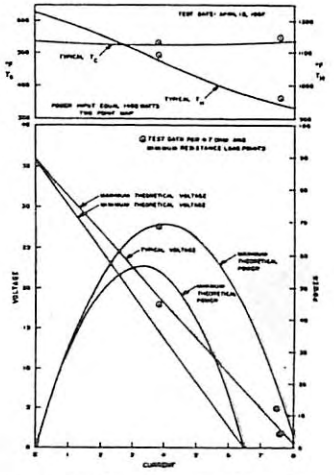

Figure 5-61. Mod 8B I-V Mapping in Air (as received from 3M)

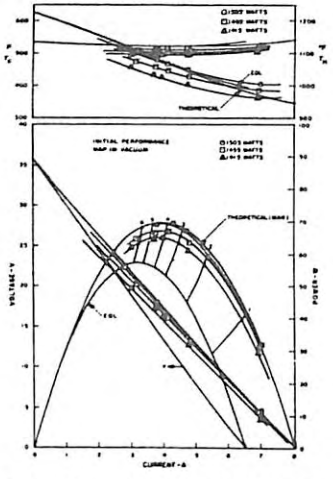

Figure 5-62. Mod 8B Performance for Lunar Day Conditions

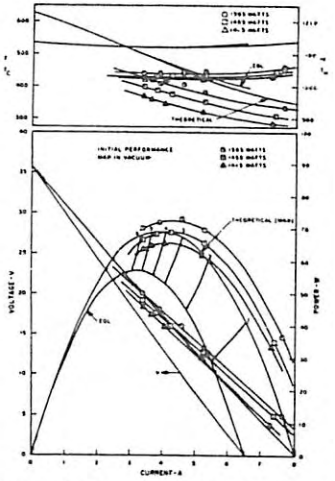

Figure 5-63. Mod 8B Performance for Lunar Night Conditions

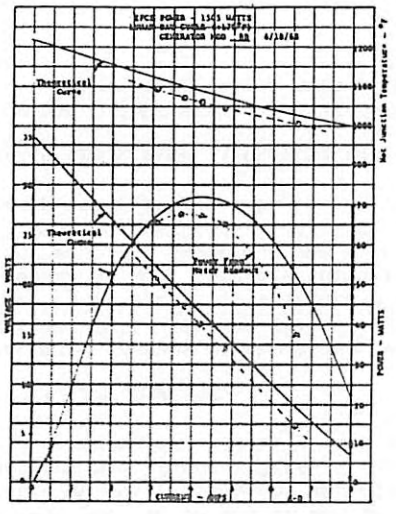

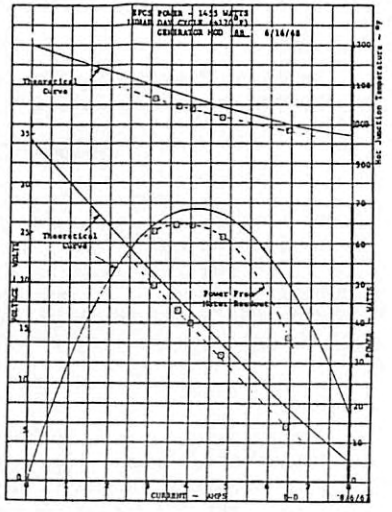

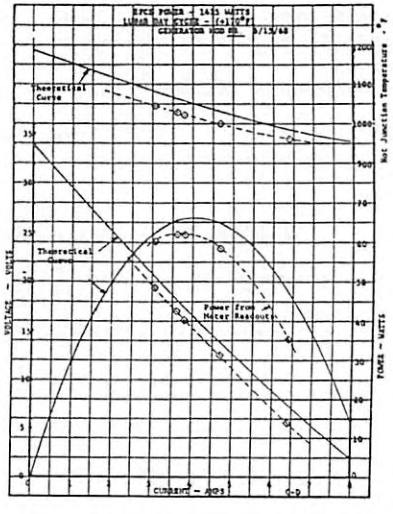

Figure 5-64. Mod 8B 7500 Hours I-V Mapping (Lunar Day Cycle)

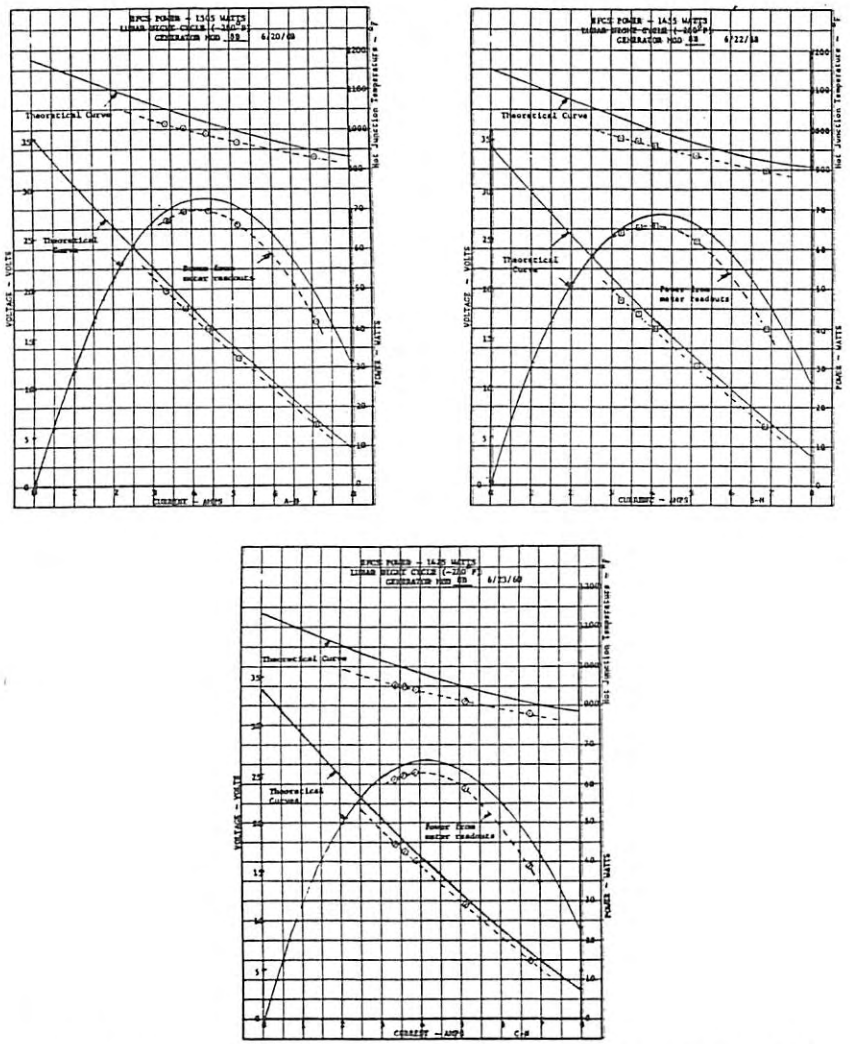

Figure 5-65. Mod 8B 7500 Hours I-V Mapping (Lunar Night Cycle)

frequency range shown below at a sweep rate of three octaves per minutes, increasing only.

FREQUENCY RANGE	VIBRATION LEVELS
5 to 20 Hz	0.39 inch double amplitude
20 to 35 Hz	± 7.8 g
35 to 100 Hz	± 10.4 g

During the test, the generator was non-operative. No indications of damage were noted at the conclusion of the test.

5.4.9.3 Random Vibration Test - Qual Levels

The generator was subjected to the random vibration spectrum shown below, at the power levels indicated, for five minutes in each of the generator's three major orthoginal axis.

FREQUENCY RANGE	VIBRATION LEVELS
23 to 80 Hz	0.244 g^2/cps
80 to 120 Hz	12 db/octave roll-off
120 to 950 Hz	0.044 g^2/cps
950 to 1250 Hz	12 db/octave roll-off
1250 to 2000 Hz	0.0148 g^2/cps

During the test, the generator was non-operative. No indications of damage were noted at the completion of the test.

5.4.9.4 Shock Test

The generator was subjected to three 15-g shocks in each direction along its three major orthogonal axes, for a total of 18 shocks. Time to peak of each shock was 11 milliseconds ± 10 percent, time of decay was equal to or less than two milliseconds (sawtooth pulse). The generator was non-operating during the test. Thermopile resistance and insulation resistance were measured after each shock. No resulting damage was experienced by the generator.

5.4.9.5 Acceleration Test

The generator was mount i in a centrifuge and subjected to three minutes of acceleration at 7.5 g's along each of the three orthogonal axes of the generator. During the test, the generator was non-operative. No resulting damage was experienced by the generator.

5.4.9.6 Operational Life Test

This test was conducted on Generator Mod 8B in the same manner as that described for Mod 5. The performance of Mod 8B over the total test period, acceptance through termination of life testing, is summarized in Figures 5-66 through 5-68. Figure 5-66 shows the normalized power output versus accumulated time; Figure 5-67 shows normalized open circuit voltage, and Figure 5-68 shows the resistance ratio.

5.4.9.7 Magnetic Evaluation Test (NASA-Goddard)

Engineering evaluation tests were performed in April 1967 at the Component Magnetic Test Facility of the Goddard Space Flight Center, Greenbelt, Maryland, to determine the resulting magnetic field of the engineering Mod 8B Generator Assembly when subjected to various magnetic environments. The tests were performed with the generator cold (no fuel capsule present). The generator's magnetic field was measured under the following conditions:

a. As received, earth's ambient field

b. As received, zero field environment

c. Depermed, zero field environment

d. After perming with a 15 oersted field

e. Rotating in a field of 0.26 oersteds

f. With selected currents flowing in the generator, in a zero field environment, with the generator depermed before the tests.

Results of this test matched closely the analysis of the model.

The test was intended to provide preliminary engineering data on the generator's magnetic characteristics, as well as to verify the procedure for the test which was to follow using the qualification generator, Mod 10, with a fuel capsule. Generator Mod 8B was identical to the qualification generator except for the presence of ten internal iron-contantan thermocouples located in the thermopile. Data obtained

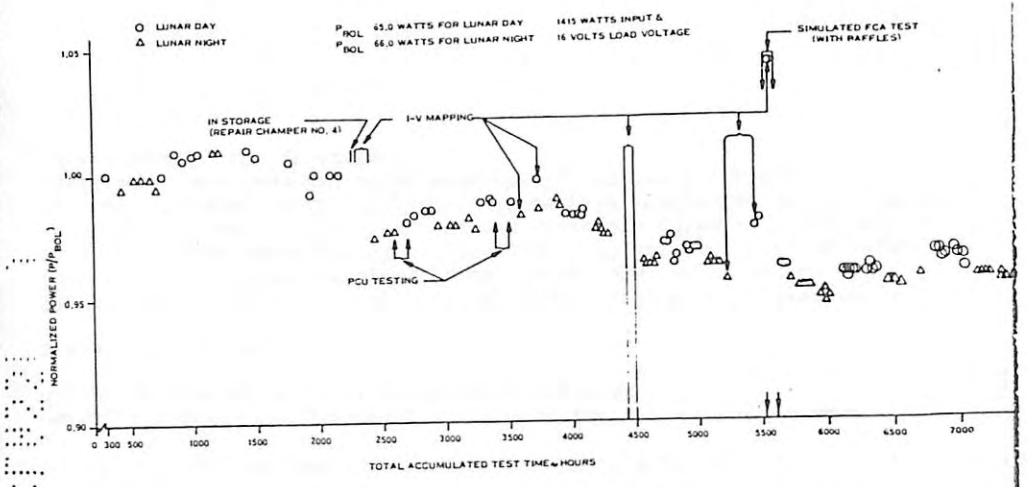

Figure 5-66. Mod 8B Normalized Power Output

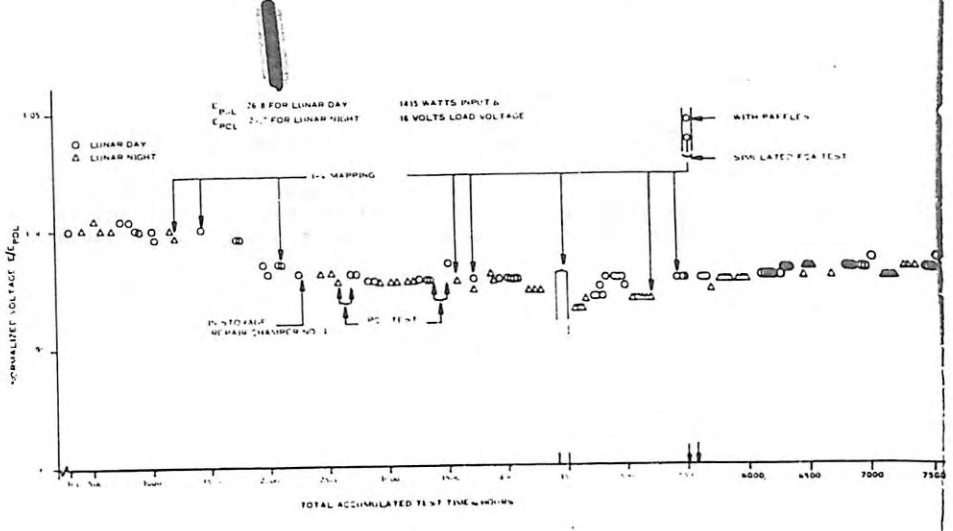

Figure 5-67. Mod 8B Normalized Open Circuit Voltage

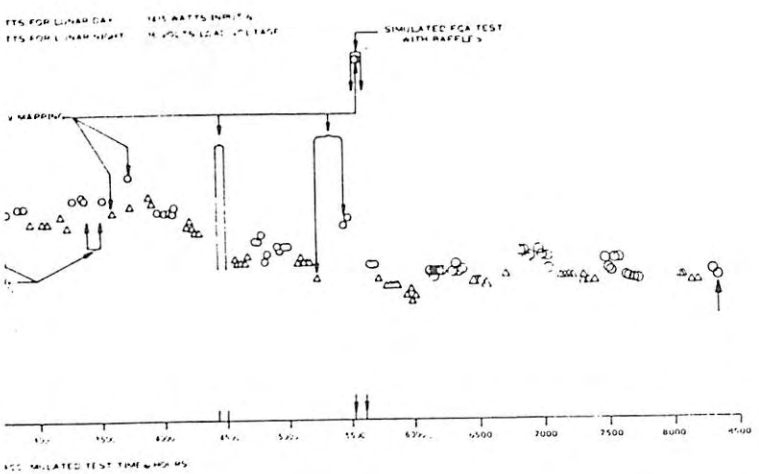

5-66. Mod 8B Normalized Power Output

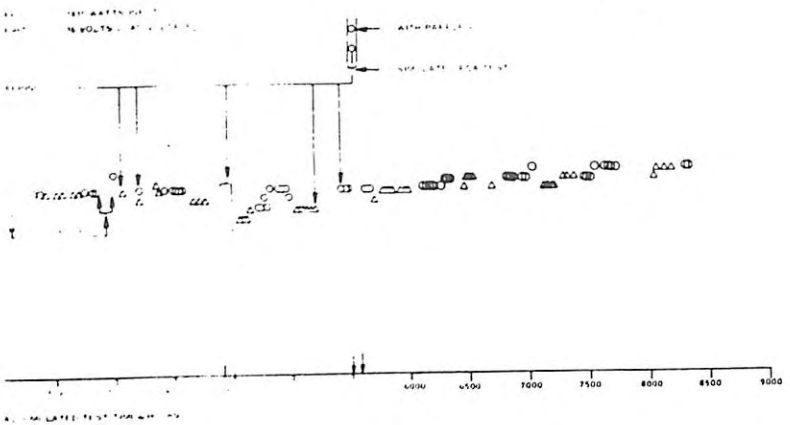

5-67. Mod 8B Normalized Open Circuit Voltage

BLANK PAGE

Figure 5-66. Mod 8B Normalized Power Output

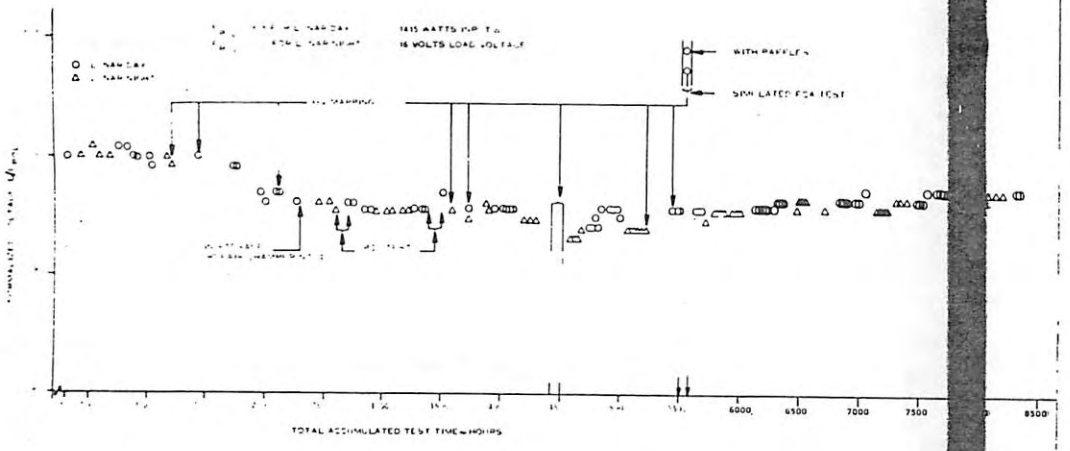

Figure 5-67. Mod 8B Normalized Open Circuit Voltage

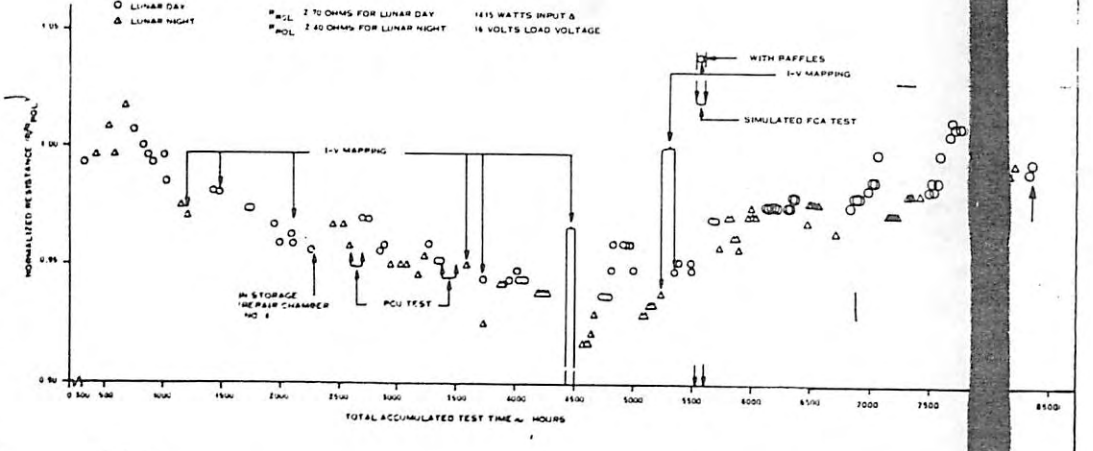

Figure 5-68. Mod 8B Normalized Resistance Ratio

BLANK PAGE

Figure 5-66. Mod 8B Normalized Power Output

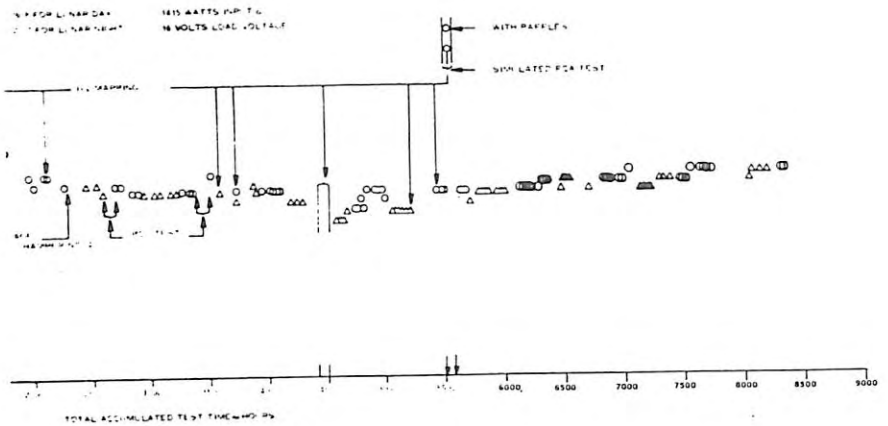

Figure 5-67. Mod 8B Normalized Open Circuit Voltage

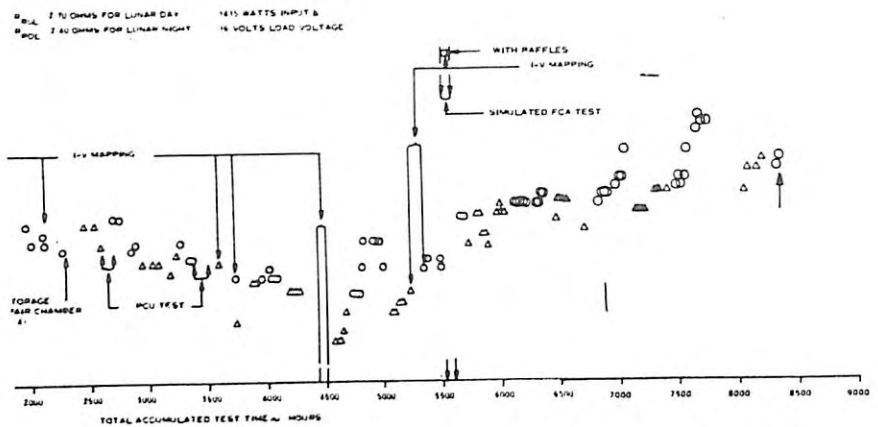

Figure 5-68. Mod 8B Normalized Resistance Ratio

4

from the test was to be compensated for the presence of these thermocouples.

Figure 5-69 identifies the generator coordinates used in the test

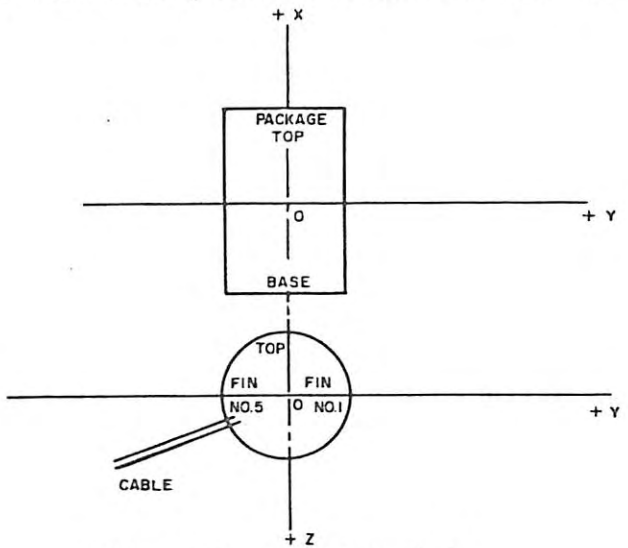

Figure 5-69. Coordinate System

The testing was performed inside a 14-foot Helmholtz coil system. The generator was tested cold, while supplied with current from a separate dc source to create stray field. A summary of the results is shown in Figures 5-70 through 5-79. The following conclusions were drawn:

a. The generator specification requirement of 0.1 γ at 50 feet was adequately met

b. The deperming tests demonstrated that the generator could be depermed to within 5 percent of its previous moment in all cases

c. The measurements of field, as received, showed that a great deal of the behavior of the generator was due to permanent magnetism in the iron-plated hot shoes as a result of perming from the ambient environment

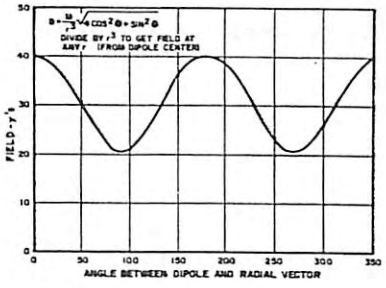

Figure 5-70. Total Field at One Meter After 15 Oersted Perm in Positive X Direction

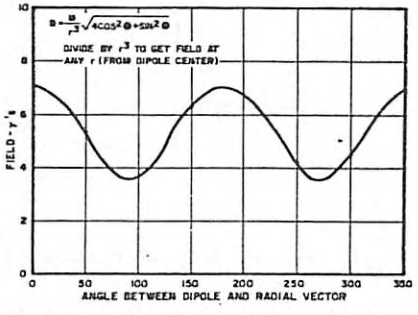

Figure 5-71 Total Field at One Meter After 15 Oersted Perm in Negative Y Direction

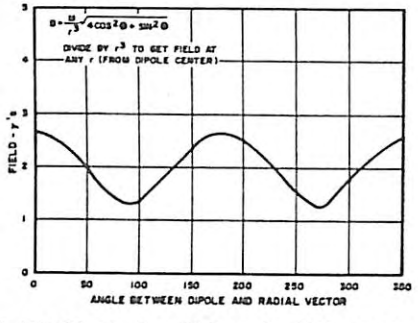

Figure 5-72. Total Field at One Meter in Presence of 0.26 Gauss Inducing Field in the Positive Y Direction

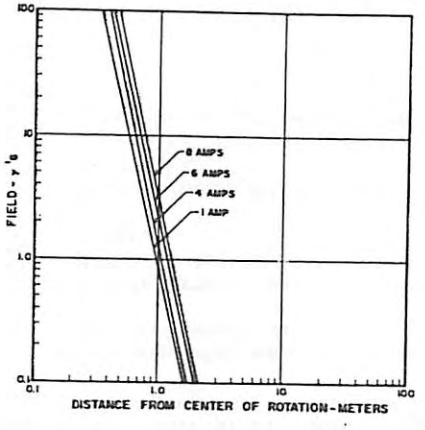

Figure 5-73. Positive X-Axis Stray Field Radial Component (Field in Negative X Direction)

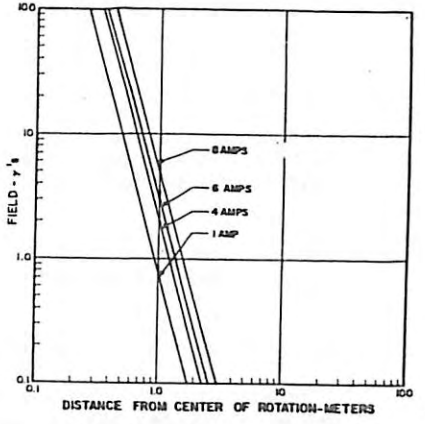

Figure 5-74. Negative X-Axis Stray Field Radial Component (Field in Negative X Direction)

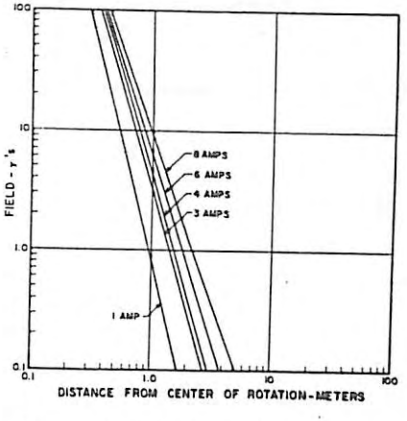

Figure 5-75. Positive Y-Axis Stray Field Radial Component (Field in Positive Y Direction)

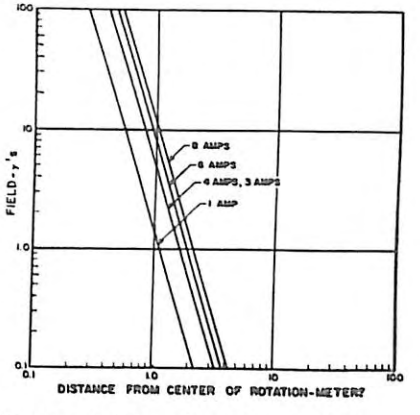

Figure 5-76. Negative Y-Axis Stray Field Radial Component (Field in Positive Y Direction)

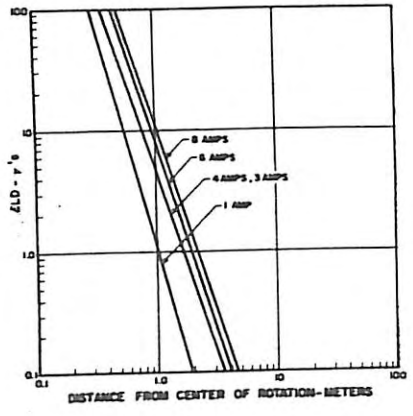

Figure 5-77. Positive Z-Axis Stray Field Radial Component (Field in Positive Z Direction)

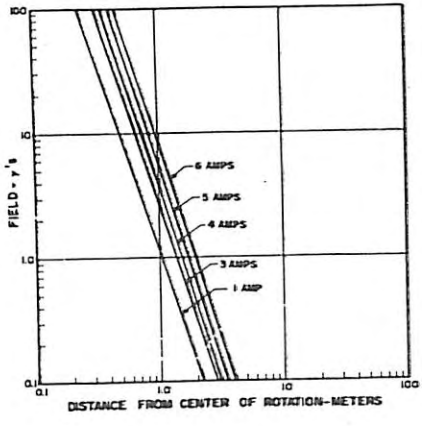

Figure 5-78. Negative Z-Axis Stray Field Radial Component (Field in Positive Z Direction)

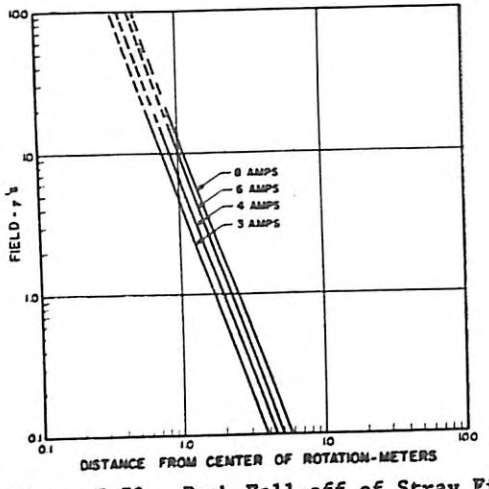

Figure 5-79. Peak Fall-off of Stray Field with Distance

d. The presence of the iron constantan thermocouple in Generator Mod 8B was additive to the total field of the generator. The actual flight hardware magnetic behavior would be less and would be more symmetrical with respect to the hot shoe configuration.

5.4.9.8 Thermal Transient Test (Hot EFCS Insertion)

A series of three simulated fuel capsule insertion tests were performed on Generator Mod 8B using an Electric Fuel Capsule Simulator (EFCS) stabilized at 1500 watts to determine the characteristics of the power buildup versus time. For minimal deployment time on the lunar surface, the fastest temperature buildup of the generator is desired. The test setup showing fixture and generator is depicted in Figures 5-80 and 5-81.

The simulated environment was maintained at $0^{o}F \pm 5^{o}F$ and at a vacuum of 10^{-5} torr or less for the duration of the three tests. The first two tests were performed with the generator in a short-circuit condition for the duration of the tests. The third test was performed with the generator in an open-circuit condition for the first sixty minutes and at a 16-volt load condition for the remainder of the test. In all three tests the EFCS was lowered into the generator within 35 ($\pm$ 1) seconds. The first 13 inches were lowered in at a rate of one inch per 1.6 seconds

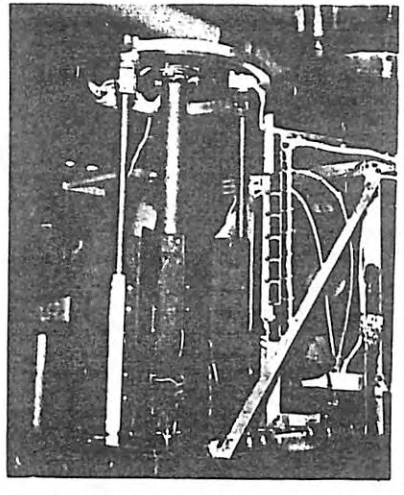

Figure 5-80. Test Fixture and Generator for Mod 8B Insertion Test

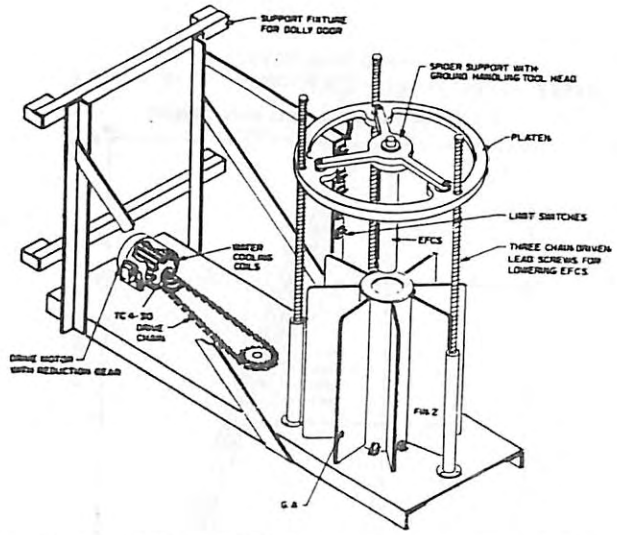

Figure 5-81. EFCS Remote Insertion Fixture

and the remaining four inches at a rate of one inch per 3.5 seconds.

The transient response of the thermopile for the two startup modes, open-circuit and short-circuit conditions, is shown in Figure 5-82. The open-circuit voltage during an open-circuit startup condition increases at a greater rate than for the short-circuit startup. The apparent difference stems from the fact that the effective thermopile conductance increases with current flow due to the Peltier effect at the hot junction. Since the Peltier cooling is directly proportional to the current flow, the difference does not become appreciable until a sizable current is flowing eight to ten minutes after capsule insertion.

Since the effective conductance of the thermopile determines the temperature difference across the thermoelements, the temperature difference will increase with decreasing current flow. The open-circuit voltage will thus be higher for lower current flow.

Figure 5-83 was developed from the I-V characteristic data obtained during the insertion tests and shows the available power at any time, T, after capsule insertion for 16-volt operation and for maximum power. As illustrated, the maximum power available using the open-circuit startup

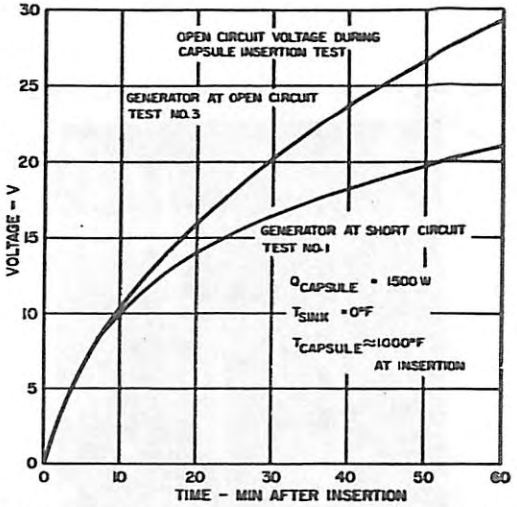

Figure 5-82. Open- and Short-Circuit Voltage During Capsule Insertion Test

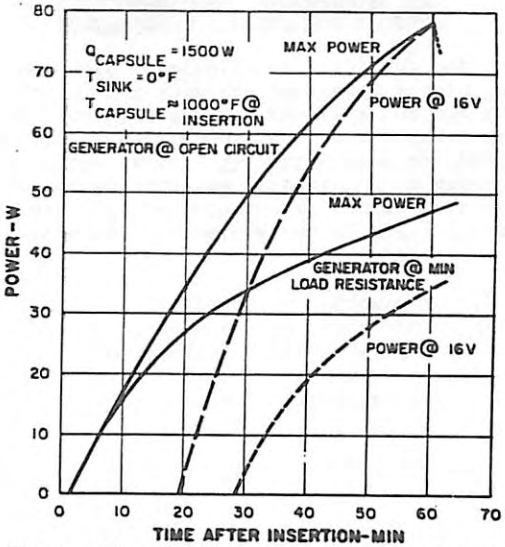

Figure 5-83. Maximum Available Power After Capsule Insertion

mode is greater than the short-circuit startup mode. It must be realized, however, that as soon as any finite load is applied to the open-circuited generator, the temperature difference across the thermoelements will decrease due to the current flow, and an initial drop in power will be experienced reflecting this temperature drop. A dashed line at T = 60 minutes indicates this behavior.

At the short-circuit condition, the power will increase at a higher rate if the load is increased, since the temperature difference will increase relatively fast after the short-circuit is removed. Therefore, a rapid increase in power, after adjustment to normal operating conditions, can be expected.

The thermal response of the generator assembly can best be illustrated in Figures 5-84 and 5-85 which depict the axial and radial response of one of the generator fins during the insertion tests.

5.4.9.9 Free Convection Baffle Test with EFCS

At the completion of the 500 hour I-V mapping, the operational life test of Mod 8B was briefly interrupted for this test. Air tests with these baffles were previously carried out using cracked Generator Mod 6. The present tests with these baffles were performed using Mod 8B under both air and thermal vacuum conditions. An electric fuel capsule

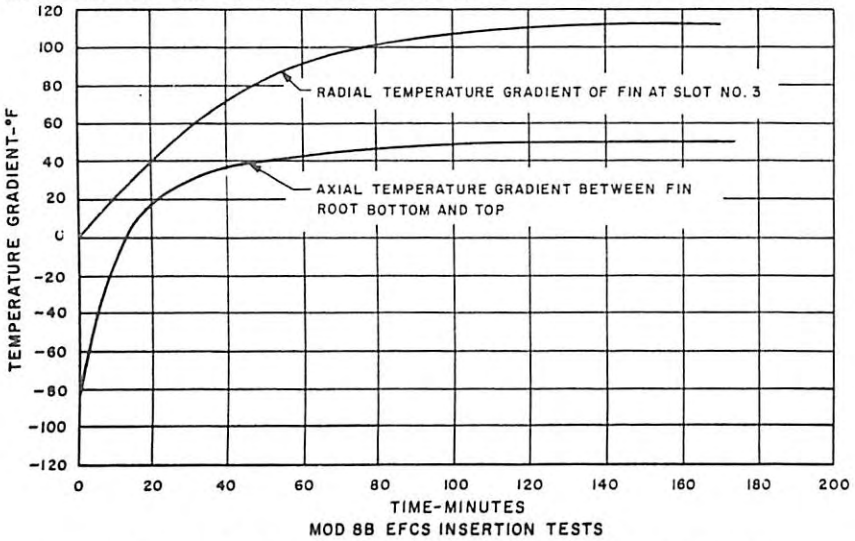

Figure 5-84. Thermal Response (Radial and Axial)

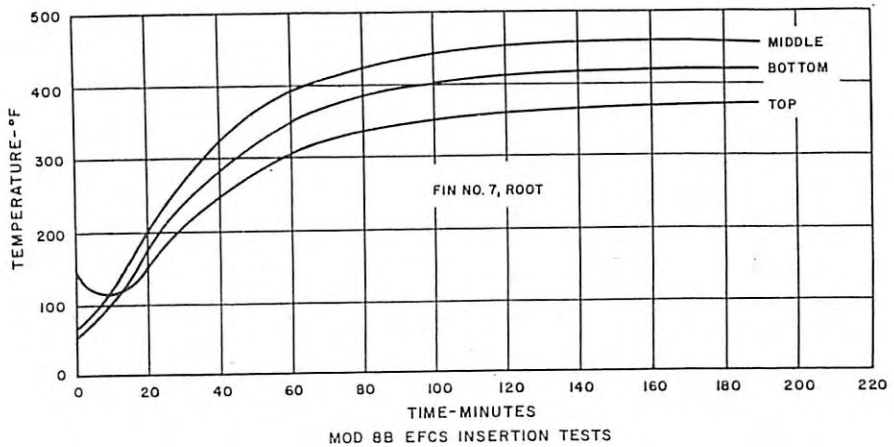

Figure 5-85. Thermal Response (Fin No. 7 Root)

was employed as the thermal source. Results of the tests are summarized in Figure 5-86. It can also be seen in Figure 5-87 that for the uncracked Mod 8B outer case, the baffles kept the gradient from the midplane to the bottom, below 90°F, compared with an estimated 150 to 180°F without the baffle.

The test confirmed the satisfactory performance of this baffle fixture. No structural damage was experienced by the generator.

5.4.9.10 Free-Convection Baffle Test with Fuel Capsule

This test was essentially a repetition of the air test performed earlier in the program using the cracked Generator Mod 6 installed in the "cake box" shroud. Since this fixture was intended eventually to be used for the magnetic tests (at NASA-Goddard) of Qualification Generator Mod 10 with a fuel capsule, it was decided that verification of its performance should be obtained first using Generator Mod 8B with the fuel capsule.

No structural damage of the generator was experienced. The generator operated successfully for four hours in air while installed in the fixture.

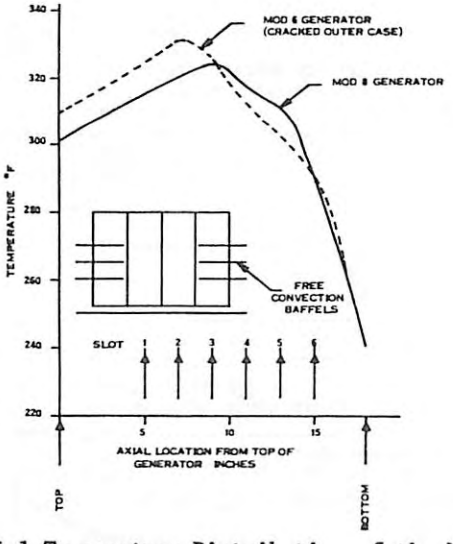

Figure 5-86. Axial Temperature Distribution of the Mod 8B Generator Outer Case During Air Operation with Convection Baffles in Place.

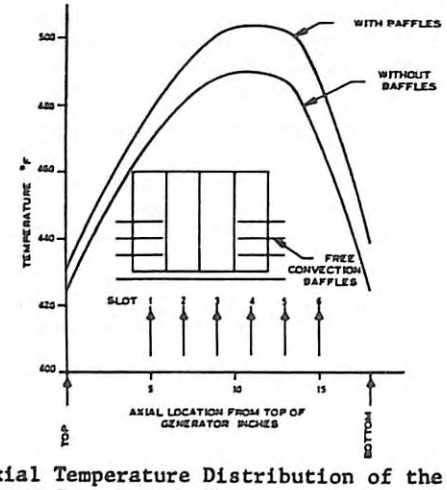

Figure 5-87. Axial Temperature Distribution of the Mod 8B Generator Outer Case During Vacuum Operation With and Without Convection Baffles in Place.

5.4.10 GENERATOR/ALSEP POWER CONDITIONING UNIT INTEGRATED PERFORMANCE TESTS

A program of integrated tests was performed using Generator Mod 8B and a Bendix Power Conditioning Unit (PCU) to evaluate the compatibility between the two units, and to, in general, determine the integrated performance characteristics of the RTG and PCU under selected conditions when they are operated as a system.

Short term compatibility between the RTG and the PCU was checked by determining whether the performance characteristics, including operating temperature, of the generator changed when it was supplying power to the PCU instead of a static load. Operating characteristics for the generator were first determined in the normal manner with the generator supplying the usual static load. Tests were then repeated under the same conditions but with the generator and the PCU interconnected.

System performance characteristics were determined by observing how well the PCU could control the generator under a range of operating conditions. Data were taken under various combinations of generator output power, PCU load and PCU temperature.

The integration tests were conducted with the PCU at room ambient conditions and again in a thermal vacuum environment at both low (-22°F) and high (+158°F) temperatures. The generator operated under lunar day conditions for all tests (+170°F, 10^{-6} torr).

Three different levels of PCU input power were used: maximum, nominal and minimum representing different conditions of generator output power. Results were as follows:

a. There was no evidence during the brief integration tests that the PCU as a load had any significant effect on the characteristics of the generator. Generator performance appeared to be the same whether it was terminated in the PCU or a static load.

b. The particular PCU tested, Serial No. 1, exhibited inadequate dynamic range. Voltage regulation was abnormal for minimum generator output-maximum ALSEP load and maximum generator output-minimum ALSEP load. Note that design changes were subsequently incorporated in the PCU and that the dynamic range is now adequate.

c. A potential problem in the utility of the built-in PCU redundancy was experienced during the testing. The PCU has two channels for receiving power from the generator, one for redundancy. The problem observed was that power is required on

the down-stream side of the switching components to activate the redundant circuitry. When the initial channel failed to operate during system startup, it became impossible to switch to the other channel since no power was provided to any part of the system. From outward indications, one had the erroneous impression that the generator failed.

d. The telemetry signal representing PCU input current generally did not follow actual PCU input current when the dynamic range of the PCU was exceeded. This characteristic makes it difficult if not impossible to analyze system performance from housekeeping data under heavy PCU load conditions.

The test program and its results are presented in a Summary Report, Reference 5-6.

5.5 REFERENCES

5-1 "SNAP-27 Quarterly Report, No. 1", General Electric GEMS 3535-1, January 1966.

5-2 "J. Quinn, "THT-D Computer Model of SNAP-27 Generator and End-of-Life Analysis", General Electric, PIR 114-ANSE, December 1966.

5-3 "SNAP-27 Quarterly Report, No. 5", General Electric, GEMS 3535-5, February 1967.

5-4 "SNAP-27 Quarterly Report, No. 6", General Electric, GEMS 3535-6, May 1967.

5-5 "Thermoelectric Leg Product Specification (TELSP) Final Technical Report", General Electric, 6300-262.

5-6 "Compatibility and Performance Testing of the ALSEP Power Conditioning Unit (PCU) with the SNAP-27 Integrated Power Unit (IPU)", General Electric, 6300-307, January 1968.

6. FUEL CAPSULE DESIGN AND DEVELOPMENT

Figure 6-1 shows an isometric cutaway of the fuel capsule; an exploded view identifying the fuel capsule's components is shown in Figure 6-2. Figure 6-3 depicts the evolution of the fuel capsule design starting with the initial one-piece construction and ending with final two-section design containing burst discs and filters.

6.1 DESIGN REQUIREMENTS

The fuel capsule design was dictated by the constraints imposed by the generator design. Basically, the following parameters were used:

Thermal loading	1500 watts
Fueled length	13.76 inches
Capsule outside diameter	2.5 inches
Fuel form	Pu-238 O_2 microspheres
Fuel geometry	Cylindrical annulus
Clad materials	Haynes-25
Liner materials	Haynes-25
Fuel specific power	0.400 ± 0.010 watts/gram
Physical density of fuel (average)	10.0 grams/cm^3
Packing fraction of fuel	75 percent
Effective fuel power density	$2.6 \pm \frac{.2}{.1}$ watts/cm^3
Cladding emissive coating	0.85
Fuel thermal conductivity	0.62 Btu/hr-ft$^\circ$F @ 1400°F clad temp

The capsule is designed to operate at temperatures between -280°F and +170°F at a pressure of 10^{-10} torr. It is required to provide containment for the fuel during a two year earth storage period, through launch

Figure 6-1. Isometric Cutaway of Fuel Capsule Assembly

Item No.	Component	GE Drawing Number	Material	Coating
1	Nut, Hex	NAS 1291C3	CR Steel AMS5525	Silver
2	Back Plate	47E300940G3	Haynes-25	
3	Flange	47C300360P1	Haynes-25	
4	Screw, Flat Head	NAS560HK3-1	CR Steel AMS5525	
5	Retainer	47B300406P1	Haynes-25	
6	Insulating Plug	47B300405P1	Min-K-2000	
7	Flange Section	47C300401P1	Haynes-25	Radifrax RC-356
8	Liner Head	47B300603P1	Haynes-25	
9	Foam Spacer, Head	47B300602P1	Haynes-25	
10	Zee Ring	47B300624P4	Haynes-25	
		47B300635P5		
		47B300606P6		
		47B300617P7		
11	Shim	47B300634P4	Haynes-25	
		47B300625P5		
		47B300616P6		
		47B300607P7		
12	Outer Liner	47B300601P1	Haynes-25	
13	Inner Liner	47B300614P4	Haynes-25	
		47B300605P5		
		47B300636P6		
		47B300627P7		
14	End Cap	47B300604P4	Haynes-25	
		47B300615P5		
		47B300626P6		
		47B300637P7		
15	Braze Ring	47B300412P1	Engaloy 243	
16	Burst Disk	47B300413P1	Haynes-25	
17	Center Section, Female	47C300608P1	Haynes-25	Radifrax RC-356
18	Foam Spacer, Center	47B300609P1	Haynes-25	
19	Center Section, Male	47C300618P1	Haynes-25	Radifrax RC-356
20	Spacer	47B300170P2	Haynes-25	
21	Filter Element	47B300335P1	Haynes-25	
22	Spacer	47B300170P3	Haynes-25	
23	Cap	47B300170P1	Haynes-25	
24	Forward Section	47C300628P1	Haynes-25	Radifrax RC-356
25	Fuel	NS4470-01-02	Pu^{238}	

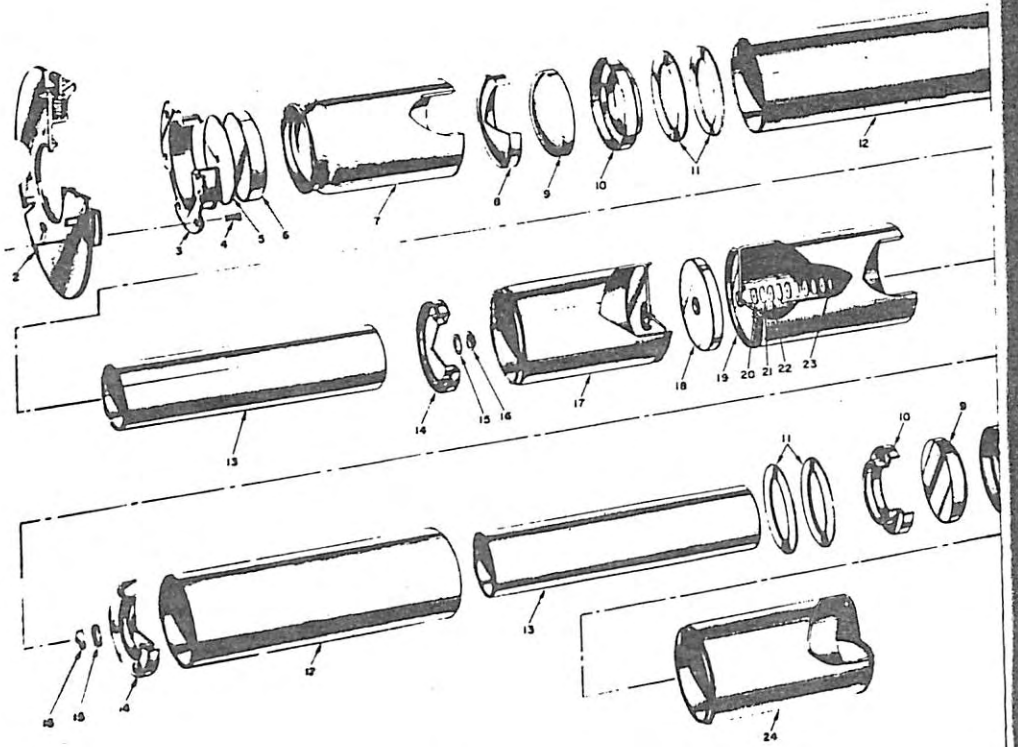

Figure 6-2. Exploded View of
Fuel Capsule Ass

BLANK PAGE

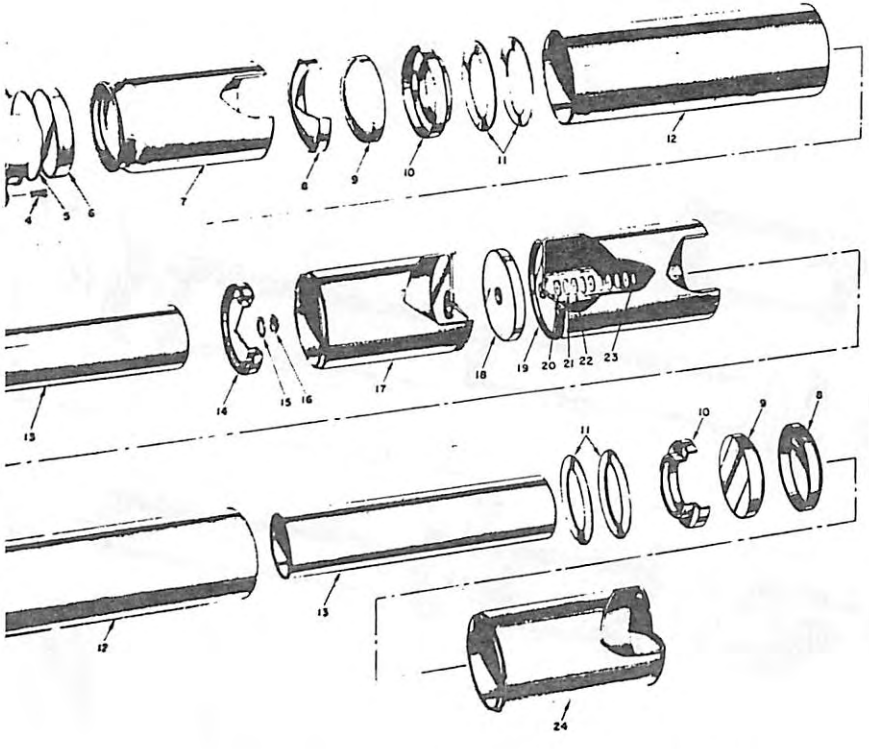

Figure 6-2. Exploded View of Fuel Capsule Assembly

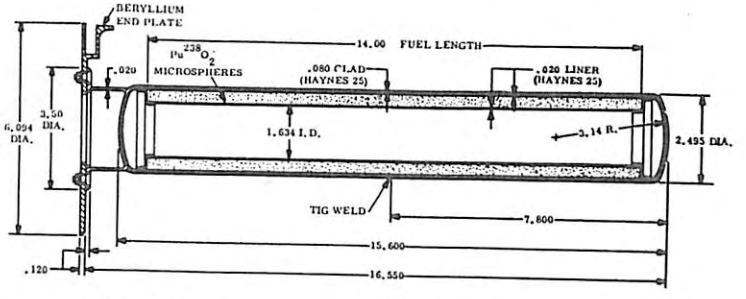

a. Initial Fuel Capsule Reference Design (Series I)

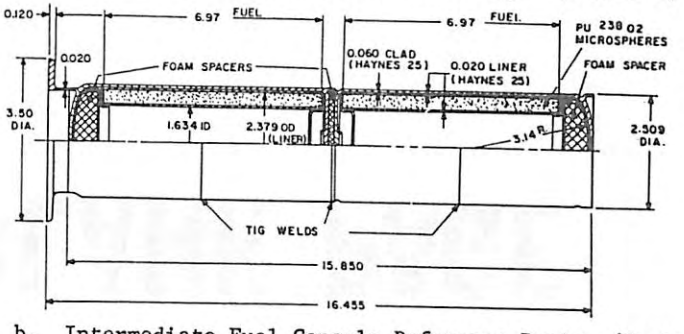

b. Intermediate Fuel Capsule Reference Design (Series II)

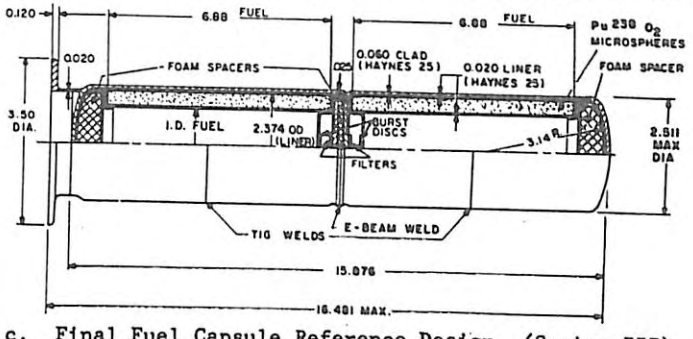

c. Final Fuel Capsule Reference Design (Series III)

Figure 6-3. Evolution of Fuel Capsule Design

and lunar landing environments and during subsequent operational deployment on the lunar surface. The design is also capable of providing fuel containment during superorbital (35,000 ft/sec), orbital and suborbital (24,300 ft/sec) abort re-entries.

Another design feature of the capsule is its helium release system which consists of a series of filters which provide a tortuous path for the helium generated by the decaying fuel such that the evolved gas is vented to the atmosphere without contaminating the area with fuel particulate.

The capsule is equipped with a latching plate which serves as a handling interface as well as locking mechanism for securing the unit in the generator, in the graphite LM fuel cask and in the storage and handling containers.

A high emissive coating is applied to the capsule's outer cladding surface to assist in providing a uniform and efficient thermal output.

6.2 COMPONENT DESIGN AND DEVELOPMENT

6.2.1 FUEL

Plutonium-238, in the dioxide of stoichiometric composition $PuO(2.00 \pm 0.004)$, was selected as the fuel. The production material contained the 238 Pu isotope as 80 a/o $\pm$ 1 a/o of the plutonium isotopes, with a total impurity content not exceed 2 a/o. The fuel has a specific power of 0.400 ± 0.010 watts/gram. The effective power density is 2.6 ± 0.1 watts/cm^3 when the average individual particle density is of 9.1 to 10.9 g/cm^3 and the packing fraction is consistent with the particle size distribution.

The fuel form selected by the AEC was spherules (microspheres). The size range of the spherules is 50 to 250 microns in diameter, with particles less than 25 microns or greater than 250 microns in diameter making up less than 1×10^{-4} percent of the total mass. The fuel was manufactured at Mound Laboratory by firing plutonium powder through an induction coupled plasma torch at 1200°F.

The fuel form is chemically and physically stable and will not undergo microscopic change in structure as a result of pyrolysis, radiolysis, spontaneous and induced fission, neutron and alpha particle bombardment, decay product ingrowth and any combination of these. The fuel is also chemically inert in contact with the primary encapsulating material which is Haynes alloy L-605 - Haynes-25 at all temperatures over the range from 0°C to 1000°C, in helium or in vacuum.

6.2.2 LINER

The function of the liner is to provide the primary envelope for containing the fuel and maintains the fuel in a desired configuration. The initial design (Series I) consisted of outer and inner tubes of Haynes-25. The inner tube was held in a concentric position with respect to the outer tube by means of end rings. The fuel was loaded into the void area formed by the outside diameter of the inner liner and inside diameter of the outer liner; the fuel was "topped off" with Haynes shims and the closure was completed by TIG-welding caps or "heads" at each end. Under each head was a Haynes foam spacer placed there for impact purposes. The resulting liner was a completely sealed annulus which distributed the fuel evenly over the entire length of the capsule. Impact testing of this Series I design showed a tendency for the capsule to fracture at its mid-section.

The capsule design was then changed to Series II to provide two separate fuel chambers in the clad such that complete containment would still occur if the capsule broke at the mid-section. The mid-section modification allowed fracture along a predetermined line to allow helium generated by the decaying PuO_2 fuel to escape. Also, by dividing the fuel load, the inertial energy from the fuel would not be transmitted to the impact end due to the slight delay resulting from deformation in the center area. The liner to accommodate this design was a shortened version of the Series I design. Other changes consisted of a liner end-cap replacing the head at one end and introduction of Haynes shims between the liner end-caps and the inner tube to compensate for a loose fit. Because of a cracking problem in making the TIG weld of the inner liner tube to the end-cap, the weld was changed to electron beam.

The final design for the liner was released as Series III. By this time it was recognized that the power density of the fuel varied from 2.5 to 2.8 watts/cc and that a weight savings in inert hardware such as shims and ZrO_2 filler could be realized if liners were sized to meet specific fuel power densities. Therefore, four different liner sizes were provided with each fuel capsule hardware set so that a selection of the proper liner could be made at the time of fueling. Also at this time, a decision was reached to vent the helium generated by fuel decay from the capsule. The liner was modified by having a hole 0.020-inch diameter placed in the center of the end cap. The hole was covered by a 0.001-inch thick Haynes-25 rupture disc brazed to the end cap through an intermediate washer or braze ring. The design for the liner was thus finalized and frozen.

6.2.3 CLADDING

In the initial phases of the program, impact survival was the prime

consideration in capsule design. Haynes-25 alloy of 0.060- to 0.080-inch thickness was selected as the clad material based on its creep rupture strength and high ductility. The critical areas of the cladding were identified as the welded sections. In Series I, there were two such welds per capsule; these were the welds which secured the flange to one cladding half and the closure weld at the capsule mid-span.

Three configurations were studied and tested for the joint design (straight-butt, flanged-butt and step-butt) and were welded using both electron beam and TIG welding processes. The TIG weld resulted in greater heat affected zones and greater change in the Haynes-25 grain structure. Electron beam welds in the step-butt configuration resulted in incomplete fusion of the joint. In straight-butt joints, both methods proved unsatisfactory due to metal shrinking in the heat affected zone and the straight-butt joint was dropped from further consideration. The flanged-butt joint with electron beam welding was selected for the flange joint but due to hot cell limitations at the fueling agency, TIG welding was selected for the closure joints. The stepped-but configuration was chosen as being the most complementary design for the TIG weld.

The Series II capsule design used the same weld parameters and joint designs as developed under Series I, but incorporated two closure welds, each being 1/4 the distance from each end and a mid-span weld to join the two half-capsules. The problem of weld penetration on the closure welds arose because there was concern that a full penetration of the joint by the weld could rupture the fuel liner directly adjacent. Subsequent development and practice of welding techniques enabled Mound Laboratory to execute full penetration without damaging the liner.

Another problem involved the mid-section weld. The assembly technique called for completing closure of two capsule halves, then joining the two fueled halves with a TIG weld. The void volume between the capsule halves is very small and pressure buildup due to heat of welding and the capsule itself caused the weld to blow open in the area that completed the closure. This was resolved by revising the manufacturing sequence by welding the center section prior to making the closure welds and by using the electron beam weld process.

During development of the cladding, provision was made for relief of the helium generated by the decaying fuel. In the Series II design, filtered apertures allowed helium to pass from the fuel chambers into the void formed by the half-capsule bulkheads and the interface joint between the capsule halves. On the female side of the center section step-joint, the clad wall thickness is 0.023 inch in a 0.130 inch band around the circumference of the part. The wall thickness of the

remainder of the cladding is 0.060-inch. When the helium pressure buildup is sufficient, the capsule (its storage/mission life being complete) will fracture in the thin section. The fuel will remain contained and continue to release helium until fuel decay is complete.

6.2.4 VENT AND FILTRATION SYSTEM

The problem of disposal of the helium gas generated by the decay of the fuel was recognized at the outset of the program. The Series I design made no provision for venting because a suitable vent design, which would vent yet prevent contamination, had not yet been developed and venting was difficult to incorporate into the Series I configuration. The Series II capsule, however, being a dual capsule was capable of being vented, and venting concepts were introduced in this design. Since venting immediately after encapsulation would result in a capsule not suitable from a safety standpoint, the capsule was designed to vent only after its useful life (two years storage plus one year operation) terminated. The venting process developed took place in three stages which were:

a. Initial release of helium from the liner

b. Filtration of the helium

c. Bursting of the thin section of the outer clad to achieve the ultimate release of the helium.

In Series II, the liner was redesigned such that the end of the liner nearest the capsule center section contained an end-cap, which positioned the inner and outer liner tabular sections concentric with one another. It was through this end-cap that the venting took place. Development tests determined the size of the vent hole, covering for the hole, weld parameters, configuration of the cover and effects of the hole and cover on the liner itself. Results of these tests indicated that a 0.020-inch diameter hole (or smaller) was needed to prevent catastropic failure of any hole covering or filter damage. Tests also showed that a 0.001-inch thick Haynes disc formed to a spherical dome with a diameter of 0.050-inch and a crown height of 0.040-inch would provide an adequate cover. The function of the cover was to provide a temporary seal for the liner such that contamination from the fuel would be contained during the capsule manufacturing and early storage stages. When the generated helium was of sufficient pressure, the cover would rupture allowing the gas to escape thru the 0.020-inch diameter hole. For this reason the cover was called the burst disc. Brazing proved to be the most satisfactory method of affixing the cover.

The bulkhead filters permit helium venting from the liner while preventing the passage of fuel particles. These consisted of Haynes-25 foil discs 0.002-inch thick with 30 holes separated by 0.008-inch thick Haynes spacers. Top and bottom spacers were 0.020-inch thick Haynes. The holes in the filter elements were initially electron beam welded, however, it was later found that laser drilling was more effective in that the holes were much rounder and maintained much more constant diameters through the disc thickness. Punching the filter element holes was tried but resulted in hole edge imperfections and required precision not common to punching operations. Also, at this time, two separate hole patterns (random and 0.25-inch diameter circle) were evaluated. The random holes provided greater flow and less of a tortuous path. Accordingly, the 0.25-inch diameter circle pattern was chosen.

The bulkhead filters provided an anti-contamination screen for the helium leaving the liner escaping to the outside of the capsule. The gas entered the filter by passing under a 0.008-inch thick tack-welded cover disc, through a center hole in a 0.02-inch disc, under the 0.020-inch thick disc to a point where it contacted the laser drilled holes in the 0.002-inch thick filter element located directly behind (under) the 0.020-inch disc. The gas passed through the laser holes contacting an 0.008-inch thick disc, moving again on to a center hole in the disc, passing through and under the disc to the next set of laser holes and so on until the helium has completed its transit over a tortuous path of four filter elements and five discs (two of 0.020-inch and three of 0.008-inch thickness).

6.2.5 BACKPLATE ASSEMBLY

The backplate assembly was developed as a device for providing a handling interface for the capsule and a latching mechanism to lock the capsule in place in its various containers during storage and deployment.

The initial design for the backplate was a circular disc of beryllium 0.125-inch thick with three pickup recesses each equipped with spring loaded locking lugs. Tabs were later added above each pickup point to serve as a guide for the various handling tools. The backplate was attached to the capsule by six threaded bolts mounted to the flange and stainless steel nuts.

When the change was made from the beryllium LM fuel cask to the Graphite LM Fuel Cask (GLFC), calculations and analysis indicated that the capsule backplate temperatures were sufficiently high on re-entry to reduce the load carrying capacity of the backplate. Since the GLFC concept required the capsule to re-enter while contained in the graphite, it was necessary to change the backplate material to Haynes-25. The

configuration was the same as that of the beryllium backplate except that the tabs above the pickup points were made integral to the plate. (See Figure 6-1.)

6.2.6 EMISSIVE COATING

In order to achieve optimum performance from the SNAP-27 generator with a minimum loading of the capsule, the thermal efficiency of the fuel capsule had to be improved by application of a high emissive coating. In addition to survival of terrestrial and lunar environments, the following requirements had to be met:

a. Total hemispherical emissivity > 0.85 at operating temperatures

b. Stable emittance in vacuum at 1500°F for > 600 hours

c. Stable emittance in air at 1100°F for > 400 hours

d. Excellent adherence in thermal shock, vibration and bend tests

e. Application to a 1100°F surface

f. Application by remote process.

Early in the program it was decided that coating the capsule prior to fueling would make the capsule difficult to decontaminate after closure. Therefore, it was decided to coat by remote control after the capsule was assembled.

Ilmenite powder has been successfully plasma-arc sprayed on substrates including aluminum, beryllium and stainless steel as an emissive coating, but would not adhere to the Haynes-25 material. The addition of lead bisilicate to the ilmenite powder in quantities of 30 to 40 percent resolved the problem. This combination was given the name Radifrax RC-353. Radifrax RC-353 was applied on electric fuel capsule simulators and appeared acceptable for the application. It was subsequently noted that when RC-353 was subjected to high temperature cycling at 2200°F, vapor disposition occurred in the form of lead indicating a breakdown of the lead bisilicate. Thermal tests of RC-353 coating continued and proved otherwise successful.

A second coating formulation, Radifrax RC-356, was prepared which eliminated the lead bisilicate and substituted calcium titanate and pure silica. The resulting composition contained 60 percent iron titanate, 30 percent calcium titanate and ten percent SiO_2.

Coatings of RC-353 and RC-356 were applied to Haynes specimens and subjected to irradiation tests at General Electric's Vallecitos Atomic Laboratory, Pleasanton, California. There were no observable changes in physical properties as a result of the neutron bombardment.

During the course of the testing, RC-356 proved to be the most favorable coating. The RC-356 proved capable of retaining a high total hemispherical emittance of greater than 0.85 following its exposure for 5000 hours at 1560°F and a pressure of 10^{-7} torr, preceded by 35 72-hour cycles in air (ambient to 1400°F). It is capable of withstanding the foregoing conditions for at least one year, maintaining optical, physical and chemical stability. In air, the coating can stand 500 hours at 1400°F without a decrease in emissivity (below 0.85).

The coating application techniques involving plasma-arc spraying under remote control was developed by General Electric-ARPO and by General Electric-Vallecitos, who also performed the coating on the deliverable live capsules. Electric fuel capsule simulators and dummy capsules were used during the coating development effort at Vallecitos.

6.3 DESIGN ANALYSIS

6.3.1 STRUCTURAL CONSIDERATIONS

The SNAP-27 Fuel Capsule Assembly is a pressure vessel, since it must contain the helium produced by the decaying fuel. Ideally, it is desirable to maintain total containment of the fuel for a period of time not less than ten half-lives of the fuel. In the case of ^{238}Pu, this is on the order of one thousand years. Realistically, however, to design for this long containment is impractical since the resulting pressure vessel would have to be excessively thick and heavy to prevent the walls from creeping and failing to hoop stresses.

The approaches suggested to resolve the problem were:

a. Find a material with excellent creep rupture material life. However, materials identified to date were not found to have sufficient creep rupture properties to allow the design to meet the containment goal without introducing a severe weight penalty.

b. A second approach was to provide a large void volume for helium storage, thus preventing the pressure from becoming too high. This was also not practical since the resultant larger system would be heavier.

c. A third approach would be to vent the helium from the capsule. This solves the problems associated with creep rupture, but introduces new problems associated with handling operations and thermal performance. The venting concept, however, if used properly, can become an effective design approach.

All three approaches were used to achieve the end goal. Suffucient void volume was provided to reduce pressure buildup, and the capsule itself does not exceed the practical volume limits defined by the generator design. Filters are mounted in internal bulkheads of the capsule which allow helium to vent to a central plenum. The helium does not vent to the outside until the capsule has completed its mission, thus eliminating the problems associated with handling and operation.

To make the vent system effective, wall thickness sizing was carefully optimized. To prevent a catastrophic rupture of the capsule, a thinned-down area of the clad was provided. This, in conjunction with the radial support offered by the bulkhead in which the filters are mounted, allowed for a predesigned controlled failure point in the clad which resulted in the positive venting of the capsule at a predetermined time without losing the primary containment of the fuel.

The clad walls were sized by using a General Electric developed computer program specifically designed to predict the life of a capsule. The analysis considered any type of fuel, quantity of fuel, capsule material, capsule geometry, initial fuel temperature, and ambient temperature. The analysis was based upon thin shell theory and considered only the hoop stress in the cylindrical portion of the cylinder. Generally, the cylindrical portion of the capsule comprises the major part of the material and weight, making its thickness specification of primary interest.

6.3.2 DYNAMIC LOADS

The fuel capsule must be able to survive loads representative of launch, lunar descent and the shock of lunar touchdown. Since the Saturn V mission loads were completely defined, test data resulting from tests performed to the anticipated environmental conditions were used for all analysis. The fluctuating stresses due to vibration were of most concern since they could result in a fatigue failure.

Capsule fatigue life is a function of varying stress amplitudes where the stress varies with time. The most commonly used method for determining fatigue life under varying amplitudes is one (proposed by Miner) in which the life of the capsule is governed by the cycle ratios at each stress level. That is, if $\sigma 1$, $\sigma 2$, $\sigma 3$, $\sigma 4$, ... σn are

the various stress levels that may be applied, n_1, n_2, n_3, n_4, ...n_{fn}, the stress cycles required to produce failure for each stress level, then by Miner's hypothesis

$$\frac{n_1}{n_{f1}} + \frac{n_2}{n_{f2}} + \frac{n_3}{n_{f3}} + \frac{n_4}{n_{f4}} + \cdots \frac{n_n}{n_{fn}} = \text{Miner's Index}$$

A Miner's Index of 0.3 was taken as the lower boundry of values to ensure structural integrity in the fatigue producing environment. The hypothesis proposes that damage is proportional to the summation of the ratios of the number of applied cycles to the number of cycles of failure, determined from constant amplitude fatigue testing at each stress level, and that as the index exceeds 0.3 the probability of failure increases rapidly.

It has been shown that only those sinusoidal cycles near resonance where the stress is greater than the rms value (i.e., greater than 0.707 times the maximum stress) contribute significantly to the cumulative fatigue damage. The number of cycles (ΔN) near resonance (during which the response is at least 0.707 of maximum) is a function of the sweep rate (β), the natural frequency (f_n), and Q (transmissibility), where:

$$\Delta N = \frac{f_n^2}{\beta^* Q} = \frac{f_n^2}{0.0347 f\ (Q)}$$

* is a function of the test sweep rate.

Since $Q = \frac{fn}{\Delta f(\text{band width})}$ and f = fn at resonance

$$\Delta N = \frac{fn^2}{0.0347 \times \frac{fn \times fn}{f}} = \frac{f}{0.0347}$$

Since the sine testing includes a sweep from 5 to 100 to 5 cps, two resonances are encountered and

$$\Delta N_{total} = 2 \times \frac{\Delta f}{0.0347}$$

The band width (Δf) at 0.707 peak stress was determined by reviewing the capsule strain gage data.

These inputs along with stress/cycle data from the S/N curve were solved in a computer program which established a Miner's Index for each stress level.

An S/N curve was generated from complete stress reversal fatigue testing of typical SNAP-27 weld joints prepared from the same Haynes-25 bar stock material and machined in the same manner as actual fuel capsule claddings. The specimens were aged to reflect the capsule pre-launch history. They were pressurized to anticipated launch conditions (400 psi) and tested at 1350°F. Failure was defined as a significant drop in pressure (5 to 50 psi). Although this is not catastrophic, post-test metallography revealed the weld area was near failure.

To establish the random contribution curve, a slightly different approach is required. The random stresses and the corresponding cycles at each level are a function of the total test time and the rms stress with an assumed Rayleigh distribution.

The rms stress value is determined by reviewing the capsule strain gage data. The total number of cycles (ΔN) encountered during random testing can be approximated by $\Delta N = f_n t$, where t is the test time in seconds.

6.3.3 FUEL THERMAL PERFORMANCE

The fuel capsule assembly was not only designed to encapsulate the fuel, but to also maintain proper temperature levels and distribution for efficient energy conversion in the thermopile. This, coupled with the need to maintain temperatures of the capsule components within the limits of the materials, results in the thermal performance being a significant design area.

The configuration of the capsule is grossly dependent on the thermal conductivity of the fuel in that the conductivity effects of inner liner temperature and the type of environment required in the fuel annulus. At the outset of the program, ΔT experiments were conducted at Mound Laboratory to obtain realistic effective thermal conductivity measurements across the fuel. A SNAP-27 liner assembly was filled with fuel and allowed to heat up. Temperatures were recorded both on the inner and outer surfaces of the liner for the length of the liner. Data at several temperatures were achieved by running the test specimen bare, with insulation around it. Tests were run both in 98+ percent pure helium and 98+ percent pure argon. From the data obtained, the effective thermal conductivity of the fuel was then calculated using the one dimensional heat transfer equation for a hollow cylinder with internal heat generation. The equation is as follows:

6.4 DEVELOPMENT TEST PROGRAMS

6.4.1 MATERIALS AND COATINGS TESTS

6.4.1.1 Materials Compatibility Tests

A test program was initiated to evaluate the compatibility of stainless steel, beryllium and Min-K 2000 insulation with the Haynes-25 fuel capsule cladding. The evaluation determined the effects of these materials when contacting the external fuel capsule surface under wide temperature and atmospheric pressure conditions. Two types of specimens were used, a beryllium/Haynes-25/stainless steel composite and a Min-K 2000/Haynes-25 composite. No compatibility problems were noted.

6.4.1.2 Emissive Coating Tests

The testing of coatings fell into three areas: coating selection tests, application technique tests, and long term performance tests. During the selection process chemical, sieve and x-ray diffraction analyses were used to determine the structure, composition and particle size distribution of the various iron titanate powders which were candidates for coating.

In the application technology phase, thermal specimens were cycled to temperatures of 1850°F for two- and five-minute cycles. These were later expanded to 1100°F for 72-hour cycles using Radifrax RC-356 coated samples. Bending tests, consisting of bending a coated test strip around a three inch diameter mandrel, were also used to determine adhesion.

Hemispherical emittance tests were made using electrically heated coated test strips and a Perkin-Elmer Model 205 Spectrophotometer. These tests were run for as long as 500 hours at 1100°F in air and 600 hours at 1560°F in vacuum.

Coated samples of Haynes-25 material were forwarded to General Electric-Vallecitos for evaluating the stability of high temperature, high emissivity coatings under neutron bombardment. Specimens of Haynes-25 alloy 0.25-inch wide by 0.020- to 0.030-inch thick by eight inches long were coated to a 0.0025-inch thickness as follows:

6 specimens	RC-353	plasma arc spray
6 specimens	RC-356	plasma arc spray
6 specimens	RC-156	paint spray

A special fixture was fabricated to support the specimens at their uncoated ends to fit the reactor test channel holes. The in-pile irradiation channel was fitted with adequate heaters, water cooling and vacuum capability to provide the required conditions for each of the test specimens. The test chamber proper was a stainless steel tube fitted with cal-rod heaters on its outer wall. A second tube enclosed the cal-rod heaters and test chamber with insulation attached to its outer wall and then a water cooled jacket encapsulated the entire assembly. The vacuum port instrumentation leads extended from the reactor through the test channel to an adequate feed through and vacuum coupling. An oil diffusion pump with mechanical backup and rough pumping provided capability to obtain vacuum to 10^{-6} torr. Vacuum is monitored utilizing an ionization gauge located as close as possible to the external shielding of reactor. Sufficient probe parts were provided to accommodate thermocouples and extentions. The tests were conducted at General Electric Vallecitos Atomic Laboratory.

The total irradiation time was approximately 200 seconds at 1×10^{11} NV ≥ 1 Mev (2×10^{13} NVT). The gamma dose was monitored using foil and wire targets placed near the specimen. Temperature and vacuum were monitored throughout the test. There was no sign of coating degradation as might be evidenced by color change, spalling or flaking.

6.4.1.3 Creep Rupture Tests

Tests to determine the stress rupture and creep characteristics of the capsule material in the as-fabricated condition were conducted. Tests were performed at General Electric-NMPO at temperatures of 1400, 1700 and 2000°F in air.

Eighty-one samples were creep rupture tested in air at temperatures of 1400, 1700 and 2000°F with test times ranging from 0.15 to 2053.8 hours. The coated and uncoated samples tested essentially the same with respect to effect of the coating in both welded and unwelded samples. The welded samples did, however, show a shorter time to rupture than the base metal samples. The welded samples had a significantly higher creep rate than base metal samples at 2000°F.

All stress rupture data were analyzed in terms of the Larson-Miller parameter $P=T(C+\log tr)$ where T is temperature in °R; tr is time to rupture in hours and C is a constant.

The conclusions of the tests were as follows:

a. Stress rupture and creep strength of Haynes-25 alloy (special heat) were higher than vendor quoted values of 1400 and 1700°F and for low stresses at 2000°F fall below

b. Welded samples gave a shorter rupture life than base metal

c. Coating of samples did not affect creep-rupture results.

6.4.2 MANUFACTURING PROCESS TESTS

6.4.2.1 Capsule Burst Tests

The mod-section weld joint in the capsule cladding is an essential element in the venting capacity of the capsule since it provides the final escape path for the helium after the useful life of the capsule or after impact. The weld provides the final seal between the filter exit and the outside during the useful life of the capsule. When the internal helium pressure is sufficient this joint will rupture permitting the capsule to vent. It is necessary, therefore, that the joint rupture non-catastrophically and at a pressure less than that required to rupture the basic cladding.

Tests were conducted on representative samples heated to a temperature typical of operating temperatures and pressurized interally until failure occurred. A test specimen was made with each of five production run of center sections. The specimens were heated to 1400°F and stabilized. The internal pressure was raised at a rate of ten psi per second until 1300 psi or failure occurred. 2500 psi was defined as minimum burst pressure. The specimens were then examined and their failure modes noted.

6.4.2.2 Liner Rupture Burst Disc Tests

The liner rupture disc is required to maintain a sealed assembly of the liner after fueling has been completed. Once the liner has been installed in the cladding and the cladding closure weld is completed the disc may rupture. The design concept for the rupture disc is a thin diaphragm brazed to a thicker washer which in turn is brazed or welded to the end cap of the liner, through which a small vent hole was drilled.

Based on calculations of gas generated by the helium decay, acceptance criteria of 250 psig at ambient temperature was established for the burst disc. After assembly of the disc to the liner a test pressurization was conducted to assure the integrity of brazed disc assembly. A second pressurization was performed to assure the disc was not damaged during subsequent handling.

Sixty-two short time burst tests were performed in which it was noted that acceptance pressurization altered the geometry of the initial design configuration and increased the burst pressure of the rupture disc.

Creep rupture tests were conducted based on a pressure anticipated one-month after fueling. The time to creep rupture failure was 8.7 weeks at 1300°F and 5.7 weeks at 1500°F.

Rupture discs were also tested to determine the effects of decontamination solution on the discs. The liner was heated to 1500°F and had an internal helium pressure of 31 psia. The decontamination solution consisted of 300 ML of water, 120 grams of oxallic acid, 67 ML of concentrated HNO_3.

The tests showed no adverse effects.

6.4.3 FILTER DEVELOPMENT TESTS

The filter permits venting of the liner while preventing the passage of fuel particles. Hence, it was required to have a helium flow rate at least equal to the helium generation rate, while having passages no larger in diameter than the minimum fuel particle expected including a large percentage of the smaller particles that may occur as a result of capsule impact. Most important, the filter must remain intact under capsule impact.

The filter development specimens consisted of Haynes-25 foil discs, with 30 holes of 0.003- to 0.0005-inches in diameter alternated with Haynes-25 spacers. The discs and spacers were welded together at the edges to form an assembly.

Flow rates were measured with helium and water. Salt particles of known size were suspended in helium to determine if passage of like size particles of PuO_2 could be passed by the filter. The results were negative.

Four capsules each containing two filters were impacted to demonstrate the ability of the filter to survive impact. Flow rates were measured before and after impact.

As a result of the filter flow rate studies, the holes in the filter elements which were drilled by the electron beam process were now drilled by the laser beam process. It was found that laser drilled holes were relatively straight whereas the electron beam holes had large entrance and exit craters which were sometimes twice the nominal diameter of the hole. This not only reduced the entrance losses but reduced the viscous losses through the exit, making the filter less efficient than supposed.

The final filter design consisted of a cover disc followed by a 0.020-inch thick Haynes disc followed by four 0.002-inch thick filter elements

in between which were 0.008-inch thick spacers (total of three) followed by a final 0.020-inch thick disc. The whole system was stacked and electron beam welded into bosses in the cladding.

It was noted that stacking at the time of welding had a significant affect on the flow rates through the filters. If the stacking pressure was severe, flow through the filters could be seriously impeded. The same was true if there was a variation in seating or alignment of the compressed filter components. A stacking tool was devised to resolve this problem.

It was also noted that helium flow rate decreased with temperature exposure and time. The flow rate, however, recovered upon increase of pressure and/or thermal relaxation.

Filter assemblies were exposed to high pressure helium at both ambient and elevated temperatures (1400°F). The filter assemblies selected for this test had low flow rates. Observations were that although the elevated temperature reduced the gas flow, post high pressure exposure measurements showed little or no permanent affect as a result of the increased pressurization.

Tests were conducted to determine the quantity and size of particles that could be passed through a filter assembly. Aluminum powder in 5 to 200 micron size placed in high purity helium gas and forced into the filter assembly under 200 psig pressure for one minute. Particles passed were 4 in 5 micron size, 8 to 12 in 10 micron size and 10 to 13 in 30 micron size.

Tests were also undertaken using salt to simulate fuel particles as to whether fuel could be leaked out through the filters should the capsule impact in water and experience a pressure reversal. Results were negative.

Life tests were conducted to determine filter performance during sustained periods of operation. The tests which simulated a capsule operating in a generator on the lunar surface were conducted at an operating temperature of 1460°F, a continuous flow of helium through the filter and the high and low pressure side of the filter to be in a helium environment. A contiunous helium flow was maintained at a ΔP of 12 psig which was raised to 180 psig once every 24 hours.

Three tests were conducted, two of which were for 1000 hours and one for 2300 hours. In the final phase of the 2300 hour test the filter assembly was subjected to a 1000 psi pressure surge to simulate normal capsule midsection failure. The filter remained intact and operable

after the pressure surge and all other filters tested performed satisfactorily with little or no degradation.

6.4.4 FUEL CAPSULE IMPACT TESTS

The fuel capsules ability to contain the fuel in the event of pad abort or re-entry was one of the major considerations in the design of the capsule. One of the most significant test series along these lines was that of impact testing.

Impact tests were to run in two series. Previous to these tests, a drop test series was conducted at Sandia Corporation to determine capsule terminal velocities.

A third series of impact tests was planned to qualify the design which evolved from the Series II and other development tests; however, the customer felt sufficient data was available and the Series III tests were cancelled. Near the end of the program a drop test of a simulated capsule in a graphite LM fuel cask furthered this decision.

6.4.4.1 Series I Impact Tests

A total of 11 Series I impact capsules were built and impacted for the purpose of determining the critical impact angle for the SNAP-27 design. The Series I configuration consisted of a single continuous fuel anulus enclosed in cladding welded at the mid-span, and loaded with a metal mixture simulating the mechanical and weight characteristics of the isotope fuel form. There were no vents or helium release mechanism. Outside appearance and dimensions were similar to those of the operational design.

The tests were conducted at General Electric's Morgantown, Pennsylvania, Impact Test facility, Figure 6-6. The mechanism used in testing was an air driven catapult. The capsule holder, which also determines the impact angle, was interchangeable and available for various angles between 0 degrees and 90 degrees. The capsule was fired at the desired velocity into a nine cubic foot granite block weighing 1360 pounds. This granite block provides a capsule to block weight ratio of 1 to 100. The capsule on the catapult was heated and pressurized prior to firing. The units were impacted at a temperature of 850°F and velocities of 265 to 240 feet per second with two at 160 feet per second. After 11 tests, Series I was cancelled owing to a major configuration change.

As a result of the tests it was observed that most clads ruptures in the center or weld area. The fuel liner, however, remained intact which was felt to be significant for containment purposes.

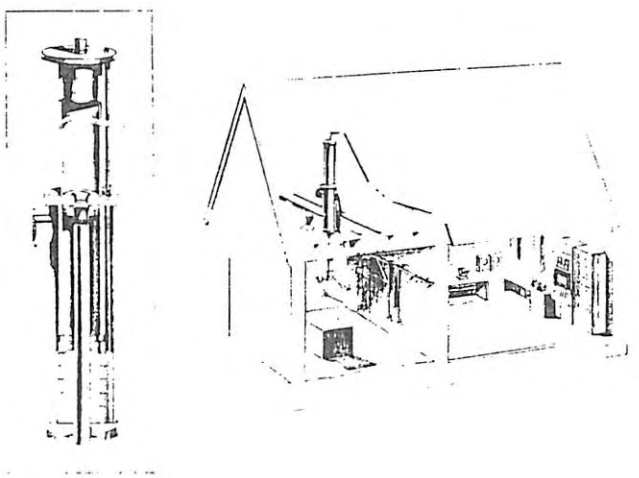

Figure 6-6. Morgantown Catapult Test Facility

6.4.4.2 Series II Impact Tests

The configuration for Series II was similar to the final design in that it has 0.060-inch clad thickness, dual liners, and three closure welds in the cladding. The liners were vented but the filters were absent since they were under development at that time.

The Series II tests originally intended for selecting cladding wall thickness was changed to determine the critical impact angle for the dual capsule configuration.

Seventeen Series II capsules were impacted using the General Electric Morgantown facility. Nine capsules split at mid-span, none of which had leaks in both half-capsule claddings. Seven half-capsules had claddings which leaked more than the minimum allowable but only three had leaks in the internal liner. Figure 6-7 shows some of the specimens following impact.

The most significant item noted was that there was no release of fuel from any impacted capsule. This was observed even in those cases where the helium leak rate exceeded the maximum allowable.

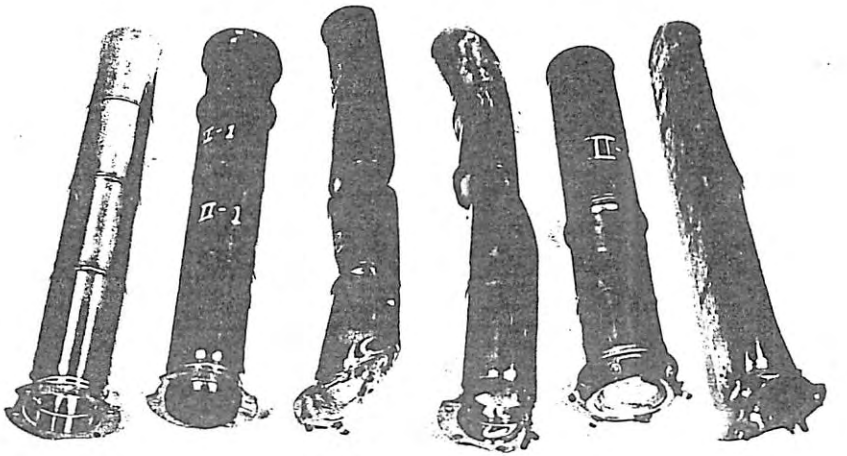

Figure 6-7. Fuel Capsule Test Specimens After Impact

The critical impact angle sought did not exist as it was originally conceived. No impact angle caused damage to the extent that fuel was released; conversely the cladding was breached on impacts from 0 degrees to 45 degrees and from 135 degrees to 180 degrees. The area of vulnerability was considered as impact at any angle within a 90 degree line centered at each extreme and opening outward. Series II impact testing indicates either end could be treated as critical with equal applicability of the test results.

6.5 REFERENCES

6-1. P. N. Flagella and W.L. McCullough, "Stress Rupture and Creep Behavior of Haynes Alloy No. 25 at 1400, 1700 and 2000°F in Air," General Electric-NMPO, 67-528, August 1967.

6-2 E. H. Sayell, "Effect of Aging on SNAP-27 Cladding," General Electric, PIR 1784, December 1967.

6-3 "SNAP-27 Quarterly Report No. 10," General Electric, GEMS 400, May 1968.

7. GRAPHITE LM FUEL CASK DESIGN AND DEVELOPMENT

7.1 DESIGN REQUIREMENTS

The design requirements for the Graphite LM Fuel Cask (GLFC) fall into two general categories:

a. Operational

b. Abort

7.1.1 OPERATIONAL

The GLFC was designed for the following operational and interface requirements:

a. Fuel capsule insertion and removal as required for test, checkout, pad safety and lunar surface operations

b. Fuel capsule heat rejection during the operational mission from fuel capsule insertion to removal to ensure that the fuel capsule temperature will not exceed 1400°F

c. Capable of meeting operational and interface requirements during or after exposure to the logical combinations of environments associated with the six phases of the ALSEP mission as defined in General Electric Specification NS-0110-07-04, "Performance and Design Requirements for the Graphite LM Fuel Cask (GLFC), SNAP-27 Program". These environments are listed in Table 7-1.

7.1.2 ABORT

The GLFC design is based on re-entry conditions associated with the following abort cases:

a. Suborbital re-entry

b. Decay from an earth orbit

c. Superorbital re-entry from translunar flight.

The first re-entry conditions were based on the latest available ALSEP mission data (see Reference 7-1) and are defined in Table 7-2. The

BLANK PAGE

TABLE 7-1. ALSEP SYSTEM OPERATIONAL ENVIRONMENTS

Environment Considered	A Handling, Assembly and Checkout	B Transportation and Storage, Packaged	C Factory and Assembly Bldg. Checkout	D Launch Pad Environment	E Launch, Flight, and Landing	F Lunar Operations
Thermal	NA	NA	NA	1. 350°F maximum with circumferential and longitudinal gradients of 150°F on the external GLFC surface for 100 hours. 2. 10 hot/cold cycles (buried/unburied) with a maximum of 600°F on the external GLFC surface reached in each cycle	1. 800°F maximum with a circumferential gradient of 150°F on the external GLFC surface for 12 hours with the RLA doors closed (earth orbit) and 72 hours with RLA doors open (translunar)	Same as E
Shock	15g peak sawtooth pulse 10 to 12 ms rise time, 6 to 8 ms decay	(1)	NA	NA	Same as A	NA
Vibration	NA	(2)	NA	NA	Random (3 axes) Frequency (H_z) / Power Spectral[2] Density (g^2/H_z) 23-80 / 0.133 80-120 / Rolloff 12db/oct 120-950 / 0.026 950-1250 / Rolloff 12db/oct 1250-2000 / 0.0087 Sweep rate-3 oct/min Sinusoidal (3 axes) Frequency (H_z) / Amplitude (g's) 5-20 / 0.3 inches D.A. 20-35 / ±6 35-100 / ±8 5 minutes per axis	NA
Acceleration	1.0g through preferred axis	2.67g vertical with 1g lateral	NA	NA	a. 60g overall design load[4] longitudinal or lateral b. 14 ± 1g longitudinal or lateral	NA
GLFC Support Assembly Band Preloads	NA	NA	Circumferential-120 psi max. Axial-450 psi max. with an avg. of 150 psi on 20 in² of GLFC end cap	Same as C	Same as C	Same as C
Ambient Temperature	-20°F to +110°F	-65°F to +160°F	+50°F to 100°F	+50°F to +100°F	0°F to 160°F	+300°F -280°F
Pressure	Ambient	Sea level to 50,000 ft.	Ambient	Ambient	1×10^{-10} torr	1×10^{-10} torr
Solar Radiation	360 Btu/ft²/hr, 6 hr/day	NA	NA	NA	NA	442 Btu/ft²/hr 6 hr/day
Humidity	15% to 50% relative	50% max. GLFC enc. in shipping cont.	50% max.	50% max.	NA	NA

(1) MIL-STD-810 A (USAF) 23 June 64 Method 516.1, Procedure III
(2) MIL-STD-810 A (USAF) 23 June 64 Method 514.1 for Equipment Class 6
(3) Forces indicated are at GLFC interface with its support structure
(4) Overall static design load factor used to design for dynamic loading based on worst possible transmissibilities

NOTE: Other induced and natural environments such as acoustics, salt spray, sand and dust, etc. are either not applicable or the levels are not critical for the GLFC.

TABLE 7-2. INITIAL RE-ENTRY CONDITIONS

SUPERORBITAL ABORT CONFIGURATION AND INITIAL CONDITIONS

Configuration

a. LM Ascent and Descent Stages Joined, All Tanks Full

b. Reference Weight - 32,000 Pounds

c. Cask Free From LM at 330,000 Feet

Initial Conditions

Condition	Altitude (ft)	$V_{Inertial}$ Down Angle (degrees)	Geodetic Inclination (degrees)	Inertial Velocity (ft/sec)
1	LM at 400,000	6.25	40	36,333
2		10	50	
3		20	60	
4		30	70	
5		38.05	90	

EARTH ORBIT ABORT CONFIGURATION AND INITIAL CONDITIONS

Configuration

a. LM Descent Stage Tanks 80 percent Full

b. Reference Weight - 18,384 Pounds

c. Cask Free from LM at 300,000 Feet

Initial Conditions

LM at 400,000 Feet

$V_{relative}$ 24,403 ft/sec (Oblate Earth)

Air Relative Geodetic Down Angle 0 degrees

Inclination 32 degrees

Latitude 0°

Longitude 0°

definition and analysis of additional abort situations, which were later defined, are contained in Reference 7-1. The abort conditions and constraints are derived primarily from LM re-entry. Under these abort conditions, which involve both earth orbit decay and superorbital re-entry, the GLFC remains attached to the LM by its mounting structure until the point of LM breakup during re-entry. From that point to earth impact, the GLFC is subsequently treated as a free unencumbered body. The re-entry flight path conditions are earth orbit and superorbital from grazing to -38.05 DFH.

The criteria used in the design of the GLFC in order to survive the operational and re-entry environment is that there is to be no yielding at limit load and no failure at ultimate load. Limit and ultimate load factors are defined in Table 7-3.

TABLE 7-3. DESIGN LOAD FACTORS

	LIMIT LOAD FACTOR	ULTIMATE LOAD FACTOR
ABORT CONDITIONS		
Aerodynamic and Inertial	1.0	1.25
Thermal	1.0	1.00
OPERATIONAL CONDITIONS		
Band Preload	1.0	1.5
60g Design Load	1.1	1.5
Thermal	1.0	1.0

7.2 COMPONENT DESIGN

The GLFC basically consists of a primary heat shield, secondary heat shield, insulation, spline locks and supports for the Fuel Capsule Assembly (FCA). The primary heat shield is the outside structure of the GLFC which completely surrounds the capsule. The external supports for the GLFC interface directly on the primary heat shield. The primary heat shield consists of a cylinder with hemispherical end caps attached to the cylinder by means of a breech joint. The breech joint

requires sixty degree rotation for installation and removal. The caps are locked to the cylinder with a spline lock consisting of a graphite/aluminum oxide tantalum wire assembly located at the cap-cylinder interface. Inside the GLFC, the capsule is supported on each end; the aft end by a latch fitting and the forward end by a capsule support. The latch fitting is the only support for the FCA in the axial direction and provides for locking the FCA inside the GLFC. The secondary heat shield is fastened inside the primary heat shield to the latch fitting and forward capsule support. The shield is cylindrical and is approximately the length of the FCA. Insulation is attached inside each end cap to protect the ends of the FCA from re-entry heating.

Figure 7-1 shows an isometric cutaway of the final GLFC design with the beryllium secondary heat shield. The GLFC is shown with a fuel capsule installed. Figure 7-2 shows an exploded view of the GLFC.

The succeeding paragraphs describe in more detail the elements of the GLFC and their functions.

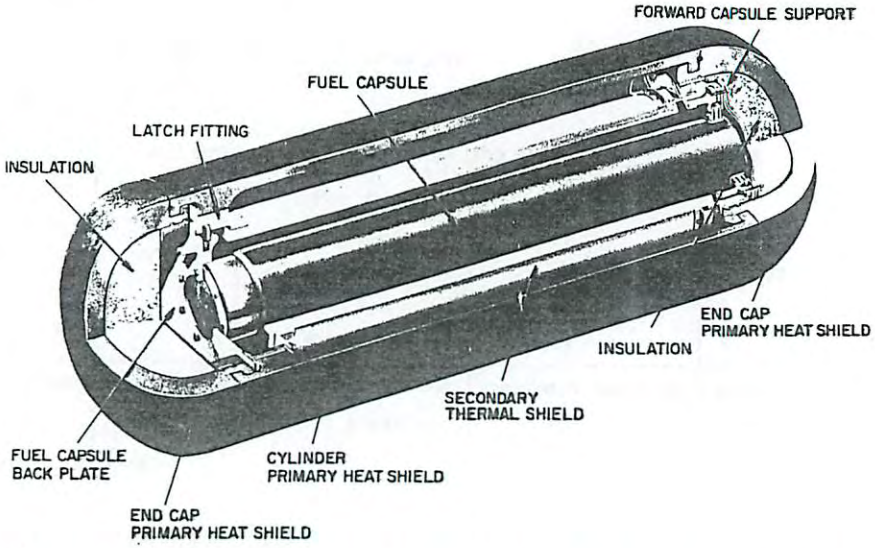

Figure 7-1. Isometric Cutaway of GLFC Final Design (with Beryllium Secondary Shield)

7.2.1 PRIMARY HEAT SHIELD

The function of the primary heat shield is to protect the FCA from the high temperatures of re-entry heating. It forms the external shell of

Item No.	Component	GE Drawing Number	Material	Coating	Melting Temperature (°F)	Density (lbs/ft^3)
1	Primary Shield Cylinder	47D301124 P1	Pyrocarb 406			98.5
2	Primary Shield End Caps	47D301124 P2	Pyrocarb 406			98.5
3	Secondary Thermal Shield	47D301251	HPB Beryllium	Silver, Rhodium, Radifrax	2360	115.8
4	Aft Thermal Shield Support Ring	47D301253	Inconel X-750	Aluminum Oxide	2540 to 2600	514.9
5	Fwd Thermal Shield Support Ring	47D301252	Inconel X-750	Aluminum Oxide	2540 to 2600	514.9
6	Fwd Thermal Shield Support Rings	47D301252	Inconel X-750	Aluminum Oxide	2540 to 2600	514.9
			Haynes L-605	(Oxidized Surface)	2425 to 2570	570.2
7	Special Nut	47D301254	Haynes L-605	(Oxidized Surface)	2425 to 2570	570.2
8	Special Bolts and Washers	47D301255	Titanium 8A1-1Mo-1V or 6A1-4V	Diffusion Barrier Formed by Na, Li, and K Carbonate Treatment	3100	269.6
9	Latch Fitting	47E300973 P1				
10	Bolt	47B301138 P1	Titanium 8A1-1Mo-1V or 6A1-4V		3100	269.6
			A-286 (Hitemp Steel)		2500 to 2660	494.2
11	Sleeve	47E300973 P5	Titanium 8A1-1Mo-1V or 6A1-4V	Diffusion Barrier Formed by Na, Li, and K Carbonate Treatment		269.6
12	Pad	47E300973 P4			3100	269.6
13	Tab	47E300973 P3	Titanium 8A1-1Mo-1V or 6A1-4V		3100	269.6
14	Housing, Fwd, Capsule Support	47E301110 P14	Titanium 8A1-1Mo-1V	Lithoid Type H17h Emissivity Coating	3100	269.6
15	Rings, Fwd. Capsule Support	47E301110 P3	Titanium 8A1-1Mo-1V		2425 to 2570	570.2
16	Guide, Fwd. Capsule Support	47E301110 P4	Haynes 25		2550 to 2610	494.6
17	Shim, Fwd. Capsule Support	47E301110 P20	CRES 302		3100	269.6
18	Flange, Fwd. Capsule Support	47E301110 P19	Titanium 8A1-1Mo-1V		3100	269.6
19	Cover, Fwd. Capsule Support	47D301254 P1	Titanium 6A1-4V			
Not Shown	Bridge Fwd. Capsule Support	47E301110 P21	Silver	Lithoid Type H17h Emissivity Coating	1700	643.7
20	Aft Cap Insulation	47D300977 P4	Fiberfrax			98.5
21	Retainer	47D301124 P5	Pyrocarb 406			
22	Forward Cap Insulation	47D300977 P1	Fiberfrax			
23	Forward Spline Lock Assy.	47D301129 G4				
24	Aft Spline Lock Assy.	47D301129 G3			5425	1037
	Cap Lock	47D301129 P19	Tantalum B21Y44A or B21Y45A or B		5425	1037
	Wire	47D301129 P6	Tantalum B21Y44A or B or B21Y45A or B		3700 to 3800	29.4
	Beads	47D301129 P3, P4, P5	Al_2O_3 171A4423		5425	1037
	Fitting Lock	47D301129 P2	Tantalum Alloy, B21Y44A or B or B21Y45A or B		2800 to 3000	276.5
	Fitting Lanyard (Aft only)	47D301129 P1	Titanium 6A1-4V		2800 to 3000	276.5
	Lanyard (Aft only)	47D301129 P7	Titanium 6A1-4V			
25	Fuel Capsule	47D30040061	See Table 3.2-1		2425 to 2570	570.2
26	Back Plate	47E30094063	Haynes 25		2425 to 2570	570.2
27	Latch Mechanism	47E300940 P4	Haynes 25			

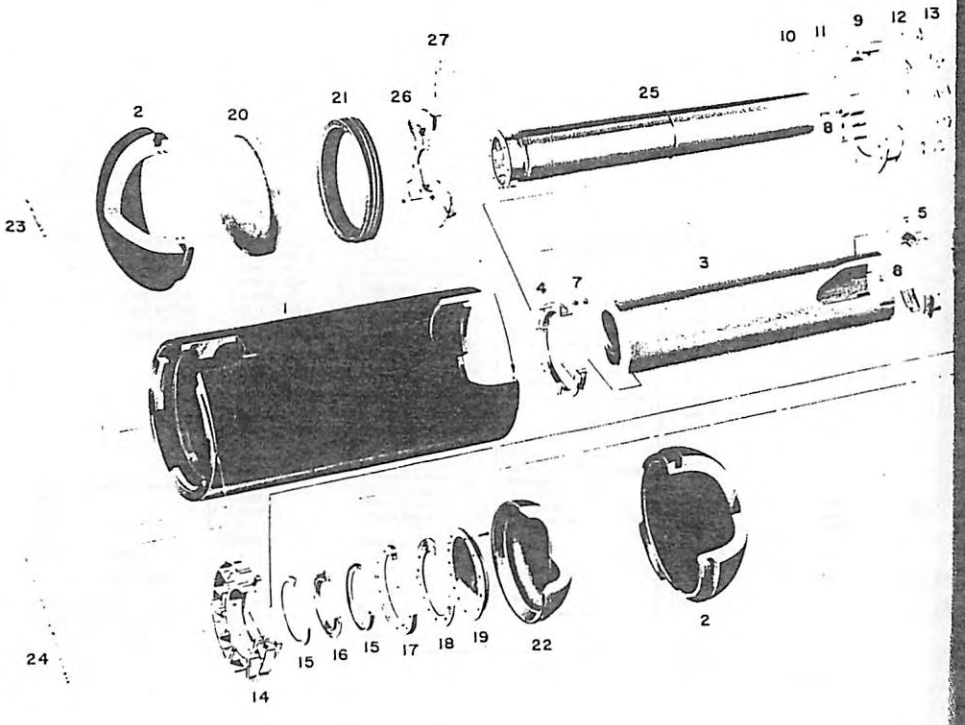

Figure 7-2. Exploded View o
(with Beryllium Secondary Sh

BLANK PAGE

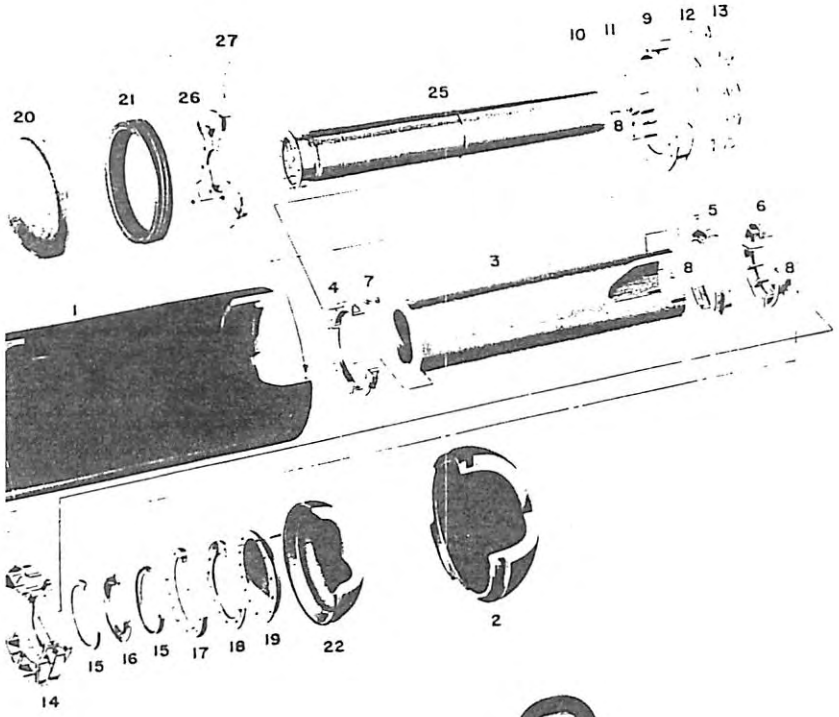

Figure 7-2. Exploded View of GLFC (with Beryllium Secondary Shield)

the GLFC and consists of a cylinder and two nominally hemispherical end caps. The cylinder wall is 0.35 inches thick, and the end cap wall is 0.70 inches thick. The graphitic material used in the heat shield is Hitco Pyrocarb-406, formed by infiltrating a pyrolized square weave graphite composite with pyrolitic graphite. The cloth layups are shown in Figure 7-3 for the end caps and Figure 7-4 for the cylinders. The primary heat shield protects the fuel capsule during re-entry by heat sink reradiation and ablation methods. The heat rejected by the fuel capsule is absorbed by the primary heat shield where it is both re-radiated to external environment and conducted to the GLFC support structure.

This material has the capability to withstand the 4500°F temperature and stresses created during re-entry thus providing a structural and thermal shield around the FCA.

The cylinder portion of the primary heat shield contains a breech joint at each end for attachment of the end caps. The end cap must be rotated 60 degrees with respect to the cylinder for installation or removal. The interface between the cylinder and end cap contains a groove to contain the spline lock. Lateral support of the GLFC from the mounting straps are at each end of the cylinder. Loads from the FCA are transmitted directly to these mounting points.

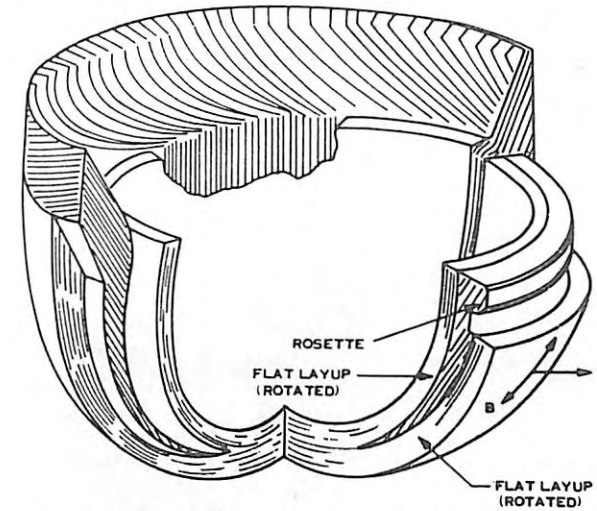

Figure 7-3. Pyrocarb-406 Ply Orientation Layup for Primary Shield End Caps.

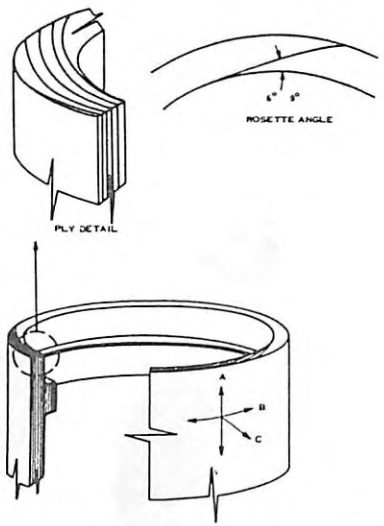

Figure 7-4. Pyrocarb-406 Layup for Primary Shield Cylinder

The wall thickness of the cylinder is designed for thermal and pressure stresses due to abort re-entry. The wall thickness is constant except at one end where it is thicker to create an attachment area for the latch fitting (FCA support).

The end caps are identical and contain a breech joint and spline groove corresponding to the cylinder. In addition, each end cap has three holes in the outer surface to interface with the axial support straps and end cap removal tool. The wall thickness of the end cap is designed for thermal and pressure stresses due to abort re-entry. The area adjacent to the cylinder is thicker to incorporate the breech joint. The minimum thickness of the end cap is greater than the cylinder due to the larger heating flux subjected to the end cap during re-entry.

7.2.2 BERYLLIUM SECONDARY HEAT SHIELD

The secondary heat shield (Figure 7-5) is needed in addition to the primary heat shield to protect the lateral surfaces of the FCA from re-entry heating since, during re-entry, the inside wall of the primary heat shield (graphite) is at high temperature and the thermal radiation to the FCA would cause a failure.

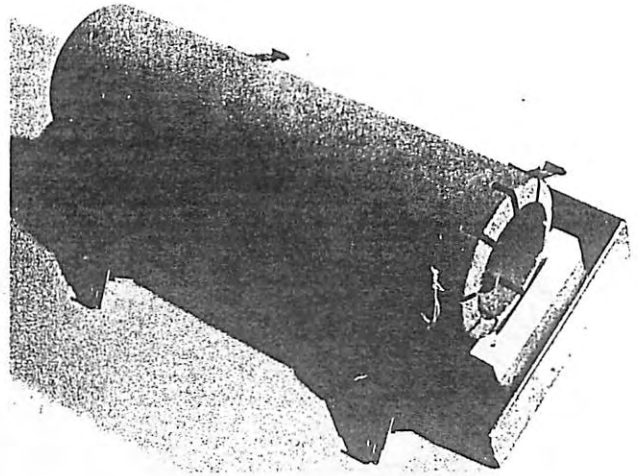

Figure 7-5. Beryllium Secondary Thermal Shield

The beryllium secondary heat shield is sized for re-entry considerations where its primary function is to act as a large heat sink for the re-entry abort. Sufficient heat can be stored through the high heat regimes to prevent the capsule from releasing fuel either by melt or "blow" due to rapid internal pressure buildup of the helium. The beryllium thermal capacitance and high thermal conductivity permits the GLFC to re-enter either spinning or side-on stable.

The secondary thermal shield consists of a beryllium cylinder 4.13 inches in diameter and 0.505 inches thick. The beryllium is coated with successive layers of silver, rhodium, and Radifrax to provide oxidation resistance and compatibility with the fuel and a high emissivity surface to promote radiant heat transfer. During normal operation, the heat rejected by the fuel capsule will be radiated to the beryllium cylinder, conducted through it, and reradiated to the graphite cylinder. During re-entry, the beryllium cylinder will act as a heat sink to protect the fuel capsule.

The cylinder is supported at the forward end on the flanges of a segmented Inconel ring which is bolted to the forward capsule support. These flanges fit into flots cut into the end of the beryllium cylinder. The slots are designed to allow radial and longitudinal thermal

expansion of the beryllium cylinder. Three Inconel clips provide the attachment required to make the internal structure a cohesive unit independent of the graphite heat shield.

7.2.3 SILICON DIOXIDE SECONDARY THERMAL SHIELD

Although this design was subsequently replaced by the beryllium shield, nevertheless, it is felt that this design should be described for information purposes. An isometric cutaway and an expanded view of the GLFC with this secondary heat shield are shown in Figures 7-6 and 7-7, respectively.

The silicon dioxide secondary heat shield was designed to have a dual function:

a. That of a sufficient thermal insulator to protect the FCA from the high temperatures of re-entry heating that would result in fuel release

b. A sufficient thermal conductor to prevent the FCA from exceeding 1400°F during normal operation.

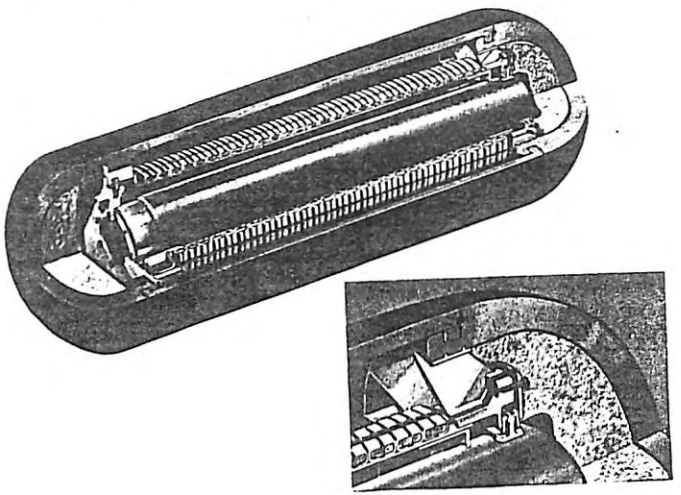

Figure 7-6. Isometric Cutaway of GLFC with Beryllium Oxide Secondary Shield

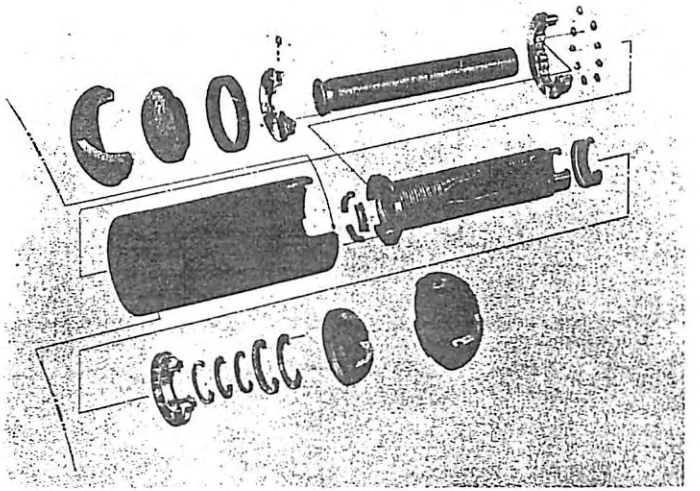

Figure 7-7. Exploded View of GLFC with Beryllium Oxide Secondary Shield

The design of the shield accomplished this by dividing the thermal insulation, which is SiO_2, into small cylindrical segments and to position around each segment a silver conduction ring as shown in Figure 7-8. The silver ring subassemblies are brazed to a columbium cylinder which serves as the structural support of the segments. The temperature of the columbium is approximately 1200°F during normal operation and as a result, requires a coating for oxidation resistance. This coating has an emissivity of 0.8 or greater. The outer surface of the silver radiation fin is coated with a General Electric Radifrax coating to produce an emissivity of 0.8 or greater. The SiO_2 insulation is also coated with Radifrax for high emissivity.

During normal operation, the heat transfer path is radially outward from the FCA by thermal radiation to the high emissivity on the inside diameter of the columbium cylinder. The heat flows by conduction across the columbium cylinder, braze joint and silver fins. The heat flow is radiated from the high emissivity of the outer silver fin surface to the inside diameter of the Pyrocarb-406 cylinder primary shield, across the wall of the cylinder and radiated to the external sink. The temperature of the silver fin is approximately 1200°F.

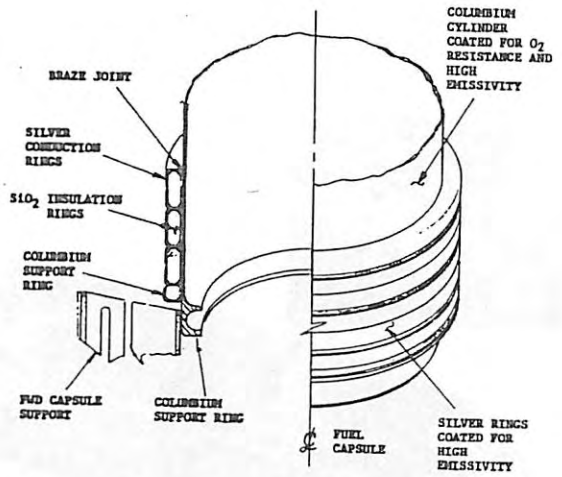

Figure 7-8. SiO_2 Secondary Thermal Shield

However, during abort re-entry, the heat flow is in the opposite direction toward the FCA during the majority of the heat pulse. This heating increases the temperature of the silver fin until it melts and opens the high conduction path to the FCA. The temperature response of the FCA is now controlled by the SiO_2 insulation.

The secondary heat shield is bolted at one end to the latch fitting; the other end maintains a close clearance pilot fit with the forward capsule support.

7.2.4 LATCH FITTING

The latch fitting serves as the aft support for the capsule during normal operation. All of the axial load from the capsule is transferred through the latch fitting, while the lateral loads are shared with the forward capsule support. The backplate of the capsule attaches directly to the latch fitting and is the only point of positive attachment and locking while inside the GLFC. The handling tool interfaces with the latch fitting and backplate to insert, lock and remove the capsule.

The latch fitting is made of titanium alloy 8Al-1Mo-1V and the surface carbonate-treated to provide a protective coating between the contacting

surfaces of the titanium latch fitting and the Haynes-25 backplate. This coating is necessary because of a reaction between titanium and Haynes-25 at high temperatures experienced during re-entry.

The latch fitting is attached for axial support to the thick lug section of the cylindrical primary heat shield by nine bolts, tabs and sleeves. This bolted joint is designed to maintain a tight joint from assembly through the higher temperatures of normal operation. This design is shown with the aft capsule support, Figure 7-9. The bolt, top flange, tab and pad shown in the figure are made of titanium while the sleeve is made of stainless steel. During heat up, the titanium bolt would expand more than the graphite and produce a loose joint. However, the stainless steel sleeve has a larger expansion coefficient that the titanium and expands in a direction to compensate for the growth of the bolt.

In the radial direction, the latch fitting initially has a clearance fit with the graphite lug. However, at temperatures of normal operation, the titanium expands to produce a tight fit. This fit is necessary to eliminate the impact of the loose surfaces during the vibration environment of launch. To prevent the titanium from expanding into and failing the graphite during re-entry, the titanium is slotted - similar to a snap ring, thus creating a flexable arch in the area that contacts the graphite. This arch yields during re-entry, and limits the load into the graphite cylinder.

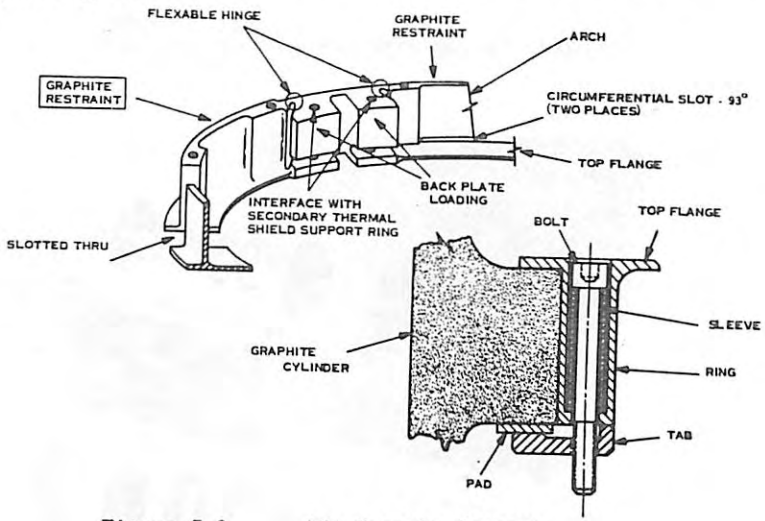

Figure 7-9. Aft Capsule Support

There is a clearance fit between the latch fitting and backplate at the normal operating temperatures. These clearances are maintained as small as possible and ensure that the FCA is free for insertion and removal.

7.2.5 FORWARD CAPSULE SUPPORT

The function of the forward capsule support is to provide for the lateral support of the forward end of the FCA. The forward capsule support is threaded into the I.D. of the forward end cap and pinned in place to prevent rotation. Support of the aft end of the FCA is provided by the latch fitting.

The forward capsule support, Figure 7-10, consists of a titanium housing ring and a Haynes alloy guide ring to support the capsule. The guide ring is mounted to the housing ring in such a way that it floats free at room temperatures but, at higher temperatures caused by fuel capsule heat rejection, tightens up to provide a firm support due to differential temperature expansions of the guide and the housing. The housing is mounted to the forward end cap by two male helical threads which mate with female threads on the end cap. This provides a heat path to the primary shield from the capsule in addition to structural support.

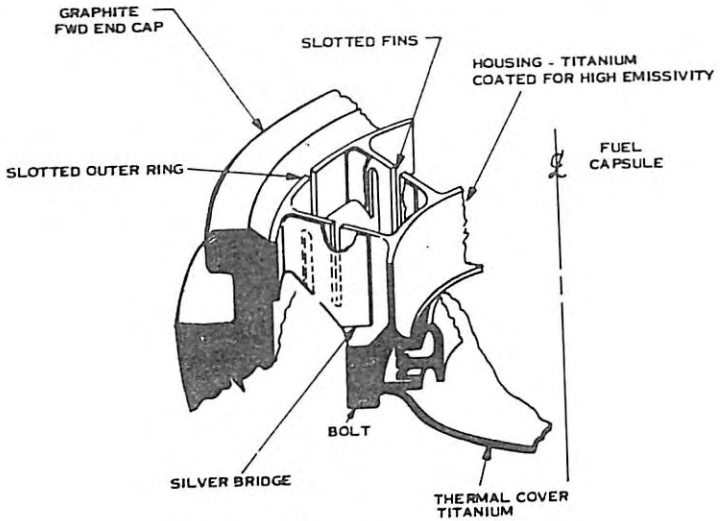

Figure 7-10. Forward Capsule Support

The titanium housing is coated with a lithoid high emissivity paint to aid the heat rejection from the end of the FCA.

The forward capsule support incorporates a thermal locking device that will allow an eccentric FCA to be installed in the GLFC and still provide a rigid support with a close clearance fit. The forward end of the FCA has this clearance with it's support to ensure freedom of movement for insertion and removal of the FCA.

The thermal lock consists of a Haynes-25 impact ring, two titanium rings and the titanium housing. The impact ring is free to move in a radial plane at ambient temperatures. When the FCA is inserted and while the "lock" is still at ambient temperatures, the FCA will, in the process of fitting inside the impact ring, move the impact ring to a radial position corresponding to eccentricity of this end of the FCA relative to the backplate. As the temperature of the "lock" increases, the differential thermal expansions between the Haynes-25 and titanium creates a thermal interference that locks the impact ring in place. The FCA is not locked to the impact ring but maintains a close clearance fit with it. It takes approximately 30 minutes, after insertion of the FCA, for the temperature to increase to the point where the lock takes place.

FCA loads are transmitted to the impact ring through the lock and out through 16 radial webs to the graphite end cap. Each web is slotted to create a spring so that the thermal expansion of the titanium during re-entry does not build up excessive interference fit stresses in the graphite end cap. The titanium spring yields during re-entry and limits the load into the graphite end cap.

Slotting the webs increases the resistance to heat conduction through the webs for normal operation. To compensate for this, a silver bridge is attached across the slots in each web.

The thermal lock is also a path of high thermal resistance. To compensate for this, a thermal cover of stainless steel is bolted to the titanium housing and bypasses the lock area.

7.2.6 AFT CAPSULE SUPPORT

The aft capsule support (Figure 7-9) is a titanium fitting which furnishes a latching point for the fuel capsule backplate latching mechanism. It is clamped to a thick internal flange on the graphite cylinder by nine titanium bolts and tabs. The overall fitting design and clamping arrangement are such as to minimize thermal stresses developed due to differential expansions of titanium and graphite materials.

7.2.7 FORWARD/AFT INSULATION

Fiberfrax T30LR insulation is located inside each end cap to protect the FCA from re-entry heat flux through the end caps. Heat rejection from the FCA in the axial direction through the insulation during normal operation is small and therefore does not contribute significantly toward increasing the operational temperature of the FCA.

7.2.8 SPLINE LOCK

This device, Figure 7-11, is used to lock the graphite end caps to cylinder. It is inserted into a hole formed by matching grooves in the graphite cylinder and end cap at their interface. A tantalum pin is attached to a tantalum wire strung with aluminum oxide beads which extends into the curved length of the hole. Upon installation, the tantalum wire deforms and takes a permanent set which prevents the tantalum pin from vibrating loose during launch or re-entry. The other end of the pin is attached to a titanium wire lanyard.

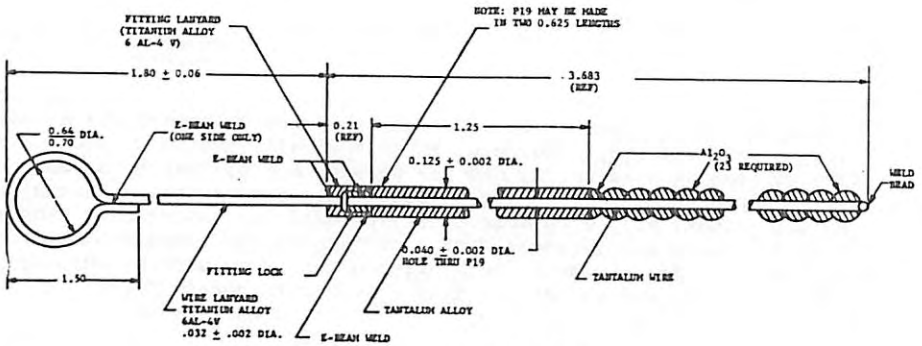

Figure 7-11. Spline Lock

7.3 DESIGN ANALYSIS

7.3.1 STRUCTURAL CAPABILITY - NORMAL MISSION

The GLFC with fuel capsule installed was analyzed for stresses due to simultaneous application of the ALSEP support structure band pre-loads and the design load at two temperature conditions, 350 and 800°F on the GLFC outer surface. These represent the critical cases, launch and lunar descent conditions. A summary of the minimum margins of safety for GLFC components is shown in Table 7-4.

TABLE 7-4. OPERATIONAL MINIMUM MARGINS OF SAFETY

Item	Loading Direction	Type of Stress	M.S.
Pyrocarb Cylinder	Lateral	Bending	+ 6.80
Pyrocarb Dome	Lateral	Bending	+ 2.30
Breech Joint Fwd	Lateral	Bending	+ 20.00
Breech Joint Aft	Lateral	Bending	+ 20.00
Fwd Capsule Support (Movable Ring on Guides)	Lateral	Bearing	+ 0.06
Back Plate	Axial	Effective Stress	+ 0.54
Latch Fitting (Tab)	Axial	Bending	+ 0.37
Secondary Thermal Shield	Lateral	Bending	> 2.00
Secondary Shield Support Rings	Lateral and Axial	Bending	> 2.00

Where margin of safety

$$\text{Margin of Safety} = \frac{\sigma_{ty}}{1.10\ \sigma_{applied}} - 1 \quad \text{(yield)}$$

$$\text{Margin of Safety} = \frac{\sigma_{tu}}{1.5\ \sigma_{applied}} - 1 \quad \text{(ultimate)}$$

Where

σ_{ty} = yield stress, psi

σ_{tu} = ultimate stress, psi

$\sigma_{applied}$ = applied or calculated stress, psi

7.3.2 THERMAL ANALYSIS - NORMAL MISSION

Three operational conditions were evaluated for the final GLFC design:

a. Stabilized on-pad operation with the GLFC's exterior surface cooled at 350°F

b. Earth orbital with SLA doors closed

c. Transient thermal response resulting from insertion of the fuel capsule into the GLFC.

A two-dimensional (axial and radial) thermal computer model was constructed for the normal operation mode. This model was used with the THT-D computer code (Reference 7-2). The model and thermal analyses are described in detail in References 7-3 and 7-4.

The maximum temperature condition occurs during earth orbit with the SLA doors closed. The resulting temperature profile of the GLFC for this condition is shown in Figure 7-12. Table 7-5 contains the principal steady-state temperatures for both the on-pad cooled conditions and earth orbital (SLA doors closed) conditions. Figure 7-13 shows the transient temperature response of the principal GLFC components after fuel capsule assembly insertion on pad (Reference 7-1).

TABLE 7-5. PREDICTED STEADY STATE GLFC TEMPERATURES

	GLFC ON LM IN VACUUM SLA DOORS CLOSED	ON PAD GLFC COOLED TO 350°F
Maximum Graphite Temperature	725°F	350°F
Maximum Beryllium SHS Temperature	1065°F	859°F
Maximum Capsule Clad Temperature	1365°F	1289°F
Maximum Inner Fuel Liner Temperature	1596°F	1520°F

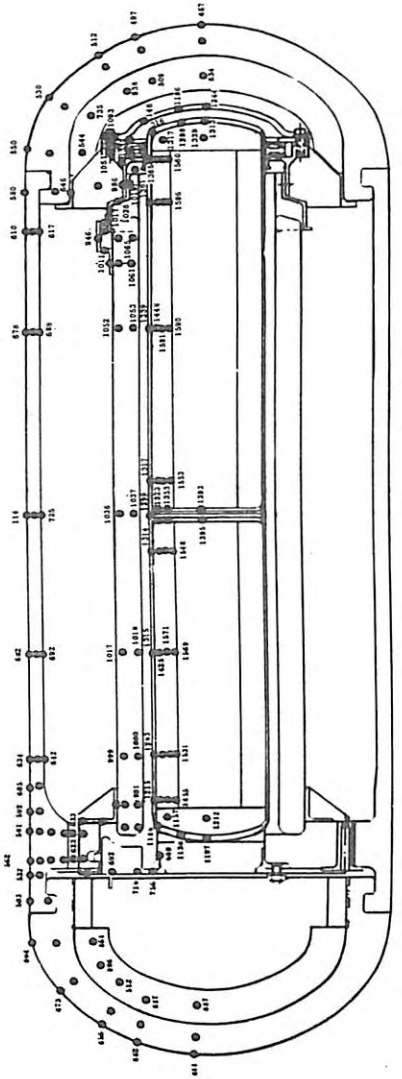

Figure 7-12. Steady State Temperature Distribution of GLFC

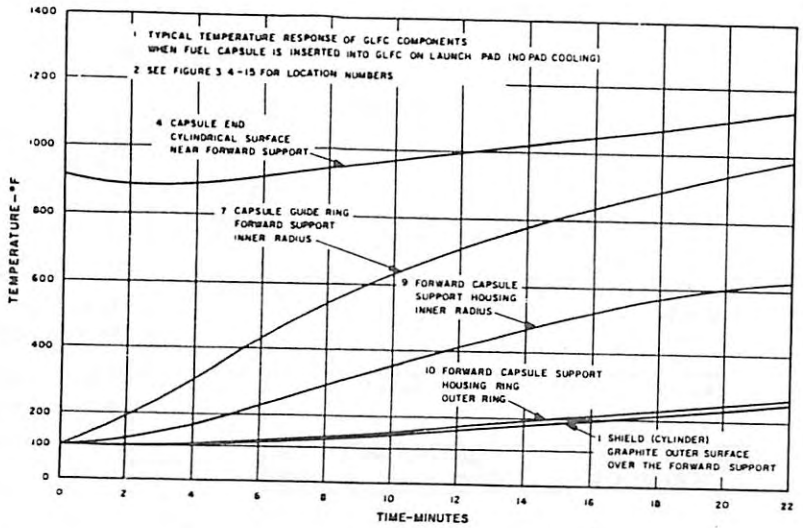

Figure 7-13. Typical Temperature Response of GLFC Components When Capsule is Inserted into GLFC in Air (No Cooling Applied)

As a result of these analyses, it has been shown that the GLFC components will operate below the maximum temperature limitations during a normal mission.

7.3.3 ABORT RE-ENTRY ANALYSIS

Aborts during normal missions may result in the re-entry of the LM with the GLFC attached into the earth's atmosphere. The LM configuration prior to re-entry, during re-entry and the initial re-entry conditions influence the GLFC re-entry environment. Information available at that time was utilized to establish the GLFC re-entry environments. These design cases were referred to as references cases. Subsequent to the initial design phase during the safety evaluation, additional information became available and a more expansive analysis was conducted. The additional cases were referred to as realistic abort cases. A complete description of the analyses is contained in Reference 7-1. A summary is presented here.

7.3.3.1 Reference Cases

These cases constitute the basis for the GLFC design. These cases assume that the LM will breakup at a specified altitude (300,000 feet for the earth orbital decay and 330,000 feet for the superorbital re-entries) and release the GLFC. The GLFC would then re-enter in a planar tumbling (end over end), random tumbling, side-on, spinning or a side-on stagnated mode of re-entry. Aerodynamic and thermal analyses showed that the side-on stagnated was the most severe and, in addition, was the most probable condition. Therefore, the design was based on analyses of the GLFC re-entering in the side-on stagnated mode.

The re-entry evaluation consisted of a series of analysis involving the following disciplines:

a. Aerodynamic - A stability analysis was performed to verify re-entry mode, and aerodynamic drag coefficients were generated.

b. Flight Mechanics - Trajectories were calculated using the initial re-entry conditions, the assumed LM breakup altitudes, and the applicable weights, areas and drag coefficients. This information is summarized in Table 7-6. The resulting trajectory data can be found in Reference 7-1.

c. Aerodynamic Heating - Stagnation heating rates and heating rate distributions were calculated using the most applicable re-entry heating correlations available. A summary of peak heating is shown in Table 7-7.

d. Thermal Analysis - One and two dimensional re-entry thermal analyses were performed using the heating rates from c. These analyses predicted the temperature response of the GLFC components during re-entry and the recession of the primary heat shield due to the graphite ablation. A summary of the results is shown in Table 7-8.

e. Structural Analysis - This analysis calculates the stress in the primary heat shield due to the temperature gradient and the aerodynamic loading. A series of one and two dimensional calculations were made using the temperature gradients from d. and the aerodynamic loads from b. The results are shown in Table 7-9 expressed as margin of safety, which is defined as:

$$\text{Margin of Safety} = \frac{\text{Tensile ultimate stress}}{\text{actual stress}} - 1$$

TABLE 7-6. BALLISTIC COEFFICIENTS $\frac{W}{C_D A}$ $\left(\frac{LB}{FT^2}\right)$

	Complete LM Full Fuel Tanks	Descent LM Tanks 80% Full	GLFC/SS Trimmed	GLFC Trimmed (side on)	GLFC Tumbling (end over end)
400 KFT	52.0	67.0	12.0	16.0	22.0
350 KFT	85.0	122.0	13.0	17.0	25.0
300 KFT	103.0	148.0	15.0	21.0	33.0
250 KFT	103.0	148.0	17.0	24.0	43.0
200 KFT	103.0	148.0	18.0	26.0	49.0
150 KFT	103.0	148.0	19.0	26.0	52.0
Weight	32,000 LB	18,383 LB	62 LB	40 LB	40 LB
Area $_{REF}$	133 FT^2	133 FT^2	0.349 FT^2	0.349 FT^2	0.349 FT^2

TABLE 7-7. PEAK HEATING RATES

Case	Trajectory	Orientation	q_c Max.[1] (Btu/Sec-Ft.^{2})	q_r Max.[2] (Btu/Sec-Ft.^{2})	q_t Max.[3] (Btu/Sec-Ft.^{2})
Reference	E. O. Decay	Stagnation	111	0	111
	=6.25° S.O.		486	13	490
	= 20° S.O.		1215	130	1250
	= 38° S.O.		1790	305	1995

NOTES: 1. Stagnation convective heating flux

2. Stagnation radiative heating flux

3. Stagnation total heating flux

TABLE 7-8. THERMAL RESULTS OF DESIGN (REFERENCE) CASES

Re-entry Trajectory	Re-entry Mode	One-Dim. or Two-Dim.	Graphite Outer Diameter			Graphite Inner Diameter			Beryllium SHS				Capsule Clad				Stagnation Point[1] Recession (inches)
			Max. Temp (°F)	Time (Sec)	Alt (Kft)	Max. Temp (°F)	Time (Sec)	Alt (Kft)	Max. Temp (°F)	Time (Sec)	Alt (Kft)	Max. Avg Temp (°F)	Max. Temp (°F)	Time (Sec)	Alt (Kft)	Max. Avg Temp (°F)	Total (Inches)
Earth Orbit Decay	Stagnated	Two-D	3480	6260	212	3113	6260	212	2317	6290	185	1870	2181	6350	119	1915	0.098
Earth Orbit Decay	Spinning	One-D	2540	6260	212	2451	6260	212	2028	6300	175	2020	2010	6360	109	2010	--
6.25° Superorbital	Stagnated	Two-D	5092	75	193	3675	80	186	2089	120	142	1608	1856	250	49	1668	0.0063
6.25° Superorbital	Planar Tumble	One-D	3700	82	181	3000	90	172	1824	155	112	1816	1784	284	30	1784	0.0257
20° Superorbital	Stagnated	One-D	5980	21	142	3950	24	120	1700	60	68	1695	1690	205	20	1690	0.0326
20° Superorbital	Planar Tumble	One-D	4440	23	132	3030	29	91	1430	140	25	1425	1570	160	119	1570	0.0131
38° Superorbital	Stagnated	One-D	6260	12	140	3630	17	82	1440	100	35	1435	1560	281	2	1560	0.0257
38° Superorbital	Planar Tumble	One-D	4750	12	135	2800	18	68	1349	180	5	1344	1498	201	2	1498	0.0085

1. Stagnation point recession given for total re-entry and at time of peak graphite OD temperatures

TABLE 7-9. SUMMARY OF MINIMUM VALUES OF MARGINS OF SAFETY CALCULATED FOR REFERENCE CASE RE-ENTRY CONDITIONS

	γ	MARGIN OF SAFETY	
		1-D Analysis	2-D Analysis
Reference Cases	6.25°	1.56	
	20°	0.48	
	38°	0.35	0.27

7.3.3.2 "Realistic" Cases

After the GLFC design was completed, additional mission abort data became available and an evaluation of the GLFC behavior during the actual mission abort re-entry was made. Where the "Reference" cases assumed a LM breakup (GLFC/LM separation) altitude, these new cases defined the actual re-entry configurations, trajectories and environments expected to result from a mission abort. Realistic GLFC/LM separation altitudes and realistic GLFC heating rates were determined and used in the analysis. The following parameters were considered and evaluated in the analyses:

a. GLFC and support structure heating while attached to the LM

b. Altitude at which the support structure separates from the LM, releasing the GLFC/support structure configuration

c. GLFC/support structure configuration re-entry (after separation from the LM) and the effect of augmented heating

d. GLFC side-on stagnated re-entry as a free and unencumbered body after separation from the support structure.

The point at which the GLFC/support structure configuration separated from the LM could not be precisely defined because of the uncertainty of the LM motion during the initial phase of the trajectory. Therefore, an altitude band was defined by calculating the maximum and minimum altitudes where separation might occur. These altitudes were determined by analyzing the thermal response of the LM structural members that interface with the support structure, for various modes of the LM

re-entry (oriented, spinning). The separation event (support structure release) is referred to as "LM breakup" and was assumed to occur when the LM structural members melted. In reality it is recognized that LM disassembly may begin before these release altitudes are reached, and that the GLFC/support structure might enter with some large portion of LM debris attached. However, assuming the LM to stay intact to the calculated release altitudes is considered to be conservative because then the LM ballistic coefficient is maintained until the lower altitudes are reached, resulting in a more severe re-entry environment. The "altitude band" shows the sensitivity of GLFC thermal and structural response to the release altitude and insures coverage of the "worst case" re-entry.

The maximum LM breakup altitude was determined by calculating the thermal response of the LM interface members to stagnation heating, without the protection of the superinsulation panels. The minimum breakup altitude was calculated in a similar manner except that average LM heating was used and the interface structure was protected by the superinsulation panels.

During the time the GLFC remains attached to the LM, it is subjected to heating generated by the LM flow field. For stagnated LM re-entry, it is assumed that the GLFC is at the stagnation point; for spinning re-entry, the GLFC is subjected to average LM heat flux for that case. The location and size of the GLFC (relative to the LM) insures that the GLFC and support structure are immersed in the boundary layer of the flow, and that both will experience nearly uniform heating. Calculations on vehicles comparable in size to the LM have shown that the shock layer is all boundary layer flow at altitudes above 200,000 feet. In the analyses, the heating distribution about the GLFC and support structure trunnion area were therefore taken as uniform.

If the GLFC and support structure separated intact from the LM, then this configuration was analyzed for oriented stable re-entry. The attitude of the GLFC/support structure was assumed to be where the flow vector is at 90 degrees to the trunnions and longitudinal axis of the GLFC. The results of aerodynamic analysis show this to be very close to a stable trim point. The effects of augmented or protuberance heating at the trunnion area were analyzed by selecting amplification factors of 1/10 and 5 times the stagnation heating. The validity of these factors were examined by performing an aerodynamic analysis of the flow caused by protuberances from the support structure and calculating the increased heat flux. The amplified heat flux in the trunnion area was applied to both the trunnion and cask until a sufficent portion of the trunnion melted, releasing the retaining straps. The GLFC was then analyzed for the remaining portion of the trajectory as a free and unencumbered body, in the side-on stagnated mode.

In those cases where the GLFC separated from the support structure before the maximum or minimum LM breakup altitudes were reached, it was analyzed as a free and unencumbered body from the separation point, and in the side-on stagnated mode.

The LM breakup analysis results are shown in Table 7-10 and Figure 7-14. The results of the GLFC thermal analyses are shown in Table 7-11, and the structural analyses results are in Table 7-12.

7.3.3.3 Suborbital Cases

If suborbital re-entry occurs with an initially intact GLFC, there will be no thermal or structural failure. However, since the most probable cause of a suborbital re-entry would be a booster malfunction which would damage the graphite, an analyses of the re-entry capability of the GLFC without the graphite heat shield was performed. The re-entry capability of the FCA/secondary heat shield is dependent upon initial conditions and the heating rate histories. Initial conditions and heating rates are shown for the cases evaluated in Tables 7-13 and 7-14.

The FCA/secondary heat shield configuration was evaluated using a two dimensional center slice thermal model. This model was used in conjunction with the THT-D computer code to calculate the thermal behavior of the FCA/secondary heat shield during re-entry including melting and ablation of the beryllium. The results of the analysis are presented in Table 7-15. Of the suborbital cases, only one case shows failure of the secondary heat shield, where failure is defined as complete ablation at the secondary heat shield on the stagnation line. The suborbital cases indicate no ablation through the secondary heat shield. The additional re-entry capability afforded by the FCA assuming it is exposed to re-entry heating following failure of the secondary heat shield was found to be negligible in comparison to the secondary heat shield due to its low heat absorptance capability.

The FCA has about one percent of the heat absorptance capability of the secondary heat shield. Therefore, it is a negligible factor in preventing fuel release after failure of the secondary heat shield. A failure of the secondary heat shield can be considered to result in an immediate failure of the fuel clad.

7.3.4 DYNAMIC ANALYSIS

This analysis discusses the results of the vibration tests performed on the engineering GLFC/ALSEP support structure assembly, as discussed in Paragraph 7.4.5.

TABLE 7-10. SUMMARY OF LM BREAKUP ALTITUDES

Re-entry Trajectory	LM Shape for Heating Rates	LM Re-entry Mode	Super-insulation Included	Time of[3] LM Breakup (Seconds)	LM Breakup Altitude (Kft)	LM Velocity at Breakup (Fps)	Path Angle at Breakup (Degrees)	Dynamic Pressure at Breakup (Lbs/Ft²)	Altitude of Insulation Release (Kft)	Time of Insulation Release	
Earth Orbital Decay	sphere	stagnated	no	5160	332	24,403	- 0.18	negig.	---		(1)
	cylinder	stagnated	no	5380	324	24,403	- 0.18	negig	---		
6.25° Superorbital	sphere	stagnated	no	38	272	35,150	- 4.7	8	---		(1)
	cylinder	stagnated	no	39	269	35,150	- 4.6	15	---		
20° Superorbital	cylinder	stagnated	no	13.7	230	35,750	-19.7	22.	---		(1)
	sphere	stagnated	no	13.7	230	35,750	-19.7	22	---		
38.05° Superorbital	cylinder	stagnated	no	7.8	225	36,400	-37.7	800	---		(1)
	sphere	stagnated	no	8.05	219	36,400	-37.7	900	---		
Earth Orbital Decay	cylinder	spinning	yes*	6345	217	23,150	- 1.0	100	270	6150	(2)
	sphere	spinning	yes*	6300	235	23,700	- 0.8	60	270	6150	
6.25° Superorbital	sphere	spinning	yes	71	195	34,000	- 2.9	310	239	51.7	(2)
	cylinder	spinning	yes	70.5	197	34,000	- 2.9	300	239	51.7	
20° Superorbital	sphere	spinning	yes	20.2	155	34,500	-19.3	190	227	14.05	(2)
	cylinder	spinning	yes	19.1	167	35,100	-19.3	110	229	13.9	
38.05° Superorbital	sphere	spinning	yes	11.4	139	35,600	-37.5	2000	214	8.3	(2)
	cylinder	spinning	yes	10.7	155	35,900	-37.5	1300	222	8.0	
Earth Orbital Decay	sphere	spinning	no	6085	279	24,300	- 0.3	negig.			
6.25° Superorbital	sphere	spinning	no	64	210	34,700	- 3.1	210			
38.05° Superorbital	sphere	spinning	no	11.1	147	34,700	-37.5	1600			

* Removed Due to Dynamic Pressure Loading, Not Thermal Loading as in the Other Cases.

(1) Cases Used to Determine Upper Band of LM Breakup Altitudes

(2) Cases Used to Determine Lower Band of LM Breakup Altitudes

(3) Time Measured From 400,000 Feet

TABLE 7-11. SNAP-27 GLFC "MISSION ABORT" THERMAL RESULTS

RE-ENTRY	ONE-D or TWO-D	BERYLLIUM MAX TEMP °F	S.H.S. MAX AVG TEMP °F	CLAD MAX TEMP °F	CLAD MAX AVG TEMP °F	TOTAL RECESSION IN.
Earth Orbit Decay, Upper Altitude[2] (.1)[3]	Two-D	2010	1978	2102	2100	-- (<.098)
" (5)	"	1997	1776	2036	1893	-- (<.098)
Lower " (.1)	"	1841	1729	1864	1806	-- (<.098)
" " (5)	"					(1)
6.25° Superorbital	One-D	2017	2000	1959	1959	.059
20° Superorbital, Lower Altitude	"	1640	1635	1650	1650	.0364
" Lower	"	1630	1625	1640	1640	.0312
38 " Upper	"	1490	1487	1550	1550	.0253
" Lower	"	1460	1458	1540	1540	.0247

NOTES:

1. THE TWO LOWER ALTITUDE CASES ARE SIMILAR IN TEMPERATURE BECAUSE OF THE VERY SHORT TIMES FOR THE GLFC/SS FLIGHT.
2. DENOTES UPPER OR LOWER LIMIT OF LM BREAKUP ALTITUDE.
3. DENOTES STAGNATION HEATING RATE MULTIPLIER IN TRUNNION AREA.

Figure 7-14. LM Breakup Altitude as a Function of Re-entry Angle

TABLE 7-12. SUMMARY OF MINIMUM VALUES OF MARGINS OF SAFETY CALCULATED FOR VARIOUS RE-ENTRY CONDITIONS

	γ	MARGIN OF SAFETY 1-D Analysis
Mission Abort (High Alt)	6.25° 20° 38°	0.81 0.40 0.39
Mission Abort (Low Alt)	20° 38°	0.46 0.46

TABLE 7-13. RESULTS OF FCA/SHS RE-ENTRY EVALUATION

	Release Alt (Kft)	Maximum SHS Temp (°F)	SHS Ablation	Conditions at SHS Failure	
				Time (Sec)	Alt (Kft)
SUBORBITAL	600	MELT	100%	400	
	560	2117	0	---	---
	480	1531	0	---	---
	180	1155	0	---	---

NOTES: 1. Be Melt Temperature - 2345°F
2. Percent Ablation shown for stagnation line

TABLE 7-14. STAGNATION HEATING RATES TO FCA/SHS CONFIGURATION

	Release Altitude (Kft)	Initial Heating Rate (B/ft^2-sec)	Conditions at Peak Heating		
			Max. Value (B/ft^2-sec)	Alt (Kft)	Time (Sec)
SUBORBITAL	600	0	300	400	400
	560	0	153	205	205
	480	0	90	130	130
	180	18.0	18.8	180	0

TABLE 7-15. INITIAL TRAJECTORY CONDITIONS FOR FCA/SECONDARY HEAT SHIELD ANALYSES

Trajectory	INITIAL CONDITIONS AT FCA/SUPPORT STRUCTURE RELEASE				Release Occurs at
	Alt (Kft)	Vel (Kft/sec)	Down Angle (Deg)	Time (Sec)	
Suborbital	600	22.0	0.2	536.2	S-IVB Ignition
	560	15.6	0.7	400.0	----
	480	11.9	5.5	300.0	----
	180	8.4	10.75	162.4	S-II Ignition
Released by explosion during ascent to Earth Orbit					

NOTE: Side-on, stagnated re-entry mode for all cases.

7.3.4.1 Strut-cask Resonances

Strut-cask resonances are here defined as those resonances in which the cask vibrates essentially as a rigid body on elastic struts. Of the six strut-cask modes, the two Y axis modes and the lowest Y axis mode are most important in that these modes are below 100 Hz and can couple with the capsule/heat shield modes of the GLFC. The resonant frequencies and responses to a three-g sine sweep are summarized in Table 7-16 for these three low frequency strut-cask modes. Comparison of the resonant frequencies indicates fair agreement with earlier test results. However, the responses to the three-g sine input vary considerably. The ratio of the hot to cold response varies from 4 to 0.4 at the various locations for the three modes. Bendix test data generally falls within the range of the General Electric hot and cold data. These variations are possibly due to inconsistencies in the behavior of the strut-fixture attachment which contained considerable free play. Another possible cause of the variation in the hot test was the fit of the forward impact ring which permitted some sliding action of the ring during the vibration test.

7.3.4.2 Random Response

The responses of the capsule, secondary heat shield and forward support were considerably lower than measured during previous GLFC hard mounted tests with the old heat shield, i.e., the maximum capsule response dropped from 38.9 g rms to 22.4 g rms, the heat shield dropped from 45.9 g rms to 9.6 g rms and the forward support dropped from 35.5 g rms to 18.3 g rms. On the other hand, the maximum vibration level at the outside of the latch plate was approximately the same, i.e., 25.4 g rms compared to 25.3 g rms. These differences can be attributed to the change in the forward support, the secondary heat shield and the vibration requirements.

A comparison of the GLFC responses between the hot and cold tests for the launch spectrum input indicates a large variation similar to that of the sine tests. A portion of this difference may be due to the variation in the input, which was not controlled as closely as the sine tests (i.e., ± 3db). Major variations in the response characteristics undoubtedly occurred during the sine tests. The 200 Hz resonance was the fundamental resonance in the Z direction.

7.3.4.3 Straingage Data

Capsule stress levels were apparently well below those levels which will cause fatigue damage. The peak sine stress was 2300 psi due to the Y axis response at station Z, which is below the threshold required to cause fatigue damage (3500 psi). Similiarly, the peak random

TABLE 7-16. GLFC RESPONSE TO 3g SINE AT STRUT-CASK RESONANCES

RESONANT FREQUENCIES			AFT CASK RESPONSE			AFT TRUNNION RESPONSE			FWD TRUNNION RESPONSE			FWD CASK RESPONSE		Axis of Vib.
	GE			GE			GE			GE		GE		
Bx	Hot	Cold	Bx	Hot	Cold	Bx	Hot	Cold	Bx	Hot	Cold	Hot	Cold	
40 Hz	40 Hz	37 Hz	21g	12g	21g*	22.5g	19g*	16g*	19.5g	11.7g*	28g*	9.5g	16.5g	Y
45	40/44	40	11g	14.5	9g*	10.5	16.5	13.5*	9	7.5	15*	15	7.5	X
75/80	87	68	2.25	2.5	3.*	2.25	10	2.5*	2.7	5.5	8.3*	8.5	3.0*	Y

* Unfiltered

stress was 1150 psi which is also well below the damage threshold (peak stress of approximately 3000 psi). The stress at the center of the capsule was approximately half that required to cause a fatigue failure and is critical for random loading in the Z axis. The latch plate end of the capsule does not appear to be critical.

A significant margin also exists on the forward support web load. The maximum measured web load was 38 pounds during the Y axis sine test at the strut-cask resonance. The estimated yield load was 105 pounds, and tests to approximately 50 pounds used for calibrating the straingage bridge did not indicate any yielding. The maximum web load is less than half the calculated yield load.

7.3.4.4 Internal GLFC Response

Two major internal resonances of the GLFC were identified in previous vibration tests and analysis. These involve the secondary heat shield and the capsule. From a Z axis three-g sine sweep, the modes were:

	Was	Now
Heat Shield/Capsule	38/54 Hz	50 Hz
Capsule/Heat Shield	60/68 Hz	80 Hz

where the "was" values refer to the old heat shield and forward support designs. These resonances are evident from the response of the capsule from Z axis input vibration where the strut-cask resonant effects are small. However, the Y axis response of the capsule reflects the Y axis strut-cask resonance; the effect of the internal resonances are minimal. The nonlinear response characteristics of the internal GLFC modes resulting from capsule free play apparently preclude significant resonant response in the Y axis at the reduced levels at the cask above the fundamental strut resonant frequency.

The responses of the internal and external accelerometers at the major resonances excited during the cold three-g sine sweep indicated that a large amount of coupling existed in the cross axes at all resonances. Comparison of these responses with those observed previously (Paragraphs 7.3.4.1 and 7.3.4.2) indicated much lower responses of the capsule and secondary heat shield responses (as indicated by x-y plots) for a 5 g transverse input were on the order of 70 g whereas levels of 16 g and 4 g are here indicated. It is not surprising that the response characteristics are significantly different since major changes were made to the design of the secondary heat shield and forward support.

7.3.4.5 Conclusions

The following can be concluded from the test results:

a. The fundamental strut-cask resonances are sufficiently separated from the internal GLFC resonances to prevent damage to the GLFC.

b. The strut-cask resonances are nonlinear, exhibiting a large variation in response amplitude, a small variation in resonant frequency, and a large amount of cross axis response. The nonlinear characteristics appear to result from free play in the strut connection to the vibration fixture which simulated the attachment to the LM structure.

c. The beryllium heat shield with the revised forward capsule support increases the resonant frequencies of the capsule and heat shield modes to 50 Hz and 80 Hz.

d. Capsule accelerations were considerably lower than measured during previous hard mounted GLFC tests, with capsule dynamic stress and forward support web loads being less than half the design allowables.

e. The response in the capsule mode was significantly different than the previous heat shield design having shorter duration impacts with the largest response at the latch plate.

7.4 DEVELOPMENT TEST PROGRAM

7.4.1 PYROCARB-406 MATERIAL CHARACTERIZATION

In order to realistically predict available safety margins for the GLFC when the severe re-entry loads were imposed, it became important to accurately determine both the mechanical and thermal properties of the outer heat shield material, pyrocarb-406. To do this required a very extensive characterization program. This graphite composite material is not only anisotropic in its mechanical and thermal characteristics, but its density also varies as a function of the distance from the surface of the layup. Since density affects both strength and conductivity, the precise characterization becomes a formidable task, demanding multiple types of material samples as well as numerous samples of each type to establish any confidence in the values obtained.

The characterization program was basically divided into two phases:

a. Flat plate testing

b. Cylinder and end cap testing.

This approach was used, due to the availability of the flat plate material, to provide preliminary properties for initial design stages. The more complex layup required for the cylinder and hemispherical end cap shapes required more time for fabrication and also demanded further characterization in order to determine any differences from the flat plate data.

Pyrocarb-406 test results show:

a. It does not fail catastrophically when loaded to tensile or compression failure stresses, but instead undergoes a "green stick" type failure where successive individual fibers fracture and some load can still be carried.

b. It is plastic in behavior

c. Strength varies as a function of material density and temperature.

The plastic behavior, shown in Figure 7-15 for a 75°F test, is more pronounced at elevated temperatures.

Table 7-17 is a summary of the properties of the primary heat shield material, pyrocarb-406 with a density of 86 lbs/ft^3. The pyrocarb-406 material, when formed for the GLFC cylinder, has a density gradient through the thickness varying from a maximum of 90 to 95 lbs/ft^3 at the outer fibers to a minimum of about 83 to 88 lbs/ft^3 near the middle of the wall thickness. Similar variations exist on the end caps. From the material characterization program and the data measured from specimens taken from each production item, curves were plotted for strength and elastic modulus similar to that shown in Figures 7-16 and 7-17.

In order to properly assign the appropriate strengths in all directions of the pyrocarb-406, it was necessary to incorporate certain testing and manufacturing effects into the design properties. Effects of the tensile specimen stress concentration and of the cloth layup angle variation were evaluated and judiciously integrated into the existing property data. Details of this property modification effort, along with various design properties used in the Re-entry Safety Analysis, can be found in Reference 7-1.

Detailed test procedures, data analysis and property information can be found in References 7-5 and 7-6.

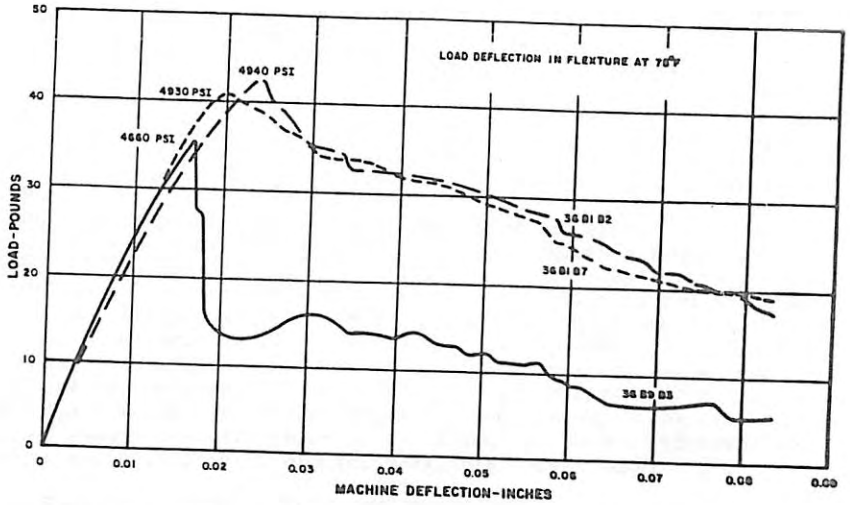

Figure 7-15. Load Deflection Characteristics of Pyrocarb Showing Plastic Deformation Capability

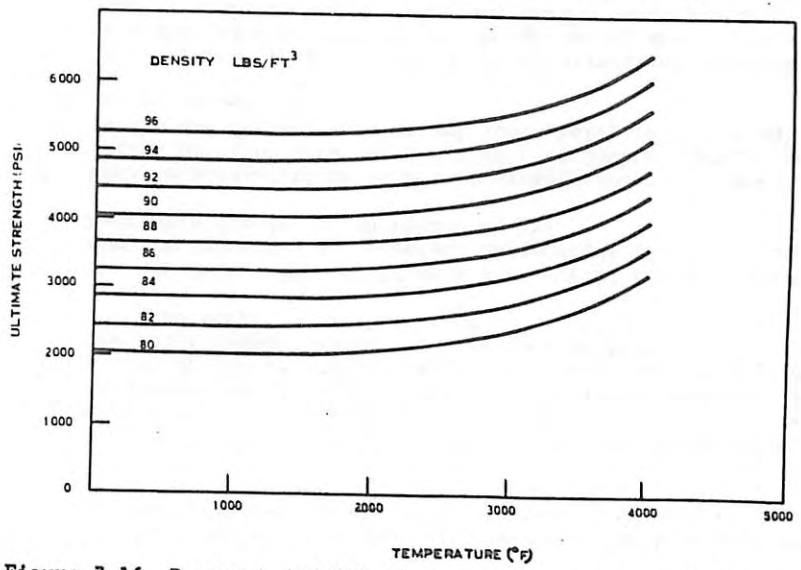

Figure 7-16. Pyrocarb-406 "B" Direction Ultimate Tensile Strength

TABLE 7-17. MATERIAL PROPERTIES OF PYROCARB 406-DENSITY 86 LBS/FT^3

Property	Temperature (°F)	Nominal Values* A	B	C	Remarks
Tensile Stress - psi x 10^3	75	10	3.3	0.62	
	2000	10.5	3.3	0.64	
	4000	15	4.4	0.89	
Compressive Stress - psi x 10^3	75	11.5	5.3	-	
	2000	11.5	5.7	-	
	4000	11.7	7.3	-	
Shear Stress - psi x 10^3	75	2200	2200	-	
	2000	2200	2200	-	
	4000	2700	2700	-	
Elastic Modulus Tension - psi x 10^6	75	2.4	1.4	0.53	
	2000	2.4	1.4	0.53	
	4000	1.5	0.8	0.36	
Elastic Modulus Compression - psi x 10^6	75	2.4	1.4	-	
	2000	2.4	1.4	-	
	4000	1.5	0.8	-	
Poissons Ratio	75	0.1	0.1	0.1	
Specific Heat - Btu/lb-°F	75	0.15	0.15	0.15	
	2000	0.47	0.47	0.47	
	4000	0.5	0.50	0.50	
Thermal Conductivity - Btu/ft-sec-°F	75	1.16	1.16	1.16	
	2000	1.35	1.35	1.35	
	4000	1.78	1.78	1.78	
Thermal Expansion - L/L	75	-	-	-	
	2000	0.002	0.002	0.0045	
	4000	0.0095	0.0075	-	
Ablation					Good Ablation Characteristics at Low Pressures
Permeability					Highly Permeable with Pyrolytic Graphite Surface Removed

* A - Longitudinal
B - Circumferential
C - Perpendicular to Surface

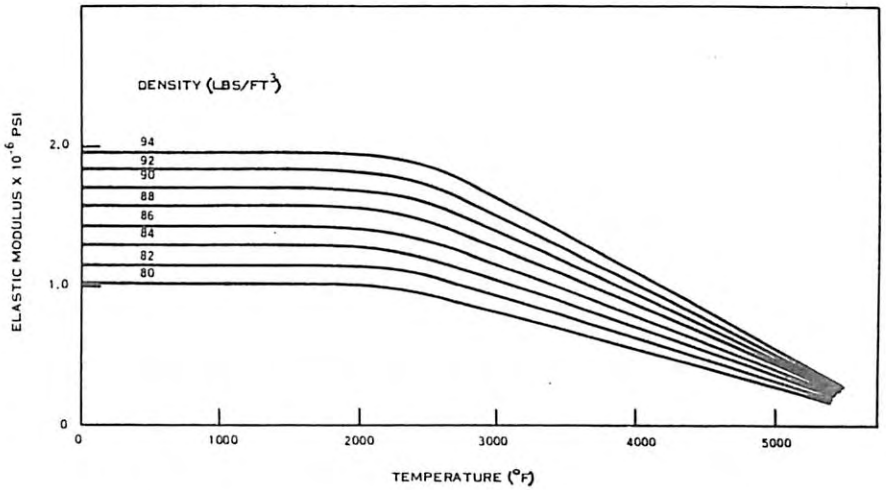

Figure 7-17. Pyrocarb-406 "B" Direction Electric Modulus

7.4.2 COATINGS TESTS

Due to the fact that no on-pad cooling of the graphite primary heat shield was originally specified, oxidation protection of the graphite in air was required since, at the normal operating temperatures of 800°F, there could be significant weight loss. Development testing was performed to provide a suitable oxidation resistant coating and to determine its total hemispherical emittance. The emittance property was required to be high enough (>0.8) to stay within defined temperature limits while in a vacuum. In the event the proposed oxidation resistant coating did not have a suitable emissivity, a second layer compatible coating whose emittance was high enough had to be provided. Details of these test efforts and results can be found in SNAP-27 Quarterly Report No. 7 (Reference 7-5).

Due to the subsequent elimination of the oxidation coating requirements, the emissivity of the selected primary heat shield material (pyrocarb-406) was still required to be high enough for heat rejection purposes during mission operation.

Emittance data on uncoated pyrocarb-406, as received, was found to be

too low (0.395 total normal). Studies were made to improve the emittance and determine variations with temperature and environment. These studies produced simple abrasive-type methods to raise the emissivity to acceptable levels. Details of methods and results can be found in SNAP-27 Quarterly Report No. 9 (Reference 7-5). Emissivity measurements were made with a Barnes Engineering Radiometric microscope in accordance with General Electric Specification SI-249194.

7.4.3 MATERIAL COMPATIBILITY TESTS

A two-part program was conducted to establish the compatibility of all materials used in the GLFC design, including the fuel. Part I of the test program investigated material interactions without the presence of fuel. Part II of the program was concerned with the materials interactions with fuel. The results of the testing, after detailed study, showed containment integrity in all but post impact and explosion situations. For surface impact, temperatures were low and materials interactions were limited except for oxidation. Burial data indicated containment in a fused or baked "cacoon" which localized interactions.

A comprehensive presentation of the testing methods, parameters, results and conclusions can be found in References 7-7 and 7-8.

7.4.4 ENGINEERING GLFC THERMAL VACUUM TEST

The objective of this test was to demonstrate that the engineering GLFC would perform as predicted and would withstand, without any degradation of performance, seventy-two hours of operation in vacuum with a maximum graphite external wall temperature of 800°F and a maximum circumferential gradient of 150°F. The heat input to the GLFC was supplied by an Electric Fuel Capsule Simulator (EFCS) energized to 1500 watts. A second objective was to demonstrate that the EFCS external surface temperature would not exceed 1400°F with a GLFC cylinder temperature of 800°F.

The GLFC and EFCS were instrumented with a total of 71 chromel-alumel thermocouples, and the thermal vacuum test fixture was instrumented with 52 thermocouples. The GLFC was placed in the GLFC thermal vacuum test fixture and installed in the eight foot by ten foot vacuum chamber. After obtaining 10^{-5} torr chamber pressure, the EFCS was energized to 1500 ($\pm$ 15) watts.

Heaters were energized in the end cap zones of the test fixture in order to raise the end cap temperatures. After two hours of adjusting test fixture heaters, it was evident that the end caps would be raised to 800°F without increasing the GLFC cylinder temperature beyond 800°F.

It was then decided to continue the test with a maximum graphite cylinder temperature of 800°F and the end caps at 650°F. These conditions are more realistic of actual mission conditions than the isothermal environment of 800°F.

Final steady state was established with the aft end cap of 650°F and the forward end cap at 685°F with a maximum graphite cylinder at 800°F. This condition was maintained for 14 hours until it was decided to terminate the test. This decision was predicated on the basis of temperature data which indicated excessive temperature gradients across the secondary thermal shield.

It was necessary to verify the validity of the thermocouple readings prior to continuing testing. Disassembly of the GLFC revealed that the thermocouples in fact were recording valid readings.

The temperature gradient across the secondary thermal shield exceeded the predicted values. The maximum EFCS surface temperature was 1518°F versus the maximum criterion of 1400°F. Both of the above conditions resulted in termination of testing until thermal testing of the secondary thermal shield on a component basis could be performed.

To confirm the results of the GLFC thermal vacuum tests, component testing of "short stack" secondary thermal shields were performed. The heater assembly was energized to produce a heater temperature of 1400°F and the system was allowed to stabilize for two hours.

The maximum ΔT between the solar sections I.D. and O.D. did not exceed 47°F during the test and the average ΔT was 41.7°F. The maximum ΔT between the Vac-Hyde thermal shield I.D. and O.D. did not exceed 45°F during the test.

7.4.5 GLFC ENGINEERING MODEL VIBRATION TEST - SiO_2/COLUMBIUM SECONDARY HEAT SHIELD

The first engineering model GLFC was subjected to a "cold" vibration test. This unit was equipped with the early design SiO_2/columbium secondary heat shield. An inert fuel capsule simulator was present within the GLFC during test and a rigid simulated ALSEP support structure was employed as the vibration fixture. Figure 7-18 depicts the test setup on a team table. Testing was carried out in each of the three major orthoginal axes of the GLFC, according to the following sequence:

a. Z axis - Sine sweeps at 1-, 3-, 5- and 7-g
   Random, 3.15 rms equivalent g

b. Z axis rerun - Random, 5.2 rms equivalent g

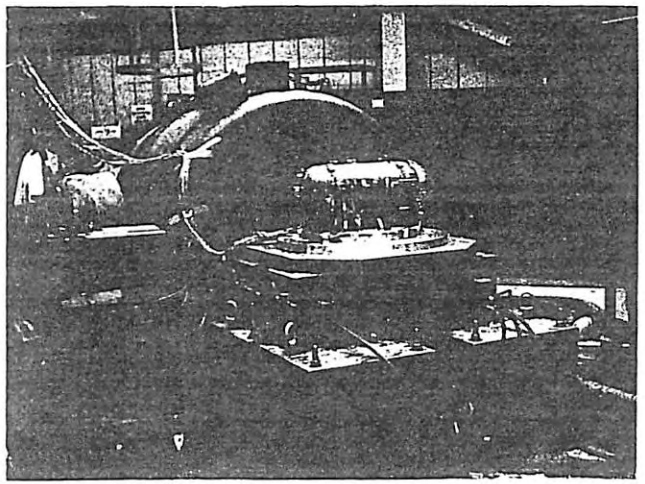

Figure 7-18. Engineering Development Test Setup

c. X Axis - Sine sweeps at 1-, 3-, 5- and 7-g
Random, 6.7 rms equivalent g for 43 seconds

d. X axis - Sine sweeps at 1-, 3-, 5- and 7-g
Random, 12 rms equivalent g for 37 seconds.

ıe results of the tests indicated nonlinear behavior in both X and Y
xes. The Y axis data was similar to that obtained previously for the
; axis and agreed favorably with analytical predictions. A Y axis
econdary heat shield resonance between 40 and 55 Hz was noted which
ıad been mistakenly identified as a forward support resonance for the
; axis test. A nonlinear stiffening of the X axis capsule mode occurred
ausing the resonant frequency to shift from 100 to 140 Hz as the input
cceleration was increased from ± 1 g to ± 7 g.

'arious mechanical failures were experienced during the testing. A de-
ailed description of the test results is contained in Quarterly Report
'o. 10 (Reference 7-5). Testing was completed on March 17, 1968.

7.4.6 SPLINE PULL TESTS

To determine the force necessary to remove the spline lock from the GLFC within a defined cone-shaped pull volume, a series of tests were conducted in accordance with General Electric procedure TR 1E14-083. Results indicated complete compliance with defined maximum pull forces attainable by the astronaut. Table 7-18 summarizes the test variations and results.

7.4.7 ENGINEERING ALSEP CASK ASSEMBLY (ACA) VIBRATION TEST

This test (Reference 7-9) was the first test performed on the GLFC with a beryllium secondary heat shield and redesigned forward capsule support. It was conducted on an assembly comprised of the GLFC and the Bendix ALSEP support structure.

The purpose of the tests was to verify the structural integrity of the integrated ALSEP Cask Assembly when subjected to qualification level sinusoidal and random vibration inputs at simulated hot conditions and at operating temperatures.

Specifically, the test was intended to:

a. Evaluate possible General Electric-Bendix interface problems and vibration response of Bendix struts upon the GLFC

b. Evaluate the stress loads imposed upon the FCA during dynamic testing, utilizing a verification FCA

c. Evaluate dynamic loads upon the beryllium secondary heat shield

d. Evaluate system assembly, interaction and response in preparation for qualification and acceptance testing

e. Evaluate the contamination safety enclosure and health physics requirements which were to apply during FCA dynamic testing

f. Establish vibration and shock inputs to test hardware in preparation for qualification and acceptance testing.

The first series of tests were performed at ambient, but with simulated operational temperature hardware clearances and without the aid of the aid of the contamination enclosure. The second series of tests were performed at operating temperatures and within the contamination enclosure.

TABLE 7-18. SPLINE PULL TEST RESULTS

Angle of Pull (in degrees)		Position of Spline Grooves	Torque on End Cap	Lanyard Length (ft)	Force Required to Remove Spline Lock
Vertical θ	Horizontal α				
0	0	Aligned	0	10	9 ounces
0	0	Aligned	0	10	10 ounces
0	0	Aligned	0	10	9 ounces
0	0	Rotated	10 in.-lb	10	46 ounces
0	0	Rotated	7 in.-lb	10	28-44 ounces
0	25	Aligned	0	10	20 ounces
0	25	Rotated (until bottomed out)	0	10	48 ounces
25	0	Aligned	0	10	12 ounces
25	25	Aligned	0	10	52 ounces
25	25	Rotated (until bottomed out)	0	10	12 pounds
25	25	Rotated (until bottomed out)	10 in.-lb	10	12 pounds

Prior to, and after subjection of qualification level dynamic loads, the ACA was subjected to a one-g sinusoidal sweep to determine if damage had occurred during the qualification level dynamic loads. The contamination enclosure intended for flight acceptance and qualification ALSEP cask assembly testing was operationally checked out during these tests.

The sequence of testing was as follows:

a. ACA cold vibration, one-g sweep

b. ACA cold vibration, full level sinusoidal

c. ACA cold vibration, full level random

d. ACA cold vibration, one-g sweep

e. Change axis and repeat a, b, c and d for each axis

f. ACA hot vibration, one-g sweep with contamination enclosure

g. ACA hot vibration, full level sinusoidal with contamination enclosure

h. ACA hot vibration, full level random with contamination enclosure

i. ACA hot vibration, one-g sweep with contamination enclosure

j. Change axis and repeat e, f, g and h for each axis

k. ACA hot vibration, lunar descent random (with contamination enclosure) in Y axis

l. ACA cold shock test (horizontal axis)

m. ACA cold shock test (vertical axis)

The vibration test levels employed were as follows:

a. Launch Boost - Qualification levels

1. Sinusoidal

Frequency Range (Hz)	Qualification Level
5 to 14	0.2 inch double amplitude
14 to 75	± 2.0 g
75 to 100	± 3.0 g

One 3-octave/minute sweep, up and down, in each of the three major axes.

2. Random

Frequency Range (Hz)	Qualification Level
20 to 100	9 db/octave increase
100 to 500	0.15 g^2/cps
500 to 2000	6 db/octave decrease

2-1/2 minutes/axis

b. Lunar Descent - Qualification Levels

1. Sinusoidal

Frequency Range (Hz)	Qualification Level
50 to 30	0.03 inch double amplitude
30 to 100	± 1.4 g

One octave/minute sweep, up and down, in each of the three major axes.

2. Random

Frequency Range (Hz)	Qualification Level
5 to 20	12 db/octave increase
20 to 100	0.01 g^2/cps
100 to 120	12 db/octave decrease
120 to 2000	.005 g^2/cps

12-1/2 minutes/axis

The results of the tests (Reference 7-10) indicated that ALSEP support structure resonances occur prior to the GLFC internal resonances, thereby minimizing the input to the major GLFC resonances. The nature of the capsule and beryllium heat shield resonances were significantly different than that of the preceding SiO_2/columbium heat shield configuration, exhibiting short duration impacts of the capsule, with the highest response occurring at the latch-plate end of the GLFC. Capsule stresses were low indicating a substantial margin. A four-to-one variation in the GLFC response occurred between the hot and cold tests which could be due to variations in the strut-to-fixture attachment and/or the slipping of the forward impact ring during the hot test. A large amount of free play in the Bendix strut attachments to the fixture was observed but was found to be in accordance with design.

7.4.8 ALSEP SUPPORT STRUCTURE VIBRATION TEST

A vibration test of the GLFC cask and ALSEP support truss system was performed by General Electric for Bendix to evaluate the effects of preload at the aft trunnion connection. The data was to be used by Bendix in the redesign of an aft trunnion release mechanism to correct for the Avdel pin failure which occurred during acceptance vibration testing of the D2/M5 mockup qualification unit. The tests were performed using a different truss assembly than the one used in previous vibration tests, and with an EFCS to provide operation temperatures. The GLFC was the same as that used for the General Electric engineering vibration tests.

The results of the tests indicated that preload has a minor effect on the GLFC response. In the Y axis, elimination of the preload without introducing free play, raised the dynamic magnification factor at the fundamental resonance from 7.5 to 9.2, a 20 percent increase. A 20 percent reduction in the second Z axis (vertical) resonant frequency also occurred with the reduced preload while the frequency shifts of other resonances were small. Comparison of this data with other cask-strut vibration data indicated that the sinusoidal responses of this unit was similar to that obtained during the Bendix-Mishawaka and General Electric engineering tests. The dynamic magnification of the D2/M5 qualification unit in the Y axis was approximately twice as high as that of this unit with no preload.

Details pertaining to the above are covered in Reference 7-11.

Frequency Range (Hz)	Qualification Level
5 to 14	0.2 inch double amplitude
14 to 75	± 2.0 g
75 to 100	± 3.0 g

One 3-octave/minute sweep, up and down, in each of the three major axes.

2. Random

Frequency Range (Hz)	Qualification Level
20 to 100	9 db/octave increase
100 to 500	0.15 g^2/cps
500 to 2000	6 db/octave decrease

2-1/2 minutes/axis

b. Lunar Descent - Qualification Levels

1. Sinusoidal

Frequency Range (Hz)	Qualification Level
50 to 30	0.03 inch double amplitude
30 to 100	± 1.4 g

One octave/minute sweep, up and down, in each of the three major axes.

2. Random

Frequency Range (Hz)	Qualification Level
5 to 20	12 db/octave increase
20 to 100	0.01 g^2/cps
100 to 120	12 db/octave decrease
120 to 2000	.005 g^2/cps

12-1/2 minutes/axis

The results of the tests (Reference 7-10) indicated that ALSEP support structure resonances occur prior to the GLFC internal resonances, thereby minimizing the input to the major GLFC resonances. The nature of the capsule and beryllium heat shield resonances were significantly different than that of the preceding SiO_2/columbium heat shield configuration, exhibiting short duration impacts of the capsule, with the highest response occurring at the latch-plate end of the GLFC. Capsule stresses were low indicating a substantial margin. A four-to-one variation in the GLFC response occurred between the hot and cold tests which could be due to variations in the strut-to-fixture attachment and/or the slipping of the forward impact ring during the hot test. A large amount of free play in the Bendix strut attachments to the fixture was observed but was found to be in accordance with design.

7.4.8 ALSEP SUPPORT STRUCTURE VIBRATION TEST

A vibration test of the GLFC cask and ALSEP support truss system was performed by General Electric for Bendix to evaluate the effects of preload at the aft trunnion connection. The data was to be used by Bendix in the redesign of an aft trunnion release mechanism to correct for the Avdel pin failure which occurred during acceptance vibration testing of the D2/M5 mockup qualification unit. The tests were performed using a different truss assembly than the one used in previous vibration tests, and with an EFCS to provide operation temperatures. The GLFC was the same as that used for the General Electric engineering vibration tests.

The results of the tests indicated that preload has a minor effect on the GLFC response. In the Y axis, elimination of the preload without introducing free play, raised the dynamic magnification factor at the fundamental resonance from 7.5 to 9.2, a 20 percent increase. A 20 percent reduction in the second Z axis (vertical) resonant frequency also occurred with the reduced preload while the frequency shifts of other resonances were small. Comparison of this data with other cask-strut vibration data indicated that the sinusoidal responses of this unit was similar to that obtained during the Bendix-Mishawaka and General Electric engineering tests. The dynamic magnification of the D2/M5 qualification unit in the Y axis was approximately twice as high as that of this unit with no preload.

Details pertaining to the above are covered in Reference 7-11.

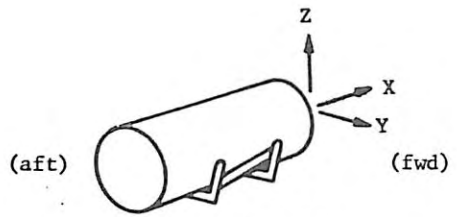

Axis Designation

7.4.9 GLFC MANNED OPERATIONAL TEST

This suited test (Reference 7-12) was performed in the man-rated Litton Industries Space Environmental Simulator. The objective of the test was to evaluate procedures, human factors, environmental effects and performance of the SNAP-27 hardware under simulated lunar operations involving removal of a fuel capsule from a GLFC.

Tests were performed at 4×10^{-6} torr. An electric capsule operating at input power of 1500 watts was utilized as the heat source. Surface temperatures of approximately 1000 to 1200°F were present on the surface of the capsule at the time of its extraction from the GLFC cavity. A Ground Handling Tool (GHT) was used to remove the electric capsule from the GLFC. A General Electric end cap removal tool was employed for removing the GLFC end cap instead of the ALSEP tool which would normally be used by the astronaut.

The procedures used inside the chamber by the astronaut were as follows:

a. Power and thermocouple leads were cut at a point as close as possible to the dome

b. Spline lock was removed using a force measuring device (force recorded as 58.5 ounces)

c. Using the torque wrench, the astronaut rotated the GLFC end cap (torque required was 19 inch-pound). The end cap was then removed

d. The astronaut engaged the GLFC and removed the EFCS placing it in a simulated generator.

The time line for the astronaut operations was as follows:

a.	Astronaut enters chamber	T + 0 minutes
b.	De-energize EFCS	T + 8 minutes
c.	Cut power and thermocouple leads	T + 11 minutes
d.	Remove spline lock	T + 13 minutes
e.	Rotate end cap	T + 15 minutes
f.	Remove end cap	T + 17 minutes
g.	Install GHT	T + 18 minutes
h.	Remove EFCS	T + 20 minutes
i.	Install EFCS in generator assembly	T + 21 minutes
j.	Exit from Chamber	T + 24 minutes

Astronaut suit temperatures recorded during testing are given in Figure 7-19. The GLFC, EFCS, and GHT temperatures are shown in Table 7-19.

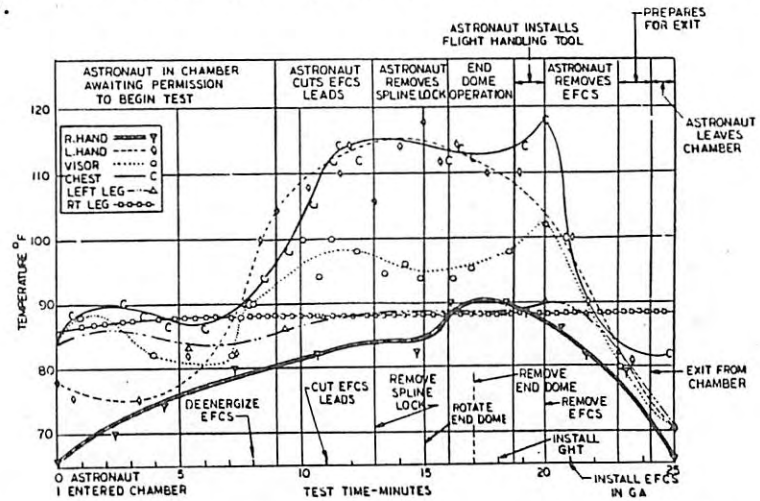

Figure 7-19. GLFC Operational Tests, Astronaut Space Suit Temperatures

TABLE 7-19. TEMPERATURE HISTORY

EFCS	
STEADY STATE	**TIME OF REMOVAL**
1. 1200°F (TOP) 2. 1305°F (MIDDLE)	1. 1070°F (MAX) - ROTATE END CAP 2. 1000°F (MAX) - REMOVE EFCS AND INSTALL IN GA
GLFC BANDS	
STEADY STATE	**TIME OF EFCS REMOVAL**
1. 565°F (FWD. - TOP) 2. 610°F (FWD. - BOT) 3. 545°F (AFT. - TOP) 4. 550°F (AFT. - BOT)	1. --- 2. 550°F 3. --- 4. ---
GHT	
STORAGE	**FUNCTIONAL USE**
1. JAW - 125°F 2. HANDLE - 125°F	1. 210°F 2. 145°F MAX. - 130°F WHEN SUIT SUBJECT GRABBED HANDLE

From all indications, the GLFC performed as expected. All handling tools proved adequate to perform the tasks involved. The GLFC operation was verified by the fact that disassembly was accomplished with ease and EFCS removal was performed with a minimum of effort. At no time was disassembly any more difficult than the same operation performed at room temperature.

Chamber operations were recorded on 35 mm film. Test results are summarized in Reference 7-13. Figures 7-20 through 7-27 depict the astronaut sequence.

Figure 7-20. Astronaut Suited and Prepared for Test

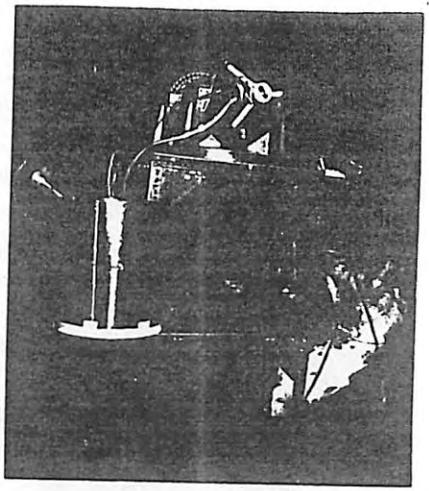

Figure 7-21. Holding Fixture (Simulated LM Mounting Conditions)

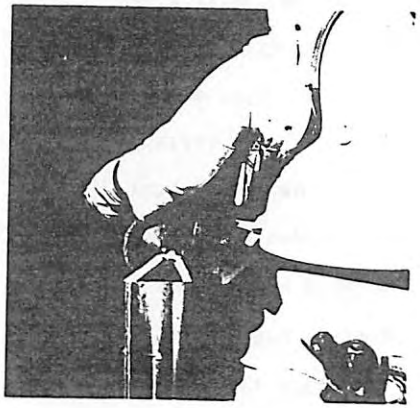

Figure 7-24. End Cap Removed

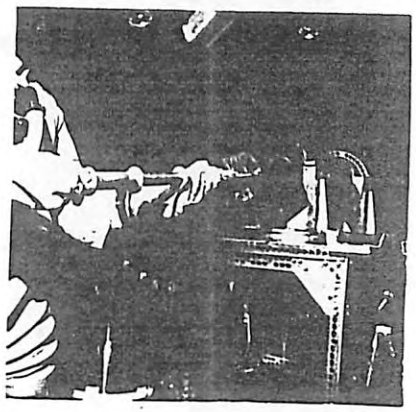

Figure 7-25. EFCS Removed Using Ground Handling Tool

Figure 7-22. Spline Lock Removed Using Force Measuring Device

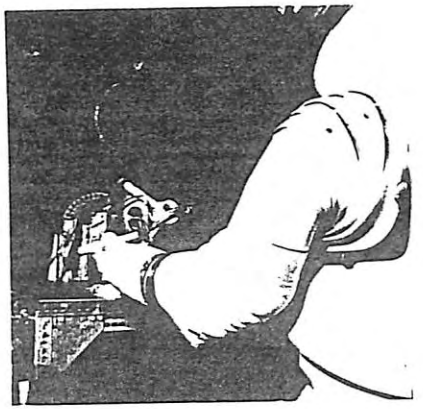

Figure 7-23. End Cap Rotated Using Torque Wrench

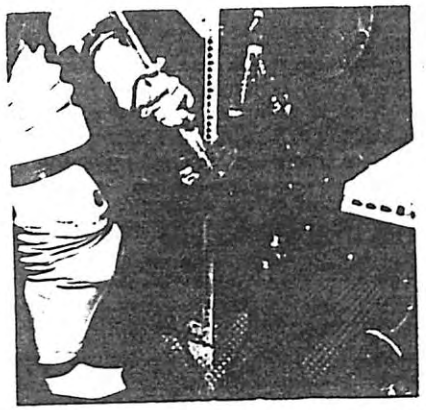

Figure 7-26. Installing EFCS in Simulated Generator

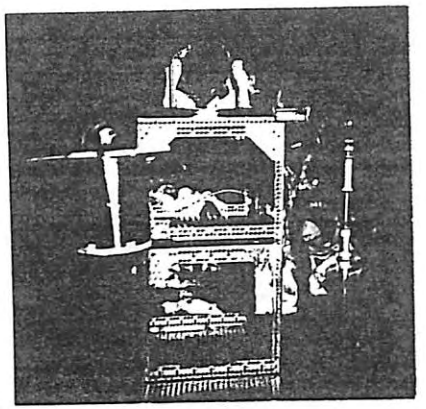

Figure 7-27. EFCS Installed in Simulated Generator

7.5 REFERENCES

7-1 "Supplement 1 to SNAP-27 Safety Report, Volume II, Accident Model Document, Appendix P. Re-entry Evaluation of GLFC and LM," General Electric, DIN 6300-300 PR1, September 1968.

7-2 Skirvin, S. C., "User's Manual for the THT-D Computer Program," GE-NMPO-P.O. No. 036-926052-T0602, June 1966.

7-3 Auxer, W., "Steady State Axial Temperature Distributions of GLFC in Operational Environments", PIR IPSO-2256, June 1968.

7-4 Auxer, W., "Steady State Axial Temperature Distribution of the GLFC", PIR ANSO-1710, November 1967.

7-5 SNAP-27 Quarterly Reports 7, 8, 9 and 10, General Electric Company, GEMS-3535-7, GEMS-3535-8, GEMS-3535-9 and GEMS-400, respectively.

7-6 General Electric Company, PIR's U8155-1949, U8157-1393, U9134-16, U9134-46, U8155-1861, U8157-1316 and U8155-1957.

7-7 "Report on Materials Compatibility, SNAP-27 GLFC Re-entry Capsule, Part I, "General Electric, GESP-7002, July 1968

7-8 "Supplement to Report on Materials Compatibility, SNAP-27 GLFC Re-entry Capsule, Part II", General Electric, GESP-7003, July 1968.

7-9 "Engineering GLFC Dynamic Testing II", General Electric, SI-249209, May 1968.

7-10 C. V. Stahle, "Results of Engineering Vibration Tests of GLFC/ALSEP Strut Assembly at GE", General Electric PIR IK75-SNAP-27-20, August 1968.

7-11 C. V. Stahle, "Sine Response of GLFC During Bendix Preload Vibration Tests", General Electric, PIR 1K75-SNAP-27-22, August 1968.

7-12 "Test Plan for the Graphite LM Fuel Cask Operational Test", General Electric, SI-249193, March 1968.

7-13 "GLFC Operational Test", General Electric, GESP-7004.

8. LM FUEL CASK DESIGN AND DEVELOPMENT

The initial approach to providing a flight cask for the fuel capsule resulted in the light-weight design referred to as the LM Fuel Cask (LFC). This configuration was the predecessor to the Graphite LM Fuel Cask (GLFC) discussed in Section 7. The description of the LFC and a summary of the supporting development effort is covered here.

ıe LFC, shown in Figure 8-1, consists of a beryllium and titanium structure fitted with ablative heat shield material on the forward and aft end. Total weight of the cask, without fuel capsule in place, is 7.5 pounds. Shape of the cask is determined by the requirement that it function as a stable aerodynamic re-entry vehicle in the event of mission abort. The central cylinder of the cask provides a free radiation surface for rejection of fuel capsule heat during all operating phases. Elastomeric heat shields on the nose and tail cone are isolated from the fuel capsule by thermal radiation barriers coated with low emissivity gold plating.

8.1 DESIGN REQUIREMENTS

Three important considerations relating to the need for free body re-entry and separation of the LFC from the LM were:

a. Weight minimization

b. Maximization of the effectiveness of heat protection applied to the LFC

c. Re-entry response of the systems.

eight minimization with an objective of 7.5 pounds for fuel capsule re-entry protection made complete spherical protection impractical with this weight constraint. Thus, the logical step was to minimize weight by providing local heat protection and to maximize the effectiveness of the heat protection provided by orienting the vehicle in a preferred direction to assure that the heat pulse would be felt only on those areas where protection was provided. Preferred orientation was to be achieved passively (aerodynamically), rather than actively through control jets or some other means.

The foregoing considerations, coupled with the need for removal of heat from the fuel capsule, led to the selection of a configuration with a

BLANK PAGE

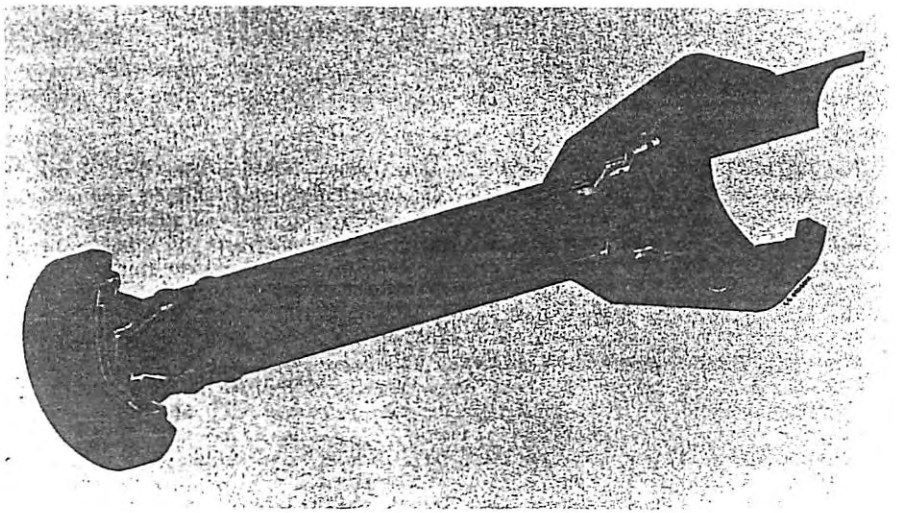

Figure 8-1. Isometric Cutaway of LM Fuel Cask (with Fuel Capsule)

blunt nose with heat protection, a cylindrical centerbody to allow for fuel capsule thermal radiation (not coated with heat protection material) and a biconic afterbody with a reverse flare.

Design requirements for the LFC differed from those of the GLFC primarily in the following areas:

a. Re-entry - Superorbital conditions were not imposed as a requirement. Only the conditions associated with a Saturn V earth orbit ascent abort and a decay from earth orbit were considered.

b. Cask/Heat Protection Bond Line - The design of the LFC was predicated on the fact that the temperature of the bond line would not exceed 450°F when integrated in the LM/Apollo.

c. Oriented Re-entry - The LFC was designed to provide oriented re-entry through the peak heating flight regime after start of re-entry in a random attitude corresponding to initial angle of attack anywhere in the range 0 to 180 degrees.

d. Vibration

1. Random

Frequency (cps)	Power Spectral Density
5 to 28	0.08 g^2/cps
28 to 45	6 db/oct. decrease
45 to 1250	0.034 g^2/cps
1250 to 2000	15 db/oct. decrease

2. Sinusoidal

Frequency (cps)	Amplitude
5 to 18.5	0.154 inch peak-to-peak
18.5 to 200	$\pm$ 3.3 g

e. Weight - The LFC was not to exceed 7.5 pounds as a design goal.

8.2 DESIGN ANALYSIS

8.2.1 THERMAL ANALYSIS

Results of a thermal analysis (Reference 8-1) conducted on the LFC for both free convection and vacuum are summarized in Figure 8-2.

8.2.2 DYNAMIC ANALYSIS

Dynamic analyses of the LFC (References 8-1 and 8-2) were performed for the lateral (most critical) condition with the fuel capsule inserted in the cask, and with the assembly at operating temperature. Responses of the cask were computed from inputs of shock, sinusoidal and random vibration. The cask and capsule were separated into a spring mass nodal model and a vibrational stiffness matrix was calculated from material properties at operating temperatures. Figure 8-3 shows the mass station locations for the critical areas of the cask.

Calculated responses for a sinusoidal input of 1 g applied to the cask at the mounting locations on the beryllium cyclinder are tabulated in Table 8-1 for fifteen nodes for the first and second frequency. The first three natural frequencies of the cask/capsule assembly were found to be 370, 464 and 722 cps. The largest response at the forward end of

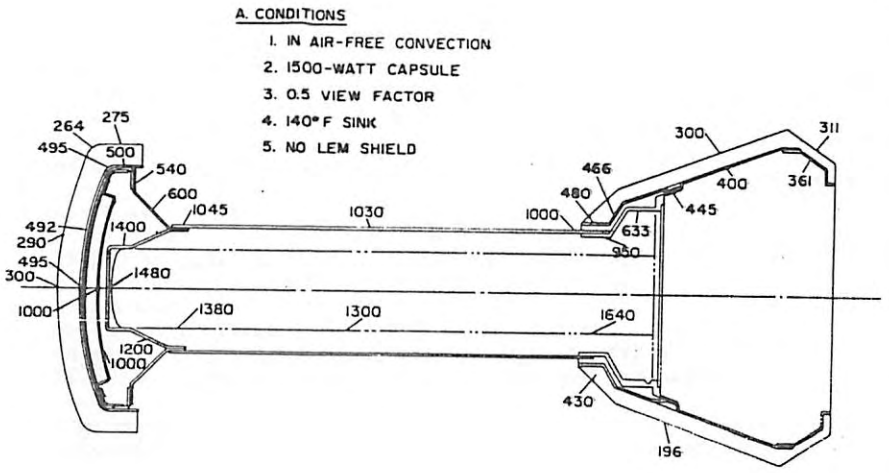

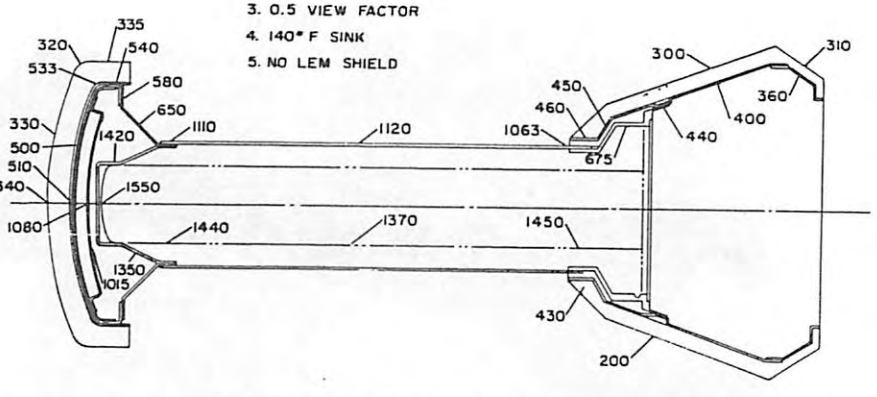

Figure 8-2. Calculated LM Fuel Cask Temperatures (°F) for Vacuum and for Air-Free Convection

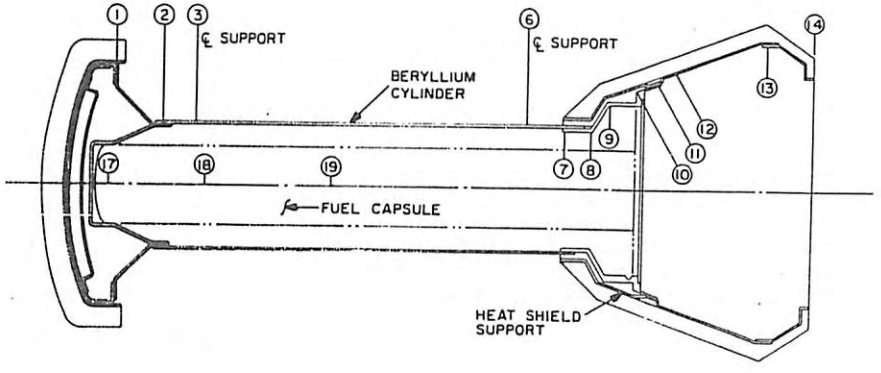

Figure 8-3. LM Fuel Cask Dynamic Node Locations

TABLE 8-1. CALCULATED DYNAMIC RESPONSES OF CASK

Station No.	1	2	3	6	7	8	9	10	11	12	13	14	17	18	19
Station Location	5.45	7.00	8.08	18.33	19.64	20.05	20.6	21.5	22.1	22.58	25.65	27.0	5.0	8.3	11.6
1 g Input 370 cps	1.36	1.1	1.0	1.0	1.21	1.33	1.42	2.41	2.80	3.19	5.35	6.0	1.56	4.5	6.7
1 g Input 464 cps	1.81	1.1	1.0	1.0	1.85	2.65	5.36	7.38	8.71	10.3	18.3	20.7	2.3	6.73	10.1
Random Input $0.075\ g^2$ cps 36 to 1200 cps g-rms	31.1	-	11.07	11.24	-	-	-	16.4	18.4	21.0	35.9	40.4	-	20.2	23.6
Shock Input Sawtooth 15g 11 ms Duration	15	15	15	15	-	15	15	15	15	15	15.2	16.7	-	-	-

the capsule was 1.8 g at Station No. 1 and 20.7 g at Station No. 14 at the end of the aft flare. The responses at the forward and aft capsule support points are 2.3 g and 7.4 g, respectively.

Calculated responses for a random vibration input of 0.075 g^2/cps applied to the cask at the mounting locations on the beryllium cylinder are tabulated in Table 8-1 for ten nodes. The largest response at the forward end of the capsule was 31.1 g rms at Station No. 1 and 40.4 g rms at the end of the aft flare at Station No. 14. The response at the aft capsule support points was 16.4 g rms.

A 15 g sawtooth shock pulse of 11.0 milliseconds duration resulted in little amplification. The calculated values are also shown in Table 8-1.

8.3 DEVELOPMENT TEST PROGRAM

A comprehensive development test program was carried out for the LM Fuel Cask. A brief description of each of these tests is given below:

8.3.1 MATERIALS AND COATINGS TESTS

8.3.1.1 Structural Materials and Bond Properties Tests

Tensile properties of titanium and tensile and compressive properties of beryllium samples were determined for temperatures ranging from 1100° to 1300°F, in a non-oxidizing atmosphere. (See Tables 8-2 through 8-6.)

8.3.1.2 Ablation Materials and Bond Properties Tests

Aging effects on the ESM 1004 LP heat shield material were determined on specimens after exposure for 42 hours at 600°F and 1 x 10^{-6} torr, followed by 600°F and 1 x 10^{-6} torr for 12 days. Bond test specimens were tested at 500°F and 600°F for lap shear strength and weight loss.

8.3.1.3 5 MW Arc Facility Tests on ESM Ablation Material

An ablation test program was conducted in the General Electric Hyperthermal Arc Facility on nose and flare sections of the SNAP-27 cask configuration covered with ablation material. Ablation materials tested were identified as ESM 1004 LP and ESM 1004 AP, with respective densities of 56 ± 4 and 35 ± 3 lb/ft^3. Three heat flux levels of 25, 75 and 125 Btu/ft^2-sec were employed. The tests indicated that the ESM bulk properties and bond to beryllium retained satisfactory integrity after exposure to the thermal/vacuum environmental tests.

TABLE 8-2. TENSILE PROPERTIES OF TITANIUM ALLOY, 6AL-4V AT FOUR TEMPERATURE LEVELS

Specimen No.	Direction and Location	Temperature (°F)	Modulus of Elasticity (psi x 10^{-6})	Yield Strength (0.2 Percent Offset)	Ultimate Strength (ksi)	Elongation 1.0-inch Gage (Percent)
25	Longitudinal L-t	RT	16.0	109.0	139.3	21.2
26			16.7	122.5	135.5	18.9
27			17.7	127.0	140.0	18.1
Average			Avg 16.8	118.1	138.3	19.4
16		1100	9.36	52.6	61.0	25.1
17			10.00	65.6	66.3	30.7
18			9.50	57.0	65.5	30.0
Average			Avg 9.75	58.4	64.3	28.6
19		1200	7.62	33.6	41.8	25.0
20			7.93	34.6	42.7	33.7
21			8.30	41.3	47.3	45.0
Average			Avg 7.95	36.5	43.9	34.5
22		1300	6.40	28.7	33.9	58.6
23			6.67	25.0	26.7	75.1
24			6.47	21.8	34.3	47.9
Average			Avg 6.51	25.2	31.6	60.3

TABLE 8-3. TENSILE PROPERTIES OF TITANIUM ALLOY, 6AL-4V AT FOUR TEMPERATURE LEVELS

Specimen No.	Direction and Location	Temperature (°F)	Modulus of Elasticity (psi x 10^{-6})	Yield Strength (0.2 Percent Offset)	Ultimate Strength (ksi)	Elongation 1.0-inch Gage (Percent)
37	Trans. M M	RT	17.1	128.0	141.0	18.8
38			16.2	122.5	133.6	23.1
39			16.9	126.2	140.0	14.8
Average			Avg 16.7	125.6	138.2	18.6
31		1100	9.0	67.3	68.2	28.10
34			11.1	74.5	79.7	19.5
33			10.1	66.1	70.3	25.1
47			10.2	58.4	63.0	22.0
Average			Avg 10.1	66.1	67.8	23.1
41		1200	7.7	37.0	48.3	27.2
42			8.6	32.5	50.5	27.6
Average			Avg 8.1	34.7	49.9	27.4
48		1300	6.2	31.0	35.0	31.0
52			6.5	29.9	31.3	32.5
53			5.6	29.5	32.5	21.0
Average			Avg 6.1	30.5	33.0	34.2

TABLE 8-4. ULTIMATE SHEAR STRENGTH OF TITANIUM ALLOY 6AL-4V, VERSUS TEMPERATURE

Specimen No.	Direction	Temperature (°F)	Ultimate Shear Strength (ksi)
121	Longitudinal	RT	100.56
122			87.40
123			75.09
			88.35
124		1100	49.35
125			46.20
126			42.46
			45.83
127		1200	36.65
128			.....
129			40.50
			38.57
142	Transverse	RT	104.75
143			112.81
144			106.74
			108.56
145		1100	43.46
146			36.64
147			46.55
			44.21
148		1200	36.84
149			39.66
150			39.00
			38.50

TABLE 8-5. TENSILE PROPERTIES OF HOT-PRESSED S-200 BERYLLIUM ALLOY* VERSUS TEMPERATURE SOLID CYLINDER (8 INCH DIAMETER BY 8 INCH LONG)

Specimen No.	Direction and Location	Temperature (°F)	Modulus of Elasticity (psi x 10^6)	Yield Strength 0.2% Offset (psi x 10^3)	Ultimate Strength (psi x 10^3)	Elongation 1.0 in.Gage (%)	Remarks
40	Longitudinal Level	R.T.	35.8	38.8	46.0	1.08	
41			34.5	38.8	48.0	1.38	
42			34.6	38.8	46.0	0.68	
			Avg. 35.0	38.8	46.7	1.05	
47		500	34.2	36.3	44.0	5.91	
48			33.8	36.8	42.5	3.61	
50			32.2	42.6	44.0	4.58	
			Avg. 33.4	36.6	43.5	4.70	
35		600	21.3	35.2	39.4	6.72	
37			29.3	36.9	40.0	7.26	
38			-	-	39.8	9.43	
			Avg. 25.3	36.1	39.7	7.87	
44		850	26.2	32.2	34.7	19.60	
57			26.2	30.4	34.5	21.55	
58			24.3	28.4	32.9	15.14	
			Avg. 23.5	30.5	34.0	18.76	
52		1050	23.2	26.0	29.0	7.1	
53			25.6	27.2	31.4	4.9	
54			23.0	21.6	24.5	4.5	
			Avg. 23.7	25.0	28.3	5.5	
59		1250	11.2	12.0	12.6	4.9	
60			11.1	9.4	10.9	6.6	
193			15.3	14.5	15.4	7.7	
			Avg. 12.5	11.9	12.9	6.4	
32		1350	10.9	8.5	9.1	5.3	
33			10.1	7.5	7.6	3.5	
34			7.0	5.5	5.9	4.1	
36			10.0	7.2	7.5	5.0	
			Avg. 9.5	7.1	7.8	4.5	
1	Transverse	R.T.	33.5	39.5	47.2	1.34	Failed at Gage Mark
5			43.2	42.5	54.3	2.81	
9			36.6	39.6	42.7	1.09	Failed Outside Gage Marks
			Avg. 37.8	40.6	48.1	1.75	
17	Transverse	500	29.1	37.4	45.0	20.70	
20			29.1	36.4	44.0	16.74	
24			31.0	37.6	44.0	13.80	
			Avg. 29.7	37.2	44.3	17.10	
2		600	32.3	35.4	42.2	24.21	
3			25.4	34.5	41.4	18.49	
4			25.0	36.0	41.0	16.25	
			Avg. 27.6	35.3	41.5	19.75	
6		850	23.4	29.5	33.9	23.36	
7			23.9	29.5	33.6	17.07	
9			23.8	31.9	35.8	24.20	
			Avg. 24.3	30.3	34.5	25.6	
10		1050	22.0	25.3	29.7	17.10	
11			21.0	25.0	30.2	19.07	
12			22.4	24.0	28.7	19.47	
			Avg. 21.7	24.8	29.5	18.54	
13		1250	14.5	14.5	15.8	6.73	Failed Outside Gage Marks
18			11.0	13.2	13.9	5.27	
19			13.4	13.9	15.3	13.20	
			Avg. 12.9	13.6	13.0	13.20	
21		1350	11.9	9.5	9.7	** 5.66	Failed Outside Gage Marks
22			9.1	10.1	10.6	10.10	
23			10.5	8.9	8.9	** 8.50	Failed Outside Gage Marks
			Avg. 10.5	9.5	9.7	8.8	

* The Brush Beryllium Company

TABLE 8-6. COMPRESSIVE PROPERTIES OF HOT-PRESSED S-200 BERYLLIUM ALLOY AT VARIOUS TEMPERATURES

Specimen No.	Direction and Location	Temperature (°F)	Modulus of Elasticity (psi x 10^{-6})	Yield Strength (0.2% Offset)	Remarks
139	Longitudinal Level 3	1050	29.2	26.8	
165			30.7	25.6	
Average			30.0	26.2	
148	Transverse Level 3	RT	42.5	39.3	
149				39.7	
Average				39.5	
138		1050	30.0	26.9	
135		1250	18.2	18.4	
141			18.8	15.4	
142			17.6	17.4	
Average			18.3	17.1	
146		1350	15.4	8.2	

8.3.1.4 Cask Structure Emissive Coating Tests

Emissivity test specimens with gold coatings applied by vapor deposition and by conversion from organometallic solutions were evaluated for adhesion and emissive properties after exposure to high temperature and vacuum conditions. Various diffusion barriers were evaluated as a check against diffusion of the low emissive coat into the structural substrate. (See Table 8-7.)

8.3.2 AERODYNAMIC AND THERMODYNAMIC MODEL TESTS

8.3.2.1 LTV Mach 17 Aerodynamic Tests

Tests were performed on a subscale model of the LM fuel cask configuration in the LTV-Vought Aeronautics Division Hypervelocity Wind Tunnel at a Mach number of 17 and a Reynolds number of 1.5×10^6 ft., for angles of attack of 0, 4, 8 and 12 degrees (static and dynamic phases). Object was to obtain preliminary static and dynamic stability data at Mach 17 for low angles of attack. Schlieren flow visualization pictures were taken at all angles of attack in the static phase.

8.3.2.2 AEDC Mach 6 Through 10 Aerodynamic Model Tests

Testing was performed at the Arnold Engineering Development Center, in their tunnels, A, B and C, for Mach Numbers 6 through 10 on subscale models of the SNAP-27 LFC configuration to determine static and dynamic stability parameters and pressure distribution using primary and back-up configurations for the LFC design. A summary of the test program is given in Table 8-8.

TABLE 8-7. EMISSIVITY DATA

Substrate Material and Thickness (in.)	Maximum Temperature of Substrate during Normal Operation (°F)	Emissivity Required	Coating	Results/Comments
Haynes-25 0.020	1500	0.85	Radifrax RC-164	Spray-gun applied and fired at 1650°F. Coating appears satisfactory.
		0.10	Diffusion barrier and gold	Organo-metallic and vapor-deposited coating processes are unsatisfactory. Work is continuing.
Titanium 6AL-4V 0.020	1100	0.85	Radifrax RC-353	Successfully grit-blasted and plasma-arc coated. Emissivity 0.88 over 70 hours
		0.10	Diffusion barrier and gold	Organo-metallic and vapor-deposited coating processes are unsatisfactory. Work is continuing.
Beryllium HPB 0.100	1100	0.85	Radifrax RC-166	Spray gun applied and fired at 1350°F. Coating appears satisfactory; however, some flaking of the coating has been observed.
	600	0.10	Diffusion barrier and gold	Test data is not conclusive

TABLE 8-8. AEDC AERODYNAMIC MODEL TEST PROGRAM

RUN NO.	TUNNEL	TYPE TEST	MACH NO.	(DEGREES)	Re (x 10^{-6} ft)	CONFIGURATION
1	C	Static Stability & Drag	10	0 to 180	0.3 to 2.2	Primary
2	C	Static Stability & Drag	10	0 to 180	0.3 to 2.2	Secondary
3	C	Dynamic Stability	10	0 to 12	0.3 to 2.2	Primary
4	B	Pressure	8	0 to 90	2.2	Primary
5	A	Static Stability & Drag	6	5 to 15	0.4 to 4.3	Primary
6	A	Dynamic Stability	6	0 to 12	0.4 to 4.3	Primary
7	A	Pressure	6	-5 to 15	4.3	Primary

8.3.2.3 Preliminary LFC Configuration Heat Transfer Tests

A series of heat transfer tests, Table 8-9, were conducted in the Rhodes and Bloxsom Hot Shot Tunnel to establish the final LFC configuration.

TABLE 8-9. RHODES AND BLOXOM HEAT TRANSFER TEST PROGRAM

MODEL NO.	ANGLE OF ATTACK (DEGREES)	FREE STREAM MACH NO.	ALTITUDE (FT)	FREE STREAM VELOCITY (FPS)
1	0	22	189,000	22,000
2	15	22	189,000	22,000
3	30	22	189,000	22,000
4	90	22	189,000	22,000

Shadowgraphs were taken on each of the models during test to determine shock layers and separate flow regions. Each of the models was sprayed with a thermopaint which responds to temperature so that heating rates on the model surface could be evaluated. Each of the four specimens was a one-half scale model of the SNAP-27 re-entry cask configuration.

8.3.2.4 LFC Configuration Re-entry Heating Test

A series of heat transfer tests utilizing standard thin wall calorimetry was conducted in Tunnel B of the Arnold Engineering Development Center, Tullahoma, Tennessee, to determine heat transfer data for the SNAP-27 LFC configuration. Test parameters included various angles of attack at several Reynolds numbers as outlined in Table 8-10. Nominal conditions for the tests were as follows:

Free stream, Mach No., $M_\infty = 8$

Total Temperature, $T_o = 1360^oF$

Total Pressure, P_o = 200 to 800 psia.

TABLE 8-10. AEDC RE-ENTRY HEATING TESTS ON LFC

GROUP	ORIENTATION (DEGREES)	PRESSURE (PSIA)	REYNOLDS NO./FT	PURPOSE
1	0 ± 90	800	3.148×10^6	To provide heat transfer data under turbulent flow Conditions
2	Same as Group 1	200	786,000	To obtain laminar heat transfer data to determine if transition does occur at high pressure
3	Same as Group 1	400	1.574×10^6	To provide interpolation of the high and low pressure test results

The test model was a full scale SNAP-27 unit configuration utilizing an electro-formed Nickel shell.

8.3.3 ENGINEERING LFC DESIGN VERIFICATION TESTS

8.3.3.1 Thermal Interfaces Test

This test was an engineering development test to verify the integrated thermal interfaces which involve the LFC, specifically the Bendix support structure and thermal shield which interfaces directly with the LFC and LM, the Grumman support structure which ties the Bendix structure to the LM vehicle, and the variations in the thermal sink which are experienced by the LFC due to the presence of the LM, the Bendix hardware and the SLA and the equivalent sink presented by the remaining sections of the launch configuration. This test represented the only planned program activity for flight proofing of the ALSEP/SNAP-27 with respect to thermal integration.

The thermal testing was performed in several phases representing: 1) the on-pad thermal environment; 2) the translunar thermal vacuum conditions with SLA closed; and 3) the translunar environment with the SLA open. A simulated on-pad ambient test was also run with the top and bottom panels of the sink removed and the SLA closed. An electric fuel capsule was used to provide the thermal input for the LFC.

The translunar thermal vacuum test with the SLA closed was conducted using the complete assembly including sink panels. Testing was conducted in a 39-foot spherical chamber under a vacuum of 10^{-5} torr or less. Panel zone heaters were used to simulate sink temperatures and a fuel capsule simulator to provide an equivalent capsule thermal input. Test duration was for 12 hours after reaching steady state temperature conditions.

The translunar thermal vacuum test simulating the SLA open was conducted under the same conditions as the SLA closed test, except that the SLA section was removed and test duration increased to 72 hours.

The test configuration comprised Engineering Model No. 1 LFC (heavily instrumented) supported by the Bendix Shield/structure, in turn, mounted to the Grumman support structure. The entire assembly was mounted to a simulated LM surface located within a thermally controllable shroud simulating the SLA interface. Testing was performed in a 39-foot space chamber at General Electric-Valley Forge. The results are given in Table 8-11.

8.3.3.2 Dynamic Verification Tests

The LM fuel cask was supported during all the tests by a rigid test fixture designed to clamp the LFC at its intended mounting points on the barrel. A heated electric fuel capsule was present within the LFC

TABLE 8-11. LM FUEL CASK THERMAL TEST SUMMARY OF TEMPERATURES

ELECTRIC FUEL CAPSULE SIMULATOR POWER - ENVIRONMENT	PHASE A 1463 WATTS 79°F AIR	PHASE B 1489 WATTS HOT VACUUM	PHASE C 1490 WATTS COLD VACUUM
EFCS - Average Temperatures	1160	1245	1230
Cask Barrel - Average Temperatures	767	914	896
Nose ESM Bond - Average Temperatures	259	466	376
Nose (ESM Bond Maximum Temperature)	299	536	453
Flare Forward ESM Bond - Average Temperature	376	525	445
ESM Aft Flare Bond Line - Maximum Temperature	408	621	569
Bendix Shield on Side Facing Cask - Average Temperature	108	433	338
Bendix Shield on Side Facing LM Blanket - Average Temperature	86	227	24
LM Blanket - Average Temperature	82	194	-122
LM Blanket - Maximum Temperature	96	217	-72
LM Leg - Average Temperature	---	---	-55
SLA (Boundary Panel) - Average Temperature	81	248	---
LM (Boundary Panels) - Average Temperature	79	71	144
Simulator Sinks	84	177	
	Temperatures in °F		

throughout the tests. The LFC/EFCS combination was subjected to vibration, shock and acoustic noise tests at levels in excess of predicted flight levels to demonstrate a factor of safety.

8.4 CASK SEPARATION STUDY

General Electric was instructed by the AEC on October 31, 1966 to perform a brief one-month study on a LM Fuel Cask Separation System to be used as a backup to the independent NASA/Bendix studies. The technical effort was completed on December 1, 1966 and reported in Reference 8-3.

Ground rules used in the study included:

a. No change in Grumman hard points

b. Stay within existing cask withdrawal envelope

c. No assistance from astronaut or ground commander

d. Use of springs for imparting separation velocity

e. Utilize flight-proven components to avoid long development programs

f. Assume the LM is removed from the SLA prior to abort.

Utilizing the ground rules and specified release criteria, a number of diverse concepts were investigated. Table 8-12 summarizes the pro's and con's of some of the concepts which were considered promising, along with the resulting decision whether or not to continue work in that particular area. Figure 8-4 is an example of one of these concepts, that employing a low temperature flare-type initiator mounted on the LM surface which ignites in the 600 to 650°F temperature range, with the resulting high temperature reaction then transmitted to a length of Pyrofuze which ignites at around 1200°F.

The search for a suitable cask separation system was subsequently abandoned in favor of the Graphite LM Fuel Cask approach.

8.5 REFERENCES

8-1. SNAP-27 Quarterly No. 3, GEMS-3535-3

8-2. SNAP-27 Quarterly No. 5, GEMS 3535-5

8-3. "Cask Separation Study, SNAP-27 Program", GE No. 6300-160.

TABLE 8-12. DECISION MATRIX

	CONCEPT	PRO	CON	RESULTS
1.	Passive, Meltable Material	Minimum interface with LM/ALSEP Lightest weight	Material development Unknown nature of LM Re-entry characteristics • No test data • Difficult to analyze • Likely to be stable	Discontinued further study
2.	Command Receiver	Highly reliable Minimal development effort Avoids aero problems (LM re-entry)	Heavy Requires difficult interface with LM Requires ground command (No authorization)	Discontinued further study
3.	Thermal flare/ Pyrofuze	Non-electrical Extremely simple	Pyrofuze release device development Ignitor development Redundancy not practical LM interface complications	Discontinued further study
4.	Thermal cell	Light weight Redundancy possible Formitable flight experience Adaptable to many separation concepts Compatible with thermal battery for multiple-squib activation	Needs development of sealed configuration Low voltage device, requires heavy wiring	Carried as prime abort-sensor concept
5.	Timer	Highly developed, reliable component Simple Avoids LM aero problems	Requires special temperature control Requires baroswitch activation and G-switch reset Ties directly to APOLLO time lines - high risk for change	Discontinued further study
6.	Ball locks	Flight experience Minimal development required Compatible with many abort sensing concepts Can be easily armed and disarmed Highly accurate release timing	Requires gas tubing and manifolding Requires pyrotechnic gas generator	Carried as prime concept
7.	Pin pusher	Flight experience Compatible with many abort sensing concepts Can be easily armed and disarmed No piping required	Requires substantial integration effort Requires nominal development effort Release timing related to tolerances and thermal expansion	Carried as backup concept

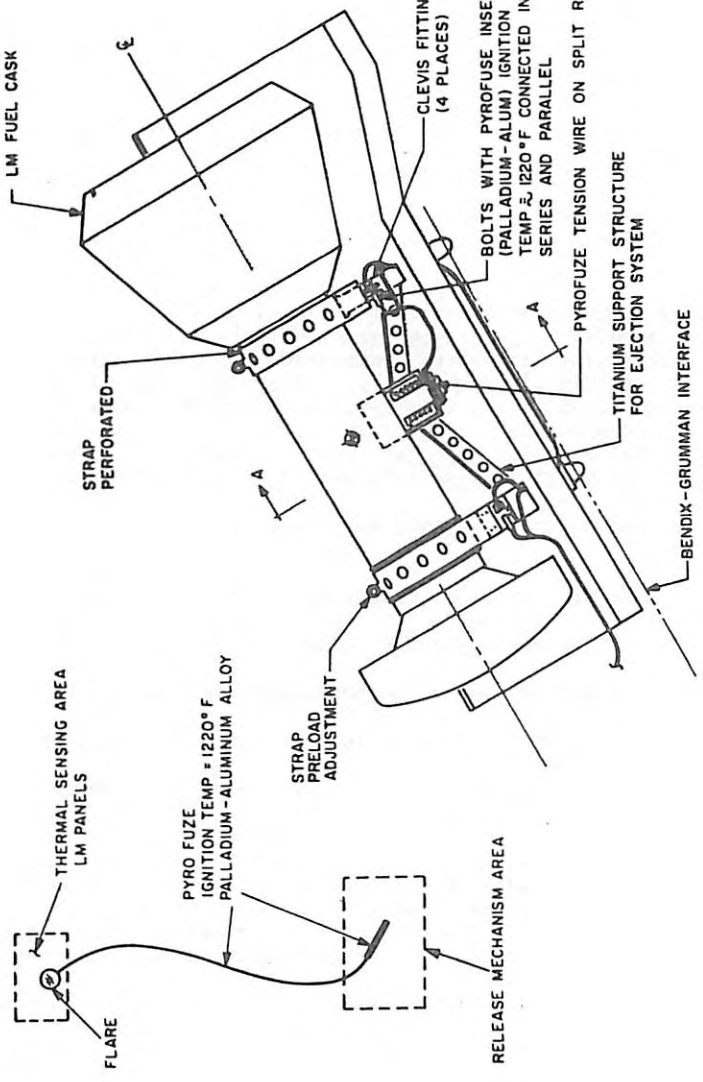

Figure 8-4. Thermal Flare/Pyrofuze Cask Release Subsystem

9. RELIABILITY

The SNAP-27 reliability program was defined in a reliability plan (Reference 9-1) which established management and technical reliability functions in support of the design, procurement, test and fabrication functions. This plan fulfilled the requirements of NASA Reliability Publication NPC-250-1 (Reference 9-2) and the NASA-MSC/AEC Plan (Reference 9-3). The plan was supplemented by the 3M Company's Reliability Program Plan (Reference 9-4).

At the request of the AEC, all direct effort by General Electric in support of the reliability program was terminated at the completion of Phase III.

Summarized in the following paragraphs are the significant results.

9.1 RELIABILITY DESIGN ANALYSIS

The primary objective of this task was qualitative and quantitative evaluation of the SNAP-27 RTG reliability. Additional complementary information was also generated, which included the uncovering of potential design problem areas, reliability input for system design tradeoffs and guidance for reliability measurements in the Integrated Test Program.

Two significant preliminary reliability analyses were performed early in the reliability program: an initial reliability estimate on the RTG and a statistical analysis of SNAP-23 life test data. The former estimated RTG reliability as 0.9943, which was slightly lower than the design goal of 0.995. It also indicated that the thermopile was the least reliable component, having a calculated reliability of 0.9974, while all the other RTG components had estimated reliabilities in excess of 0.999. The statistical analyses of SNAP-23 life test data indicated that the electrical resistance variation of a thermocouple was a function of operating time, while the variation of open circuit voltage and output current was a function of hot and cold temperature fluctuations as well as operating time. Analytical relations for the resistance, open circuit voltage and output current as a function of operating time and hot and cold junction temperatures were fitted to the test data. The results of these preliminary analyses were used to guide the direction of the subsequent reliability investigations.

A failure mode and effects analysis was performed on the thermopile since this was the component having the lowest reliability. The results,

BLANK PAGE

summarized in Table 9-1, indicated that the most critical failure locations were the thermoelement hot junctions, the cold follower and the thermal insulation.

A reliability prediction analysis on the RTG indicated that it possessed a 0.9994 probability of successfully completing its one year lunar mission, as compared to its reliability design goal of 0.995. For the analysis, the RTG was considered as comprised of three major subsystems: the thermopile assembly, the generator structural assembly and the fuel capsule assembly. The fuel capsule was treated in this analysis as part of the structure.

The thermopile reliability was assessed for the condition that the predominant failure mode for the thermocouple was that of open circuit. Both the mode of short-circuiting between thermoelectric element and that of short-circuiting to either the hot or cold frame were considered to be negligible and not included in the reliability assessment because the thermopile design includes features which are intended to minimize the probability of occurrence of these failure modes.

The reliability calculations were made as follows:

a. Thermopile Reliability Mathematical Model - For the condition that 17 non-adjacent couple failures in the open mode are permitted with no premissible adjacent open-circuited couples, the thermopile reliability is given by:

$$R\ (\text{Thermopile}) = \sum_{X=204}^{221} \binom{221}{X} P_1^{\ X} \cdot P_2^{\ 221-X}$$

where:

$P_1 = R_o^{\ 2}$

$P_2 = 2R_o \cdot (1-R_o)$

R_o = Couple reliability (open mode) = $e^{-\lambda t}$

λ = Failure rate in failures/hour

t = Mission time = 10,000 hours

TABLE 9-1. SNAP-27 FAILURE MODE AND EFFECT ANALYSIS FORM (SHEET 1 OF

Item No.	Item Description	Assumed Failure Mode	Assumed Caused of Failure	Effect on Mission Performance	Compensating Provisions	Failure Class	Prob. of Occur.	Proposed Course of Action
1	Hot end insulation (Boron Nitride)	A. Electrical short circuit to frame.	Impurities, metal particles, cracked insulation, condensate from brazing operations.	Varies from reduction in output to total loss of generator output. A short to ground could possibly produce an undesirable condition for the load.	Two independent shorts must occur, since the generator is a floating ground.	A_f	B_o	
		B. Increased thermal impedance.	Cracked insulation.	Reduced output from the affected elements. Increased hot frame temperature may cause excessive heating of the other elements.	Most likely type of crack would have minor effect.	B_f	B_o	
		C. Transverse crack separates hot end insulation into two or more pieces.	Excessive coefficient of friction and thermal cycling.	Excessive relative motion causes an increase in hot junction resistance.	Boron nitride may slide on hot frame.	U_f	A_o	Consider M_o strip with Boron Nitride inserts as prime design.
		D. Lack of transient thermal expansion compensation.	Insertion of fuel capsule.	Same as 1C.	Magnitude of effect can be determined from prototype.	U_f	A_o	Perform a simulated fuel loading.
2	Hot Strap	Spalling of plating.	Improper fabrication, improper processing of plating.	Sublimation products from elements travel to hot shoe and react with copper. This compound returns to the element and causes a change in element doping, resulting in reduced output. The growth of copper whiskers also poses a potential electrical short hazard.		B_f	B_o	Requires Q.C. test of plating for tendency to blister. Ensure that iron plating is not cracked during assembly.
3	Hot Button	A. Electrical open circuit at hot strap or at element.	1. Foreign material during assembly.	Reduced output due to excessive resistance.	Would be detected during checkout and processing.	B_f	C_o	
			2. MIN-K insulation works into the area between the element and hot button during thermal cycling and/or vibration.	Same as 3.A.1		B_f	A_o	Use of preformed strip of Microquarts surrounding the element at the hot end.
		B. Element not properly seated in hot button.	Improper assembly.	High thermal and electrical resistance and possibly a cracked element.	Would probably be picked up by test for proper spring length.	C_f	C_o	Call out in visual Q.C. check.
4	Thermoelectric Element	A. Cracking, especially under thermal cycling.	1. Excessive thermal gradient causes cracking at cold end.	Internal resistance will increase with proportionate decrease in power output.	Spring pressure may maintain nearly constant output, but sensitivity to shock and vibration will be increased.	B_f	B_o	Post-test analysis required to detect occurrence.
			2. Bonding at hot junction causes cracking at hot end. See Section 4.D.					
			3. Improper fabrication of element.					
			4. Improper assembly of generator.					
			5. Excessive force exerted on element during fabrication.					
		B. Excessive	1. Excessive oper-	Gradual deter-	Reduction in	B_f	B_o	Post test anal-

9-1. SNAP-27 FAILURE MODE AND EFFECT ANALYSIS FORM (SHEET 1 OF 3)

Assumed Failure Mode	Assumed Caused of Failure	Effect on Mission Performance	Compensating Provisions	Failure Class	Prob. of Occur.	Proposed Course of Action	Criticality Ranking
A. Electrical short circuit to frame.	Impurities, metal particles, cracked insulation, condensate from brazing operations.	Varies from reduction in output to total loss of generator output.		A_f	B_o		
		A short to ground could possibly produce an undesirable condition for the load.	Two independent shorts must occur, since the generator is a floating ground.				2
B. Increased thermal impedance.	Cracked insulation.	Reduced output from the affected elements. Increased hot frame temperature may cause excessive heating of the other elements.	Most likely type of crack would have minor effect.	R_f	B_o		4
C. Transverse crack separates hot end insulation into two or more pieces.	Excessive coefficient of friction and thermal cycling.	Excessive relative motion causes an increase in hot junction resistance.	Boron nitride may slide on hot frame.	U_f	A_o	Consider M_o strip with Boron Nitride inserts as prime design.	3
D. Lack of transient thermal expansion compensation.	Insertion of fuel capsule.	Same as 1C.	Magnitude of effect can be determined from prototype.	U_f	A_o	Perform a simulated fuel loading.	3
Spalling of plating.	Improper fabrication, improper processing of plating.	Sublimation products from elements travel to hot shoe and react with copper. This compound returns to the element and causes a change in element doping, resulting in reduced output. The growth of copper whiskers also poses a potential electrical short hazard.	2	R_f	B_o	Requires Q.C. test of plating for tendency to blister. Ensure that iron plating is not cracked during assembly.	4
A. Electrical open circuit at hot strap or at element.	1. Foreign material during assembly.	Reduced output due to excessive resistance.	Would be detected during checkout and processing.	R_f	C_o		8
	2. MIN-K insulation works into the area between the element and hot button during thermal cycling and/or vibration.	Same as 3.A.1		R_f	A_o	Use of preformed strip of Micro-quartz surrounding the element at the hot end.	1
B. Element not properly seated in hot button.	Improper assembly.	High thermal and electrical resistance and possibly a cracked element.	Would probably be picked up by test for proper spring length.	C_f	C_o.	Call out in visual Q.C. check.	3
A. Cracking, especially under thermal cycling.	1. Excessive thermal gradient causes cracking at cold end.	Internal resistance will increase with proportionate decrease in power output.	Spring pressure may maintain nearly constant output, but sensitivity to shock and vibration will be increased.	R_f	B_o	Post-test analysis required to detect occurrence.	
	2. Bonding at hot junction causes cracking at hot end. See Section 4.D.						4
	3. Improper fabrication of element.						
	4. Improper assembly of generator.						
	5. Excessive force exerted on element during fabrication.						
Excessive	1. Excessive oper-	Gradual deter-	Reduction in	R_f	B_o	Post test anal-	4

BLANK PAGE

				not short and react with copper. This compound returns to the element and causes a change in element doping, resulting in reduced output. The growth of copper whiskers also poses a potential electrical short hazard.				blister. End that iron plat is not cracke during assem
3	Hot Button	A. Electrical open circuit at hot strap or at element.	1. Foreign material during assembly.	Reduced output due to excessive resistance.	Would be detected during checkout and processing.	B_f	C_o	
			2. MIN-K insulation works into the area between the element and hot button during thermal cycling and/or vibration.	Same as 3.A.1		B_f	A_o	Use of prefor strip of Micr quartz surro the element a hot end.
		B. Element not properly seated in hot button.	Improper assembly.	High thermal and electrical resistance and possibly a cracked element.	Would probably be picked up by test for proper spring length.	C_f	C_o	Call out in vi Q.C. check.
4	Thermo-electric Element	A. Cracking, especially under thermal cycling.	1. Excessive thermal gradient causes cracking at cold end.	Internal resistance will increase with proportionate decrease in power output.	Spring pressure may maintain nearly constant output, but sensitivity to shock and vibration will be increased.	B_f	B_o	Post-test ana required to de occurrence.
			2. Bonding at hot junction causes cracking at hot end. See Section 4.D.					
			3. Improper fabrication of element.					
			4. Improper assembly of generator.					
			5. Excessive force exerted on element during fabrication.					
		B. Excessive Sublimation	1. Excessive operating temperature.	Gradual deterioration of generator performance. Condensation of sublimation product on the insulation increases thermal loss and results in an eventual change in doping level as in Section 4.C.3. If cold follower freezes, an open circuit will result. Oxidized manganese collects at hot junction and increases resistance.	Reduction in element resistance partially compensates for reduction in hot junction temperature. MIN-K insulation confines sublimation product to the area near the element.	B_f	B_o	Post test ana ysis required detect occur- rence.

KEY:

DEFINITION OF MISSION

The time and stress encountered subsequent to IPL acceptance testing, including shipping, two-year storage, preparation for launch, fueling, and one year of ope

DEFINITION OF FAILURE CLASSES

A_f This condition is sure to cause severe reduction in performance, or a complete failure.

B_f This condition may cause severe reduction in performance.

C_f This condition will not cause mission failure by itself.

U_f Insufficient data to indicate class of failure.

DEFINITION OF PROBABILITY OF OCCURRENCE

A_o Probably will occur within the mission sequence.

B_o Remote possibility of occurrence within the mission sequence.

C_o Probably will not occur within the mission sequence.

U_o Probability of occurrence unknown.

3

9-3/9-4

BLANK PAGE

ri- oper d	Sublimation ducts from elements travel to hot shoe and react with copper. This compound returns to the element and causes a change in element doping, resulting in reduced output. The growth of copper whiskers also poses a potential electrical short hazard.		R_f	B_o	Requires Q.C. test of plating for tendency to blister. Ensure that iron plating is not cracked during assembly.	4
ent- (as- nula- ute the a the : hot g ther- and/or assembly.	Reduced output due to excessive resistance. Same as 2. A. 1 High thermal and electrical resistance and possibly a cracked element.	Would be detected during checkout and processing. Would probably be picked up by test for proper spring length.	R_f R_f C_f	C_o A_o C_o	Use of preformed strip of Micro-quartz surrounding the element at the hot end. Call out in visual Q.C. check.	8 1 9
ve dient hing of at hot ses hot ction r fabri- ment. r as- mer- ne force rement cation.	Internal resistance will increase with proportionate decrease in power output.	Spring pressure may maintain nearly constant output, but sensitivity to shock and vibration will be increased.	R_f	B_o	Post-test analysis required to detect occurrence.	4
low oper- erature.	Gradual deterioration of generator performance. Condensation of sublimation product on the insulation increases thermal loss and results in an eventual change in doping level as in Section 4.C.3. If cold follower freezes, an open circuit will result. Oxidized manganese collects at hot junction and increases resistance.	Reduction in element resistance partially compensates for reduction in hot junction temperature. MIN-K insulation confines sublimation product to the area near the element.	R_f	B_o	Post test analysis required detect occurrence.	4

...ceptance testing, including shipping, two-year storage, preparation for launch, fueling, and one year of operation.

...e in performance, or a complete failure.

...erformance.

...itself.

...ion sequence.

...ace.

4

TABLE 9-1. SNAP-27 FAILURE MODE AND EFFECT ANALYSIS FORM (SHEET 2

Item No.	Item Description	Assumed Failure Mode	Assumed Cause of Failure	Effect on Mission Performance	Compensating Provisions	Failure Class	Prob. of Occur.	Proposed Co of Action
4	(Continued)	B. (Continued)	2. Insufficient gas pressure in generator.	Same as 4. B. 1		A_s	C_o	
		C. Change in doping level.	1. Diffusion of silver solder constituents through or around stainless steel barrier disc.	Deterioration of generator output within several thousand hours. Possible deterioration of mechanical bond.	Observed failures on other programs may have been due to poor assembly technique.	R_f	U_o	a. Evaluatio of isothermal 10-couple tes module. b. Evaluate silver solder
			2. Diffusion of barrier disc constituents into elements, especially at high temperatures.	Gradual increase in element resistance and thermal conductivity.	Has occurred in only a few instances in other programs.	R_f	B_o	Same as 4. C.
			3. Reaction of sublimation product with MIN-K insulation. Resulting compound condenses on element. Sodium in condensate diffuses into element.	Rapidly increasing degradation trend after a period of apparently stable performance. The length of the stable period depends strongly on operating temperature. This effect applies to the N element.	SNAP-23 generators are operating without change. These generators use MIN-K insulation. This effect has not been proven.	R_f	B_o (B_o rather than A_o due to relatively short mission).	Same as 4. C. and 3. A. 2
			4. Outgassing of insulation results in water vapor inside of generator. This water vapor oxidizes the manganese dopant in the P element.	Gradual reduction generator output power. Extent of reduction will be limited.		R_f	B_o	
			5. Water vapor in generator due to failure of case seal. This water vapor oxidizes the manganese dopant in the P element.	Same as 4. C. 4		R_f	C_o	
			6. Impurities introduced in handling.	Possible increase in element resistance or change in open circuit voltage.	No definite data indicating that failures have been caused by this effect.	R_f	U_o	
4	(Continued)	D. Bonding at hot junction followed by thermal cycling.	1. Water vapor in generator due to outgassing of insulation.	Thermal cycling causes cracking at hot end of the element. This cracking increases the generator resistance.	Small quantities of water vapor reduce hot junction resistance.	A_f (A_f rather than C_f due to thermal cycling).	B_o	
			2. Water vapor in generator due to failure of case seal.	Same as 4. D. 2.		A_f	C_o	
		E. Poor bond between element and barrier disc (cold end)	Improper fabrication.	High generator resistance. Increased sensitivity to vibration.	Spring pressure vents complete failure. This condition could possibly be detected by Ultrasonic measurement technique, resistance versus length measurement, and/or pull test.	C_f	B_o	Specify addit on tests.
		F. Excessive resistance at hot junction.	1. Proprietary	Low output power due to high generator resistance.	Would be detected during processing.	R_f	A_o	Proprietary

AP-27 FAILURE MODE AND EFFECT ANALYSIS FORM (SHEET 2 OF 3)

Assumed Cause of Failure	Effect on Mission Performance	Compensating Provisions	Failure Class	Prob. of Occur.	Proposed Course of Action	Criticality Ranking
2. Insufficient gas pressure in generator.	Same as 4. B. 1		A_a	C_o		5
1. Diffusion of silver solder constituents through or around stainless steel barrier disc.	Deterioration of generator output within several thousand hours. Possible deterioration of mechanical bond.	Observed failures on other programs may have been due to poor assembly technique.	R_f	U_o	a. Evaluation of isothermal and 10-couple test module. b. Evaluate other silver solders.	6
2. Diffusion of barrier disc constituents into elements, especially at high temperatures.	Gradual increase in element resistance and thermal conductivity.	Has occurred in only a few instances in other programs.	R_f	B_o	Same as 4. C. 1. a.	4
3. Reaction of sublimation product with MIN-K insulation. Resulting compound condenses on element. Sodium in condensate diffuses into element.	Rapidly increasing degradation trend after a period of apparently stable performance. The length of the stable period depends strongly on operating temperature. This effect applies to the N element.	SNAP-23 generators are operating without change. These generators use MIN-K insulation. This effect has not been proven.	R_f	B_o (B_o rather than A_2 due to relatively short mission).	Same as 4. C. 1. a and 3. A. 2	4
4. Outgassing of insulation results in water vapor inside of generator. This water vapor oxidizes the manganese dopant in the P element.	Gradual reduction generator output power. Extent of reduction will be limited.		R_f	B_o		4
5. Water vapor in generator due to failure of case seal. This water vapor oxidizes the manganese dopant in the P element.	Same as 4. C. 4		R_f	C_o		8
6. Impurities introduced in handling.	Possible increase in element resistance or change in open circuit voltage.	No definite data indicating that failures have been caused by this effect.	R_f	U_o		6
1. Water vapor in generator due to outgassing of insulation.	Thermal cycling causes cracking at hot end of the element. This cracking increases the generator resistance.	Small quantities of water vapor reduce hot junction resistance.	A_f (A_f rather than C_f due to thermal cycling).	B_o		2
2. Water vapor in generator due to failure of case seal.	Same as 4. D. 2.		A_f	C_o		5
Improper fabrication.	High generator resistance. Increased sensitivity to vibration.	Spring pressure vents complete failure. This condition could possibly be detected by Ultrasonic measurement technique, resistance versus length measurement, and/or pull test.	C_f	B_o	Specify additional tests.	7
1. Proprietary	Low output power due to high generator resistance.	Would be detected during processing.	R_f	A_o	Proprietary	1

BLANK PAGE

			4. Outgassing of insulation results in water vapor inside of generator. This water vapor oxidizes the manganese dopant in the P element.	Gradual reduction generator output power. Extent of reduction will be limited.		R_f	B_o
			5. Water vapor in generator due to failure of case seal. This water vapor oxidizes the manganese dopant in the P element.	Same as 4.C.4		R_f	C_o
			6. Impurities introduced in handling.	Possible increase in element resistance or change in open circuit voltage.	No definite data indicating that failures have been caused by this effect.	R_f	U_o
4	(Continued)	D. Bonding at hot junction followed by thermal cycling.	1. Water vapor in generator due to outgassing of insulation.	Thermal cycling causes cracking at hot end of the element. This cracking increases the generator resistance.	Small quantities of water vapor reduce hot junction resistance.	A_f (A_f rather than C_f due to thermal cycling).	B_o
			2. Water vapor in generator due to failure of case seal.	Same as 4.D.2.		A_f	C_o
		E. Poor bond between element and barrier disc (cold end)	Improper fabrication.	High generator resistance. Increased sensitivity to vibration.	Spring pressure vents complete failure. This condition could possibly be detected by Ultrasonic measurement technique, resistance versus length measurement, and/or pull test.	C_f	B_o
		F. Excessive resistance at hot junction.	1. Proprietary	Low output power due to high generator resistance.	Would be detected during processing.	R_f	A_o
			2. See also Sections 3 and 4.D.1.				
5	Cold Cap	A. Poor bond between cold cap and barrier disc.	Improper fabrication.	Increased sensitivity to vibration.	Same as 4.F, except that it would probably not show up in a resistance versus length measurement.	C_f	C_o
		B. Poor thermal contact to cold follower through ball and socket.	Build-up of mechanical tolerances.	Excessive cold junction temperature causes excessive hot junction temperature. This results in shorter life and reduced output.		R_f	B_o

3

9-5/9-6

BLANK PAGE

	element.					
	Gradual reduction generator output power. Extent of reduction will be limited.		R_f	B_o		4
in r e it	Same as 4.C.4		R_f	C_o		8
- iing.	Possible increase in element resistance or change in open circuit voltage.	No definite data indicating that failures have been caused by this effect.	R_f	U_o		6
in u-	Thermal cycling causes cracking at hot end of the element. This cracking increases the generator resistance.	Small quantities of water vapor reduce hot junction resistance.	A_f (A_f rather than C_f due to thermal cycling).	B_o		2
in eal.	Same as 4.D.2.		A_f	C_o		5
a-	High generator resistance. Increased sensitivity to vibration.	Spring pressure vents complete failure. This condition could possibly be detected by Ultrasonic measurement technique, resistance versus length measurement, and/or pull test.	C_f	B_o	Specify additional tests.	7
	Low output power due to high generator resistance.	Would be detected during processing.	R_f	A_o	Proprietary	1
:a-	Increased sensitivity to vibration.	Same as 4.F, except that it would probably not show up in a resistance versus length measurement.	C_f	C_o	Specify additional tests.	9
	Excessive cold junction temperature causes excessive hot junction temperature. This results in shorter life and reduced output.		R_f	B_o	Test equipment is required to ensure uniform quality.	4

4

TABLE 9-1. SNAP-27 FAILURE MODE AND EFFECT ANALYSIS FORM (SHEE

Item No.	Item Description	Assumed Failure Mode	Assumed Cause of Failure	Effect on Mission Performance	Compensating Provisions	Failure Class	Prob. of Occur	Propos of A
5	(Continued)	C. Failure of ball and socket to pivot.	Mechanical tolerance, foreign material.	Thermal cycling will result in cracking of element. This increases generator resistance, thereby reducing power output.		R_f	B_o	
6	Cold Follower	A. Electrical short circuit.	1. Burr on cold follower prior to hard coat. 2. Burr on cold frame. 3. Foreign material at ball and socket joint. 4. Bend spring or projection from spring. 5. Cracking of hard coat insulation due to thermal cycling or loss of water or crystallization.	Same as 1.A.	Two independent shorts must occur since the generator is a floating ground.	A_f	B_o	
		B. Loss of freedom of cold follower.	1. Seizing of cold follower due to insufficient clearance. 2. Seizing of cold follower due to foreign material. 3. Blocking of cold follower action by MIN-K insulation.	Electrical open circuit due to thermal expansion and/or sublimation (see also Section 4. B). Increase of cold junction temperature due to reduction in the force on the ball and socket. (See Section 5. B).		A_f	B_o	
		C. Loss of water of crystallization from hard coat.	Excessive operating temperature.	Source of water vapor. (See Section 4.C.4, 4.D).		R_f	U_o	
7	Jumper Wire	A. Electrical open circuit.	1. Nick or excessive flexure which has weakened the wire. 2. Poor bond between jumper and cold shot.	Breakage results in the loss of at least a portion of generator output. Vibration sensitivity is increased. Slight reduction in output.	Series-parallel connection reduces chance of complete failure. Same as 7.A.1.	R_f R_f	B_o C_o	
		B. Electrical short circuit.	Improper assembly.	Same as 1.A. Vibration may cause a change in output.	Would probably be detected by acceptance tests.	A_f	B_o	
8	Insulation	A. Caking or sintering.	Time, excessive operating temperature or foreign materials.	See Item 6.B.3.		R_f	A_o	
		B. Outgassing of water vapor.	Property of insulation or insufficient processing.	See Items 4.A.2 and 4.C.4.		R_f	A_o	
		C. Increased thermal conductivity after a period of operation.	1. Characteristic of insulation. 2. Caused by foreign material.	Reduced output from increased thermal loss.		R_f	U_o	Testing of (is being pla
		D. Force of packing overstresses generator case.	Improper assembly, lack of allowance for additional forces.	Rupture of case		A_f	U_o	Evaluate co and propos tion.
		E. Change in element doping level.	Reaction of insulation with sublimation products.	See Item 4.C.3.	See Item 4.C.3.	R_f	B_o	
9	Spring	A. Reduction in spring force.	Change of material properties with time at operating temperature.	Increased electrical resistance reduces output. Increased thermal impedance increases temperature of hot and cold junction.		R_f	B_o	
		B. Broken Spring.	Improper manufacturing.	Loss of at least a portion of generator output.	Series-parallel connection reduces the chance of complete failure.	R_f	C_o	
		C. Electrical short.	Bent spring or metal whisker.	See Item 1.A.		A_f	B_o	
10	Generator Case	A. Failure of case weld.	Poor weld quality.	1. Loss of generator gas pressure. See Item 4.B.2.		A_f	B_o	
				2. Entrance of water vapor. See Items 4.A.2, 4.C.3, and 4.D.2.	Would occur only in earth environment.			
		B. Failure of seal around electrical connections.	Internal stresses, improper assembly, rough handling.	Same as Item 10.A.		A_f	C_o	
		C. Rupture of case.	1. See Item 8.D.	See Items 4.A.2, 4.B.2, 4.C.3, and 4.D.2.		A_f	C_o	
			2. Meteorite Impact.	See Items 4.A.2, 4.B.2, 4.C.3, and 4.D.2.		A_f	C_o	

NAP-27 FAILURE MODE AND EFFECT ANALYSIS FORM (SHEET 3 OF 3)

...ssumed Cause of Failure	Effect on Mission Performance	Compensating Provisions	Failure Class	Prob. of Occur	Proposed Course of Action	Criticality Ranking
...ical tolerance, foreign ...l.	Thermal cycling will result in cracking of element. This increases generator resistance, thereby reducing power output.		B_f	B_o		4
...r on cold follower prior ...t cont. ...r on cold frame. ...sign material at ball and ...joint. ...d spring or projection ...spring. ...cking of hard cont in... ...n due to thermal cycling ...t water or crystallizat...	Same as 1.A.	Two independent shorts must occur since the generator is a floating ground.	A_f	B_o		2
...ng of cold follower due ...fficient clearance. ...ing of cold follower ...foreign material. ...king of cold follower ...by MIN-K insulation.	Electrical open circuit due to thermal expansion and/or sublimation (see also Section 4. B). Increase of cold junction temperature due to reduction in the force on the ball and socket. (See Section 4. B).		A_f	B_o		2
...ive operating temper...	Source of water vapor. (See Section 4.C.4, 4.D).		B_f	U_o		5
...or excessive flames ...as weakened the wire. ...- bond between jumper ...cold shot.	Breakage results in the loss of at least a portion of generator output. Vibration sensitivity is increased. Slight reduction in output.	Series-parallel connection reduces chance of complete failure. Same as 7.A.1.	B_f B_f	B_o C_o		4 3
...or assembly.	Same as 1.A. Vibration may cause a change in output.	Would probably be detected by acceptance tests.	A_f	B_o		2
...xcessive operating temp... ...or foreign materials.	See Item 4.B.1.		B_f	A_o		1
...y of insulation or in... ...it processing.	See Items 4.A.7 and 4.C.4.		B_f	A_o		1
...acteristic of insulation. ...ed by foreign material.	Reduced output from increased thermal loss.		B_f	U_o	Testing of this parameter is being planned.	6
...or assembly, lack of ...on for additional forces.	Slippage of seam		A_f	U_o	Evaluate current design and properties of insulation.	3
...n of insulation with mois... ...products.	See Item 4.C.3.	See Item 4.C.3.	B_f	B_o		4
...material properties ...at operating temper...	Increased electrical resistance reduces output. Increased thermal impedance increases temperature of hot and cold junctions.		B_f	B_o		4
...e manufacturing.	Loss of at least a portion of generator output.	Series-parallel connection reduces the chance of complete failure.	B_f	C_o		3
...ing of metal whisker.	See Item 1.A.		A_f	B_o		2
...ld quality.	1. Loss of generator due power drain. See Items 4.B.2.		A_f	B_o		2
	2. Extrusion of water vapor. See Items 4.A.2, 4.C.5, and 4.D.2.	Would occur only in earth environment.				2
...ckness, improper ...), rough handling.	Same as Item 14.A.		A_f	C_o		5
...on 4.D.	See Items 4.A.2, 4.B.2, 4.C.5, and 4.D.2.		A_f	C_o		5
...ume Impact.	See Items 4.A.2, 4.B.2, 4.C.5, and 4.D.2.		A_f	C_o		5

The couple failure rate is given by:

$$\lambda \leq \frac{X^2_{\alpha,2(F+1)}}{2T}$$

where:

X^2 = value of the chi-squared distribution at $1 - \alpha$ confidence and $2(F + 1)$ degrees-of-freedom

F = number of observed failures

T = number of observed couple hours of testing.

b. Couple Failure Rate - The calculations were based on a total of 4,821,088 part hours of thermocouple testing. Of this, 4,169,088 part hours included data from the SNAP-23 life tests with the remaining 652,000 part hours representing the SNAP-27 module testing. In both test programs, no failures of the thermocouples were observed. The failure rate is calculated below for a 50 percent confidence level, i.e., $1 - \alpha = 0.5$.

$$\lambda \leq \frac{1.386}{2 \times 4.82 \times 10^6} = 0.14 \times 10^{-6} \ \frac{\text{failures}}{\text{hour}}$$

where: 1.386 = value of the chi-square distribution at 50 percent confidence and 2 degrees-of-freedom (F = 0).

The reliability of the thermocouple for a 10,000 hour mission is:

$$R_o = e^{-0.14 \times 10^{-6} \times 10^4} = e^{-0.0014} = 0.9986$$

c. Thermopile Reliability - Using the above thermocouple reliability,

$$P_1 = (0.9986)^2 = 0.9972$$

$$P_2 = 2(0.9986)(1 - 0.9986) = 0.0027$$

Substituting the above values into the expression for the reliability of the thermopile,

R (Thermopile) = 0.99943

The reliability block diagram representing the thermopile as used in these calculations is shown below.

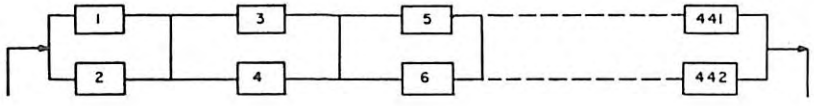

d. Structural Reliability - The analytical procedure used in assessing the reliability of the various structural members was that described in Reference 9-5.

The reliability of each component in the generator structural assembly was defined as the probability that the material strength of the component minus its applied load was greater than zero. The individual component reliabilities and the overall generator structural assembly reliability of 0.99998 are listed in Table 9-2.

The fuel capsule assembly reliability was based on a structural analysis of the backplate presented in Reference 9-3. The estimated reliability is 0.999999.

The reliability of the structure is given as:

$$R\,(\text{Structure}) = R\,(\text{Outer Case Assembly}) \cdot R\,(\text{Hot Frame Assembly}) \cdot R\,(\text{Cold Frame}) \cdot R\,(\text{Hermetic Seal, Fwd}) \cdot R\,(\text{Hermetic Seal Assembly, Aft}) \cdot R^{8}\,(\text{Generator Mounting Lugs}) \cdot R\,(\text{Fuel Capsule})$$

Substituting the reliability values estimated for the structure components, the reliability of the structure becomes:

$$R\,(\text{Structure}) = (0.999999) \cdot (0.999985) \cdot (0.999999) \cdot (0.999999)^{8} \cdot (0.999999) = 0.99998$$

TABLE 9-2. SNAP-27 RTG RELIABILITY PREDICTION ANALYSIS

COMPONENT DESCRIPTION	QUANTITY	RELIABILITY
Thermopile Assembly	1	.99943
Generator Structural Assembly	1	.99998
Outer Case	1	$.999999^{+}$
Hot Frame	1	.999985
Cold Frame	1	≈1.0
Forward Hermetic Seal	1	≈1.0
Aft Hermetic Seal	1	.999999
Mounting Lugs	8	$.999999^{+}$
Fuel Capsule Assembly	1	$.999999^{+}$
RTG		.9994

The reliability for the cold frame and the forward hermetic seal were not included in the calculations since their estimated reliability was ≃ 1. The follower springs are not included since failure of a spring does not constitute structure failure.

e. Generator Reliability - The generator reliability is given by:

$$R\,(\text{Generator}) = R\,(\text{Structure}) \cdot R\,(\text{Thermopile})$$

Substituting the reliability values computed for the structure and thermopile into the above expression, the reliability of the generator becomes:

$$R\,(\text{Generator}) = (0.99998) \cdot (0.99943)$$

$$R\,(\text{Generator}) = 0.9994$$

The RTG reliability is the product of the thermopile assembly reliability, the generator structural reliability and the fuel

capsule reliability. As summarized in Table 9-2, the RTG reliability is 0.9994 which exceeds the reliability goal of 0.995.

9.2 RELIABILITY MEASUREMENT

A Reliability Measurement Plan (Reference 9-6) established the means for reliability measurement of the RTG through the development, qualification and flight hardware phases. In order to satisfactorily measure the RTG reliability, it was necessary to plan and conduct a test program which would produce sufficient testing with equal emphasis on the mission critical environments so that a statistically sound reliability value could be established. It was determined that acceptable reliability measurement data sources were the development tests of the 104-couple modules, the engineering tests of the Mod 5 and Mod 8B generators, and the qualification tests of the Mod 10 generator.

A statistical method for determining reliability measurement information from test data was developed and documented (Reference 9-7). A primary aim of the statistical method was to simultaneously demonstrate required performance and predict ultimate performance from initial operating information. This can be accomplished by testing the unit and analyzing a critical variables performance or "signature" data. The most meaningful critical parameter was found to be the power ratio, Po/P_{th}, which is the actual power relative to the theoretical power both under matched load conditions. The specification against which performance was measured was a lower limit of 0.73 for the power ratio. Subsequent statistical analysis at 3000 hours for B-2 and C-4 10-couple module tests indicated a generator lifetime ($Po/P_{th} > 0.073$) in excess of 12,000 hours. This was varified by the results of the Mod 5 generator life tests.

9.3 SELECTED MATERIALS, PROCESSES AND PARTS LISTS

Three SNAP-27 documents were generated by General Electric based on References 9-3 and 9-8 to control SNAP-27 material, processes and parts (References 9-9, 9-10 and 9-11).

9.4 REFERENCES

9-1 "SNAP-27 Reliability Plan", GE No. 6300-013, February 1966

9-2 "Reliability Program Provisions for Space Systems Contractors", NPC-250-1, July 1963.

9-3 "NASA/AEC Plan for Development of an Electrical Power Subsystem for the Apollo Lunar Surface Experiment Package", September 1966.

9-4 "SNAP-27 Reliability Program Plan," 3M Company, MMM 8460-0011.

9-5 "Structure Reliability Report", Martin Marietta Corporation, ER11862, December 1961.

9-6 "SNAP-27 Reliability Measurement Plan:, GE No. 6300-014, April, 1966.

9-7 "Reliability Estimate Analysis of SNAP-27 Generator Assembly, GE No. 6300-012, February, 1966.

9-8 "General Specification for Approved Materials for use in the Apollo Spacecraft", MC999-0058, July, 1964.

9-9 SNAP-27 Selected Materials List, NE 0060-07-03,

9-10 SNAP-27 Selected Process List, NE 0060-12-01,

9-11 SNAP-27 Selected Parts List, NE 0060-03-10,

10. FABRICATION AND ASSEMBLY

10.1 GENERATOR FABRICATION

10.1.1 FABRICATION OF BERYLLIUM COMPONENTS

The following sequence delineates six major steps in the SNAP-27 generator fabrication (see Figure 10-1):

a. Rough Milling of the Outer Case - The outer case is shown set up in a Gorton Model B-360 milling machine. The material for the outer case is hot pressed block beryllium, 7.5 inches OD, 4.875 inches ID and 19 inches long. The operation shown is rough milling between the mounting flanges.

b. Finish Milling of the Outer Case - The outer case is shown set up in a Gorton Model 9J tracer. The operation shown in this picture is finish milling of the outer case. Eight grooves for the fins have been milled.

c. Initial Fin Installation in Outer Case - The fins made of cross-rolled beryllium sheet, are installed in the configuration shown here.

d. Final Brazing of Fin Structure - After the outer case assembly has been installed in the graphite crucible and subjected to a complete examination (braze alloy placement and case alignment), nine baskets filled with titanium chips are inserted between the fins and in the center of the assembly. The titanium chips act as a getter, absorbing oxygen, moisture and all other contaminants generated during the braze cycle.

e. Rough Machining of Cold Frame - The cold frame is shown set up in an American Pacemaker lathe. The material for the cold frame is hot pressed block beryllium. Undercutting of the hot pressed block beryllium is shown here.

f. Final Hole Boring of the Cold Frame - The cold frame is shown set up in a Pratt and Whitney, Model B, Tape-O-Matic drill. The drilling sequence of the cold frame employs in excess of 7200 tape commands.

BLANK PAGE

10.1.2 GENERATOR ASSEMBLY PROCESS

The following sequence delineates four major steps in the assembly of the SNAP-27 generator (see Figure 10-2):

a. Thermopile Assembly - The thermoelements are mounted in strips and inserted on the hot frame inside the cold frame. The followers, springs and end caps are then installed from the outside. Figure 10-3 shows the assembly of the leg components into the loading tray.

b. Thermopile Wiring - The thermoelements are connected in series-parallel by conducting metal strips. Electrical leads are led down the outside of the cold frame to the power headers. The electrical leads are looped around each end of the cold frame to act as degaussing loops. SNAP-27 magnetic test data show that the magentic field is a factor of six lower than the SNAP-27 specification of 0.1 gamma at 50 feet, for the worst case test condition.

c. Final Assembly - The completed thermopile is shrink-fitted within the outer case and the assembly closed by seal welding the end plates. Prior to closure, all voids are filled with a powdered thermal insulation.

d. Finished Generator - These major steps in the generator assembly culminate in the finished SNAP-27 Radioisotope Thermoelectric Generator.

10.2 FUEL CAPSULE FABRICATION

The plan for fabrication of live fuel capsules involved General Electric as the capsule design agency with the added responsibilities of furnishing hardware and performing finishing operations such as backplate installation, ultrasonic inspection, gauging and coating. Mound Laboratories of Miamisburg, Ohio, was the fueling agency whose function was to develop closure welding and manufacturing techniques, and fuel and seal the capsule.

During the latter stages of the design and development program, General Electric delivered representative hardware for Mound to develop weld parameters and techniques. TIG welding in a helium atmosphere within a glove box was selected as the weld method.

At the outset, the approach to capsule fabrication was based on the following considerations. The capsule consisted of three major component assemblies. These were the liners, cladding and fuel. The

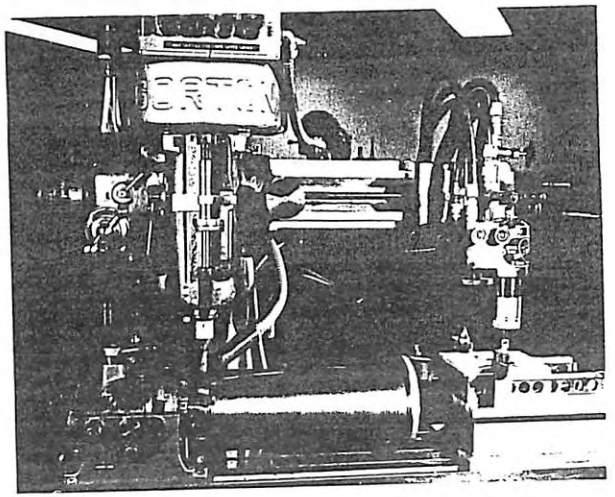

Rough Milling of Outer Case

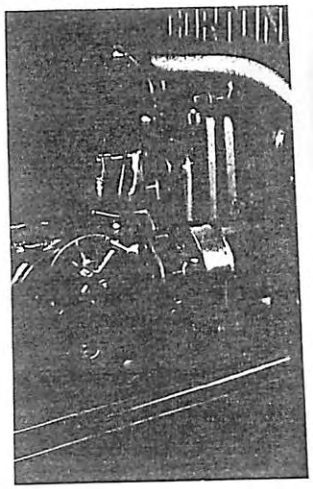

Finish Milling

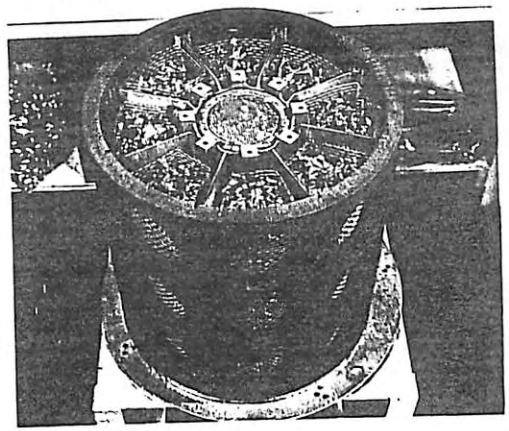

Final Brazing of Fin Structure

Rough Machinir

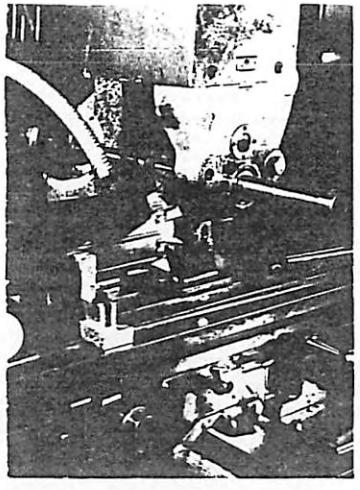

ling of Outer Case

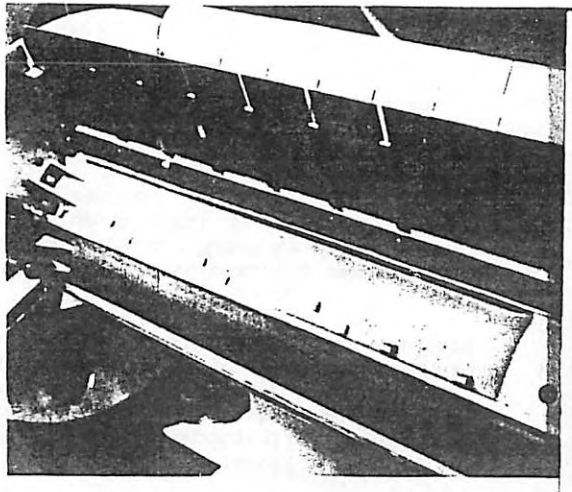

Initial Fin Installation in Outer Case

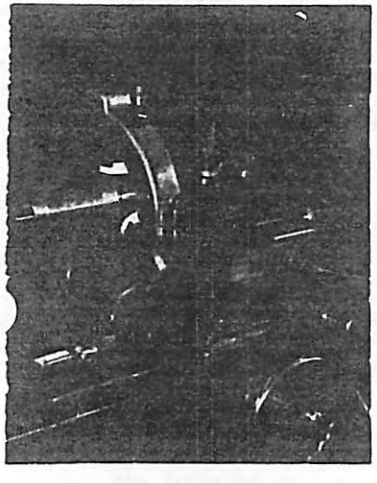

hining of Cold Frame

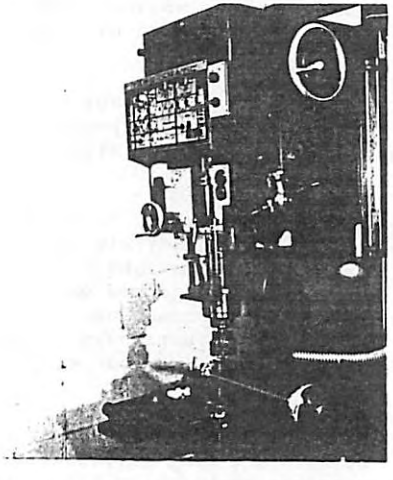

Final Hole Boring of Cold Frame

Figure 10-1. Fabrication Beryllium Components

2

BLANK PAGE

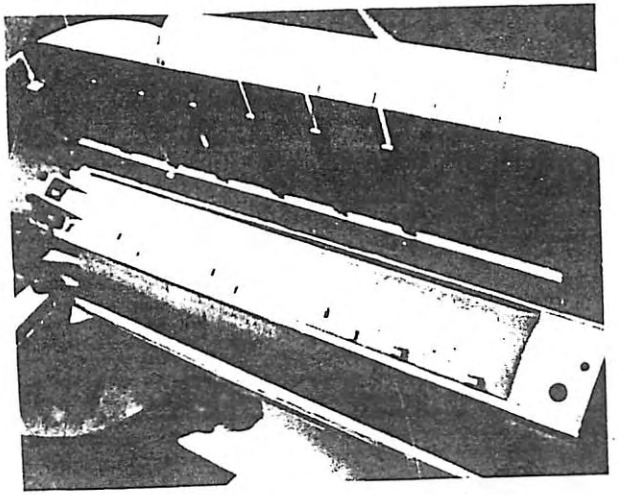

Initial Fin Installation in Outer Case

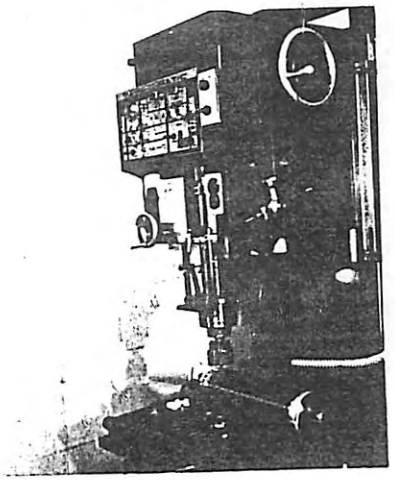

me

Final Hole Boring of Cold Frame

Figure 10-1. Fabrication of Beryllium Components

3

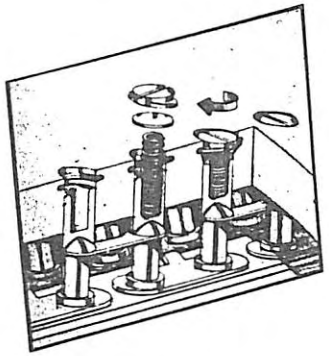

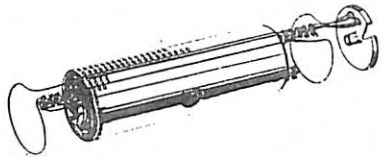

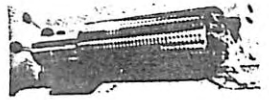

Thermopile Wiring

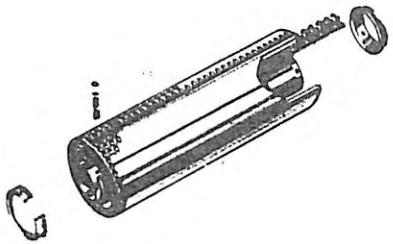

Thermopile Assembly

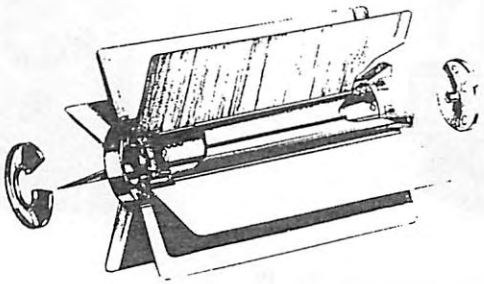

Final Assembly

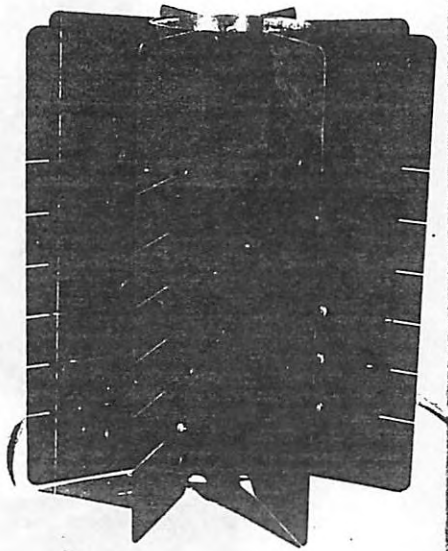

Finished Generator

Figure 10-2. Generator Assem

BLANK PAGE

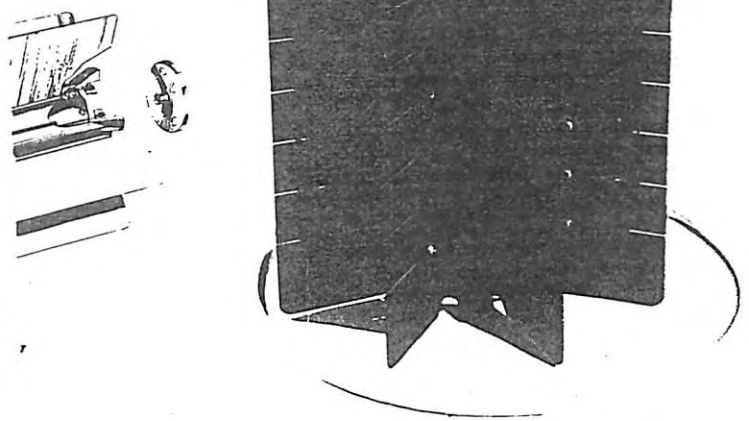

Finished Generator

3

Figure 10-2. Generator Assembly

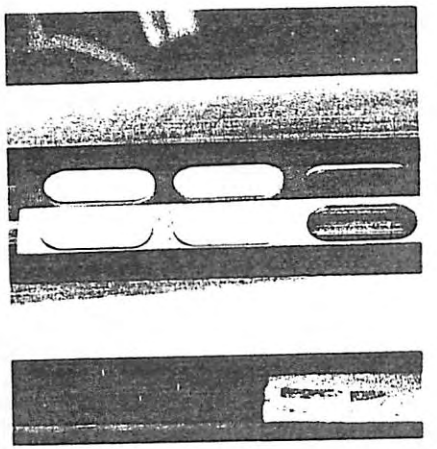

Step 1. Boron Nitride Inserts Set into Molybdenum Grid Strip

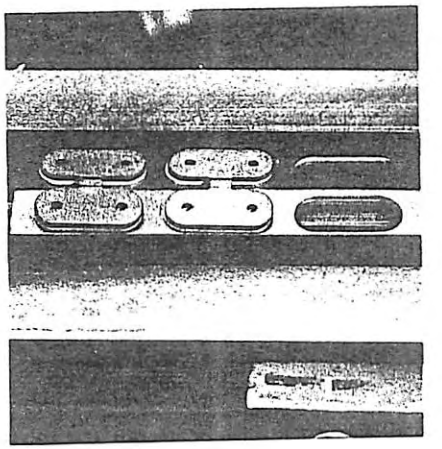

Step 2. Addition of Hot Junction Electrodes

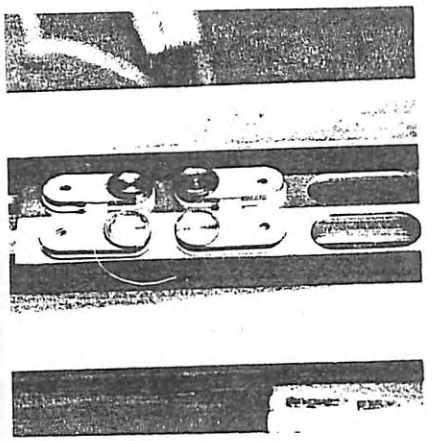

Step 3. Addition of Hot Junction Buttons

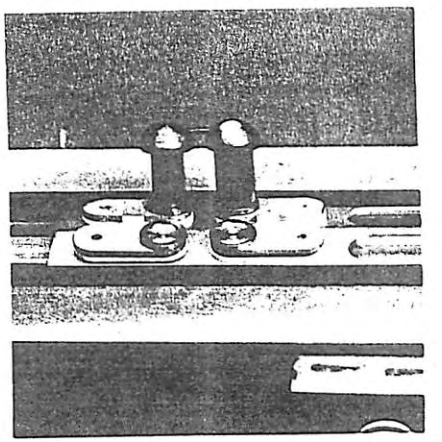

Step 4. Couple Assembly Added

Figure 10-3. Assembly of Components into Loading Tray

hardware making up the liners was made from 0.40 inch sheet stock rolled to 0.020 inch thickness, formed by vendors and finally assembled by General Electric/Valley Forge. The liner hardware consisted of a fuel annulus ring, a Z ring, a head, Haynes shims (0.008 inch thick), and a foam spacer. Hardware such as end caps, braze discs and annular tubes made up the fuel annulus ring. These were assembled by General Electric. The annular tubes were formed by rolling 0.020 inch sheet stock into a right cylinder and welding the juncture using the electron beam process. Properly sized tubes were placed concentric to one another and held in place by an end cap which was TIG welded to the outer tube and electron beam welded to the innermost tube. Prior to the installation of the end cap, a burst disc (01001 inch Haynes) was brazed over a small gas port in the center of the end cap. The fuel annulus ring thus assembled along with the Z ring and other hardware mentioned previously was delivered to Mound for fueling.

Because there was a variation in effective fuel power density, each set of capsule hardware delivered for fueling consisted of four different size liner sets. Each capsule contained two liners and there were actually eight liners in each capsule set.

The clad hardware consisted of a flange section assembly, center section male, center section female, and forward section. These parts were machined from solid Haynes bar stock, and in several cases, assembled at General Electric. For example, the flange section assembly consisted of a flange section to which was butt-welded a flange using the electron beam process. Screws for attaching the capsule backplate were welded into place in the flange. Another cladding assembly operation consisted of placing filter elements and spacers into bosses on the center section male and center section female components and electron beam welding them into place.

With the hardware assembled as described above, hardware sets were collected, match mated, and forwarded to Mound for fueling. A backup set of hardware was available on a one-for-one basis prior to the commencement of an individual fueling. In addition to the hardware sets, General Electric also forwarded representative capsule hardware for example welding which was done prior to and after each production weld to insure parameters were correct and the welding during that series of welds was adequate and consistent.

When Mound and General Electric felt the process for assembly was established, a Mound Specification MD-1-11391 was published with the assistance of General Electric. This specification covered the complete assembly operation and provided the capsule program bench mark.

In fueling, Mound would begin with two example welds on the liner

closure, using the aforementioned representative hardware. Example welds were made under the same conditions as the prime welds. The liners were mounted in copper chill blocks containing cooling water; a Z ring was added to close the open end of the annulus; a foam spacer placed on top of the Z ring and a cap called a head covered the entire capsule end forming a butt-joint with the outer tube of the liner. The assembly was placed in a glove box in a helium atmosphere and TIG welded. The weld was a full penetration head to annulus and underlying Z ring.

The two example welds were made and subjected to visual, dye penetrant and leak test inspections prior to beginning the production weld. A metallographic inspection of these was also made, but not necessarily prior to the production weld.

In fueling the liner, PuO_2 microspheres were added to the annular portion of the liner to achieve a thermal output of 740 $\pm$ 15 watts. Selection of the properly sized liner was made on calorimetry data from the fuel itself. The fuel loading was predetermined for each liner prior to fueling. After the fuel was loaded into the liner the final void volume in the fuel chamber was filled with zirconium dioxide microspheres topped off by Haynes-25 shims. The zirconium dioxide provided the final measure of control on fuel volume and the shims provided a fuel barrier as well as a void filler. Z-ring, foam spacer and head were added and with the water system activated in the chill blocks, the TIG weld was made.

Immediately following the production weld, another example weld was made and evaluated to ensure the weld parameters and quality of the weld was the same as that made just previous to the production weld. Since only visual and leak tests could be performed on the production welds, consistency noted between before and after welds that could be destructively tested provided an indication of the quality of the production weld.

Initially, the planned encapsulation sequence involved sealing one liner in the flange section assembly/center section female clad and another fueled liner in the forward section/center section male clad, forming two half capsules, then joining these with a center section weld. The void volume in the chamber formed by the half capsule bulkhead walls at the juncture was small and the capsule halves were hot resulting in concern that blowout would occur due to pressure buildup in the void. General Electric suggested that in their processing of the fuel capsule parts that they make the mid-span weld. This permitted welding while the hardware was cold and enabled use of an electron beam weld. General Electric was then given this assignment and throughout the program delivered center section assemblies (male and female center sections

joined) to Mound for fueling.

At the completion of the liner fueling, calorimetry measurements were made on the liners and they were readied for encapsulation. The same "two before", "one after" practice weld criteria applied to the clad or closure welds as it did in the liner welding. After making two example welds, the flange end liner was encapsulated by placing the flange assembly and the center section assembly in chill blocks in a helium atmosphere and making the TIG weld. The forward closure weld was made in the same fashion. Following encapsulation, visual, dimensional, leak test, neutron count and tangential radiography inspections were made.

The fuel used in the capsule was processed from plutonium powder into 238 PuO_2 microspheres at Mound by passing the powder through in induction coupled plasma torch. The fuel was characterized and placed in 200 gram batches.

Upon completion of manufacturing and inspection activities at Mound, the capsule was shipped to General Electric-Vallecitos for final processing. Upon receipt, the capsule was leak checked in a vacuum chamber, gauged for roundness and maximum OD, and inspected visually using a 10X Questar telescope. The capsule was ultrasonically inspected, then coated.

In the coating process, the capsule was grit blasted then sprayed with an iron titanate coating of 0.0020 $\pm$ 0.0005 inch thick. The strips were coated with the capsule, measured for thickness, bend tested and checked for total hemispherical emittance.

The final step of processing was attaching the capsule backplate by means of stainless steel nuts and screws, the latter being an integral part of the capsule flange. Prior to placing the backplate, a Min-K insulation plug was inserted into the flange hollow. A Haynes retainer was placed over the Min-K, then the backplate was installed. The capsule was weighed and packaged for shipment to General Electric-Valley Forge for test.

During the course of capsule manufacture several problems were encountered, all of which were overcome without impact to the ALSEP program.

After the design freeze the initial difficulty involved the final weld in the liner assembly. It was observed that as the closure of heat to liner to Z ring was made, the weld blew out. Several remedies were implemented including baking out in vacuum the foam spacer head and machining a step in the heat foam spacer.

A second problem arose in that cracking was observed in the same liner closure weld. This was attributed to copper contamination of the hardware by the various tooling used in forming the parts and making the weld. Of particular note was inclusions and other contaminants in the heads. Steps were taken to nickel plate the tooling and to remove the suspect heads from the program.

The next serious problem occurred during fueling operations of Fuel Capsule No. 2. A small (less than five gram) portion of teflon "O" ring from the fuel calorimetry can fell into the fuel in the capsule liner. After the capsule was completed a question was raised as to whether the fluorine constitute of the teflon would attack the tungsten in the Haynes-25, thus causing a breach in the liner and possibly the clad. Mound conducted a very thorough study into the matter and proved to the satisfaction of all parties that such a reaction would not take place with the small quantity of teflon involved. Radiation measurements served to further confirm this in that no increase in radiation levels was noted.

Subsequent to the closure of each capsule, Mound performed dimensional, neutron count, visual, leak test and radiographic inspections on the capsule and cladding closure welds. The radiographic inspection was made tangentially to the welded surface in a direction perpendicular to the long axis of the capsule. Using this technique a small arc of weld could be inspected with a radiographic shot. Radiographs were taken in 22-1/2 degree increments around the closure weld.

Since the joint being inspected was of a stepped configuration, and the metal thickness through which the radiographic beam was passed varied from the outermost portion of innermost, there was concern that radiography could possible miss certain defects depending on their nature and orientation. For this reason, General Electric-Vallecitos, as part of their processing, inspected capsule closure welds using ultrasonic techniques.

In the untrasonic process, the capsule, prior to coating, was placed on rollers powered by an electric motor allowing the capsule to rotate about its major axis. A lithium sulphate transducer was positioned at a 30 degree angle (to the vertical) one-half inch above the weld being inspected. The inspection was conducted under water because a uniform medium such as water or oil is required for the faithful transmission and reflection of the high frequency sound waves.

Using this process, a suspect area was found in the forward closure weld of Fuel Capsule 1. Fuel Capsule 2 exhibited similar anomalies in the same weld. The status of Fuel Capsules 1 and 2 were being resolved when Fuel Capsule 3 was fueled.

Several deviations occurred during the fueling of Fuel Capsule 3. After the liners were fueled, it was noticed upon removing one of the liners from its calorimetry can, a burst disc was dented and the nickel shot surrounding the liner was damp. It was concluded that water may have gotten into the can, was turned to steam by the heat from the fueled liner, causing a resultant pressure that dented the burst disc. To eliminate the possibility of water having entered the fueled area, the liner was dismantled, the fuel removed and allowed to heat for 30 minutes to drive off moisture.

After fueling another liner, an attempt at closure of the liners in the clad was made. The weld wandered on the first sample and after cleaning of the weld head and replacing the electrode a second attempt was made. Two pre-production welds and the flange to center section welds were made without incident; however, the weld bead wandered on the dome-to-center section closure weld, leaving an unwelded section. With the concurrence of General Electric, Mound made a second weld over the dome-to-center section closure. Double welded test specimens were also made at this time in which wander was experienced. The test specimens were subjected to ultrasonic inspection at General Electric-Vallecitos; however, agreement could not be reached between General Electric and Mound as to the defects and correlation of defects as verified later by metallography. The capsule itself was subjected to ultrasonic inspection and found to have (according to ultrasonics) defects in both closure welds, the most severe in the dome end which extended continuously for 150 degrees around the perimeter.

At this point, although agreement as to whether Fuel Capsule 3 was defective could not be reached, Mound did realise there was a problem with the weld equipment and made modifications to the weld head and changed weld parameters accordingly.

Fuel Capsule 1 in the meantime was recoated by General Electric-Vallecitos because the original coating was marred in handling. Prior to coating, it was again scrutinized by Mound's radiographic inspection and pronounced to be defect-free.

Fuel Capsule 2 was shipped to Mound for gamma and neutron dose rate and spectra measurements in the generator.

After their equipment modifications, Mound assembled Fuel Capsules 4, 5 and 6 plus two radiant heat test capsules (dummy fuel) and two verification capsules (dummy fuel) without incident, although Fuel Capsules 5 and 6 did exhibit minor ultrasonic indications.

After considerable deliberation the AEC directed Mound to destructively inspect Fuel Capsule 3 by performing metallography on the suspect areas.

This would serve the dual purpose of confirming whether Fuel Capsule 3 was sound and also provide a basis for the significance of ultrasonic testing with respect to the SNAP-27 program.

The results of the metallography showed that the fuel capsule was free from defects as defined by the model specification; however, grain boundary liquations were observed in the heat affected zone adjacent to the weld, that could have caused the defect indications detected by ultrasonic testing.

During the course of manufacturing, several important studies were conducted in an attempt to better understand the capsule welding. These included the fatigue testing of Haynes-25 alloy tubular weld test specimens in which General Electric built test rings of Haynes-25, welded them, fatigued them under heat and internal pressure, subjected them to radiography, ultrasonics and metallography. Experiments were conducted by General Electric-Vallecitos in alternate electronic inspection methods such as delta scan and eddy current. Mound investigated numerous radiographic schemes and techniques for improved inspection. Mound and General Electric-Vallecitos collaborated on two studies to attempt to find correlation between ultrasonic and radiographic inspection. Sandia added to the field of knowledge in performing hot (radioactive) metallographic studies of capsule hardware.

At the conclusion of the fabrication program the following recommendations were made:

a. Improve joint design by shortening the lip

b. Determine if post-machining stress relief annealing is practical and incorporate it into component fabrication

c. Consider repair welding as a necessary part of weld development

d. Incorporate axial loading of the joint during welding as a requirement

e. Include, during welding development, a study correlating weld defects with total weld heat input

f. Use ultrasonic testing as an inspection aid; however, begin early in the program and develop the process with the welding.

11. QUALIFICATION TEST PROGRAMS

11.1 MOD 10 GENERATOR ASSEMBLY QUALIFICATION TESTING

Mod 10 Generator, S/N 6320005, was selected as the prime generator for qualification testing in accordance with the requirements of References 11-1 and 11-2. The tests performed were as follows:

- Acceptance Tests
  - Visual examination
  - Resistance measurements
  - I-V mapping, in air
  - Leak rate test (non-operating)
  - Resistance recheck
  - Operability assurance vibration test
  - Thermal vacuum test
  - I-V mapping in vacuum
  - Leak rate test (operating)
- Sinusoidal Vibration Test, Qual Levels
- Random Vibration Test, Qual Levels
  - Resistance
  - I-V mapping (vacuum)
  - Leak rate check (operating)
- Shock Test
  - Resistance
  - I-V mapping
  - Leak rate check (operating)

BLANK PAGE

Acceleration Test

Resistance

I-V mapping (vacuum)

Leak rate check (operating)

Operational Life Test

Magnetic Evaluation Test (with fuel capsule)

Operational Life Test (continuation)

All performance testing was conducted with an electric fuel capsule, except that during the magnetic evaluation testing, a nuclear fueled capsule was employed. The test sequence is presented by Figure 11-1.

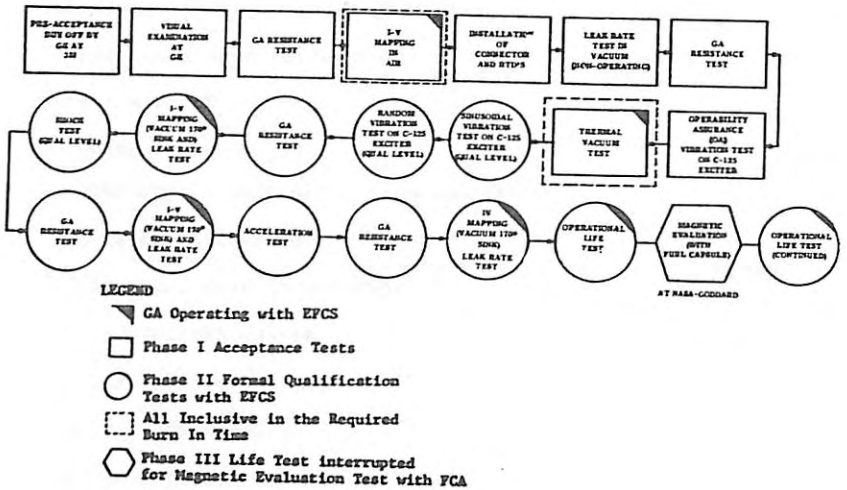

Figure 11-1. Generator Mod 10 Test Flow Chart

11.1.1 I-V MAPPING

Performance characteristics of Generator Mod 10 are summarized in Figures 11-2 through 11-16. Figure 11-2 shows the first mapping in air after its receipt from the 3M Company. Figures 11-3 through 11-8

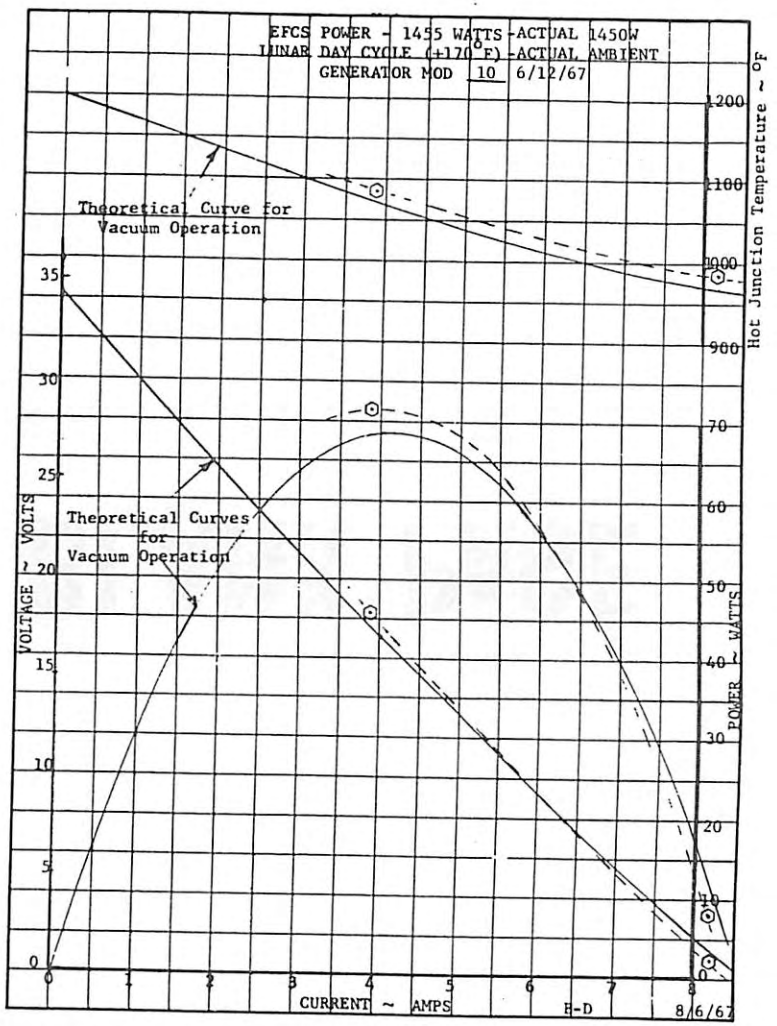

Figure 11-2. First I-V Mapping in Air

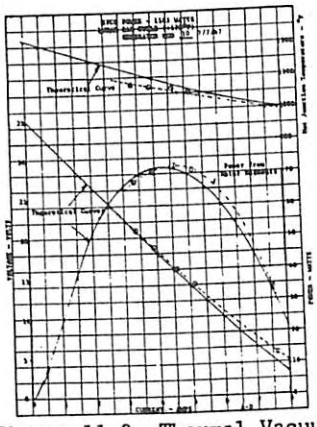

Figure 11-3. Thermal Vacuum Test-Lunar Day Cycle (EFCS Power 1505 Watts)

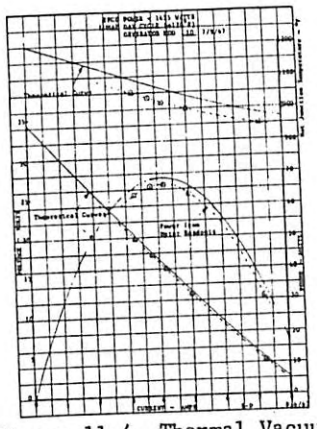

Figure 11-4. Thermal Vacuum Test - Lunar Day Cycle (EFCS Power 1455 Watts)

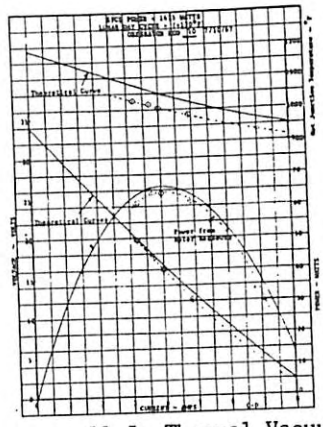

Figure 11-5. Thermal Vacuum Test - Lunar Day Cycle (EFCS Power 1415 Watts)

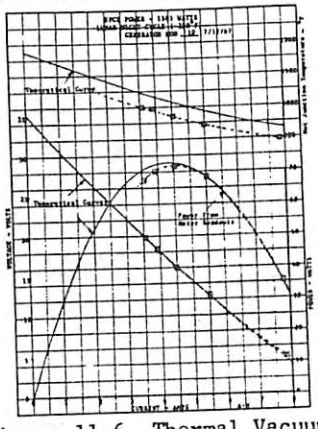

Figure 11-6. Thermal Vacuum Test-Lunar Night Cycle (EFCS Power 1505 Watts)

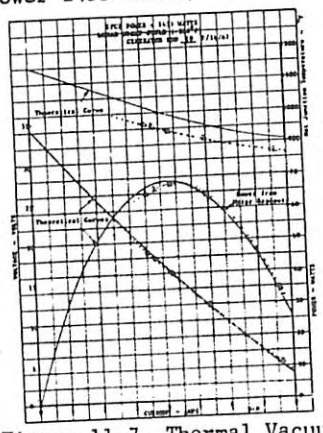

Figure 11-7. Thermal Vacuum Test-Lunar Night Cycle (EFCS Power 1455 Watts)

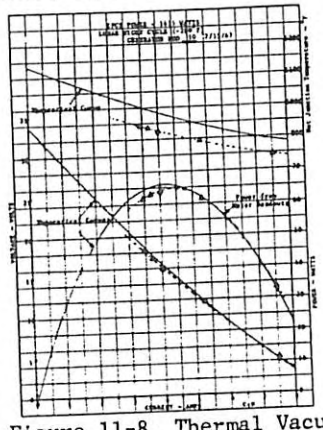

Figure 11-8. Thermal Vacuum Test-Lunar Night Cycle (EFCS Power 1415 Watts)

BLANK PAGE

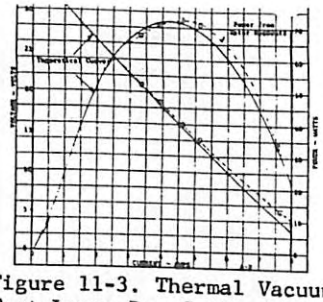

Figure 11-3. Thermal Vacuum Test-Lunar Day Cycle (EFCS Power 1505 Watts)

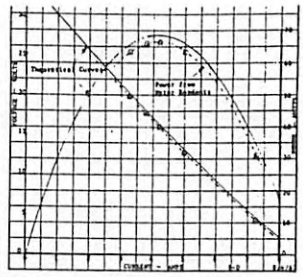

Figure 11-4. Thermal Vacuum Test - Lunar Day Cycle (EFCS Power 1455 Watts)

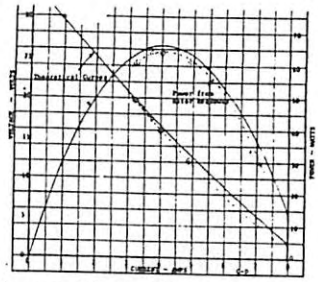

Figure 11-5. Thermal Vacuum Test - Lunar Day Cycle (EFCS Power 1415 Watts)

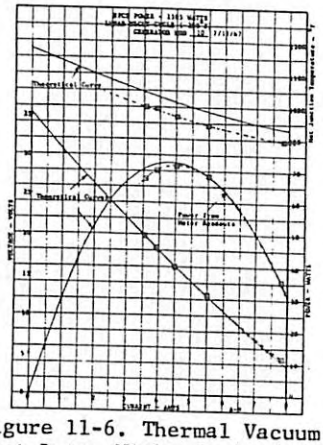

Figure 11-6. Thermal Vacuum Test-Lunar Night Cycle (EFCS Power 1505 Watts)

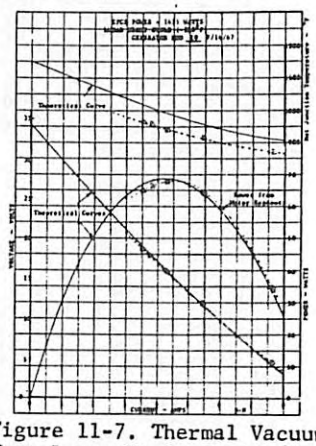

Figure 11-7. Thermal Vacuum Test-Lunar Night Cycle (EFCS Power 1455 Watts)

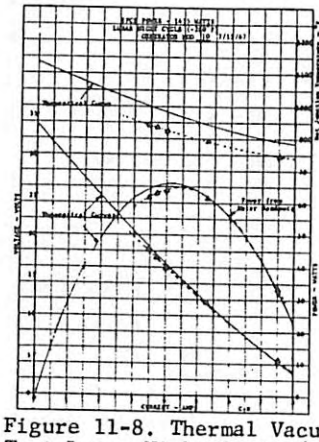

Figure 11-8. Thermal Vacuum Test-Lunar Night Cycle (EFCS Power 1415 Watts)

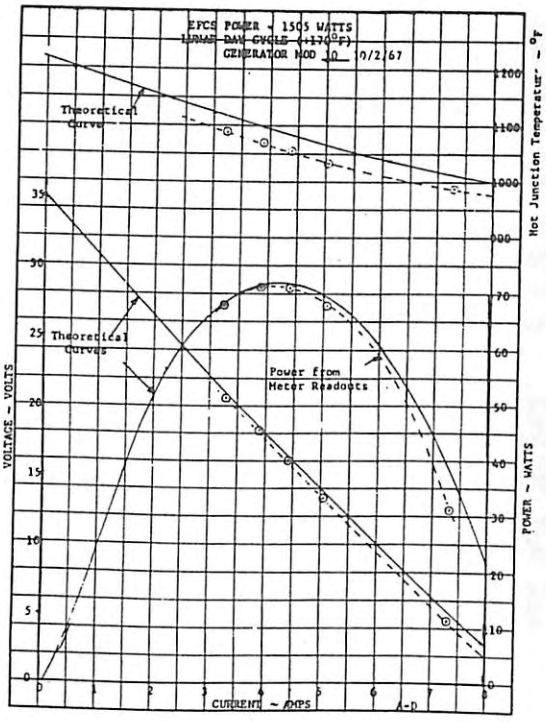

Figure 11-9. I-V Mapping after 1000 Hours (Lunar Day Cycle)

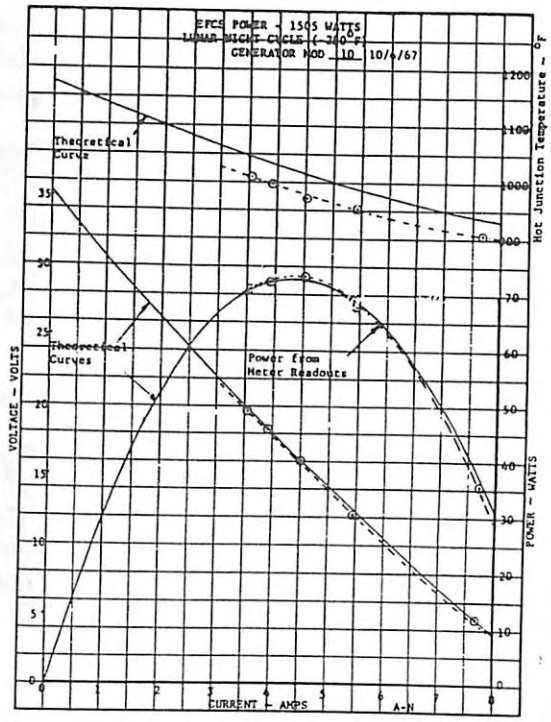

Figure 11-10. I-V Mapping after 1000 Hours (Lunar Night Cycle)

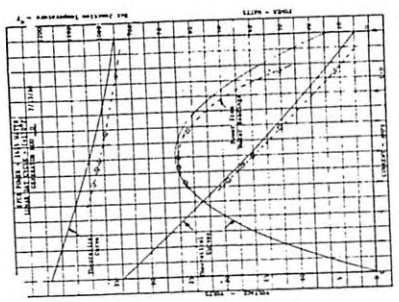

Figure 11-13. Final I-V Mapping-Lunar Day Cycle (EFCS Power 1415 Watts)

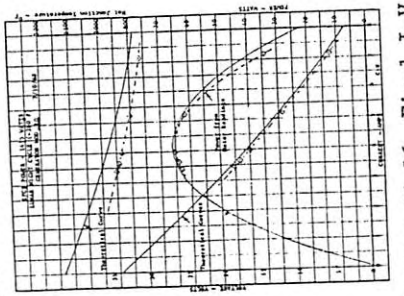

Figure 11-16. Final I-V Mapping-Lunar Night Cycle (EFCS Power 1415 Watts)

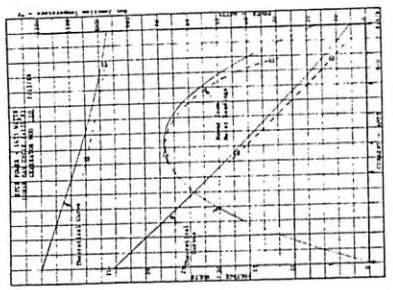

Figure 11-12. Final I-V Mapping-Lunar Day Cycle (EFCS Power 1455 Watts)

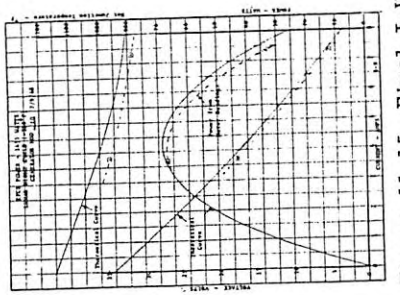

Figure 11-15. Final I-V Mapping-Lunar Night Cycle (EFCS Power 1455 Watts)

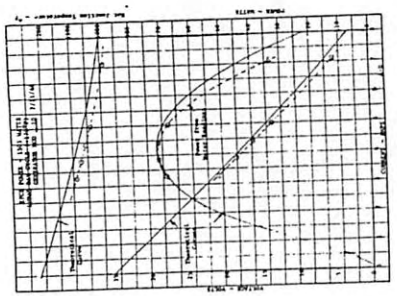

Figure 11-11. Final I-V Mapping-Lunar Day Cycle (EFCS Power 1505 Watts)

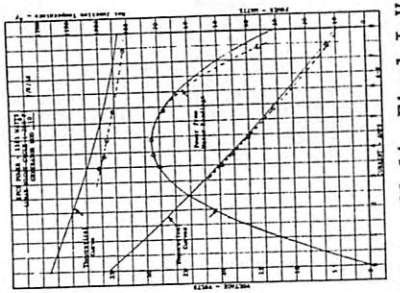

Figure 11-14. Final I-V Mapping-Lunar Night Cycle (EFCS Power 1505 Watts)

cover the initial thermal vacuum mapping at both lunar day and night conditions for three power inputs and five load conditions. Figures 11-9 and 11-10 are of thermal vacuum mapping after 1000 hours of operational life. Figures 11-11 through 11-16 are the concluding maps at lunar day and night conditions just prior to shutdown of the testing, after total of 7,771 hours, including 7,429 at vacuum. Data sheets for these curves are included in the Appendix.

11.1.2 ARGON LEAK RATE MEASUREMENTS

a. Initial leakage of the non-operating (cold) generator: 9.01×10^{-7} std cc argon/sec

b. Initial leakage of the operating generator (hot) under thermal vacuum conditions: 2.45×10^{-7} std cc argon/sec

c. Final leakage of the operating generator under thermal vacuum conditions, after 7,429 hours: 3.84×10^{-7} std cc argon/sec

(Specification limit = 4×10^{-6} std cc argon/sec)

11.1.3 SINUSOIDAL VIBRATION TEST - QUAL LEVELS

The generator was subjected to sinusoidal vibration along each of its three orthogonal axes over the frequency range shown below and at the input levels indicated:

Frequency	Vibration Levels
5 to 20 Hz	0.39" double amplitude
20 to 35 Hz	± 7.8 g
35 to 100 Hz	± 10.4 g

The frequency range was covered at a rate of three octaves per minute, once, in increasing direction only. The generator was non-operative during this test. No resulting damage was experienced.

The Generator Assembly (GA) was then installed in a 4 foot by 5 foot vacuum chamber and a four point post-test I-V mapping performed to verify the integrity of the GA. The GA successfully passed the qual vibration test. Figure 11-17 depicts the setup on the shaker.

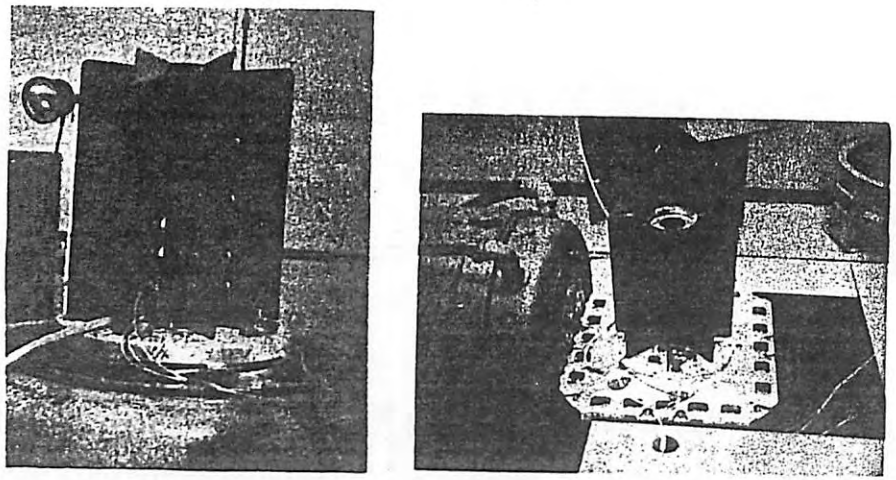

X Axis

Y and Z Axis

Figure 11-17. Vibration Setup

11.1.4 RANDOM VIBRATION TEST - QUAL LEVELS

Frequency Range	Vibration Levels
23 to 80 Hz	0.224 g^2/cps
80 to 120 Hz	12 db/octave roll-off
120 to 950 Hz	0.044 g^2/cps
950 to 1250 Hz	12 db/octave roll-off
1250 to 2000 Hz	0.0148 g^2/cps

The generator was subjected to five minutes of random vibration in each of its three orthogonal axes over the frequency range and input levels indicated.

The GA was then installed in a 4 foot by 5 foot vacuum chamber and a four point post-test I-V mapping performed to verify the integrity of the GA. The GA successfully passed the qual vibration test.

11.1.5 SHOCK TEST

The generator was subjected, non-operating, to three 15 g shocks in both directions of each of the generator's three major axes. The time to peak of each shock was 11 msec $\pm$ 10 precent with a time decay equal to or less than two msec. Figures 11-18 and 11-19 depict, respectively, the shock test equipment and a typical 15 g shock waveform obtained during the test.

The GA was then installed in a 4 foot by 5 foot vacuum chamber and a three point post-test I-V mapping performed to verify the integrity of the GA. The GA successfully passed the qual shock test.

11.1.6 ACCELERATION TEST

The generator was installed in a centrifuge and rotated non-operating for a period of three minutes along both directions of the vertical axes and in a positive direction of the two lateral axes to produce a rotational force of 7.5 g's.

The GA was then installed in a 4 foot by 5 foot vacuum chamber and a five point post-test I-V mapping performed to verify the integrity of the GA. The GA successfully passed the qual acceleration test.

11.1.7 OPERATIONAL LIFE TEST

An operational life test of Mod 10 was started on August 7, 1967. During the test, the chamber temperature was cycled every fourteen days from +170 $\pm$ 5°F to -280 $\pm$ 20°F simulating lunar day and night conditions while maintaining a vacuum in the 10^{-9} torr range. The generator load voltage was maintained at 16 volts during the test, except for I-V mapping. All testing was performed using an electric capsule as the generator heat source.

A five point performance map and leak rate test was conducted during the test (same as in the acceptance thermal vacuum test) at the following periods:

After 1000 hours of operation

After 3000 hours of operation

After 5000 hours of operation

After 7500 hours of operation.

The details and qualification test results are covered in Reference 11-3.

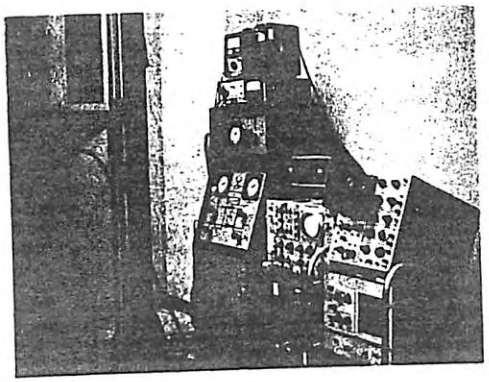

Figure 11-18. Shock Test Equipment

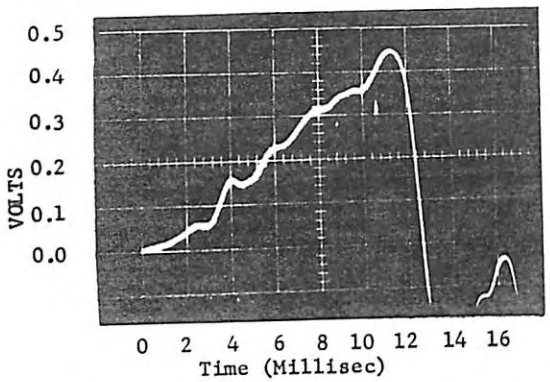

Accelerometer Calibration: 29.8 MV/G

$$\text{"G" Level} = \frac{0.44 \text{ volts}}{0.0298 \text{ volts/G}} = 14.76 \text{ G's}$$

Figure 11-19. Typical 15g Shock Waveform

11.1.8 MAGNETIC EVALUATION TEST

The Operational Life Test on the Mod 10 generator was interrupted (on February 22, 1968) to make the GA available for the magnetic testing at NASA-Goddard. Fuel capsule, S/N 6330001, was employed as the heat source for the generator during the test. Figure 11-20 depicts the RTG inside a special non-magnetic test fixture within the coil system. Figures 11-21 through 11-23 summarize the results of the magnetic test. Reference 11-4 documents the details and results of the test.

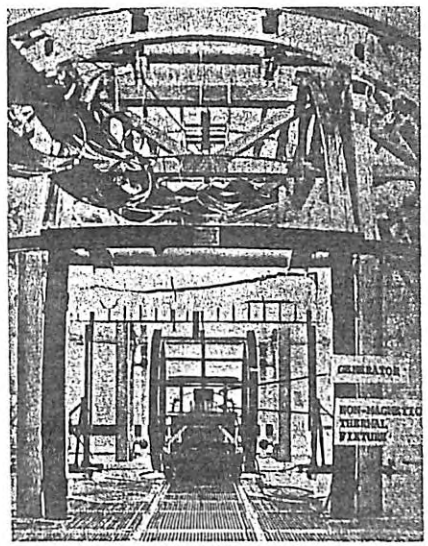

Figure 11-20. Magnetic Evaluation Test at NASA-Goddard's Space Center

At the completion of the magnetic evaluation test, the generator was reinstalled in the 4 foot by 5 foot vacuum chamber and the operational life test resumed in the same manner as before. The operational life test was terminated by AEC direction on July 15, 1968.

Figures 11-24 through 11-26 are normalized curves of generator power, voltage and resistance, respectively, as a function of time covering the complete operation life test. The data for these curves is presented in Appendix D.

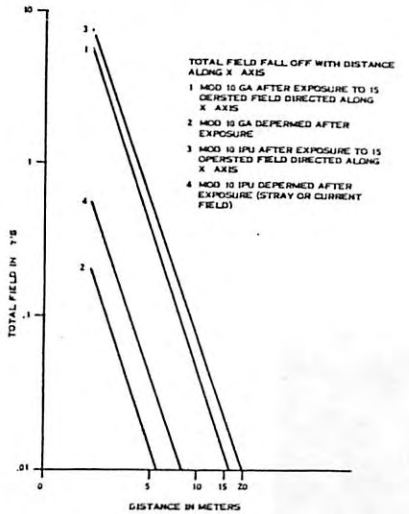

Figure 11-21. Total Field Fall-off with Distance Along X Axis

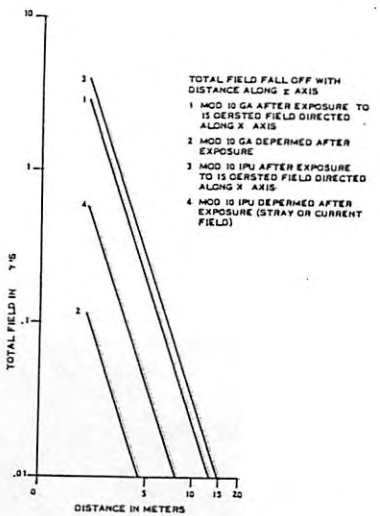

Figure 11-22. Total Field Fall-off with Distance Along Z Axis

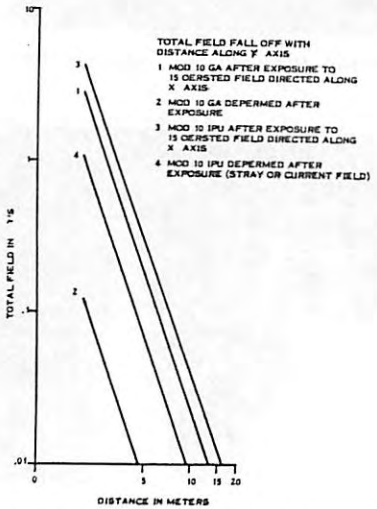

Figure 11-23. Total Field Fall-off with Distance Along Y Axis

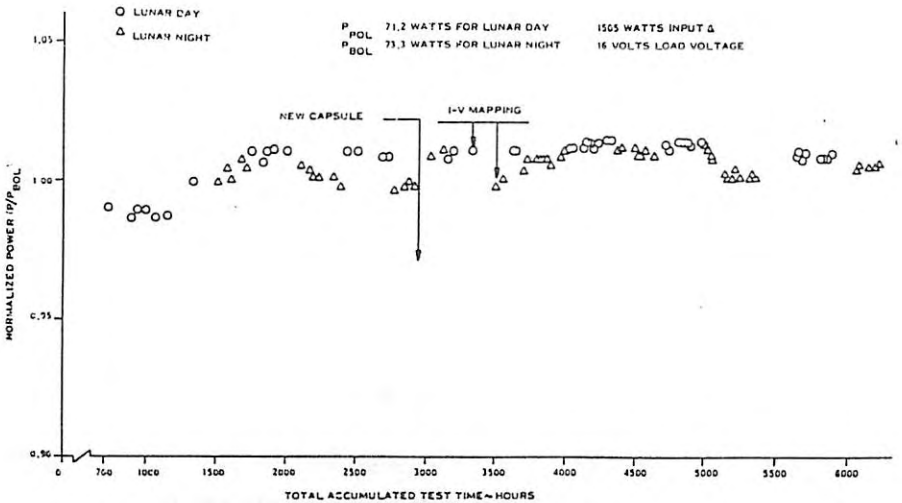

Figure 11-24. Mod 10 Generator Normalized Power Outpu

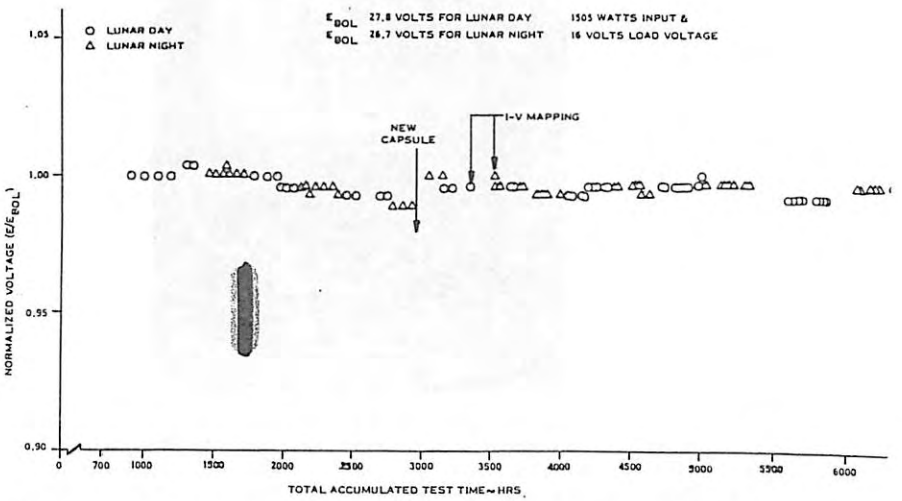

Figure 11-25. Mod 10 Generator Normalized Open Circuit V

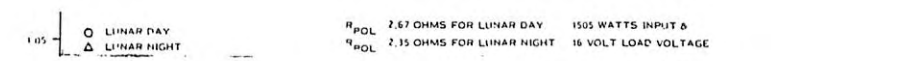

P_{POL} 71.2 WATTS FOR LUNAR DAY 150S WATTS INPUT &
P_{BOL} 73.3 WATTS FOR LUNAR NIGHT 16 VOLTS LOAD VOLTAGE

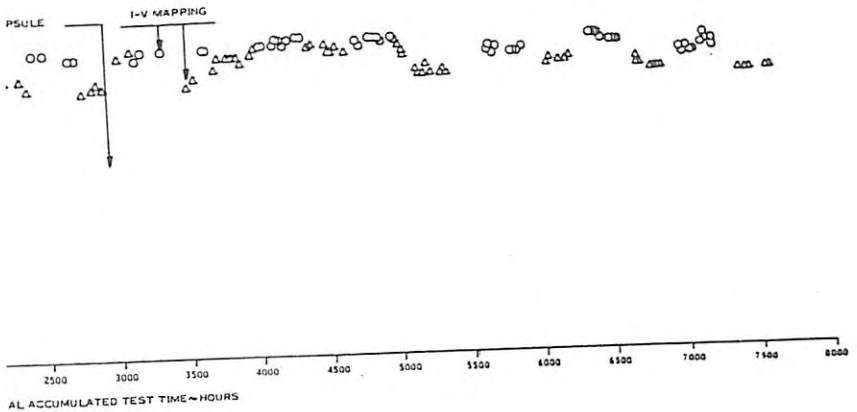

11-24. Mod 10 Generator Normalized Power Output

E_{BOL} 27.8 VOLTS FOR LUNAR DAY 150S WATTS INPUT &
E_{BOL} 26.7 VOLTS FOR LUNAR NIGHT 16 VOLTS LOAD VOLTAGE

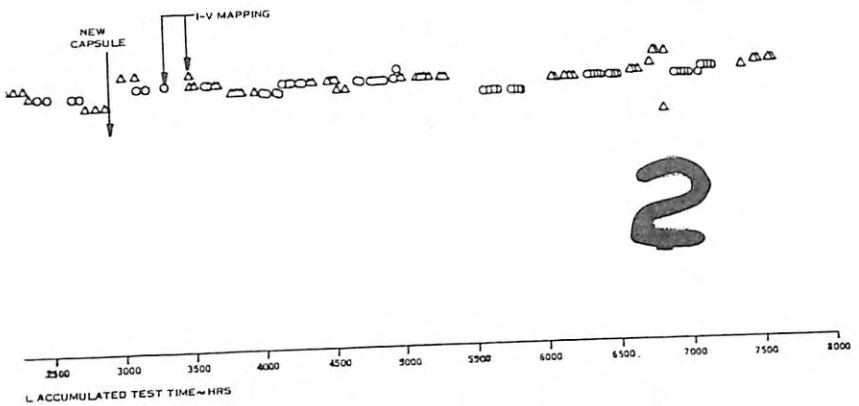

. Mod 10 Generator Normalized Open Circuit Voltage

R_{POL} 2.67 OHMS FOR LUNAR DAY 150S WATTS INPUT &
R_{POL} 2.15 OHMS FOR LUNAR NIGHT 16 VOLT LOAD VOLTAGE

BLANK PAGE

Figure 11-24. Mod 10 Generator Normalized Power Output

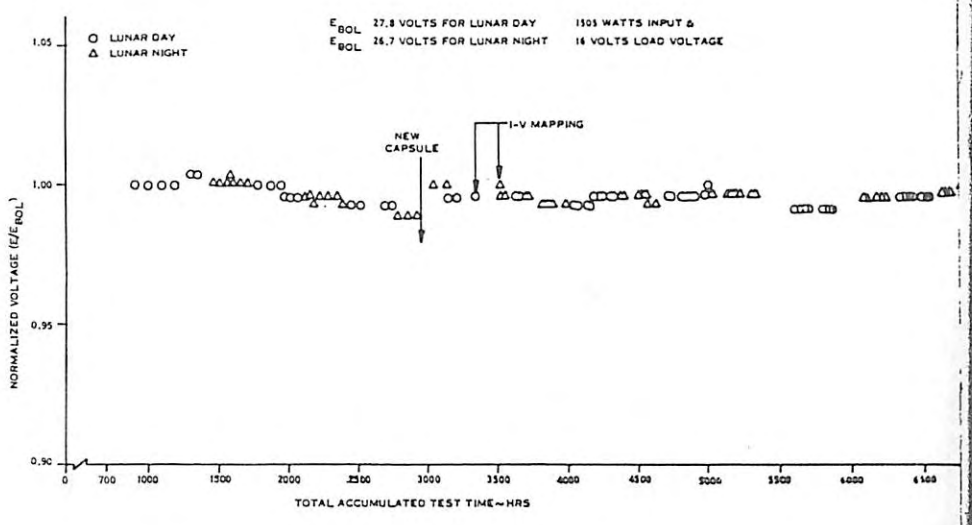

Figure 11-25. Mod 10 Generator Normalized Open Circuit Voltag

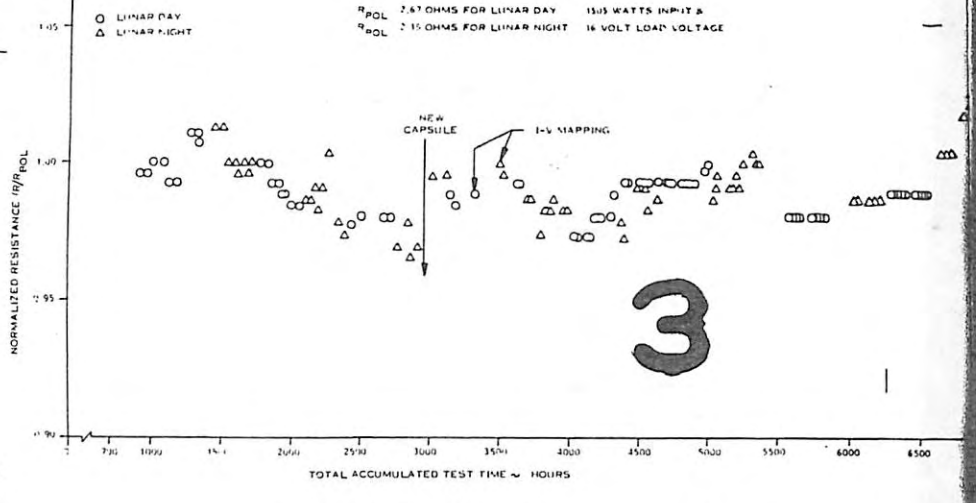

Figure 11-26. Mod 10 Generator Resistance Ratio

BLANK PAGE

Mod 10 Generator Normalized Power Output

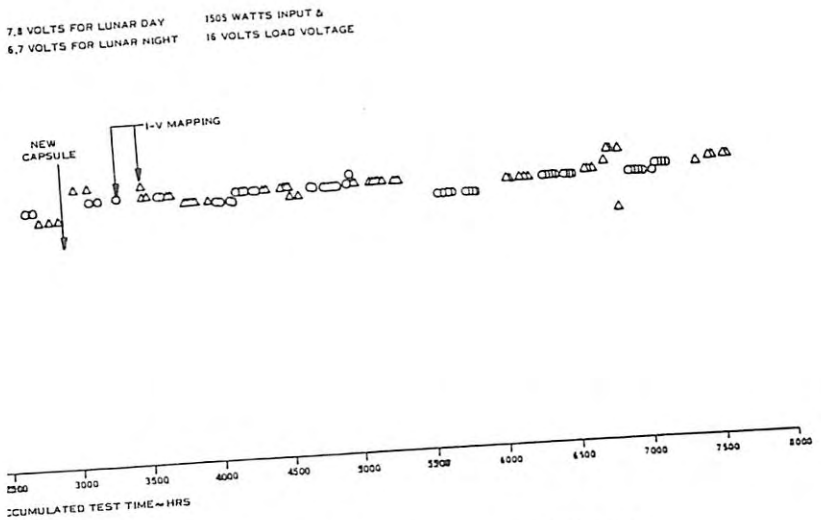

Mod 10 Generator Normalized Open Circuit Voltage

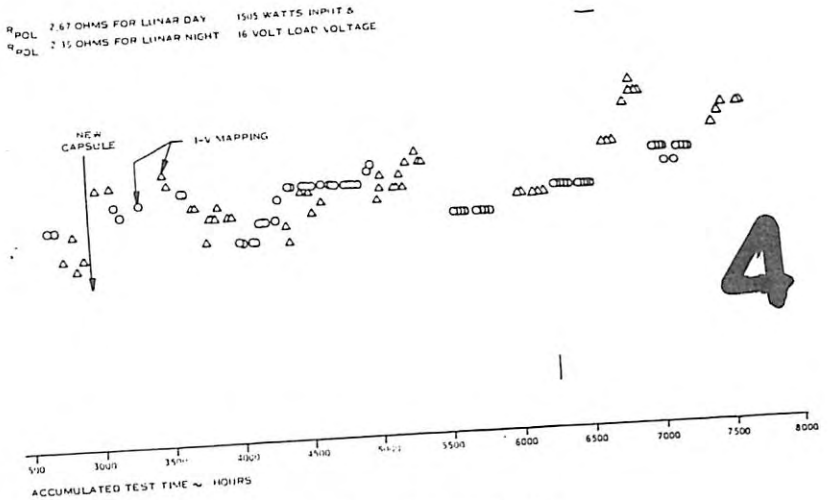

11-26. Mod 10 Generator Resistance Ratio

11.2 FUEL CAPSULE ASSEMBLY, S/N 6330004, QUALIFICATION TESTS

The qualification test program conducted on fuel capsule, S/N 6330004, consisted of initial acceptance tests on the capsule by itself followed by tests on the capsule when integrated with the GLFC and the ALSEP Support Structure. These latter tests, referred to as the ALSEP Cask Assembly (ACA) tests, are covered in Subsection 11.4. In the ACA configuration, the capsule thus experienced the benefit of being supported and housed in a GLFC which provided a realistic capsule environment. Figure 11-27 depicts the sequence of activities.

The acceptance tests performed initially on the capsule were:

a. Receiving Inspection

b. Thermal Mapping - vacuum

c. Helium Leak Check

d. Flange Weld Inspection

e. Operability Assurance Vibration.

The qualification tests which the capsule experienced as part of the ACA configuration consisted of:

a. Thermal Air Test

b. Thermal Vacuum Test

c. Sinusoidal and Random Vibration Tests

d. Shock Test

At the completion of the above vibration and shock tests, the fuel capsule was removed from the GLFC and inspected for damage, thermally remapped and helium leak checked. Tables 11-1 and 11-2 summarize the results. Figure 11-28 is a temperature profile of the capsule before and after vibration testing.

11.3 GRAPHITE LM FUEL CASK, S/N 6406001, QUALIFICATION TESTS

The GLFC was not qualified as a component by itself. Instead, it participated in all the qualification tests which were performed on the ALSEP Cask Assembly which went through qualification testing as described in Subsection 11.4.

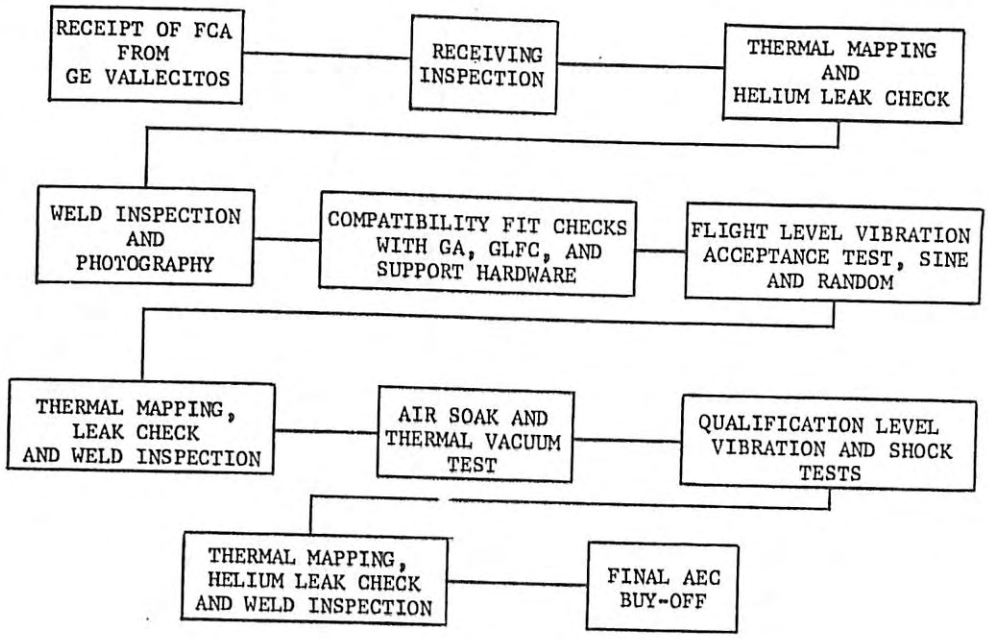

Figure 11-27. FCA Flow Sequence, Qualification Hardware

TABLE 11-1. SNAP-27 QUALIFICATION FCA, S/N 6330004, AVERAGE THERMAL PROFILE DATA (^{o}F)

LOCATION	PRE-VIBRATION	POST ACCEPTANCE LEVEL VIBRATION	POST QUALIFICATION LEVEL VIBRATION
0.3 in. from dome	734	749	762
1.0 in. from dome	818	833	835
4.5 in. from dome	999	991	995
8.0 in. from dome	958	945	955
11.5 in. from dome	999	994	990
15.2 in. from dome	772	795	817

TABLE 11-2. SNAP-27 QUALIFICATION FCA, S/N 6330004, HELIUM LEAK RATE DATA

PRE-VIBRATION	3.4×10^{-8}
POST ACCEPTANCE LEVEL VIBRATION	8.3×10^{-8}
POST QUALIFICATION LEVEL VIBRATION AND SHOCK	2.3×10^{-8}